# Estimation and Control Methods for Active Reduction of Engine-Induced Torsional Vibration in Hybrid Powertrains

**Methoden zur Schätzung und Regelung für aktive Beruhigung von verbrennungsmotorisch erregten Torsionsschwingungen im hybriden Fahrzeugantriebsstrang**

Zur Erlangung des akademischen Grades Doktor-Ingenieur (Dr.-Ing.)
genehmigte Dissertation von Raja Sangili Vadamalu aus Tuticorin, Indien
Tag der Einreichung: 16.10.2018, Tag der Prüfung: 19.12.2018
Darmstadt — D 17

1. Gutachten: Prof. Dr. techn. Christian Beidl
2. Gutachten: Prof. Dr.-Ing. Stephan Rinderknecht

TECHNISCHE UNIVERSITÄT DARMSTADT

vkm

Estimation and Control Methods for Active Reduction of Engine-Induced Torsional Vibration in Hybrid Powertrains
Methoden zur Schätzung und Regelung für aktive Beruhigung von verbrennungsmotorisch erregten Torsionsschwingungen im hybriden Fahrzeugantriebsstrang

Genehmigte Dissertation von Raja Sangili Vadamalu aus Tuticorin, Indien

1. Gutachten: Prof. Dr. techn. Christian Beidl
2. Gutachten: Prof. Dr.-Ing. Stephan Rinderknecht

Tag der Einreichung: 16.10.2018
Tag der Prüfung: 19.12.2018

Darmstadt — D 17



**Estimation and Control Methods for Active Reduction of Engine-Induced Torsional Vibration in Hybrid Powertrains**

Am Fachbereich Maschinenbau
an der Technischen Universität Darmstadt

Zur Erlangung des akademischen Grades

**Doktor-Ingenieurs (Dr.-Ing.)**

eingereichte

**Dissertation**

vorgelegt von

Raja Sangili Vadamalu M.Sc.

aus Tuticorin, Indien

| | |
|---|---|
| Referent: | Prof. Dr. techn. Christian Beidl |
| Korreferent: | Prof. Dr.-Ing. Stephan Rinderknecht |
| Tag der Einreichung: | 16. Oktober 2018 |
| Tag der mündlichen Prüfung: | 19. Dezember 2018 |

Darmstadt 2018

D17

**Erklärung**

Hiermit erkläre ich, dass ich die vorliegende Arbeit, abgesehen von den in ihr ausdrücklich genannten Hilfen, selbständig verfasst habe.

Darmstadt, 16. Oktober 2018

Raja Sangili Vadamalu

*Dedicated to my Father, who is with me through memories and my Mother*

குஞ்சி யழகும் கொடுந்தானைக் கோட்டழகும்
மஞ்சள் அழகும் அழகல்ல - நெஞ்சத்து
நல்லம்யாம் என்னும் நடுவு நிலைமையால்
கல்வி அழகே அழகு.

-நாலடியார், பதினெண் கீழ்க்கணக்கு (ca. 300 BCE - 7th century CE)

## Vorwort

Die vorliegende Arbeit entstand während meiner Tätigkeit als wissenschaftlicher Mitarbeiter am Institut für Verbrennungskraftmaschinen und Fahrzeugantriebe der Technischen Universität Darmstadt.

Ich bedanke mich bei meinem Doktorvater und Institutsleiter Herrn Prof. Dr. techn. Christian Beidl für die Möglichkeit an hochinteressanten Themen zu forschen und die Infrastruktur am Institut nutzen zu können. Ich schätze das mir entgegengebrachte Vertrauen sehr, die Themen mit dem größtmöglichen wissenschaftlichen Freiraum bearbeiten zu können.

Herrn Prof. Dr.-Ing. Stephan Rinderknecht danke ich für sein Interesse, seine Ratschläge und die Bereitschaft das Koreferat zu übernehmen. Mein besonderer Dank gilt Herrn Prof. Dr.-Ing. Günter Hohenberg für sein stets offenes Ohr und die fachlichen Gespräche, die mir geholfen haben, meine Gedanken zu strukturieren und zu schärfen.

Insbesondere Herrn Dr. Karthikeyan Kottaisamy (Ph.D) und Dr.-Ing. Ramakrishnan Ambur danke ich für das Gegenlesen dieser Ausarbeitung und die inhaltlichen Diskussionen. Für die interessanten fachlichen Anregungen und für die Zusammenarbeit in den Projekten bedanke ich mich herzlich bei Herrn Dr.-Ing. Maximilian Bier.

Darüber hinaus möchte ich mich herzlich bei den StudentInnen bedanken, die durch ihre Abschlussarbeiten und Tätigkeiten als Hilfswissenschaftler meine Forschungsarbeit unterstützt haben. Mein herzlicher Dank gilt allen Mitarbeiterinnen und Mitarbeitern des VKM für die kollegiale Zusammenarbeit und das gute Arbeitsklima. Der mechanischen und elektrischen Werkstatt danke ich für die schnelle und zuverlässige Unterstützung, sowohl bei terminierten als auch kurzfristigen Aufträgen. Ebenso danke ich Frau. Renate Schreiber für die Unterstützung in organisatorischen und verwaltungstechnischen Anliegen.

Mein herzlichster Dank gebührt meinen Eltern und meiner Familie, die mich in der Zeit der Entstehung dieser Arbeit stets unterstützt haben. Ich danke besonders Bernhard und Gerti Hein für alle Unterstützung seit meinem Masterstudium. Ich bedanke mich auch bei allen nicht von mir beeinflussbaren Faktoren, die mir geholfen bzw. nicht gestört haben.

## Abstract

Automotive powertrain development faces the formidable challenge of reducing fuel consumption, improving driving performance, meeting regulatory demands and satisfying customer demands. Besides powertrain hybridization, continuous optimization of the internal combustion engine (ICE) is actively pursued. Engine refinement using technologies like Miller/Atkinson cycle and Variable Compression Ratio leads to higher peak pressure values in the cylinder from the improved thermodynamic processes. This trend along with rightsizing and downspeeding of the ICE give rise to torque pulsations with higher amplitude and low frequencies. These resulting oscillations cause passenger discomfort and affect component durability.

Measures for passive torsional vibration isolation essentially modify the mechanical characteristics of the powertrain. Approaches employing isolation with the use of tuned mass dampers to reduce such torsional oscillations have also been applied. The increasing complexity and the tuning effort required for the passive mechanisms have increased the interest in adopting active vibration reduction measures. Active torsional vibration reduction uses the onboard electric machine for realizing compensation torque to reduce engine-induced powertrain oscillations.

The objective of this thesis is to develop methods for estimation and control to realize the active reduction of engine-induced torsional oscillations in automotive powertrains. The oscillatory dynamics of the powertrain is governed by the torsional dynamics of the powertrain system and external excitations, in the form of torque pulsations from the ICE. The developed estimation methods study both the torsional powertrain system and the excitations. The dynamic engine torque is estimated using Unknown Input Observer (UIO) techniques. The filtering of the mean value and harmonic components of the dynamic torque is performed using a Linear Parameter Variant (LPV) estimator. The characteristics of the torsional system are identified using Errors-In-Variables (EIV) setup in closed loop operation.

In this work, before initiating the development of control methods, a methodology has been defined to analyze the potential available for active vibration reduction. Besides, the developed vibration reduction controller shall be integrated with the hybrid vehicle energy management controller. A modular architecture has been presented to enable the integration of the controller irrespective of their realization. To characterize the losses associated with the active vibration reduction control, a harmonic characterization of the actuation unit efficiency has been formulated. Beyond the analysis of the losses involved, the harmonic efficiency characterization

can be used to develop electric machines specific to vibration reduction of various harmonics. A generic approach has been employed for the development of vibration reduction controllers using measurements for feedback. This approach involves an abstract definition of the active vibration reduction problem. Such an abstract viewpoint offers an opportunity to apply different control methodologies such as adaptive, robust and time-delayed control. The developed controllers have been analyzed with simulations and validated using the experimental setup, demonstrating the desired torsional vibration reduction.

## Zusammenfassung

Die Entwicklung von zukünftigen Fahrzeugantriebskonzepten wird von Herausforderungen wie der Reduktion des Kraftstoffverbrauchs, der Erfüllung von Kundenansprüchen wie Fahrspaß und Fahrkomfort sowie der Erfüllung von gesetzlichen Rahmenbedingungen geprägt. Neben der Hybridisierung der Antriebsstränge wird der Verbrennungsmotor kontinuierlich verbessert und optimiert. Weiterentwicklungen des Verbrennungsmotors mit Hilfe von Technologien wie dem Miller/Atkinson-Zyklus oder dem variablen Kompressionsverhältnis resultieren dabei aufgrund der verbesserten thermodynamischen Prozesse in höheren Spitzendruckwerten im Brennraum. Dieser Trend in Kombination mit dem Rightsizing und Downspeeding des Verbrennungsmotors führt zu Drehmomentschwankungen mit erhöhter Amplitude und niedrigen Frequenzen. Die resultierenden Torsionsschwingungen wirken sich nachteilig auf den Komfort der Fahrgäste aus und beeinträchtigen die Lebensdauer der Komponenten.

Passive Maßnahmen verändern im Wesentlichen die mechanischen Eigenschaften des Antriebsstrangs. Sie beruhen auf Änderungen der Trägheit und/oder der Isolation durch Schwingungstilger, um derartige Torsionsschwingungen zu reduzieren. Durch die zunehmende Komplexität des Antriebsstrangs und dem dadurch erforderlichen hohen Applikationsaufwand verschiebt sich der Fokus in der Entwicklung immer stärker in Richtung aktiver Schwingungsreduktionsmaßnahmen. Die aktive Drehschwingungsreduktion verwendet die elektrische Maschine des Fahrzeugs zum Erzeugen eines Kompensationsdrehmoments, um die verbrennungsmotorisch erregter Torsionsschwingungen zu reduzieren.

Ziel dieser Arbeit ist die Entwicklung von Methoden zur Abschätzung nicht messbarer Schwingungsgrößen und die Entwicklung von Regelungsansätzen für aktive Beruhigung von verbrennungsmotorisch erregten Drehschwingungen in Fahrzeugantriebssträngen. Die Schwingungsdynamik des Antriebsstrangs wird durch die Torsionsdynamik des Antriebsstrangsystems und externe Anregungen in Form von Drehmomentpulsationen aus dem Verbrennungsmotor bestimmt. Die entwickelten Schätzverfahren untersuchen sowohl das torsionale Antriebssystem als auch die Anregungen. Das dynamische Motordrehmoment wird mithilfe von Unknown Input Observer (UIO) Verfahren geschätzt. Die Filterung des Mittelwerts und der harmonischen Anteile des dynamischen Drehmoments wird unter Verwendung eines linearen Parametervariantenschätzers (LPV) durchgeführt. Die Eigenschaften des Torsionssystems werden durch den Einsatz eines Errors-In-Variables (EIV) im Closed-loop Betrieb ermittelt.

Bevor mit der Entwicklung des Reglers begonnen wird, wird eine Methodik abgeleitet, um das für die aktive Schwingungsreduktionsmethode verfügbare Potential zu analysieren. Darüber hinaus soll der entwickelte Schwingungsreduzierungsregler in den Energiemanagementregler des Hybridantriebsstrangs integriert werden. Eine modulare Architektur wird vorgestellt, um die Integration des Reglers unabhängig von dessen Realisierung zu ermöglichen. Um die mit der aktiven Schwingungsreduktionsregelung verbundenen Verluste zu quantifizieren, wird eine harmonische Charakterisierung des Wirkungsgrads des Aktors formuliert. Außerdem kann die harmonische Effizienzcharakterisierung dazu verwendet werden, elektrische Maschinen auszulegen, die für die Schwingungsreduktion verschiedener Oberschwingungen prädestiniert sind.

Ein generischer Ansatz wurde für die Entwicklung der Schwingungsreduktionsregler unter Verwendung von Messungen als Rückkopplung angewendet. Der Ansatz basiert auf einer abstrakten Definition des Problems der aktiven Schwingungsreduktion. Diese abstrakte Ansicht bietet die Möglichkeit, verschiedene Regler wie adaptive, robuste und zeitverzögerte Stabilisierungsansätze anzuwenden. Die entwickelten Regler wurden mit Simulationen analysiert und im Versuchsaufbau validiert, um die erwünschte Torsionsschwingungsreduktion nachzuweisen.

## List of Figures

## List of Tables

## List of Abbreviations

| | |
|---|---|
| ACF | Auto-Correlation Function. |
| ANC | Active Noise Control. |
| ARMAX | AutoRegressive Moving Average with eXogeneous inputs. |
| ARX | AutoRegressive with eXogeneous inputs. |
| BSG | Belted Starter Generator. |
| CASMA | Crank Angle Synchronous Moving Average. |
| CCA | Canonical Correlation Analysis. |
| CEA | Combustion Engine Assist. |
| CG | Conjugate Gradient. |
| CPA | Centrifugal Pendulum-type Absorber. |
| DFT | Discrete Fourier Transform. |
| DMF | Dual Mass Flywheel. |
| DOF | Degrees of freedom. |
| ETFE | Empirical Transfer Function Estimates. |
| ECU | Electronic Control Unit. |
| EGR | Exhaust Gas Recirculation. |
| EIV | Errors-In-Variables. |
| EM | Energy Management. |
| ETM | Electric Traction Machine. |
| GD | Gradient Descent. |
| HV | High Voltage. |
| ICE | Internal Combustion Engine. |
| IIR | Infinite Impulse Response. |
| IQC | Integral Quadratic Constraints. |
| IV | Instrumental Variables. |
| FIR | Finite Impulse Response. |
| FRF | Frequency Response Function. |
| FxLMS | Filtered x-Least mean squares. |
| HANN | Harmonic Activation Neural Network. |
| LFT | Linear Fractional Transformation. |
| LMI | Linear Matrix Inequalities. |
| LMS | Least Mean Squares. |
| LPF | Low Pass Filter. |
| LPM | Local Polynomial Method. |
| LPV | Linear Parameter Variant. |
| LTI | Linear Time Invariant . |
| MA | Moving Average. |

| | |
|---|---|
| MIMO | Multi Input Multi Output. |
| ML | Maximum Likelihood. |
| MPC | Model Predictive Control. |
| MSE | Mean Squared Error. |
| NLMS | Normalized Least Mean Squares. |
| NVH | Noise Vibration Harshness. |
| OE | Output Error. |
| PEM | Prediction Error Method. |
| PRBS | Pseudo Random Binary Sequence. |
| PSD | Power Spectral Density. |
| RDE | Real Driving Emissions. |
| RLS | Recursive Least Squares. |
| RMS | Root Mean Square. |
| SA | Spectral Analysis. |
| SISO | Single Input Single Output. |
| SML | Sample Maximum Likelihood Estimator. |
| SNR | Signal-to-Noise Ratio. |
| SOGI | Second Order Generalized Integrator. |
| SOC | State of Charge. |
| SSARX | Subspace AutoRegressive with eXogeneous inputs. |
| SSV | Structured Singular Value. |
| SVD | Singular Value Decomposition. |
| WLS | Weighted least squares. |
| UIO | Unknown Input Observers. |
| UUT | Unit Under Test. |

## Contents

# 1 Introduction

The development of automotive powertrain faces the challenging task of balancing between the conflicting goals of meeting stringent regulations and satisfying customer demand for better fuel economy, performance and comfort. A development phase relying solely on improving the efficiency of the internal combustion engine (ICE) or meeting regulatory demands for reduced emissions shall not result in a desirable customer appeal in terms of fun-to-drive. Presently, gasoline engines enjoy the biggest market share for passenger car powertrains. This can be attributed to the potential for low exhaust gas emissions and high robustness against fuel quality variation as well as high power density. Though the market share of electric powertrains in the long term is forecasted to be higher, in the short term (till 2025), the major powertrain shall be gasoline-powered including hybrid as well as Plug-in-Hybrid vehicles [1].

Powertrain hybridization helps to shift the operation of the engine to higher loads, which further emphasizes the need for improvement of the maximum engine specific power. This also motivates the consideration of the trade-off between maximum engine thermal efficiency and maximum engine specific power for future engine development. Presently, Miller cycle and Atkinson cycle offer the most cost-effective $CO_2$ solution [2]. Figure 1.1 gives an overview of the futuristic concepts that are currently pursued in case of light-duty gasoline engines along with short-term target and future potential. The figure depicts a representation of the engine concepts with the maximum specific power (in kW/liter) and engine displacement (in liter). One of the investigated concepts, Turbo Gasoline Direct Injection using the Miller cycle with external cooled Exhaust Gas Recirculation (EGR) can achieve a maximum thermal efficiency of 42% with a specific power greater than 90 kW/liter.

The planned concepts for the short term and long term are only possible with higher mean effective pressure, assuming the engine operating speeds are in the same order of magnitude. This assumption is justifiable in order to increase engine efficiency which serves as an additional goal. Hence the common feature among all the currently investigated futuristic concepts is, that their mean effective pressure is higher than that of the current engines leading to higher torque pulsations. A similar trend is also seen in the case of diesel engines. The attractiveness of the diesel powertrain is declining due to the current discussions regarding the "Dieselgate affair", the complexity required to meet the Real Driving Emissions (RDE) regulations and the introduction of limited driving bans in cities (Hamburg and Frankfurt). Nevertheless, the mean effective pressure of diesel engines is higher

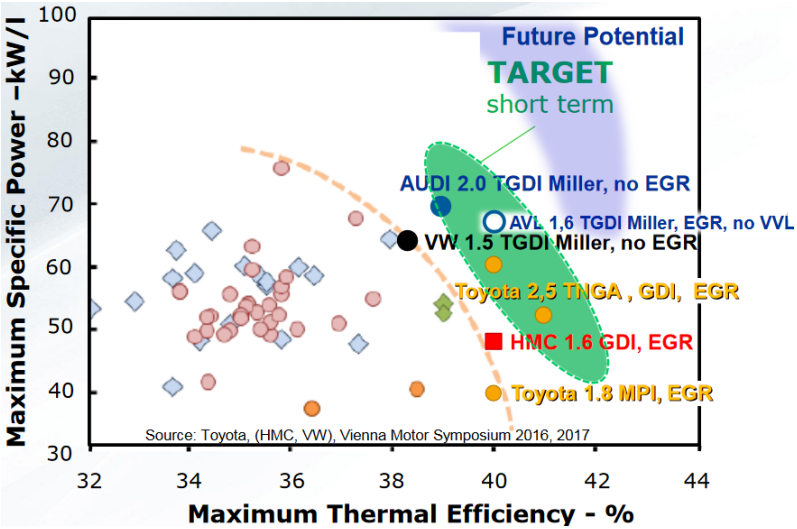


**Figure 1.1:** Trade-off between the maximum efficiency and the maximum specific performance as key development target for future gasoline engines [6]

than the gasoline engines [3], this is one of the reasons for an early introduction of passive isolation measures in the diesel engines [4].

Additional efficiency improvement measures such as down-speeding, which refers to the modification of the transmission ratios to operate at lower engine speeds lower are the frequencies excited. The combination of the above-mentioned measures increase the mean effective pressure and shift the engine operation to lower operating speeds. This shifts the spectrum of torsional excitation, due to the combustion engine torque oscillations, towards lower frequencies with higher amplitude. Such regions have increased human sensitivity to vibrations according to ISO 2631 [5].

## 1.1 Motivation

ICE torque pulsations are a result of the displacement of eccentric masses, associated gas dynamics and periodic energy conversion in the cylinder resulting in pulsating engine torque. Engine development trends such as rightsizing lead to increasing peak pressure resulting in higher amplitude torque oscillations. These measures along with down-speeding shifts the spectrum of torque oscillations to

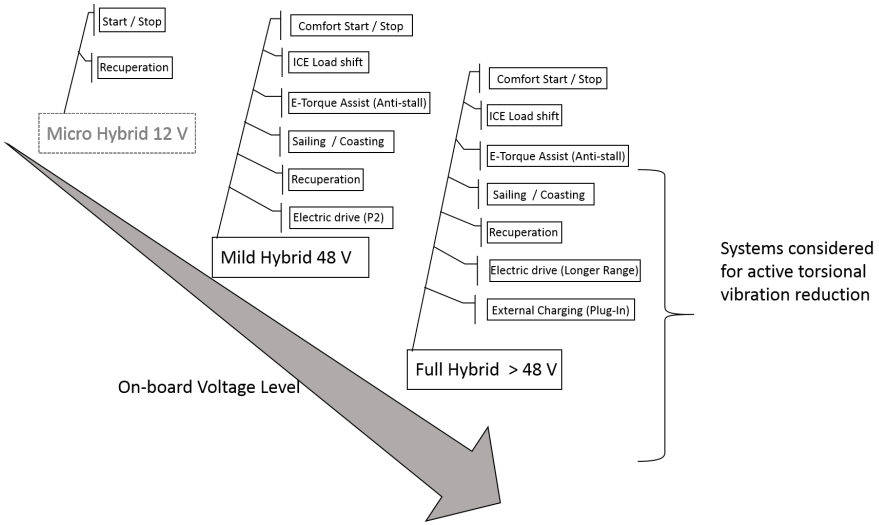


**Figure 1.2:** Overview of hybrid powertrains with realizable operating modes or functionality

lower frequency region. These periodic torque fluctuations lead to speed oscillations around the mean operating speed termed as rotational irregularity, which propagates through the flexible powertrain, affecting component durability and passenger comfort.

### Hybridization as an enabler for torsional vibration reduction

Powertrain hybridization will be one of the key focus areas for automotive powertrain development in the forthcoming years. On the one hand, continuous development of the ICE over the last decades has led to a level of technical maturity, where any improvement shall be incremental and can be realized only with considerable effort. On the other hand, stringent regulatory framework placing binding targets, pose challenges for the development of conventional combustion engine based powertrains. One such objective by the European Union is to reduce the $CO_2$ emissions in the transportation sector by 60% compared to levels in 1990 [7], resulting in a fleet-level regulatory limit of 95 g $CO_2$ per driven kilometer for registration of new vehicles in 2020. Achieving such a target without hybridization measures would require an average combustion engine efficiency of 40% or more [8].

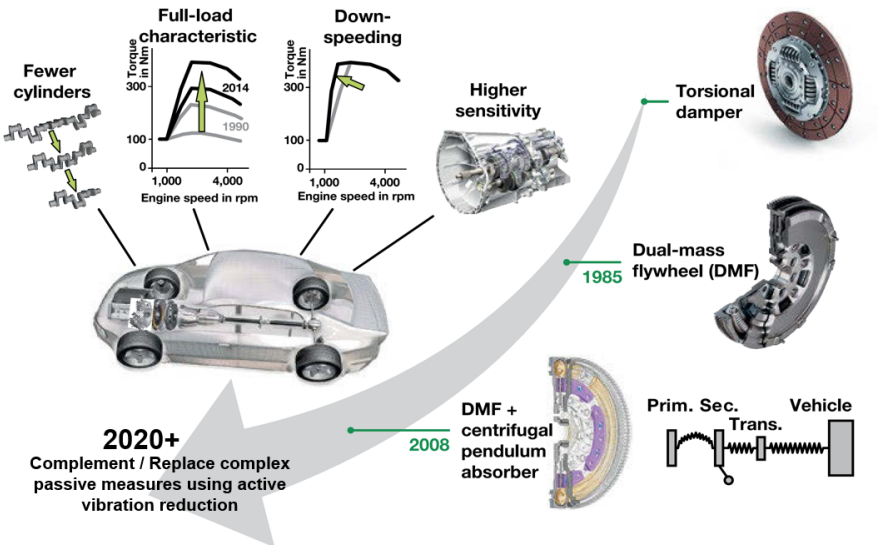


**Figure 1.3:** Chronological development of torsional vibration reduction measures : Motivation for active vibration control development adapted from [9]

The bandwidth of possible hybridization extends from 12 V micro hybrid systems through 48 V mild hybrid systems to high voltage hybridization. Figure 1.2 depicts the possible hybridization categories based on the operational voltage level. Depending on the buffer for energy interchange provided by the onboard power system, different functionality can be realized or existing functionality can be enhanced. The depiction does not consider the availability of external charging facility as a criterion for classification since the focus of the representation in Figure 1.2 is on the realizable hybrid modes. As indicated in the figure, the active torsional vibration methods discussed in this work are applicable to High Voltage (HV, voltage level > 48 V) and 48 V systems. Besides, the shift to 48 V hybridization allows for auxiliary component electrification, reducing the power demand from the engine.

With the availability of additional power source, different functionalities have been conceptualized which extend beyond the regulatory emission levels and fuel consumption reduction. Focus areas of such developments have mainly been drivability/driving dynamics and comfort/Noise Vibration Harshness (NVH). The comfort measures thus achieved have been restricted to the low frequency of operation

due to the high fidelity torque control required for the realization of such functionalities.

One such concept is ActiveHybrid Damping function (AHD) developed by BMW and was introduced in ActiveHybrid 5 [10]. The goal was to reduce torsional vibrations of the drivetrain during dynamic maneuvers using the ICE in combination with the electric machine during acceleration. The usual approach to reduce longitudinal acceleration is to filter the driver's torque request to avoid excitation of vehicle shuffle or surge frequency. Such a filter is termed as anti-surge filter [11]. It leads to a reduced dynamic response. In case of the gasoline powertrain combustion engine, the realization of the filtering can also be performed using short-term interventions [11] of ignition timing. Such interventions deteriorate the fuel economy due to the shift from the fuel-optimal ignition timing. In the case of hybrid powertrains, the torque from the electric machine can be used to reduce the longitudinal vibrations without negatively influencing driving dynamics [10]. With high fidelity torque control of the Electric Traction Machine (ETM), such measures can be used for the active reduction of rotational irregularity.

Reduction of engine-induced torsional oscillations/rotational irregularity using passive measures is achieved by using a modification of the inertial/stiffness properties of the powertrain system and/or using isolation devices such as tuned mass dampers. A chronological overview of the developed passive torsional vibration reduction devices is presented in Figure 1.3. Clutch disc with a torsional damper uses a modification of stiffness characteristics to achieve torsional vibration reduction. Dual Mass Flywheel (DMF) achieves vibration reduction by shifting the eigenfrequency from the frequency range excited by the ICE using the torsional spring and the secondary inertia. The DMF is equipped with Centrifugal Pendulum Absorber (CPA) to meet the increasing demands of modern ICE. The CPA realizes a speed-dependent tuned damper, using the centrifugal force variation over rotational speed. It can be tuned to a specific order of torsional excitation. In addition to the increasing complexity of the passive devices along with the required tuning effort, packaging constraints in case of modern powertrains have shifted the focus from passive measures to active vibration reduction.

Active vibration reduction uses the compensation torque generated by the electric machine to reduce the engine-induced torsional oscillations of the powertrain. The active vibration reduction methods in contrast to passive measures can be activated on-demand and hence ideally supplement the passive damping measures. This flexibility of the active methods renders them attractive for supplementing passive measures. The advantages specific to (but not limited to) active torsional vibration reduction approach are listed in the following.

- *Comfort and durability*: Apart from being perceived as disturbing, increased torsional vibrations lead to higher loads on the powertrain components affecting their structural durability [12].
- *Packaging advantages*: Besides exploiting the synergy of the electric traction machine in the powertrain, active torsional vibration techniques do not require additional packaging space only for the torsional dampening purpose. These techniques use the existing electric traction machine introduced to achieve $CO_2$ or emission targets, not requiring additional components. They represent a functional integration of vibration attenuation along with $CO_2$ or emission reduction measures.
- *Cylinder deactivation*: It leads to improvement of the part-load engine efficiency by operating the active cylinders at a higher specific load. Nevertheless, higher torque can be realized from the inactive cylinders when needed, in contrast to downsizing and downspeeding technologies. With an increased interest in new cylinder deactivation strategies, an increase of the engine-induced excitations can be expected during deactivation mode changes.
- *Influence on consumption and driving style*: With reduced torsional oscillations, the ICE can be operated at lower speeds. This is in addition to the possibility of reducing the ICE idling speed leading to advantages in fuel consumption. It is claimed that isolation of torsional vibrations results in a change of driving style due to better comfort at lower engine speeds. The changed driving style shifts the engine operation to lower speeds during normal driving leading to fuel consumption advantages [13].

## 1.2 Problem statement

The goal of this work is to realize active vibration reduction using the compensation torque from the onboard electric machine to attenuate engine-induced torsional oscillations. This shall supplement the passive vibration reduction measures or replace them in certain situations. With the increasing peak pressure in the cylinder due to improved combustion processes, the passive measures reach their limit [14].

The operational range shall be primarily restricted to speeds below 2000 rpm due to two reasons. The first one being the increased sensitivity of the flexible powertrain to torsional oscillations at low speeds [15], [16]. Further, alternative methods have to be developed which demonstrate both performance and efficiency such

as clutch slip control [4] that are efficient at higher speeds [17]. These methods can be used to supplement the developed controller at higher speeds if required.

From the perspective of structural analysis, two features characterize a vibrating system under external forcing function. They are structural properties of the system and characteristics of the excitation. In the case of torsional oscillations, these features would be the torque pulsations resulting from the ICE and the flexibility of the powertrain. To develop control methods to reduce the torsional vibrations, the above-mentioned effects have to be studied, which is the focus of the first part of the thesis. The controllers developed in the second part use the estimated dynamics quantities and the identified parameters to realize the controller. Each control method is validated using simulations with a 3-cylinder engine and experimentally validated using a 2-cylinder engine. This helps demonstrate the applicability of the controller to various engine concepts.

Every mechatronic solution has certain prerequisites on the base (mechanical) system for its realization. One such condition is that in the working range of the active vibration control, the coupling between the component generating the compensation torque and the inertia in the ICE torque transmission path should be in subcritical operation. Otherwise, higher compensation torque amplitude would be required to realize vibration reduction through the coupling operating in isolation mode. This conclusion is satisfied in case of the P2 powertrain where the ETM is both the compensation torque generating device and also the inertia in the torque transmission path. However, both these components are different in the case of 48 V belt-driven system as discussed in [18]. A detailed discussion of the basic requirements on the powertrain for the realization of active torsional vibration reduction is presented in section 2.6.

The required sub-critical operation can be realized using a stiff or a non-stiff interconnection between the ICE and ETM, which generates the compensation torque. The depiction of the active vibration reduction controller in case of the stiff powertrain is presented in Figure 1.4. The figure displays only the torque signals, which is the forcing function since only engine-induced torque oscillations are considered. The torque signals are presented with respect to crankshaft angle to aid correlation with the different strokes of the ICE. As it can be seen, the compensation torque shall be out-of-phase to the ICE torque oscillations. This is because a stiff interconnection does not introduce any phase lag between the torque signals. The figure also presents two variants with low and high compensation torque and the resulting torque at the gearbox input are presented. Active vibration reduction in powertrain with such a stiff coupling was the main focus of the work [19]. To best of the author's knowledge all realizations of passenger vehicle powertrains

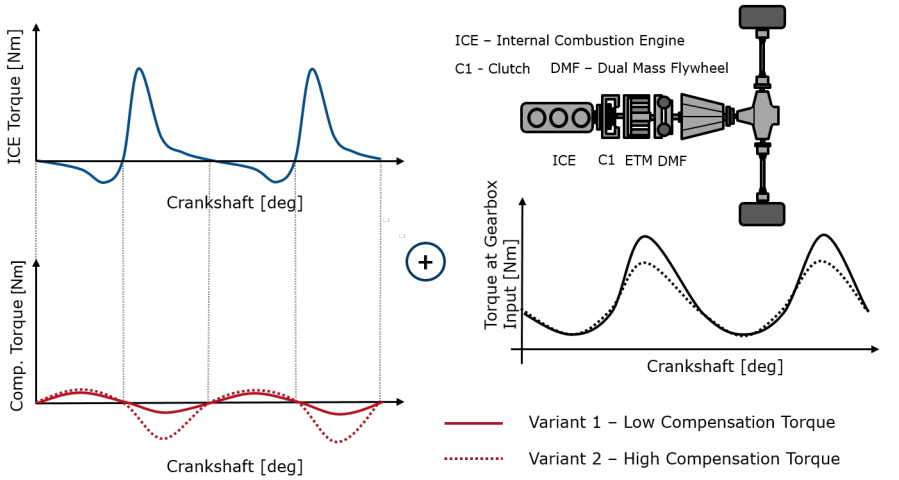


**Figure 1.4:** Conceptual representation of the active vibration reduction control in a stiff powertrain

both hybrid [20] and conventional powertrains [21] use flexible interconnections between ICE and ETM or the rest of the powertrain.

Figure 1.5 depicts the active vibration reduction in case of the non-stiff / flexible coupling. Due to the flexibility of the coupling, there exists a phase lag between the ICE torque and the torque transferred through the DMF and clutch. The compensation torque shall be out-of-phase to the torque acting on the inertia of the electric machine. However, sensing the torque acting on the electric machine inertia poses practical difficulties. This is the core motivation to develop controllers which use only speed measurements to realize the desired active torsional vibration reduction. A passive equivalent system to the stiff/non-stiff variants presented here would be the variants with the CPA positioned on the primary and secondary masses as presented in [22].

## 1.3 Outline of the thesis

The structure of the thesis is presented in Figure 1.6. The work comprises of two parts. The first part deals with the estimation of unknown parameters of the powertrain and internal torque of the combustion engine. The second part handles active vibration reduction control using different control approaches with each chapter

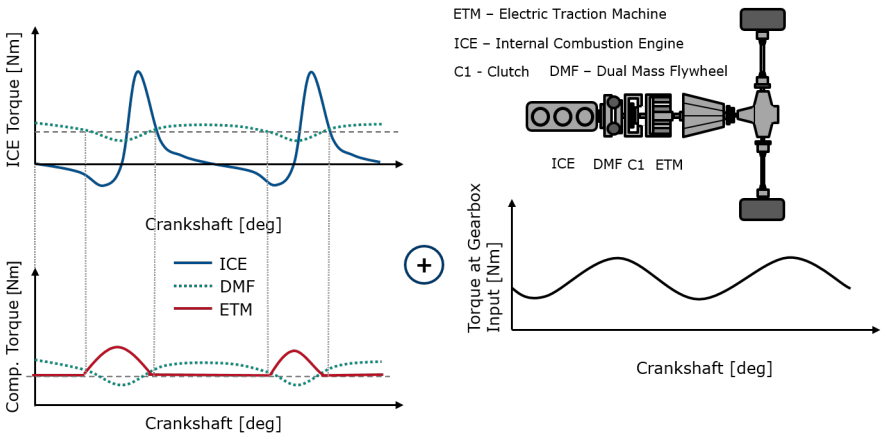


**Figure 1.5:** Conceptual representation of the active vibration reduction control in a non-stiff powertrain

conceptualized as a stand-alone unit. The demarcation between the parts is also motivated by its applicability. The methods discussed in part A are directly applicable for generic oscillatory systems and are restricted neither to automotive powertrains/energy converters nor just to torsional vibrations. The controllers presented in part B focus on the problem of engine-induced torsional vibration specific to automotive powertrains. Nevertheless, with necessary extensions, it can also be applied to other torsional vibration reduction problems. Each chapter in part B is dedicated to a certain control philosophy.

The *Chapter 2* introduces the problem of torsional vibration problem specific to automotive powertrains. It discusses the currently available passive vibration reduction measures to motivate the development of active vibration reduction. It goes on to present an overview of the proposed active vibration reduction controllers in the literature. A methodological approach has been proposed for the potential analysis for active vibration reduction controller. This analysis helps get an idea of the achievable torsional vibration reduction before the actual controller implementation. A novel approach to characterize the efficiency of the electric machine and inverter from the perspective of vibration control is presented. Given the modularity of the developed vibration reduction controller, its integration with the hybrid vehicle energy management system has been simplified. This simplification aids independent development of both the involved functionalities. The

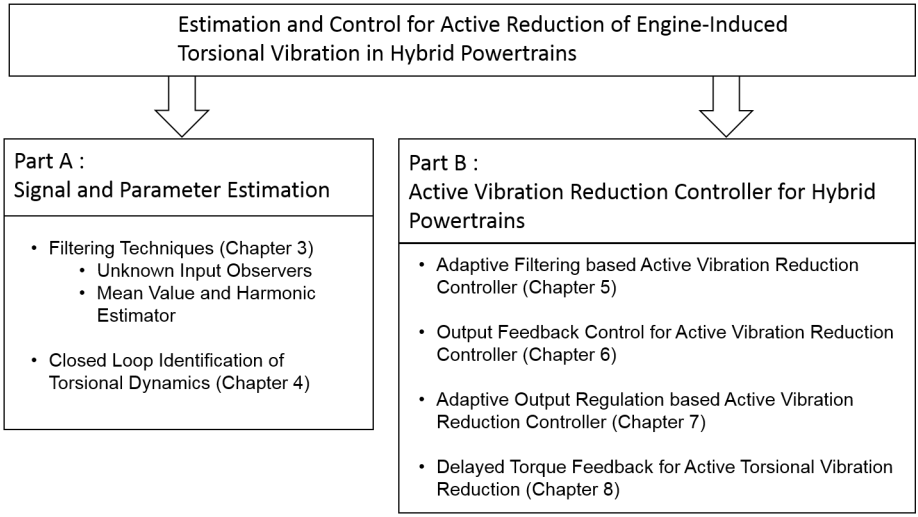


**Figure 1.6:** Overview of the thesis structure

interface required for the integration is discussed along with the use case of a model predictive torsional vibration reduction controller. Finally, the test setup used for experimental validation of the developed controller is presented.

The main source of torsional excitation under study in this work is the ICE. These torque pulsations result due to the discrete combustion events and the crankshaft mass distribution. *Chapter 3* presents methods to estimate the oscillatory combustion engine torque. The methods compute not only the oscillatory torque based on available measurements but also perform its harmonic separation into different frequency components. The generic nature of the estimation approach is not restricted to either ICE torque or just torque signals. This specifically refers to the harmonic separation which is extended to speed and angular deflection signals.

Besides the external excitations, the system dynamics determine the oscillatory behavior of the powertrain system. Hence it is vital to understand the dynamics before attempting to achieve the desired reduction using a controller. The approaches to identify the torsional dynamics of the powertrain system are developed in *Chapter 4*. The identification of the dynamics is performed at the test setup, since the excitations required to characterize the system, cause passenger discomfort if realized in the real vehicle. In addition, the developed method is also employed

to identify the experimental test setup which is used for validation of the torsional vibration reduction controllers. Apart from the controller validation, dynamic characterization of test benches which is advantageous from other viewpoints shall be presented.

*Chapter 5* presents an adaptive filter based solution to the vibration reduction problem. The approach uses an adaptive filter realization but without requiring sensing of a reference signal. From the algorithmic perspective, two different realizations have been presented to select the one that offers the best performance with the least computational complexity.

A (robust) output feedback control approach is proposed in *Chapter 6*. The robustness is against the uncertainties of the model used for controller synthesis. An advantage of this approach is that the controller developed can be applied to variants of powertrains such as with an ICE with reduced inertia or a clutch with a stiffer coupling characteristic. The only prerequisite being, the variations are covered by the uncertainty in the parameters. In addition, a method to realize the desired compensation torque amplitude with the robust controller is presented.

A harmonically tuned controller to reduce the torsional oscillations is developed in *Chapter 7*. The controller rejects the oscillations using an output regulation based disturbance rejection approach. It uses the estimation methods developed, to compute the harmonic content to suppress them using feedback control.

Using the developed identification and filtering techniques, the estimation of the oscillatory torque transferred from the ICE to the ETM can be computed. This estimated torque can be split into its (non-periodic) mean value and harmonics. Using feedback of this harmonic shaft torque a reduction in vibration can be achieved. However, delays in the feedback loop lead to stability problems. The approach presented in *Chapter 8* introduces an additional delay to realize torsional vibration reduction using oscillatory shaft torque feedback.

A summary of the main findings and conclusions of the work is presented in *Chapter 9*. Further, an overview of the outstanding issues and recommendations for future research are given.

# 2 Active Torsional Vibration Reduction

This chapter presents the torsional vibration problem of automotive powertrains with rightsized/downsized, downspeeded engines. It serves as an introduction to the subsequent chapters focusing on the synthesis of active vibration attenuation controllers for the problem.

## 2.1 Powertrain-induced vehicle vibrations

Vibra-acoustic problems in vehicles can be classified into two major classes [23].

- Internal or vehicle-induced vibrations
- External vibrations which result from external sources such as road unevenness

One feature of the internal or vehicle-induced vibrations is its deterministic nature, while external vibrations are mostly stochastic. This characteristic of the vehicle-induced vibrations motivates the development of methods to reduce such vibrations and their effects. The main subsystems which influence the vibra-acoustic characterization of the vehicle from vehicle-induced phenomena are suspension, chassis and powertrain [23]. This work focuses on vehicle vibrations generated by powertrain components, specifically the torsional oscillations induced by the ICE. In case of a vehicle, with ICE being part of its powertrain, the vibra-acoustic characterization is mainly defined by the engine [16], [23]. Besides torsional oscillations, powertrains also exhibit axial and bending vibrations, which are usually reduced by constructive measures such as modification of journal bearing and thrust bearing with reference to a timing-drive mechanism [24].

Different driving situations shift the operation of the components of the automotive powertrain to specific operating regimes leading to different vibration phenomena. The result of such vibration phenomena can range from mild discomfort to critical failures and durability issues. The major sources of vibration of a powertrain with an internal combustion engine are enlisted in Table 2.1. The table presents mechanisms along with their effects that can lead to torsional vibrations besides the ICE [16].

- *Imbalance excitation of the elements excite the first order*: Imbalance excitation of an out of balance propeller shaft leads to bending oscillations around its centerline. These bending oscillations are synchronous with the shaft rotation speed and can potentially lead to resonance. Depending on the

**Table 2.1:** Components and sources of vibration excitation in an automotive powertrain [25]

| Components | Sources of vibration |
|---|---|
| Engine | Dynamic torque, Ignition, Irregularities in Ignition |
| Clutch | Chatter |
| Torsion damper | Periodic change in damping characteristic |
| Transmission | Gear meshing, Gear pitch error, Torque spikes during shifts |
| Crankshafts | Bending angle |
| Tires | Road irregularities |
| Rotary components | Rotational imbalance |

stiffness of the bearing supports these oscillations are transferred to the vehicle.

- *Excitation by Cardan joints excite the second order*: In case of a Cardan shaft with the non-zero joint angle, there are two torque fluctuations for every revolution. The amplitude of the torsional oscillations depends on the bending angle. At certain vehicle speeds, these torque fluctuations can lead to the resonance of the drivetrain.
- *Friction coefficient fluctuations*: Friction coefficient variation in friction based power transfer can excite torsional oscillations. Among such effects, self-excited oscillations with a negative friction coefficient and friction-excited flutter through non-conservative coupling have attracted much attention [26].
- *Excitation of the second order due to pitch errors of the gears*: Excitation of the torsional modes can be also through gear meshing and tooth pitch errors [27].

In addition, external sources such as road surface unevenness and wheel slip variations as a result of friction coefficient change can also excite the powertrain [26]. The undesirable effects due to torsional vibrations are knocking of components within play range (transmission rattling and clonk), transfer of excitation energy to the body through supports (load change clonk or whining) and coupling with bending as well as translation vibrations [16]. This work emphasizes the effects of the torsional vibrations due to the main excitation source, which is the ICE with its torque pulsations. In specific, the emphasis is on the vibra-acoustic problems

**Table 2.2:** Classification of drivetrain problems along with the corresponding driving situation based on [28]

| Drivetrain problem | Problem Class | Driving situation |
|---|---|---|
| Gear rattle | Acoustic | Idle, Drive, Coast, Engine stop, Launch |
| Body boom | Acoustic | Drive, Coast |
| Clatter | Acoustic | Engine stop |
| Judder/Chatter | Driveability | Launch |
| Surging | Driveability | Tip-in, Back-out, Launch |

resulting from the chemical-thermal-mechanical energy conversion of ICE as well as power transfer to the wheels and not that resulting from its auxiliaries.

### Engine-induced torsional vibration

This section presents the engine-induced torsional vibration of the drivetrain. The term drivetrain refers to all the powertrain components excluding the ICE. Its usage is justified as the torsional vibration of the powertrain-induced by the ICE is studied. The important drivetrain problems can be classified into three categories namely acoustic, driveability and durability problems [28]. Durability problems lead to deterioration of the component strength and mainly occurs during sub-idle (resonance speed) drive and engine start. This classification of the acoustic and driveability problem along with the relevant driving situations is listed in Table 2.2.

Surging is a low frequency (2-10 Hz) vibration phenomena as a result of driver triggered load change events [29]. It becomes perceptible through the resulting longitudinal vehicle oscillations. Chatter is defined generically as the vibrations arising in the slip phase of the clutch due to periodic torque change [30]. It can be either triggered due to material properties, in this case, the use of ceramic clutches could be a solution [31]. In the case of forced judder, the resulting torque fluctuations can be reduced using slip control discussed in Section 2.2.

Driver (or) driving profile-induced torsional oscillations such as surging due to step changes or transients in pedal value shall not be studied. Besides, torsional vibrations of powertrain due to driver triggered events such launch and gear shift are not the focus of this work. Among the vibration phenomena, gear rattle and driveline boom are mainly influenced by the torque pulsations of the ICE and the associated rotational irregularity and shall be discussed.

### Gear rattle and clatter

Rattle and clatter result from the vibrations of idler gears or gear wheels which are not involved in the power flow. These idler gear wheels oscillate within their functional clearances. These oscillations result in the change of contact surfaces and contact loss due to the backlash in the gear toothing. The difference between rattle and clatter triggered by the same source namely rotational irregularities is the driving state [26].

Clatter refers to the noise when the transmission is in neutral whereas rattling refers to the noise under driving and coasting situations. If the amplitude of rotational irregularities is high, not actuated idler gears lift and oscillate within the tooth backlash. The amplitude of oscillations depends on the inertia of the idler gear, drag torque and excitation from the rotational irregularities. Likewise, synchronizer rings and sliding shift sleeves can also exhibit rattle. In this case, the impacts on contacting the idler gears are the source of excitation [21]. Passive measures on the level of transmission to reduce rattle involves the reduction of gear play and reduction of axial tolerances as well as the use of wedge gears [16]. This work deals with methods to reduce the excitation of rattle by reducing the rotational irregularity which is the source of excitation.

### Driveline boom

As the powertrain is mounted on the vehicle, its vibrations also excite the vehicle body. Driveline boom is a result of the excitation of the driveline resonances by the dominant orders of the ICE. Besides the torsional oscillations that excite the resonances, the mounting of the powertrain plays an important role.

The motor-transmission block is usually tuned to be supercritical over the engine operation region. The transmission path of torsional oscillations to the differential is supported by the torque transferred through the differential housing and mounts on the chassis. In case of powertrains with the DMF, the eigenfrequencies in the range 70-100 Hz lead to higher amplitude oscillations at the differential. This vibration mode, when excited by the torsional oscillations, is termed as differential boom [26]. These vibration phenomena are pronounced in case of the rear wheel driven vehicles [32].

Reduction of rotational irregularity is necessary irrespective of the transmission type. To increase efficiency, future automatic transmissions engage the lock-up clutch at speeds around 800 rpm increasing the demand for isolation of torsional

oscillations. Dual-clutch transmissions have reduced tolerance to rotational irregularity as part of the transmission is not involved in the power flow, hence subjected to rattling noises [33]. Hence subsequently the torque pulsations which is the main source of torsional oscillations or the rotational regularities shall be presented.

### ICE torque pulsations

The main source of excitation of the flexible powertrain is the torque pulsations of the ICE. These torque pulsations are a result of the energy conversion process, gas exchange process and inertial torque. The magnitude of the ICE torque pulsations is influenced by the number of cylinders, firing order and interval as well as combustion stability and cycle-to-cycle variability in mean effective pressures in each cylinder [34]. Misfire or combustion instability additionally excite the torsional system, such effects shall not be the focus during the controller development for active vibration reduction.

The dynamic torque $T_{\text{dyn}}$ from the ICE can be expressed as the sum of torque due to pressure variation in the cylinder resulting from the energy conversion process $T_{\text{gas}}$, torque due to acceleration forces working on the oscillating piston mass $T_{\text{inertia}}$ and friction torques well as parasitic torque due to accessories denoted by $T_{\text{friction}}$ in equation (2.1).

$$T_{\text{dyn}} = T_{\text{gas}} + T_{\text{inertia}} + T_{\text{friction}} \tag{2.1}$$

$$T_{\text{trans}} = m_{\text{trans}} r^2 \omega^2 (\cos\phi + (\frac{r}{l})\cos(2\phi)) \tag{2.2}$$

$$T_{\text{gas}} = rF(\sin\phi + \frac{\lambda\sin(2\phi)}{2\sqrt{1-\lambda^2\sin^2(\phi)}}), \lambda = \frac{r}{l} \tag{2.3}$$

The inertial effect of the moving masses can be split into rotating and translating masses. The effective rotating mass includes the crankshaft and portion of the mass of the connecting rod. The forces due to these rotating masses rotate with a speed synchronous to the engine speed. The effect of the rotating masses can be counteracted by counterbalance weights [34]. The inertial torque due to the translating masses $m_{\text{trans}}$ of the engine such as the piston along with part of the connecting rod for a stationary speed can be expressed as in equation (2.2) [29]. The quantity $\omega$ stands for the engine speed, $r$ and $l$ denote the radius of the crankshaft and length of the connecting rod respectively. Friction torque is dependant on the lubricant condition and the temperature. Methods to compute the friction torque by measurements operating the engine at stationary speeds are discussed in [35].

**Table 2.3:** Critical orders of the combustion engine [16]

| Engine | critical orders |
|---|---|
| 3-cylinder in-line engine | 1.5 , 3, 4.5, ... |
| 4-cylinder in-line engine | 2, 4, 6, ... |
| 6-cylinder in-line engine | 3, 6, 9, ... |
| 8-cylinder V-90 engine | 4, 8, 12, ... |
| 12-cylinder V-90 engine | 3, 6, 9, ... |
| 12-cylinder V-60 engine | 6, 9, ... |

The gas forces acting on the piston (denoted by $F$) resulting from the combustion process and the resulting torque at the crankshaft is given by equation (2.3) as in [26]. The effective value of the gas torque depends on the pressure in the combustion chamber. The increasing values of peak pressure in the combustion chamber of modern combustion engines lead to higher torque pulsations. The resulting dynamic ICE torque $T_{\text{dyn}}$ at the crankshaft is a resultant of the individual cylinder torques as in equation (2.1) depending on the cylinder configuration and ignition order.

From the equation (2.3), the inertial torque is proportional to the square of the engine speed and is independent of the mean engine torque. Whereas, the gas torque depends on the cylinder pressure which is a function of the commanded mean torque. As the resultant torque is the sum of the torque components, the inertial torque dominates in higher engine speeds. The higher value of gas torque which is the main reason for high torque pulsations is dominant at low engine speeds and high torque. In addition, to the higher torque amplitude, the lower frequency of the torque pulsations contributes to passenger discomfort [5].

The frequency of the torque pulsations depend on the engine ignition frequency and hence a direct function of the operational speed and engine configuration [29], [16]. In the case of a 4-stroke 4-cylinder engine, the dominant frequency is the second harmonic of the engine speed. Table 2.3 gives an overview of dominant harmonic (in multiples of engine speed) for common engine configurations.

Figure 2.1 presents the dynamic torque from the simulation models for 2, 3 and 4 cylinder inline engines operating at a mean speed of 1200 rpm. The top plot of the figure presents the time-domain representation, whereas the bottom plot display frequency domain representation. The model of the ICE was done

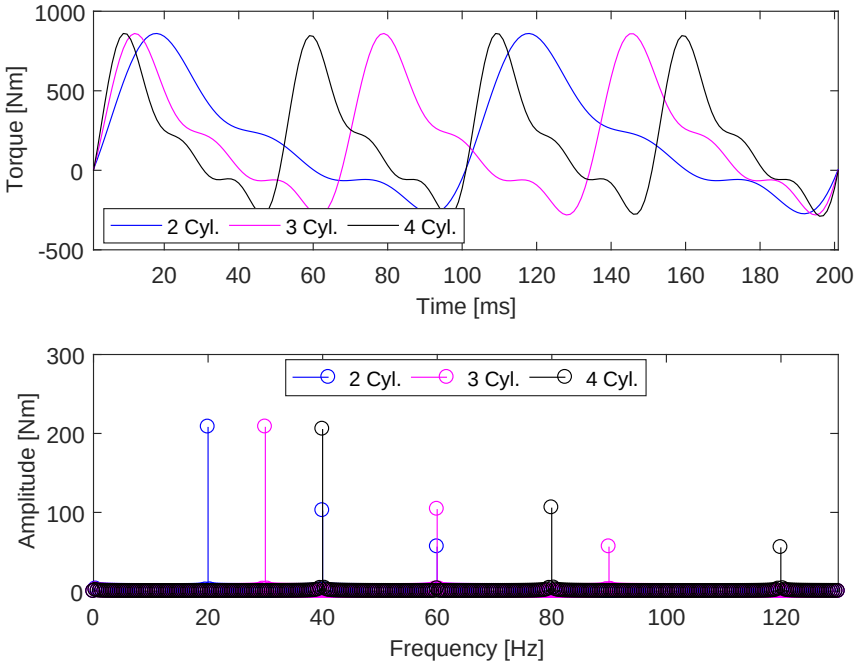


**Figure 2.1:** Time domain and frequency domain representations of torque generated by 2,3 and 4-cylinder engines at a mean speed of 1200 rpm

in [36] and was parameterized from test bench measurements. The ICE model along with the powertrain model is used for potential analysis and validation of the developed controllers in the simulation. The set value torque for the engine model was parameterized for the depiction in the figure in such a way that, the different torque harmonics have the same amplitude. This naturally results in the same peak amplitude of the torque for all the engine configurations which can be seen in the top plot. From the bottom plot, the amplitude of the torque at the harmonic frequencies can be seen. The lesser the number of cylinders in the engine lower is the frequency of excitation due to the dominant harmonic component. In addition, the overlapping of the frequencies of the engine configurations is also visible. For example, the dominant harmonic of the 4-cylinder engine coincides with the second harmonic (non-dominant) of the 2-cylinder engine. This shift of the frequency spectrum was the motivation for the development of the directE compensation strategy [19].

**Table 2.4:** Component and sources of vibration excitation in an automotive powertrain based on [37]

| **Feature** | **Damping** | **Isolation** | **Compensation** |
|---|---|---|---|
| Effect | Damping around resonant frequency | Reduction of the amplitude above resonant frequency | Compensation of either the excitation or the resonance |
| Passive realization | Elastomer elements or fluid damping | Introduction of flexibility | Vibration neutralizer / absorber |
| Active realization | Damping around resonant frequency | Reduction of the amplitude above resonant frequency | Compensation of either the excitation or the resonance |

## 2.2 Passive and Semi-active measures for Torsional Vibration Reduction

To develop active vibration reduction methods to replace or supplement the passive vibration reduction/isolation mechanisms, their working principle has to be studied. This section presents a review of generic vibration reduction methods followed by passive measures for torsional vibration reduction in automotive powertrains. Different approaches have been investigated for vibration reduction in the case of flexible structures [37]. Besides the reduction of vibration excitation and detuning the structure, three different methods for vibration reduction exist irre-

spective of their realization using passive or active measures. An overview of these methods is given in Table 2.4.

The different passive measures for torsional vibration reduction shall be presented in the chronological order of their development as shown in Figure 1.3. The single mass flywheel is one of the primitive methods to reduce rotational irregularity. By increasing the inertia the speed oscillations of the engine can be reduced. The flywheel stores energy during the power stroke of the engine and uses it during the negative torque phase to push the exhaust gas out of the combustion engine, compress the fresh air-fuel mixture prior to combustion and overcome the inherent friction and other parasitic action in the engine [34]. The larger the flywheel the lesser is the engine speed oscillations. A demerit of the approach is that the additional inertia has a negative effect on the dynamic performance and fuel consumption. Further, the higher inertia on the engine side increases wear on the synchromesh units due to the higher inertia that has to be synchronized [38]. In addition, increased inertia also increases the bending load of the flywheel requiring modifications of the crankshaft bearing [39], [40]. These disadvantages motivate the use of alternative methods for the reduction of torsional vibration which shall be discussed in the subsequent section.

#### Clutch discs with torsional dampers

Clutch disc with a torsional damper is the simplest and cost-effective solution for torsional vibration reduction with relatively low packaging demand. The depiction of such a clutch disc with torsional dampers is presented in Figure 2.2a. In addition, they are equipped with centering cone that compensates the possible axis offset between the engine and the transmission and axial spring elements to improve comfort [38]. One of the disadvantages of using dampers against torsional oscillations in the subcritical region is the reduction of the effect of isolation in the supercritical region.

The main challenge in its development is to ensure torsional damper characteristics with defined spring stiffness and hysteresis for the realization of damping effect for all operating conditions. This conflicting demand is a result of spring characteristics, which can be compensated by using springs with variable stiffness characteristics. Figure 2.2b depicts the damper characteristic curve with the torsion angle relative to the transmitted torque. The stiffness characteristics of the torsional damper consist of a soft first stage with additional stiffer stages. This ensures higher isolation when traversing the resonance during start/stop events and low loads. The stiffer stage provides sufficient isolation during high loads.

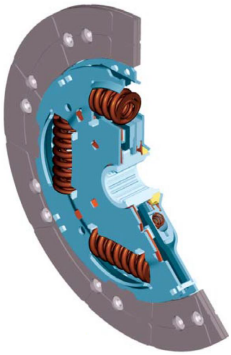

**(a)** Torsional vibration damper

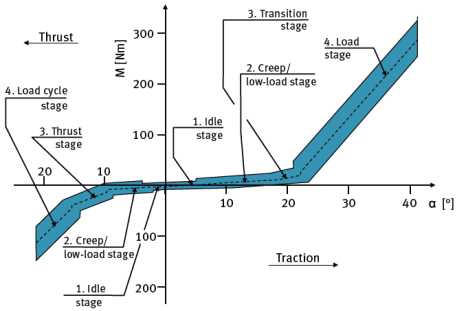


**(b)** Characteristics of the clutch disc with torsional damper

**Figure 2.2:** Clutch discs with torsional vibration dampers [38]

With the further development of clutch disc with dampers, Valeo offers 4KKIT, a single mass flywheel-based aftermarket solution for selected vehicles with factory-mounted DMF [41]. The 4KKIT comprises of a flywheel and modified clutch disc with long-travel dampers as well as a pre-damping technology to achieve isolation similar to that of DMF.

### Dual mass flywheel (DMF)

DMF consists of a primary and secondary inertia coupled by lubricated bow spring set. The key advantage of the DMF when compared to the clutch discs with torsional dampers is the shift of the resonance speed below the idle speed of the engine to ensure supercritical operation in the driving. Due to the elimination of the gearbox rattling and reduction of body boom, driving at low engine speeds was possible with the DMF leading to consumption advantages [28]. Besides the value of the primary and secondary inertia, the spring element determines the filtering characteristics of torsional oscillations.

The DMF spring elements are realized as a bow/arc spring by LuK and set of compression springs [44], with compression spring guide elements made of polyamide plastics [43]. One advantage of a small spring element solution is its lesser sensitivity to centrifugal loads. Additional springs can be added to the flange to provide additional damping capacity without increasing packaging demand. DMF from LuK using bow springs uses nested springs of the same length to achieve linear characteristics. Bi-linear stiffness is achieved using springs of differ-

**(a)** DMF with arc spring [42]

**(b)** DMF with linear compression springs [43]

**Figure 2.3:** Realization variants of DMF [42], [43]

ent lengths with the outer spring being active during idling and low load conditions [17]. Similar multi-stage torsional characteristic curves are achieved by ZF by combining different quantities of compression springs with different rigidities [43]. As in the case of torsional springs, the soft stage provides isolation during start/stop, whereas the stiffer stages ensure overload protection and decoupling during normal driving. The DMF products by Sachs initially featured guiding planets to avoid LuK patents, which were removed after the expiry of the respective patents [17].

From the perspective of bending loads, the DMF does not introduce any disadvantage. The mass of the primary flywheel is reduced which is favorable for bending load at the crankshaft. The secondary flywheel supported by the roller bearings does not generate high reaction forces as in case of the single flywheel with the combined mass of the primary and secondary flywheel [39]. The continuous development of DMF has led to the elimination of its demerits, some of which are enlisted here. Since 1990, one of the main focuses of DMF development was to improve isolation during driving situations [45]. In order to compensate for higher torque pulsations of the modern ICE, the spring rate would have to be made stiffer. The stiff bow spring leads to insufficient isolation during driving. With the introduction of inner dampers with compression springs, the isolation during the driving situation can be improved. The inner dampers are active in the start-up phase, supported by the stiffer outer arc springs. The compression springs are in serial connection, enclosed in a ring to avoid friction due to centrifugal forces [22].

In case of an arc spring, the centrifugal forces push the spring outside and lead to increased friction between the spring and the shell. Moving the spring to-

wards the center reduces the centrifugal forces quadratically, which in turn also reduces the friction. This leads to conflicting goals due to the associated reduction in spring capacity and hence not suitable for engines with higher torque. Another approach would be to reduce friction, without affecting friction during the engine start-up. This was realized by integration of slide shoes in the arc spring, achieving noticeable vibration reduction in the tip-in/back-out cycles [22]. This improvement is of specific interest with the introduction of 48 V belt driven hybrid systems, which increase the load during coast and also alternating load cycles during recuperation.

#### Centrifugal pendulum-type absorbers (CPA)

Despite the continuous innovations of the dual mass flywheel, it was not able to meet the isolation requirements due to the increased torque pulsations of the modern combustion engines with a higher power-to-volume ratio [22]. One solution to the problem was to introduce pendulum-type absorbers. In contrast to the secondary mass of DMF, the pendulum masses are not in the torque transmission path, thereby functioning as a tuned mass absorber. The functional principle of the CPA is expressed by the equations (2.4) and (2.5) [46]. The quantity $\Omega$ denotes the rotational speed and $p$ stands for the harmonic order that shall be attenuated. The dimensions $L$ and $l$ stand for the distance from the center of the DMF with CPA to the center of the arc traced by the pendulum and radius of the arc traversed by the pendulum mass respectively. This is then the resonance tuning condition for the simple point-mass CPA when the pendulum oscillation angles are small and the rotor is rotating at a steady speed with small fluctuations. As it can be seen in (2.5) the anti-resonant frequency is proportional to the rotational speed, the realization of good isolation over the operating speed range is possible theoretically.

$$p = \sqrt{\frac{L}{l}} \tag{2.4}$$

$$f_{cpa} = \frac{\Omega}{2\pi} p \tag{2.5}$$

CPA is a relatively recent development with its introduction in 2006 and start of production in 2008. Factors such as modular design and good isolation have led to use of centrifugal pendulum-type absorbers not only in DMF but also in clutch discs and torque converters [13]. Different locations for integration of the pendulum masses have been investigated. Positioning the pendulum masses within the DMF is favorable as the grease of the DMF serves as a lubricant also for the

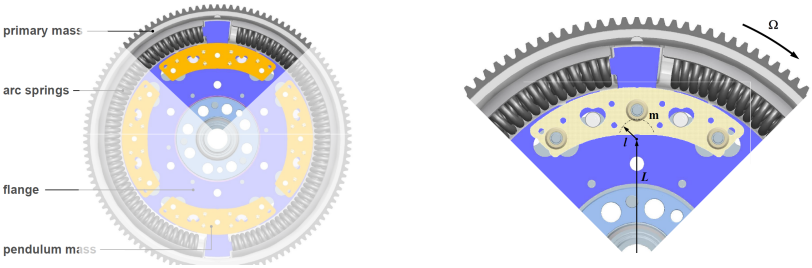


**(a)** DMF with CPA on secondary mass

**(b)** Enlarged view of CPA

**Figure 2.4:** Dual Mass Flywheel with centrifugal pendulum-type absorbers [17]

masses. Integration of the pendulum masses on the primary flywheel requires masses of about 3-5 kg. Although an integration on the secondary flywheel reduces the masses to about 1 kg [22]. However, integration of the masses on the secondary flywheel does not reduce rotational irregularities of the engine accessories. In case of trucks, the CPA is arranged on the primary flywheel ensuring, reduced oscillations at the gearbox input and the belt [13].

The integration of CPA and hence the additional masses in the powertrain is not always disadvantageous from the perspective of the dynamics. In case of a wet clutch DCT, the inertia of the clutch is low compared to that of the dry clutch system. In order to realize a DMF function in such a configuration, additional mass must be added. This additional mass can be added in the form of pendulum absorbers without additional packaging space and demerits for the vehicle dynamics.

The isolation effect due to the pendulum depends on the mass and the vibration angle. The integration of the CPA is done by bifilar (two-thread) mounting with rollers to reduce the mass required for achieving the required harmonic order reduction. This advantage of the bifilar mount has been derived theoretically in [47]. At low speeds above the idling speed, the CPA requires large vibration angle (large path curvature) to store the associated vibration energy. In addition, irrespective of the engine speed, the arc-length traversed by the pendulum mass has to increase for reducing dominant harmonics. Assuming a constant pendulum vibration angle, it can be seen from equation (2.4) that the smaller the harmonic order the larger is the path curvature of the pendulum.

The second generation pendulum by LuK [13] exhibits larger vibration angles than the first generation pendulum, making better use of the available pendulum

mass to absorb the vibration energy. This is achieved by guiding one of the bifilar mount points radially outside and the other radially inside to achieve a trapezoidal oscillation rather than a parallel oscillation as in the case of first generation pendulum. In addition, a stop damper and intermediate plate were implemented in the second generation CPA. This increases the damping capacity while maintaining stopping functionality that reduces noise risk in start-stop cycle [17].

The tuning of the CPA requires close interaction between powertrain construction and damper design [13] for the exploitation of its potential. Based on linear (small angle) models, the tuning rule given by equation (2.5) seems obvious. But in practice, additional instabilities have to be accounted for during the tuning of the CPA with multiple masses. This requires CPA tuning slightly above the main excitation order, termed as positive mistuning or overtuning to ensure a stable and reliable operation. Two types of instabilities due to nonlinear effects have to be considered. When the amplitude of the fluctuating torque reaches a certain level, a jump of the absorber through a saddle-node bifurcation to another solution happens, leading to undesired vibrations. The classic approach to avoid the jump condition is to intentionally mistune the CPA in relation to the applied torque. Positive mistuning pushes the jump condition to higher torque levels at higher absorber amplitudes. However, an increased mistuning would lead to performance degradation, requiring a compromise between performance and operational torque range [48], [49], [50].

The second nonlinear effect is termed bifurcation to non-unison. It is an instability in the case of CPA with multiple absorbers. A unison motion of all the absorbers in the same direction in a synchronous fashion is desired. The instability here occurs with certain absorbers active and others inactive leading to complex interactions between the absorbers. These effects depend on the levels of mistuning and damping of the individual absorbers. Besides positive mistuning, use of cycloidal or epicycloidal path for the pendulum travel can also improve its stability [48], [49], [50]. As can be seen, the tuning of the CPA absorbers is an art in itself, which serves as a motivation to develop methods such as active vibration reduction.

#### Clutch slip control

Slip control of the clutch offers an alternative method to reduce torsional vibrations in powertrains. The basic principle of clutch slip control is to dissipate the oscillatory energy thermally using the slipping of the clutch disc. Such condition of operation of the clutch is known as partial slip [51]. It is characterized by the

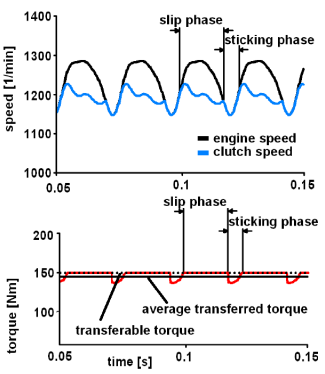


**(a)** Torsional vibration reduction using clutch slip control realizing partial slip

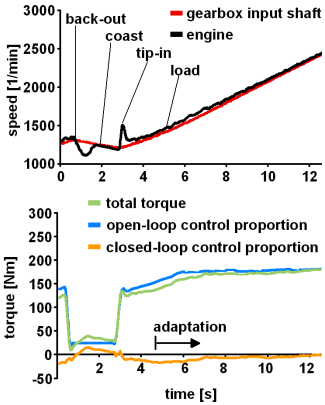


**(b)** Clutch slip control realizing partial slip

**Figure 2.5:** Clutch slip control [51]

alternation of the sticking and slip phases with the combustion engine ignition frequency. The clutch slip control can be integrated with the clutch release system [28], making it attractive for powertrains with the clutch-by-wire system.

In contrast to the CPA, clutch slip control does not require additional packaging space as it uses the existing clutch release system and can be combined with passive solutions such as DMF and torsional damper systems. In the case of an automatic transmission, the lock-up clutch slip control can be employed to reduce torsional oscillations with the availability of cooling [23],[38]. One obvious restriction of the clutch slip control is that it can be employed only for driving situations with a closed clutch. An important disadvantage of the method is the generated thermal losses in the clutch which are proportional to the slip speed. Furthermore, increased wear leads to insufficient vibration reduction, indirectly influencing driver behavior to drive at higher engine speeds. The higher excitation frequencies at such higher speeds with low human sensitivity lead to increased fuel consumption. The achievable reduction in cyclic irregularity depends on the performance of the clutch friction coefficient and bandwidth of the clutch slip controller. A higher bandwidth slip controller in combination with an ideal clutch friction coefficient can achieve a better reduction.

Clutch slip control requires a positive clutch friction coefficient to achieve the required damping effect [30]. The positive friction coefficient introduces a stabilizing effect. If the slip is increased as a result of an increase in engine torque, the

torque transferred by the clutch increases reducing slip. A negative clutch friction coefficient introduces instability due to chatter and requires higher controller dynamics. Chatter can be influenced not only by the clutch and its actuation systems but also by powertrain components. It results in periodic torque fluctuations in a slipping clutch which lead to longitudinal vehicle vibrations.

Figure 2.5a presents the operation of the clutch slip control to reduce rotational irregularities. The clutch actuator is modulated to realize alternating slip and stick phase to reduce the variation of the rotational speed at the gearbox input. The control is achievable without any perceptible impact on vehicle dynamics. This is depicted in Figure 2.5b with different driving situations.

In the case of an automatic transmission with such wet clutches, a slip speed of about 100 rpm leads to effective damping of driveline boom effects [23]. However, the effect of lubricant degeneration over lifetime affects the controllability of the clutch slip and has to be considered [16]. It was reported in [51] that, clutch control with single mass flywheel was able to achieve isolation comparable to DMF. An endurance test resulted in extra clutch wear of 0.2 to 0.4 mm per 100,000 km. Further, it is well-argued that the additional fuel consumption in the test procedure with slip control can be compensated by the better responsiveness of the vehicle compared to that with a DMF.

A comparison of the effect of active vibration reduction with that of a clutch slip controller is presented in [52]. It concludes based on simulation results at full load of the ICE that the combination of clutch slip control and active vibration reduction can achieve the required vibration comfort with better efficiency. It proposes the use of active vibration reduction at low speeds, use of slip control at higher speeds and use of both for moderate engine speeds up to 2000 rpm.

## 2.3 Overview of related studies

Active torsional vibration reduction has been pursued since 1990 [52]. One demerit that deterred introduction in a commercially available (non-research prototype-) vehicle was additional energy required and the questions regarding battery durability. The introduction of Plug-in-Hybrid vehicles with larger battery capacity, reduce the energy consumed for active compensation to less than 2% of the entire capacity [52]. Under such cycling operation for vibration reduction, the cell behavior deterioration is lesser than believed earlier [53]. This has given an impetus to recent research in the field of active torsional vibration reduction also motivated by the problems faced by passive measures.

Approaches discussed in [18], [19] avoid charging, discharging behavior of the battery during vibration reduction. The feedforward control approach in [19] was developed for high voltage battery systems. The methods in [18] use feedback control focusing on belt-driven 48 V systems. The controller approaches discussed in this work are also capable of realizing vibration reduction either in motor or in generator operation.

From the perspective of controller design, the objective of active torsional vibration reduction controller is to suppress multi-tonal disturbances introduced by the ICE. The disturbance source that excites the flexible powertrain is the torque fluctuations from the ICE. The ETM serves as the sources of compensation torque to reduce the torsional oscillations. Depending on the ICE variant (3- or 4-cylinders) the harmonic to be rejected can vary. Frequency of the engine torque disturbances is a factor of the current engine operation speed and the engine configuration. In case of inline 4-stroke engines with $z_{cyl}$ cylinders, the maximum frequency in Hz ($f$) of interest can be computed using equation (2.6) in terms of the engine operating speed ($n$).

$$f = (n \times z_{cyl})/120 \tag{2.6}$$

Different approaches have been investigated for the realization of active vibration reduction. The approach discussed in [54] uses a gain scheduling harmonic controller which estimates the Fourier parameters of the oscillating engine speed to adapt the Fourier coefficients of the command signal to the ETM. The feedback law computes the Fourier parameters of the command signal, which are adapted during transient conditions to ensure convergence. The results of the controller were analyzed in a simulation environment. Harmonic controllers to suppress the main order of torque fluctuations were synthesized using $H_\infty$ performance specifications in [55] using Linear Matrix Inequalities (LMI). The developed controller was tested on a hybrid test bench with mono-cylinder ICE. The approach in [56] applies Hilbert transformation of the speed signals to convert the estimate of torque pulsations acting on the powertrain to constant valued disturbances. Synthesis of the PI controller to reject the constant disturbances is performed using LMI as a static output feedback $H_\infty$ controller. In [57], an active filter with a parameter-dependent state feedback gain using engine speed, as scheduling signal is used to realize vibration damping. The design of the controller is done using mixed $H_2/H_\infty$ synthesis.

In [58], different control techniques for periodic disturbance attenuation such as lead-lag compensator, $H_\infty$, PID and inverse notch filter were investigated to

mitigate torsional oscillations along with the analysis of real-time capability. The notch filter with high frequency lead compensation was shown to have better performance than the other schemes under operation at a constant speed. Linear Parameter Varying (LPV) dynamic-output feedback controller is proposed in [59]. By using the internal model principle [60], a polytopic description is used to synthesize LPV controller using LMI. Experimental validation is performed using a mono-cylinder ICE. Recently model predictive control was also investigated for the active vibration reduction problem [61]. In spite of the higher computational effort, it offers flexibility for integration with the energy management system of hybrid electric vehicles by offering tunable compensation torque limits.

Adaptive control methods have also been applied to solve the problem. Feedforward control in [19] uses pulsed compensation torque from the ETM for torsionally stiff powertrains. The triggering of the compensation pulses is adapted with respect to the ignition signal of the ICE. In [62], Harmonic Activation Neural Network (HANN) was used with the filtered estimate of the engine acceleration to adapt the HANN coefficients. In addition operation point, speed and torque of the engine and the crank angle were used as input signals for the compensation network. Estimation of the ICE torque was used to generate compensation torque without considering the torsionally flexible coupling between the ICE and ETM as in [19]. Combination of feedforward and feedback control to realize disturbance input decoupling in a hybrid vehicle with an integrated starter/alternator (SA) for active vibration reduction is proposed in [63]. An adaptive notch filter based controller using filtered least mean square (FxLMS) algorithm for adaption has been reported in [64]. In [61] a model predictive control approach for the active vibration reduction problem is presented. Further, it was shown that online constraint tuning of compensation torque amplitude offers flexibility for integration with the energy management system of hybrid electric vehicles.

Adaptive notch filter method as presented in [65] was employed in [64] to realize vibration reduction control using a filtered ETM speed signal as the reference signal. The implementation computes the electric current required for the realization of compensation moment and requires models of both the mechanical system and the current controller. Evaluation of the controller was performed only in stationary operation without discussion of transient performance, analyzing the usage of filtered speed as the reference signal. [66] implements a narrow band FxLMS algorithm, using a pulse train generator based on the measured engine speed and discrete-time oscillator to generate the reference signal for feedforward adaptive control.

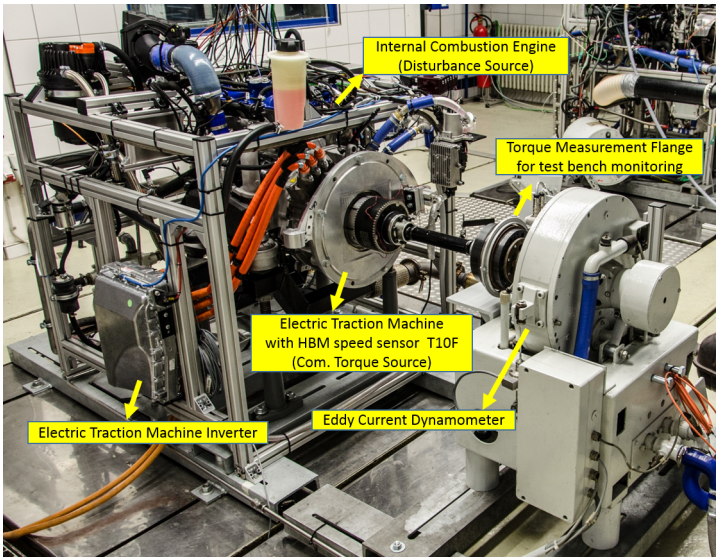


**Figure 2.6:** Test setup used for the experimental validation

## 2.4 Test bench used for Experimental Validation

Due to the complexity of hybridized powertrain systems, synthesis and validation of control algorithms for specific powertrain functionality on the real prototype is time-consuming and involves increased effort. Furthermore, development and validation of the control algorithms of concepts where the corresponding prototype vehicles are not yet realized can be validated on the system level with test setups built up by integration of the individual powertrain components.

Experimental validation of the developed controllers is performed at the test bench depicted in Figure 2.6. The experimental setup was initially developed to closely represent the powertrain dynamics at the test bench. The Unit Under Test (UUT) is the Combustion Engine Assist (CEA) Powerpack unit. The powerpack unit constituted by the ICE and ETM separated by the clutch is coupled to the eddy current dynamometer using a shaft coupling. The ICE and ETM are commanded using set torque values. The speed control of the powerpack unit in the test bench is realized using the eddy current dynamometer. The dynamometer receives torque input based on the speed controller implemented in the real-time system. The real-

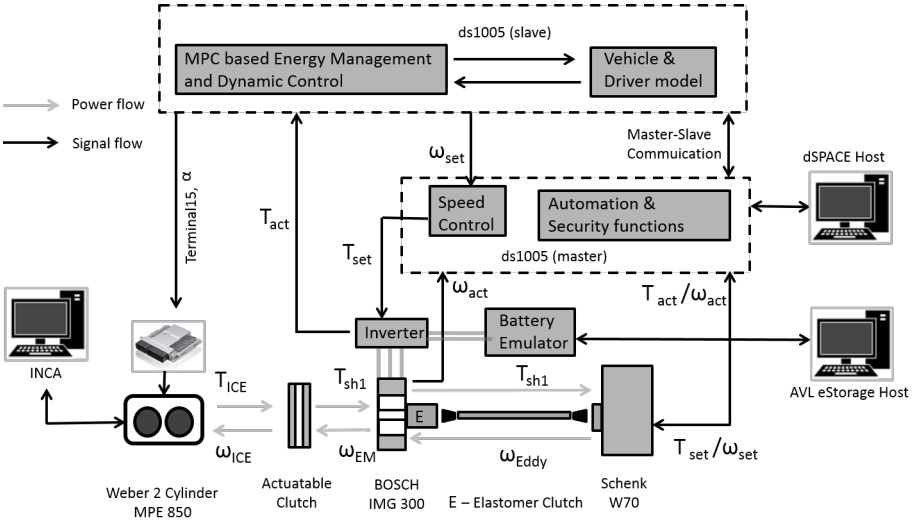


**Figure 2.7:** Control architecture of the Powerpack test setup used for experimental validation

time system used to realize the test bench automation system is implemented using dSPACE ds1005 hardware.

The developed active vibration reduction controllers are executed on this real-time hardware with a sampling frequency of 1 kHz. Shaft torque measurement is performed using HBM torque measurement flange (T10 F/FS) on the connecting shaft on the dynamometer side. Speed measurements at the ICE flywheel, ETM and the dynamometer are realized using optical measurement devices. Experimental validation uses the 2-cylinder engine at powerpack test bench. But the simulation analysis employs a 3-cylinder engine to demonstrate the applicability of the controller to different engine configurations. In order to ensure reproducible ICE behavior at the powerpack test bench, the vibration reduction controller is activated with a warm ICE.

The experimental setup from [19] was developed to a master-slave configuration test setup. The master and the slave threads are executed on separate ds1005 processors on the dSPACE processor board. The dSPACE processor board interfaces to the different IO boards (ds2211 HIL board, ds4002 timing und digital-I/O board and ds3002 incremental encoder-interface board) for data acquisition and

to realize set value commands. The schematic of the control architecture of the powerpack test bench is depicted in Figure 2.7. The size of the components and the distance between them are not to scale. Methods for parametric and non-parametric test bench identification for such test bench configurations have been developed in chapter 4. Control-oriented identification of the CEA powerpack torsional dynamics and the test bench torsional dynamics are discussed in section 8.1.1 and section 5.3.6 as well as 6.3.3.

## 2.5 Energetic aspects of Active Vibration Reduction Controller

### 2.5.1 Harmonic efficiency characterization

As discussed, a whole collection of market-ready and development stage solutions are available for non-active torsional vibration reduction. The term non-active used here refers to both passive mechanisms and semi-active approaches such as slip clutch control. In [19], simulation of a DMF using linear torsional spring characteristics was used to compute the losses involved. These computed losses were compared to the losses in case of active torsional vibration reduction. Such an approach is not pursued in this work for two reasons. Complex powertrain components with impact phenomena such as DMF (and its variants) as well as DMF with CPA require complex models which have to validated with experimental results. Using a non-validated simulation model affects the credibility of the conclusions thereby derived.

The dissipated mechanical power in the case of passive mechanisms, when compared to the electrical energy required for the active method, should consider the source of the electrical energy. Contrary to the usual assumption, the mechanical energy, in this case, is more valuable than the electrical energy as it can be directly used for traction. Whereas, the electrical energy would have to be converted to mechanical energy using loss involving conversion using the electric machine and inverter to aid traction. In simpler terms, this would be analogous to compare $CO_2$ emissions from conventional powertrain with that of claimed zero $CO_2$ emissions of an electric vehicle. With the advances in the field of energy management using model predictive control and online optimization-based approaches, an equivalence between the onboard energy source has to be performed considering the past and future driving scenarios.

In order to realize active torsional vibration reduction, the ETM has to generate an oscillating torque to counteract the torque oscillations introduced by the ICE in the flexible powertrain. The energy required for the active damping is supplied

from the onboard battery. The required power for vibration reduction has been a reason for the active vibration reduction system not being widely accepted. An analysis of the power required to perform the active vibration compensation with and without a mean value torque of the ETM was performed in [19]. In practice, this would occur when the hybrid vehicle energy management commands a mean value torque in addition to the oscillatory torque demand from the active vibration reduction functionality. The conclusion of the analysis was that for a pulsed compensation torque operation, the power required for active torsional vibration compensation is less with motoring (positive) mean value torque than zero mean value torque for the same oscillations.

### Core idea

This work proposes a new method to arrive at a metric to quantify the active torsional vibration reduction from the perspective of energy efficiency. The system boundary used for the definition of the metric involves the electric traction machine and the inverter used to realize the desired compensation torque. As the metric is applied for experimental investigations at the powerpack test bench, the battery is not part of the efficiency characterization. The inclusion of the battery in the metric would require the battery along with its power management system to be set up. In addition, with the current development dynamics in the field of energy storage systems, such a characterization would have to be repeated frequently to keep pace with the new developments. However, if required, the influence of energy storage systems can be included.

The utility of the proposed efficiency characterization is two-fold, from an analysis perspective and viewpoint of synthesis/development of the ETM.

- On the basis of the harmonic characterization, inputs for the electric machine design can be formulated to design a machine that is efficient for the reduction of certain harmonics. This design step can be adapted based on the combustion engine which shall be used in tandem with the electric machine. Using such an approach, processes can be formulated that aid a co-design of the combustion engine and the electric machine in close coordination to exploit the potential of active vibration reduction systems from the comfort and energetic viewpoints.
- The harmonic efficiency characterization serves to study the operating regions of the ETM which have an energetic advantage over other regions for the harmonic to be suppressed. This understanding can be used to perform

activation of the vibration reduction along with the hybrid energy management functionality. Such an approach, aids calibration of both the active vibration reduction functionality and hybrid energy management.

### Measurement procedure

The harmonic efficiency characterization is based on a specific measurement procedure at the experimental setup. The setup discussed in Section 2.4 is operated with an open clutch, thereby decoupling the ICE from the test setup. In such a condition, the ETM can be operated with the eddy current dynamometer. The ETM is operated in torque control mode and the dynamometer receives a set speed command signal.

One restriction of the used test setup from the perspective of harmonic efficiency characterization is that the dynamometer can only brake the ETM to a certain speed. This requires the ETM to generate a positive torque so that the setpoint speed can be regulated using the dynamometer. Hence, the characterization is limited to ETM with positive torque (ETM motor operation). It has to be mentioned that, the restriction is specific to the test setup. In the case of an active dynamometer (with positive and negative torque generation), the procedure can be performed around zero and negative torque (ETM generator operation).

From the test bench mechanics perspective, the setup shall be operated in supercritical operation. The harmonics for which the characterizations are desired shall be above the eigenfrequency of the setup with a safety margin of ($\sqrt{2}$). This supercritical operation ensures that the test setup is operated in its isolation region. This is a pre-requisite as the constant speed operation of the dynamometer is possible even with the speed oscillations from the ETM which shall be commanded by sinusoidal signals. During the process, depending on the amplitude of ETM speed oscillations (which in turn depends on the amplitude of the superimposed sinusoidal signal) energy shall be stored and retrieved in the torsional shaft.

The measurement procedure involves the measurement of the input and output power operating the ETM at different operating points. The operating points are defined by the mean (constant) values of torque and speed. Based on the dominant harmonic to be canceled, efficiency characterization around different harmonics can be of interest. In this work, only the first and second harmonic shall be considered. As the method of efficiency characterization is generic it can be employed also for 1.5 th or other odd-numbered harmonics.

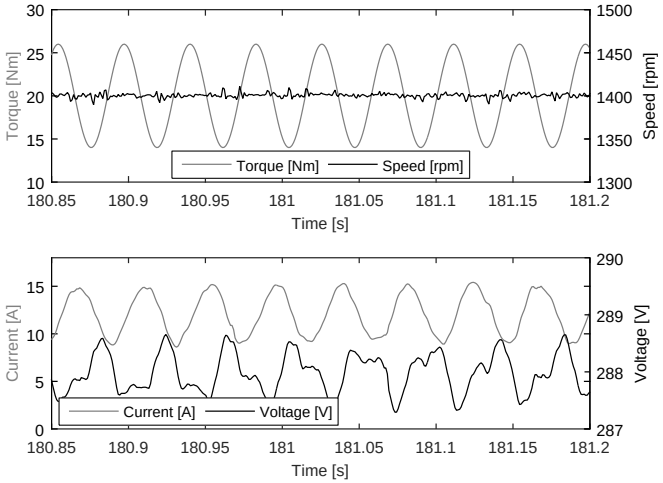


**Figure 2.8:** Measured input and output signals for computation of efficiency at first harmonic operation, $\eta_{1h}$ cf. Table 2.5

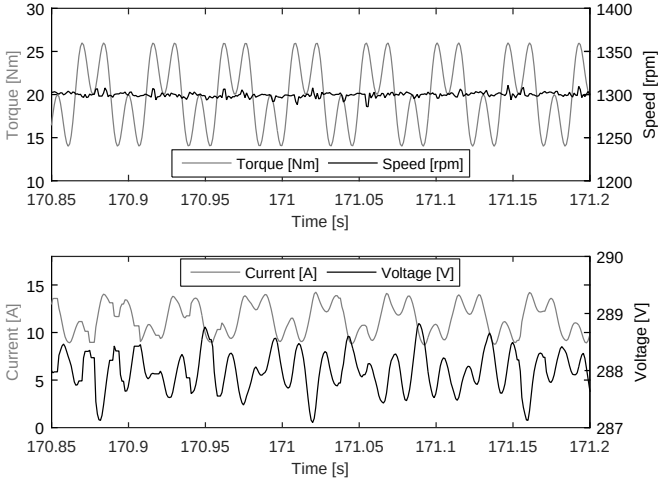


**Figure 2.9:** Measured input and output signals for computation of efficiency at second harmonic operation, $\eta_{2h}$ cf. Table 2.5

**Table 2.5:** Overview of the experimental procedure for the harmonic efficiency characterization of the ETM and inverter

| Variant | Torque set point (ETM) | Speed set point (Dynamometer) |
|---|---|---|
| Efficiency at mean value operation ($\eta_{DC}$) | constant torque | constant speed |
| Efficiency at first harmonic operation ($\eta_{1h}$) | constant torque with first harmonic oscillation | constant speed |
| Efficiency at second harmonic operation ($\eta_{2h}$) | constant torque with second harmonic oscillation | constant speed |
| Efficiency at first and second harmonic operation ($\eta_{1+2h}$) | constant torque with first and second harmonic oscillation | constant speed |

In case of the characterization for the first harmonic, the torque setpoint of the ETM shall be driven by a sinusoidal signal with the corresponding frequency and suitable amplitude. The setpoint of the dynamometer is kept constant during the procedure. Figure 2.8 presents measurements at the test bench during such operation. The torque setpoint is varied around the mean value of 20 Nm with a frequency of 23.3 Hz, whereas the speed setpoint is kept constant at 1400 rpm. The battery current and battery terminal voltage is measured which are also shown in the figure. The current varies with the same frequency as that of the demanded torque, which again is a verification that the superimposed sinusoidal torque is being generated. This verification is required as the actual torque generated from the ETM is transmitted using CAN bus with a frequency of 100 Hz. The battery voltage is to be maintained constant but shows negligible variations.

Similar measurements were performed using ETM torque excitations with the first and second harmonic at a mean operating speed of 1300 rpm. The results are shown in Figure 2.9. The torque setpoint has a mean value of 20 Nm and superimposed sinusoidal oscillations of 21.6 Hz and 43.3 Hz. As in the case of Figure 2.8,

the battery current also shows oscillations similar to that of the commanded torque value. The battery voltage also depicts minimal variations. These fluctuations can be reduced if required by proper calibration of the inverter in the battery simulator, which is beyond the scope of this work. An overview of the experimental procedure used for the harmonic efficiency characterization is shown in Table 2.5. The table includes the discussed first and second harmonic characterization along with the characterization with the mean value and the second harmonic.

**Post-processing / Characterization**

In contrast to the time-domain based averaging procedure employed for computation of the efficiency, a frequency-domain based approach is adopted. From the measurement inputs (battery terminal voltage, battery current) and outputs (shaft torque using HBM torque flange and speed signal), the input and output power is determined. These input and output power are transformed to frequency domain using FFT. This transformation is valid as the measurement procedure involves only stationary (periodic) operation. Care should be taken to use complete periods of the signals or chose appropriate windowing techniques. After the frequency domain transformation, using the amplitudes of the input and output power the corresponding efficiency can be computed. These computations can be performed for the respective harmonics and also for the mean value operation (or) DC value. The term DC is from electrical engineering jargon referring to non-alternating value. If nonlinearities are present, then they would manifest themselves with appropriate amplitude and lower or higher frequencies than the one used for the excitations. It was not the case in the measurements obtained from the experimental setup.

The delays involved in the processing of the signals do not create a problem, as only the amplitude of the power is used. The delays would cause variation in the phase of the computed frequency-domain input and output power but not in their amplitudes. The resulting maps of the harmonic efficiency characterization are presented in Figure 2.10. The measurement is performed at around mean torque set points of 10, 20, 30, 40 and 50 Nm with a corresponding sinusoidal amplitude of 5 Nm. The speed set points were chosen to be 1000-2000 rpm with a spacing of 100 rpm between them. The form of the computed map is the same for the DC and the higher harmonics. However, quantitatively the efficiency in case of the first and second harmonic has one order of magnitude lesser than the mean value efficiency. Further, a certain kind of superposition effect can be observed. When performing the characterization with the first and second harmonic, the efficiency further degraded by one order of magnitude in compared to the case with only the first or the second harmonic. The harmonic efficiency computation was repeated

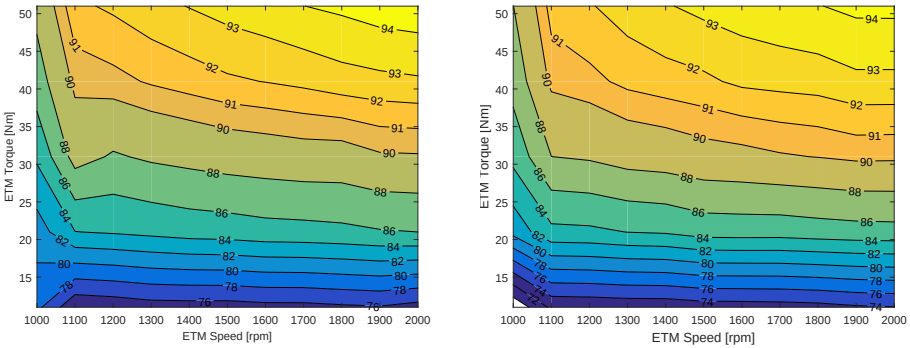


**(a)** $\eta_{DC}$ **(b)** $\eta_{1h}$

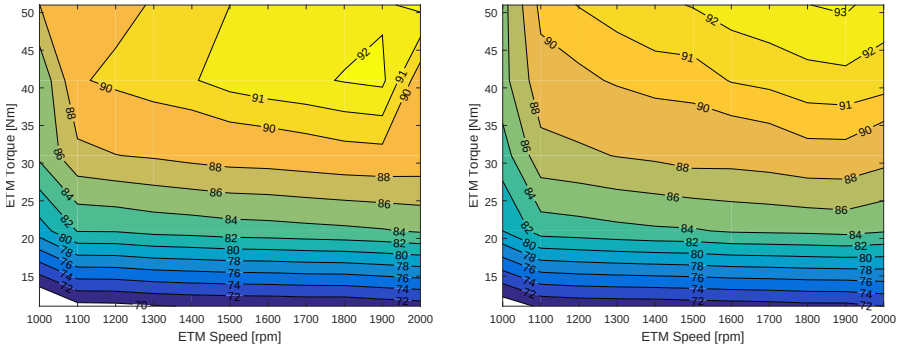


**(c)** $\eta_{2h}$ **(d)** $\eta_{1+2h}$

**Figure 2.10:** Measured efficiency characterizations at the experimental test setup

to ensure statistical guarantees. The results showed a similar trend with different harmonics.

The main conclusion from the harmonic efficiency characterization is that for the employed ETM and inverter combination for operation around certain mean value torque and speeds with motoring operation there is no significant power loss due to the harmonic energy conversion. In the previous statement, the harmonic efficiency is compared to that of mean efficiency without effects like active torsional vibration reduction. Further [53], [52] concludes that during the battery loading with such active vibration operation does not lead to battery life deterioration.

### 2.5.2 Integration with energy management

Active measures integrate the functionality of vibration reduction with the traction demand of the existing onboard Electric Traction Machine (ETM). This requires a clear definition of the interfaces between the active torsional vibration reduction and the hybrid vehicle Energy Management (EM).

In this work, an approach for the integration of the controller shall be presented. The approach is based on the specific realization of neither the EM controller nor the vibration reduction. The schematic of the integration is presented in Figure 2.11. The approach uses a frequency-based control allocation to clearly differentiate the task of the respective controllers. As shown in the figure, the integration demarcates between low frequency and high frequency control. The separation between the low and high frequency components is achieved by an estimator. The task of the estimator is to compute the mean value (dc value) and the harmonic estimates (ac values) of the states of the torsional powertrain system. Further details of the theory, implementation and experimental validation of the estimator are discussed in chapter 3. The resulting command torque sent to the ETM is the sum of the torque requests calculated by the low and high frequency component.

The low frequency control component is responsible for tracking the battery state of charge (SOC). The main input is the reference state of charge denoted by $\mathrm{SOC}_{ref}$ and the actual SOC. The specification of the reference SOC does not restrict it to a tracking model predictive control [67] (MPC) implementation, if the EM is realized using MPC theory. The reference SOC can thereby be computed by an economic MPC [67]. The low frequency component receives the low frequency (also referred to dc values) components of the state of the torsional system. The state of the torsional powertrain, here approximated with a three mass approximation.

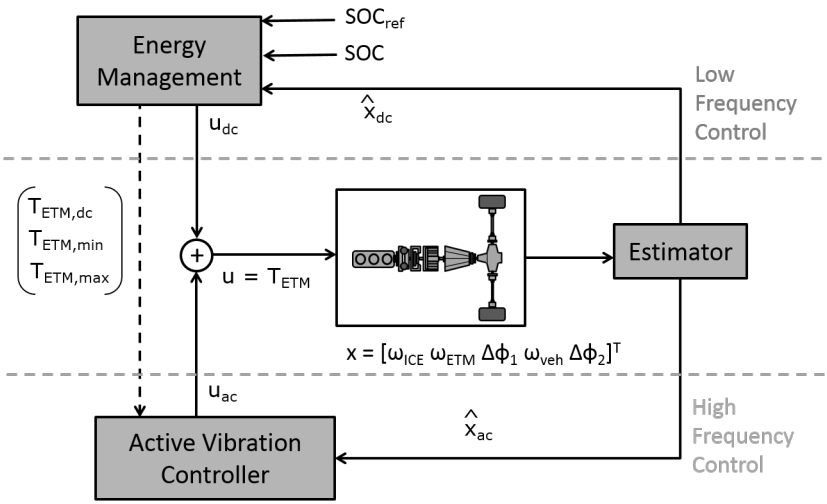


**Figure 2.11:** Integration of Model Predictive Control based Energy Management and Active Vibration Reduction Controller

The task of this component is to compute the power split between the onboard energy converters to track the desired SOC trajectory. Based on the current demand torques, it also computes the maximum and minimum torque margin available for active vibration reduction. The available torque margin refers to the torque limits of the ETM (over the operating speed) taking into account effects such as thermal derating.

The high frequency control component commands the set torque for the ETM inverter for active torsional vibration reduction. The term high frequency is used to refer to the fact that this component works with the harmonic estimates. The values of frequency depend on the region of vibration reduction (1000 - 2000 rpm) and engine configuration as presented in Table 2.3. It receives the estimated states or just the outputs of the torsional powertrain and computes the compensation torque. The compensation torque shall be computed in a way that the maximum and minimum limits for the compensation torque set by the low frequency component is adhered to. Control techniques for the low frequency component is discussed in the Chapters 5, 6, 7 and 8.

Figure 2.12 depicts the results of the integration of active vibration reduction control and EM controller. The architecture presented in section 2.5.2 was used for

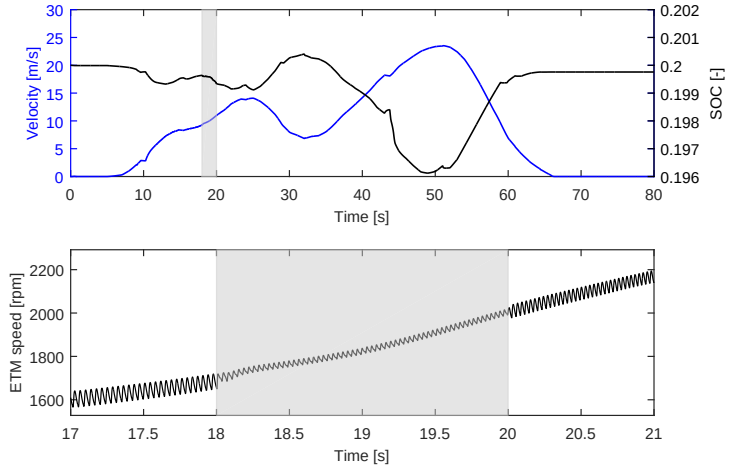


**Figure 2.12:** Integration of MPC based EM with the active vibration reduction controller [61]. MPC based active vibration reduction controller is activated in the gray-shaded region.

the integration. The vehicle velocity and the SOC profile for the considered driving scenario are presented in the top plot. During the considered scenario, the active vibration reduction control is activated between 18 and 20 seconds as shown in the bottom plot. The achieved vibration reduction can be seen in the reduced oscillations of the ETM speed signal without affecting its mean value. This mean value is determined by the current gear selection and vehicle velocity. In other words, the low frequency operation of the powertrain is determined by the low frequency component, the EM controller. The high frequency performance of the powertrain is governed by the vibration reduction controller. Thus a clear demarcation of the objectives is achieved by frequency dependent control allocation.

## 2.6 Methodology for Potential Analysis

The knowledge of the dynamic behavior of the powertrain is an important prerequisite for the development of both passive and active vibration reduction systems. Before the development and realization of the active torsional vibration are initiated, an analysis of the powertrain shall be performed. This analysis serves to determine whether the powertrain system offers the possibility for active vibra-

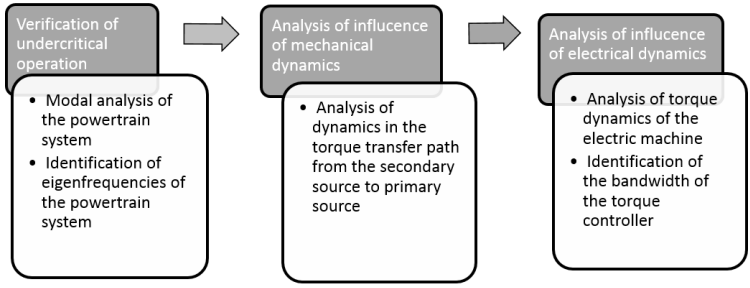


**Figure 2.13:** Potential analysis methodology for the development of active torsional vibration reduction

tion reduction. This section presents a methodology for such a potential analysis. The analysis involves the study of the torsional coupling between the primary and secondary source. The primary source refers to the source, which in the case of torsional vibration is the ICE. The secondary source is the electric machine which generates the compensation torque to act against the oscillations. The steps of the potential analysis methodology are depicted in Figure 2.13.

The first step is the modal analysis of the torsional vibration system. Modal analysis helps to compute the frequencies at which a structure can oscillate, in which eigenmodes (vibration shapes) the structure oscillates at these frequencies and the amplitude of oscillations at certain frequencies [28]. To study the torsional vibration phenomenon, the powertrain is discretized into finite-dimensional torsional mass-spring-damper system [16]. The degree of discretization, in other words, the number of degrees of freedom of the discretized system depends on the vibration effects under study [68]. Torsional vibration phenomena such as shuffle arise due to abrupt load changes or change in drive torque exciting the first drivetrain mode requiring a simpler model with the inertia of the drive unit and the vehicle mass coupled by a powertrain dependent stiffness. On the other hand, transmission noise such as rattle from unloaded gears, whine due to transmission error and dynamic mesh forces from loaded gears in kHz range require finer discretization of the model used for the study.

The vibration effect of interest is in the range of engine operating speeds from idle speed to 2000 rpm. Depending on the engine configuration this range translates to a frequency band of 16.67 - 33.33 Hz or 25 - 50 Hz in case of 2-cylinder and 3-cylinder engines respectively. Employing models with eigenfrequencies out-

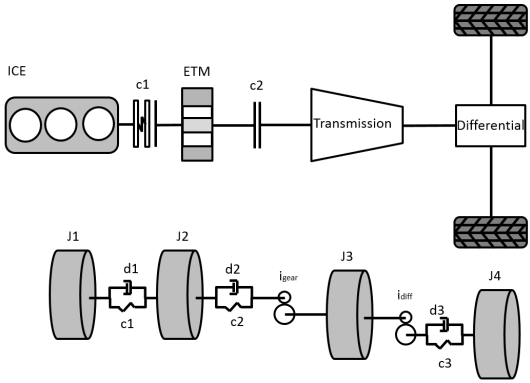


**Figure 2.14:** Powertrain and its discretization used for potential analysis

**Table 2.6:** Parameters for the powertrain modal analysis

| Parameter | Description | Value |
|---|---|---|
| Inertia ICE | Moment of inertia of the combustion engine, flywheel, bearing sleeve clutch release plate, clutch disc | 0.2 $kgm^2$ |
| Inertia ETM | Moment of inertia of the electric traction machine, clutch C2 input and output inertias | 0.12 $kgm^2$ |
| Inertia Gearbox | Moment of inertia of gearbox on input and output side | 0.03 $kgm^2$ |
| Inertia Vehicle | Inertia of wheels together with differential inertia, equivalent rotational inertia of the vehicle translation mass | 123.7 $kgm^2$ |
| Stiffness C1 | Stiffness of clutch C1 | 600 $Nm/rad$ |
| Stiffness C2 | Stiffness of clutch C2 | 3000 $Nm/rad$ |
| Stiffness C3 | Stiffness of drive shaft connecting the gearbox output to the wheels | 10000 $Nm/rad$ |

**Table 2.7:** Computed eigenfrequencies for three degree of freedom torsional powertrain

| | Eigenfrequencies and Speeds | | |
|---|---|---|---|
| Gear | First | Second | Third |
| Second Gear (i=2.5) | 3.6 Hz | 14.8 Hz | 129.5 Hz |
| Speeds (3-cylinder engine) | 144 rpm | 592 rpm | 5180 rpm |
| Fifth Gear (i=1) | 7 Hz | 17.7 Hz | 62 Hz |
| Speeds (3-cylinder engine) | 280 rpm | 708 rpm | 2480 rpm |

side the above-discussed bandwidth increases the complexity of the model without additional benefits. As discussed in section 2.1, gear rattle and driveline boom are the major vibration phenomena of interest. This requires in minimum a four inertia approximation the torsional powertrain [23]. Figure 2.14 depicts this four-dimensional approximation of the torsional powertrain. The torsional dynamics of the crankshaft is neglected modeling it as a rigid body. The reason being the frequency range of interest lies below the eigenfrequency of the crankshaft [26]. Similarly, the axial engine vibrations and bending modes of the crankshaft shall not be modeled [34]. The modal analysis performed here does not consider nonlinear effects such as play or lash, nonlinear bearing stiffness, variable tooth stiffness normal to the plane of contact during meshing of gears and clutch judder (due to friction variation). The inertia and flexibilities of the powertrain components are parameterized based on the technical specification when available and from the literature such as [26], [16]. The parameter values used are presented in Table 2.6. The transmission ratio corresponding to the first gear and the differential is chosen as 4 and 3 respectively [16]. The computed eigenfrequencies and corresponding engine speeds (3-cylinder engine) are listed in Table 2.7.

The main observation from the computation of the eigenfrequencies is that the active vibration controller operates between the first and second eigenfrequencies around an engine operating speed of 1000-2000 rpm. The operating speed is well above the DMF mode shape [32] or the second mode shape at lower gears. This would mean that there is a supercritical operation of the coupling between the ICE and the ETM, which helps in attenuation of the torque pulses from the ICE through the coupling. This supercritical operation is beneficial for the realization of active torsional vibration reduction, as it reduces the magnitude of torque required by the ETM to attenuate the resulting torque oscillations at the ETM. In case of belt-driven systems [18] such an analysis has to be performed to confirm that the

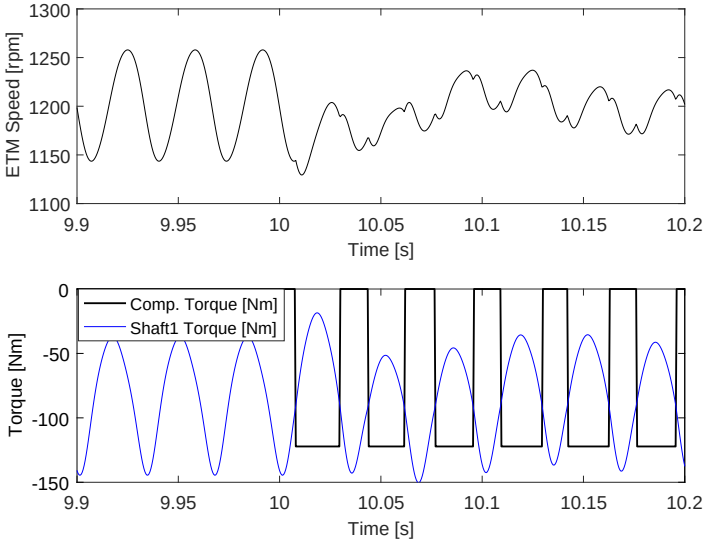


**Figure 2.15:** Potential Analysis: Performance of the active vibration reduction strategy in stationary operation

eigenfrequency of the belt drive between the belt starter generator (BSG) and the inertia coupled to by the belt, is above the frequency range of operation (25 - 50 Hz in case of 3-cylinder engines). This sub-critical operation of the belt drive ensures effective transmission of the BSG torque on to the inertia in the path of the ICE torque along the powertrain.

The subsequent steps in the potential analysis methodology are to analyze the mechanical and electrical dynamics. The mechanical dynamics refers to the dynamics between the air gap torque of the electrical machine and the torque at the shaft in case of the presented powertrain in Figure 2.14. In the case of the presented powertrain, this dynamics is linear provided the shaft flexibility is linear in the operating range and can be computed using linear system identification techniques. The methods of identification developed in Chapter 4 can be used to identify the torsional dynamics. Further, there is no delay involved in the mechanical path. Nevertheless, the electrical path may involve delay effects such as magnetization delay in case of an asynchronous machine. The effect of delays in the realization of the active vibration reduction controller along with a method for stabilizing the controller in the presence of delays is discussed in chapter 8. The potential analysis and the validation of the developed controllers using simulations employ

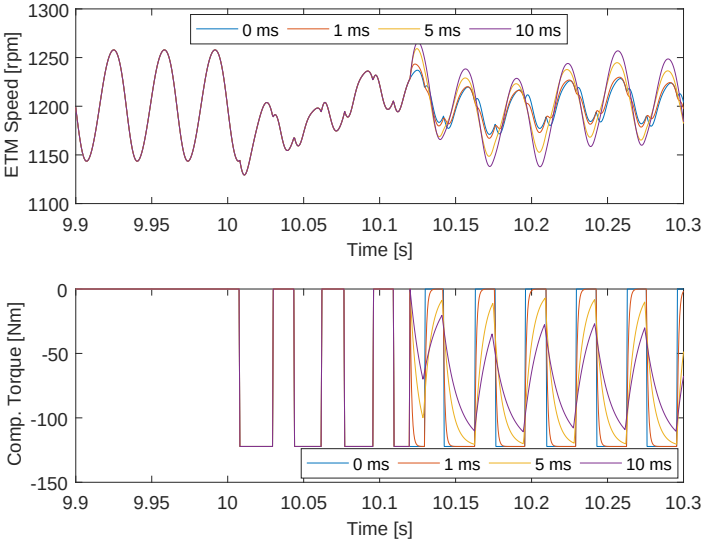


**Figure 2.16:** Potential Analysis: Performance of the active vibration reduction strategy in stationary operation with varying PT1 dynamics in the actuation path

the same simulation model. Using the eigenvalue analysis of the linearized system (obtained from the modal analysis) and the numerical stability region of fixed step solvers [69], Runge-Kutta with a sample time of 1 ms was chosen as the solver for the simulation used in the potential analysis. Introduction of time lag (PT1) elements in the actuation path can be due to electrical or mechanical effects. As the simulation is performed before the development of the controller, an appropriate control strategy is used.

Due to the flexibility of the coupling between the ICE and ETM, the torque transmitted to the ETM will have a phase shift with respect to the ICE torque. Hence using the value of the transmitted shaft torque, the ETM shall be commanded to counteract the effect of the shaft torque. By using this strategy and tuning the value of shaft torque above which the compensation has to be performed along with the maximum and minimum of the compensation torque, a compensation strategy is realized. The limits on the compensation torque are motivated by energetic considerations and effects that are machine dependent (such as derating).

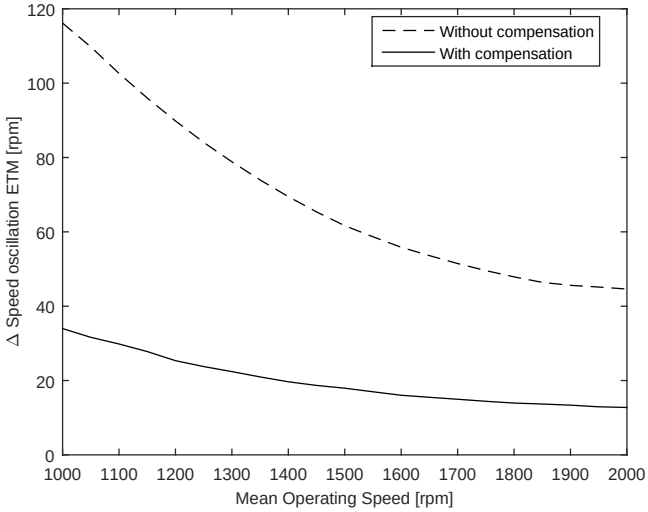


**Figure 2.17:** Potential Analysis: Performance of the active vibration reduction strategy presented in terms of speed fluctuation over the operating speed with and without active compensation

Figure 2.15 shows the result of simulation around a mean operating speed with the developed compensation strategy. In the subsequent discussion, the ICE torque ranges between 850 Nm and -266 Nm during the part-load operation (70% pedal value). The maximum value of the compensation torque was set to zero, to realize compensation using generator operation. This is of specific interest, to recharge the battery in case of low SOC. This can also be realized with a negative mean value compensation torque for the case of 48 V belt-driven system as presented in [18]. The compensation was activated at 10 seconds. It can be seen that the compensation torque counteracts the shaft torque leading to reduced speed oscillations which can be seen in the top plot. The bottom plot presents both the shaft and the compensation torque. The minimum value of the compensation torque employed thereby is -120 Nm.

The simulation model can also be used to study the effect of PT1 dynamics of the actuator on the vibration reduction. In the case of the electrical path, the lowest possible time constant depends on the resistance and inductance of the machine. In addition, the inverter controller can introduce an additional time delay. The study with time constants is performed by inserting additional time lag blocks

in the simulation irrespective of their source. The results of such an analysis are presented in Figure 2.16 for different time constants of 0, 1, 5 and 10 ms. The PT1 dynamics was activated at 10.12 seconds, whereas the controller was turned on at 10 seconds. Till 10.12 seconds after the controller activation, the compensation torque and the speed oscillations coincide. After activation of the different PT1 elements, the larger the time constant the lower is the effective compensation torque realized by the actuator. This can be seen in the bottom plot. This dynamic effect is also reflected in the resulting vibration reduction as it can be seen in the top plot. By using such an analysis, the minimum dynamics required by the electric machine along with its torque controller to realize a certain degree of vibration reduction can be computed as in [18].

Various metrics have been discussed in the literature for the quantification of the achieved vibration reduction. A survey of these methods used both for data from simulation and real measurements is presented in [19]. The methods use either the variation of the rotational speed or rotational acceleration. The rotational speed is directly measurable at the test bench and accessible in the simulation model used for potential analysis. Hence the metric shall be based on the rotational speed with and without compensation. In case of controllers that act against the dominant harmonic, comparison of the harmonic amplitudes computed by the estimator discussed in chapter 3 shall be performed for both stationary and transient speed conditions.

The final result of the potential analysis is presented in Figure 2.17 with the maximal speed difference as a metric. The simulation that was performed in Figure 2.15 was repeated for different speeds and the resulting vibration reduction is plotted over the operating speed range. No additional PT1 elements are added to the simulation model. The maximum and minimum speed oscillation reduction achieved is 71.5% at 1000 rpm and 71.4% at 2000 rpm. The compensation torque used is between 0 and -120 Nm. A similar analysis can be performed with the additional time lag (PT1) elements. As it can be seen in the figure active vibration reduction is capable of achieving vibration reduction over the entire operating speed range as in case of CPA, hence offering an effective alternative.

## 2.7 Active Torsional Vibration Reduction in 48 V systems

48 V technology is forecasted to play a major role in future mild hybridization technology. This is a result of not only the possible $CO_2$, driveability and emission advantages compared to conventional powertrains, but also due to lower system costs and additional effort required to fulfill safety requirements in comparison with high

voltage systems. With the introduction of LV 148 standard defining 48 V vehicle power system, the leading German auto manufacturers have increased focus on 48 V power systems. This 48 V Hybridization trend can be viewed as systematic electrification of the powertrain from the perspective of ICE based powertrains. Among the possible 48 V powertrain architectures, the Belt Starter Generator currently is the most accepted variant due to benefits such as low integration cost.

The first step of the potential analysis can be directly applied to the 48 V belted drive system. It requires the proper parameterization of the torsional dynamics considering the transmission ratio due to the belt drive. The belt drive system has to be equipped with a tensioner to ensure dynamic pre-tensioning when changing from motoring to generator operation. In comparison to the shaft system depicted in Figure 2.14, the belted drive system along with the decoupling tensioner exhibits nonlinear behavior. The analysis of the mechanical path in case of 48 V belt driven system was used to formulate the compensation strategy without exciting the dynamics of the decoupling tensioner [18].

The final step of analyzing the electrical path dynamics involves the definition of the required bandwidth of the torque controller of the belted starter generator (BSG). Another potential source of delay in the electrical actuation path is the (physical) location of the active vibration reduction controller. If the active vibration reduction controller is realized as a part of the BSG inverter then there is a minimal delay. If the active vibration reduction controller is implemented in the hybrid control unit along with the EM, then the torque requests have to be transferred to the inverter using a high frequency bus connection, which can introduce delay effects in the system. For reasons of brevity, a detailed presentation of the potential analysis performed for 48 V belt-driven system shall not be done. The interested reader is referred to [18].

## 2.8 Conclusion

Trends in the continuous ICE refinement such as rightsizing in tandem with forced induction, speed reduction (down-speeding) result in higher cyclic non-uniformity This leads to higher ICE torque pulsations and rotational irregularities causing passenger discomfort. Besides subjective perception, the ability to operate the ICE during normal driving situations slightly above idle speed results in advantages in fuel consumption. The vibration phenomena due to the rotational irregularities such as rattle and boom are discussed. Besides, the vibration phenomena, the ICE torque pulsations which are the main cause for the torsional vibrations is presented.

Passive mechanical solutions rely on inertial and/or isolation by tuned mass dampers to reduce such torsional oscillations. However, with the increasing adoption of turbo/supercharging technology together with the improving power-to-volume ratio of the combustion engines, these measures become increasingly ineffective over the entire operating spectrum of the powertrain. If tuned for robust operation, DMF with CPA offers good vibration isolation. But this solution requires additional effort in tuning for different driving situations considering the nonlinear effects and packaging space to accommodate the pendulum masses increasing its complexity. This encourages the investigation of active torsional vibration reduction methods.

A review of the methods investigated in the literature for active torsional vibration reduction is presented. This discussion serves as basis to demarcate the novelties in the approaches presented in chapters 5, 6, 7 and 8. The test setup used for the experimental validation of the developed methods is presented along with its control architecture. The setup uses the CEA powerpack with an eddy current dynamometer and offers the flexibility to identify the torsional dynamics and to validate the controllers.

Active vibration reduction offers a mechatronic solution to the torsional vibration problem. For the proper and efficient functioning of the mechatronic system, the boundary conditions of the underlying mechanical system have to be defined. The developed methodology for potential analysis presents an approach to evaluate the achievable torsional vibration reduction before the begin of the actual controller development. From the energetic perspective, the harmonic characterization of the ETM and inverter used for active vibration reduction control is proposed. A modular architecture for the integration of the vibration reduction controller and hybrid vehicle energy management is presented. The proposed integration architecture is evaluated from a non-synthetic driving situation. The evaluation presented the ability of the architecture to handle conflicting demands by formulating constraints on the ETM torque used for traction and vibration reduction.

# 3 Filtering Techniques for Automotive Rotatory Energy Converters

Filters are dynamic systems commonly employed in the fields of control, identification and fault detection. Filtering refers to the process of extracting a certain quantity of interest from measurement signals, which usually is internal to the system and is either not directly measurable or only measurable using a complicated measurement setup. In this chapter, two variants of filters are studied, namely Observer and Estimator.

Observers estimate unmeasurable quantities of a process using measurements and model assumptions of the process along with the parameters associated with the model. They are tools for engineering motivated by applications not limited to condition monitoring, eliminating the use of costly measurement devices and estimation of disturbances as well as estimating states for output regulation control. Observers use knowledge about the deterministic part of the system. The absence of the noise model offers degrees of freedom for the realization of the observers.

Estimators are filters that are not structured as an observer, they employ simpler signal models. One practical situation is when the system is affected by uncertainty, the idea of using a copy of the system for observer design is not realizable practically unless robustness can be ensured. Estimator in this work refers to the dynamic system used to compute the non-periodic mean value as well as the harmonic components of the combustion engine speed and torque from the respective oscillatory signals using simpler signal models rather than the copy of the system.

The chapter is structured as follows. Section 3.1 motivates the need for filtering techniques along with an overview of the related literature. Subsequently, section 3.3 introduces observers for mean value torque estimation with results. This is followed by section 3.4 which discusses filters for estimation of oscillatory combustion torque. Validation of the developed filtering techniques in simulation and at experimental setup is presented in section 3.5, followed by concluding remarks.

## 3.1 Introduction

Signals corrupted with harmonics and noise are becoming increasingly common in engineered systems. In the field of power converters, the increased use of switching based devices and also due to nonlinear loads, lead to higher harmonic content in the signals. Specifically, in the field of powertrains, the torque generated by the combustion engine comprises of the non-periodic mean value in addition to higher order harmonics depending on the engine configuration. This is a consequence of the gas torque resulting from the cyclic combustion process and also the inertial as

well as frictional torque from the components. Proper knowledge of the harmonic components can be used for diagnosis in case of the combustion engine for misfire detection [70]. The non-periodic mean estimate can be used for actual value for feedback control, termed as certainty equivalent control, separating the feedback control problem to a (non-stochastic) control problem and a statistical estimation problem. A delay-free separation of the signal into its mean value and different harmonics is important from various perspectives.

Observers are filters that use a deterministic representation of the dynamic system and noise assumptions to compute the quantity of interest. A common realization of which is the Kalman filter which operates under Gaussian noise assumption. The task of an observer in this work is to estimate the inner torque generated by automotive rotatory energy converters. In case of the internal combustion engine, this torque is termed as the effective torque (also termed as brake torque in stationary operation). Effective combustion torque is the torque that accelerates the inertia of the combustion engine and the coupled loads. The effective torque results from the indicated torque, as a consequence of the pressure variations in the combustion chamber without the effects of friction torque and other parasitic torque resulting from the auxiliary devices. Robust measurement equipment for indicated torque sensing is established, however, the subsequent computation of the effective torque requires knowledge of the engine friction characteristics. Engine friction characterization is difficult and is usually performed during motoring of the engine [3]. Such indication based techniques are limited to the laboratory environment and vehicle prototypes as an adaption for series production vehicles have not been successful due to packaging, durability and cost reasons. Hence the task of the observer in case of ICE test bench would be to compute the ICE effective torque using the available measurements. The developed observer considers the internal combustion engine torque as an unknown input of the system and uses the measurements available at the test bench to estimate its value. Both the methods are evaluated using simulations and validated at the test bench for both stationary and transient operation.

An estimator relying on the fact of harmonic separation with a low-pass filtering and linear parameter variant component has been developed. It estimates the non-periodic mean value of the combustion engine torque along with the additional harmonics. The estimator is designed generically based on the frequency dependence of the harmonics to the mean value non-periodic component of the oscillatory signal. Hence it can be used to estimate the corresponding components of torque, speed or other harmonically corrupted signals and its application is not restricted to reciprocating machines. The functionality of the estimator is vali-

dated using test bench measurements for combustion engine as well as for electric machines, establishing its universal applicability. Any such noisy signal such as acceleration of the ICE block can be used as input, but the focus in this work shall be to study the estimator performance for speed and torque signals.

## 3.2 Overview of related studies

The estimation of the ICE effective torque is of practical significance, some of the possible applications of the estimate are listed below.

- *Engine control*: Torque control structure: Modern Engine Electronic Control Unit (ECU) use a torque based control structure to translate driver demand to the corresponding actuator set points [71], [11]. One of the reasons for its wide adaption is its practical interpretability and correlation to vehicle acceleration and hence driver demand. Further torque based control offers flexibility in the design phase with adaptability to different components, ideally decoupling ICE control functionality development from driveline and vehicle control functionality. Torque based control involves a backward propagation of the torque request to the engine ECU and forward propagation of the generated torque to the motive torque at the wheels. In addition to coordinating the torque demand among the different actuators such as air path control and fuel injection control, the torque control structure handles the different timescales of the dynamic process involved. Hence the availability of the effective torque, a crucial non-measurable quantity helps improve the dynamic torque control.
- *Engine diagnosis*: Engine misfire detection: ICE cylinder misfire is a result of combustion instability which may occur during transient operation under conditions such as inappropriate air-fuel ratio, advanced ignition timing, higher levels of dilution through exhaust gas recirculation. Misfires create problems not only from comfort perspective due to non-uniformity of the generated torque but also from the viewpoint of emissions due to unburnt hydrocarbon emissions usually along with higher amounts of $NO_x$ due to improper functioning of the catalytic converter. Different methods have been investigated for diagnosis of engine misfire, estimation of effective torque has been employed for misfire diagnosis [72].
- *Gear shift control*: The estimation of effective torque in the vehicle can be used for controlling the gear shift process. The stages of gear shift include a phase where the transmission is made free of torque before and phase with

the ramp-up to the driver defined torque in case of shift control in the automated manual and dual-clutch transmissions [73]. The stages before and after the speed synchronization require precise tracking of the pre-defined torque trajectory realizable using the combination of torque observer and an output feedback tracking controller.

- *In-the-Loop architecture*: Engine and Powertrain In-The-Loop test benches gain importance for emulation of real-world driving scenarios in a reproducible manner. In [74] and references therein different approaches for the integration of real-time simulation models with automotive test benches to realize In-The-Loop test benches are presented. Based on analysis of the different approaches, [74] concludes that the approach using an observer to compute the effective torque of the energy converters at the test benches offers both stable realization and transferability of real-world driving effects at such In-The-Loop test benches.
- *Active torsional vibration attenuation*: Estimates of the mean value and the harmonics of the ICE speed signal and the shaft torque can be used to realize vibration attenuation as discussed in chapter 5 as well as chapter 7 and chapter 8 respectively.

Widely used torque estimation methods are physically motivated using the variables such as engine speed, the quantity of fuel injected, engine geometry, pressure and temperature conditions that influence the torque generation process in the combustion engines. These methods are implemented as lookup tables which are parameterized using an extensive measurement campaign. The references in [75] enlist the publications and patents that discuss such lookup table based effective torque estimation techniques. Time and effort involved in the calibration of such lookup table approaches have motivated the application of observers to estimate the effective torque using the available measurements.

A survey of different observers from a practical perspective characterizing them based on the extent of knowledge of the plant including its structure and required input signals is presented in [76]. There are two different schools of thought. The first approach considers observer as a dynamic system that optimizes some cost formulation on observed states using measurements, based on assumptions on disturbances or uncertainties in the system. Another approach presents the estimation of disturbances along with the states using measurements and known inputs. This work uses the second approach along with the assumption of linear systems and Lipschitz nonlinear systems modeling the unknown torque to be estimated as an unknown input. Test benches are the dynamic systems under

consideration in this work, nevertheless, the approaches are applicable to entire powertrain systems. From the control perspective, the rotational dynamics of the test bench can be modeled as damped oscillatory systems. It is common practice to model the UUT and the dynamometer as inertia and the shaft using the damping and stiffness elements. The focus is to develop torque observers for test benches, however, the methods can be also employed for in-vehicle operation.

The system dynamics used for the observer synthesis can be linear or nonlinear. In the approaches in [77], [78] the nonlinearity results from the torque generation dynamics of the internal combustion engine (ICE). ICE torque generation is modeled as an Extended Hammerstein System, motivated by input affine representations of the nonlinear dynamical system [77] and [78]. The input affine system approximation facilitates the design of inversion based controllers for output tracking [79]. From the ICE perspective, such nonlinear approximation of the ICE torque generation is restrictive. It neither includes the coupling effect between different controllers such as air or fuel path controllers nor physical effects such as temperature accounting for warm/cold start ICE operation. Additionally, the ICE torque behavior deteriorates over time and hence invalidating the assumed model representation as well as the parameters of the model.

A high-gain Kalman filter neglecting the dynamometer dynamics, to estimate the engine torque is developed in [80]. One drawback of this approach due to high gain is the resulting noisy estimate which requires subsequent denoising. [81] presents two torque estimation methods specifically for ICE, both the methods are based on high gain observers presented in [82]. The first method uses high gain observers to estimate the engine torque as the unknown variable using the engine speed and load torque as measurements. In contrast to [80], the filtered measurements of engine speed and load torque are used as input to the observers. The second method models the effective torque as a function of variables such as mass flow rates and engine speed and uses the idea of adaptive parameter estimation to compute estimates of effective torque using their measurements.

Besides high gain Kalman filtering, time-varying Kalman filtering [83] has been studied for estimation of resultant torque at the crankshaft using only crankshaft speed measurements. The implementation of time-varying Kalman filter is motivated and parameterized by the crankshaft dynamics. A parametric Kalman filter using crank angle as parameter and crank speed as well as shaft torque as inputs to estimate the inner combustion torque is used in [72]. The authors in [84] propose a new class of asymptotic observers for estimating an unknown periodic input entering a linear time-periodic system. It based on approximation using cer-

tain numbers of Fourier modes and obtain similar performance with the reduced computational burden compared to Kalman filter-based methods.

In contrast to the time-triggered filtering, the crank angle synchronous moving average (CASMA) filter performs sampling triggered by signals from an incremental encoder. The signals to be filtered are averaged over a predefined window of crank angle. This makes the CASMA filter independent of the mean speed of the rotatory energy converter. However, the implementation requires variable sampling time and may suffer from aliasing at low mean speed values. The approach in [80] models the combustion oscillations as a parameter varying exosystem and uses an observer based on the internal model principle to reconstruct the combustion oscillations and separate the non-periodic mean value of the combustion torque. Further, a cascaded structure comprising of a high gain Kalman filter cascaded with the internal model observer is used to estimate the mean value torque from the measurements. It has to be observed that the engine torque is considered as an additional state without any dynamics in conjunction with the high gain approach. A fixed-sampling interval moving average (MA) filter is proposed in [85] to filter non-periodic mean value of harmonically corrupted signals. The implementation uses a fixed-depth method for MA filtering to make it adaptive during transient situations with the variation of the mean speed.

Approaches to solve the estimation of the engine torque using unknown input observers (UIO) was investigated in [86]. The approach used angular velocity measurements in the crankshaft to compute the instantaneous torque in each cylinder. The resulting instantaneous engine torque can be computed using the cylinder torques. The approach was motivated by indicating measurements common in the field of combustion engines. Further, the approach involves complex measurement setup due to speed sensing at locations of the crankshaft. In contrast, the approach in the work uses external signals to construct the unknown input observer (UIO). The term external signals refer to signals measured at the components attached to the ICE and not internally within the crankshaft as in [86]. This approach benefits from simpler measurement equipment and can also use estimated speed signals if available to compute the unknown quantity of interest.

The unknown inputs affecting the system in this study shall be focused on unknown inputs acting on the dynamic system. In other words, other effects unaccounted for in the model of the observer such as uncertainties shall not be studied. In addition to the oscillatory torque, the non-periodic mean value torque is of interest. In the case of the ICE, the mean effective torque contributes to the acceleration of the associated inertial masses. Different approaches have been proposed to estimate the non-periodic mean value of oscillatory quantities. The method proposed

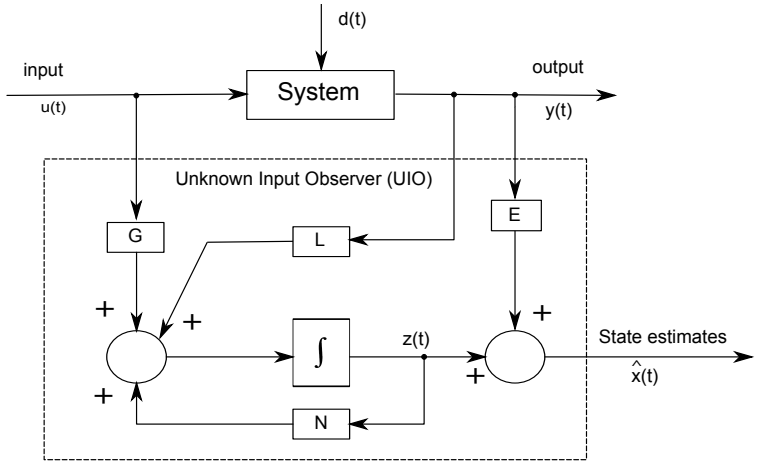


**Figure 3.1:** Structure of the Unknown Input Observer with parametrization from the LMI approach

in this work uses the dependency of the harmonic frequencies to estimate the mean value of the oscillating signal. This is of specific interest in applications such as ICE speed signals which contain harmonic content, with the harmonics being a multiple of the mean value speed signal.

## 3.3 Unknown Input Observer

Estimation of the non-periodic combustion engine torque is a filtering problem [35]. The state estimate $x$ at the current instant given data up to the current time instant $k$ which is given by equation (3.1), where $Z^N$ denotes the set of measurements up to time instant $k$, comprising of both inputs and outputs as given by $Z(k) = [u(k) \quad y(k)]^T$.

$$\begin{aligned} &\text{estimate } x(k|Z^N) \\ &\text{given } Z^N = \{Z(1), Z(2), ..., Z(k)\} \end{aligned} \tag{3.1}$$

Classical realizations of such filters are not restricted to Wiener- and Kalman filters. Recently methods that estimate unknown disturbance in addition to estimates of states have been gaining more attention [76]. Estimation of disturbances can be employed in conjunction with feedback control leading to realize disturbance

rejection controllers. The estimation of engine torque has been adopted based on the assumption that the engine torque as an unknown input to the dynamic system using the theory of Unknown Input Observers (UIO). The UIO method uses a deterministic system approximation relying on the absence of coupling between the state estimates and the disturbances. This section introduces both the approaches, followed by its application to the synthesis of UIO.

When used in tandem with active disturbance attenuation controllers, the employed observers shall provide delay/phase-free estimates. For a dynamic operation of powertrain components on a test bench, the knowledge of the dynamic behavior of the test bench is essential. The model used in the observer is parameterized using the identification of the test bench. Chapter 4 investigates different approaches for non-parametric and parametric identification of the test bench dynamics in closed loop operation.

Let us consider a linear dynamical system described by the equations (3.2), where $x(t) \in \mathbb{R}^n$ is the state vector, $y(t) \in \mathbb{R}^m$ is the output vector, $u(t) \in \mathbb{R}^r$ is the known input vector and $d(t) \in \mathbb{R}^q$ is the unknown input. With knowledge of the disturbance estimate $\hat{d}$, the tracking control law $u_t$ can be extended to eliminate effects of the disturbance by extending it with the pseudo-inverse of the input matrix as given in equation (3.3).

$$\dot{x} = Ax + Bu + Fd, y = Cx \tag{3.2}$$

$$u = u_t - B^{\dagger} F \hat{d} \tag{3.3}$$

**Definition 3.1.** Unknown Input Observer [87] of the system in equation (3.2) is defined as the dynamic system whose state estimation error $e(t)$ as defined in equation (3.4) approaches zero asymptotically regardless of the presence of unknown inputs or additive disturbances acting on the system. The asymptotic convergence is given by the equation (3.5) where $\hat{x}(t)$ represents the state estimates.

$$e(t) = x(t) - \hat{x}(t) \tag{3.4}$$

$$\lim_{t \to \infty} \|\hat{x}(t) - x(t)\| = 0 \tag{3.5}$$

The state estimates are given by the dynamic system defining the observer dynamics as listed in equations (3.6) and (3.7). The states of the system can

be computed using the states of the UIO and the measured outputs as given by equation (3.7). The block diagram of the UIO is depicted in Figure 3.1.

$$\dot{z} = Nz + Ly + Gu \tag{3.6}$$

$$\hat{x} = z - Ey \tag{3.7}$$

*Theorem* 3.1. Necessary and sufficient conditions [87] for the system in equations (3.6) and (3.7) to represent an UIO for the system in equation (3.2) are given by equations (3.8) and (3.9).

$$\text{rank}\,(CF) = \text{rank}\,(F) = q \tag{3.8}$$

$$(C, A_1) \text{ is a detectable pair, with } A_1 = A - F[(CF)^T CF]^{-1}(CF)^T CA \tag{3.9}$$

The existence of the full order UIO depends on two conditions namely relative degree condition (3.8) and minimum phaseness condition (3.9) which shall be checked before the UIO synthesis.

The relative degree condition is $rank(CF) = rank(F) = q$. This condition implies equation (3.10) and the existence of a regular output and state transformations as in equation (3.12), define new coordinates of the linear system. This condition expresses the number of measurements needed, which shall be greater than or equal to the number of unknown inputs. Further, the states that are directly coupled to the unknown input shall be obtainable from the measurements. One consequence of this condition is the possible variants based on the input signals for the realization of the UIO discussed in section 3.3.3, describing the variants of the UIO.

$$dim(y) >= dim(d) \tag{3.10}$$

$$\bar{y} = \begin{pmatrix} \bar{y_1} \\ \bar{y_2} \end{pmatrix} = \begin{pmatrix} H_1 \\ H_2 \end{pmatrix} y, \tag{3.11}$$

$$\begin{pmatrix} \bar{y_1} \\ \xi \end{pmatrix} = \begin{pmatrix} H_1 C \\ M \end{pmatrix} x = Tx \tag{3.12}$$

$$\dot{\bar{y}} = A_{11}\bar{y_1} + \bar{A_{12}}\xi + \bar{B_1}u + w \tag{3.13}$$

$$\dot{\xi} = \bar{A_{21}}\bar{y_1} + \bar{A_{22}}\xi + \bar{B_2}u \tag{3.14}$$

$$\bar{y_2} = \bar{C_{22}}\xi \tag{3.15}$$

The minimum phaseness condition is fundamental to estimate the disturbance from the outputs, which is equivalent to the extension of Hautus criteria for observability:

$$rank\begin{pmatrix} sI-A & -F \\ C & 0 \end{pmatrix} = n+q, \forall\, s \,\epsilon\, \mathbb{C}_0^+ \tag{3.16}$$

where $\mathbb{C}_0^+$ is the closed right half complex plane. The minimum phaseness condition results from the fact that the UIO uses an implicit inversion of the system. The inversion operation makes the transmission zeros of the system the poles of the UIO. Hence prerequisite of a stable UIO is the stability of the transmission zeros of the system.

In contrast to the techniques proposed in the literature the observer synthesis in this work handles nonlinearities in the torsional mechanical system and not in the ICE torque generation process as in [78], [88]. Modern powertrains are equipped with torsional damping systems such as DMF with CPA [9]. The torsional characteristics of such devices are designed to have two-staged damper characteristics which can be approximated using Lipschitz nonlinearities to be handled by UIO synthesis using Linear Matrix Inequalities (LMI) techniques.

### 3.3.1 Linear matrix inequalities based approach

Linear Matrix Inequalities (LMI) define convex constraints on the decision variables applicable to shows that wide range of problems in the field of systems and control theory that can be formulated as standard convex or quasi-convex optimization problems [89], [90]. The use of LMI methods for controller or observer design is based on the formulation of the controller parameterizations (assuming certain structure such as a rational form) as decision variables and the desired specifications as constraints. The solution of the formulated optimization problem under the assumptions of feasibility leads to the desired controller or observer. LMI constraints used for the observer synthesis are formulated as feasibility problems. LMI feasibility problem solves the question of existence of an element $x \in \mathscr{X}$ such that the conditions defined in form of the convex constraint $\{\mathscr{F}(x) \prec 0\}$ hold. The LMI

defined by $\{\mathscr{F}(x) \prec 0\}$ is feasible if such an element can be found else it is said to be infeasible.

$$N = MA - KC, \quad G = MB \tag{3.17}$$

$$L = K(I + CE) - MAE \tag{3.18}$$

$$M = I + EC \tag{3.19}$$

Based on the observer dynamics defined in equation (3.6)-(3.7) and using the definitions of the matrices $N$, $G$, $L$ and $M$ as given by the equations (3.17) - (3.19). The error dynamics of the UIO can be formulated as in the equations (3.20) - (3.21).

$$e = \hat{x} - x = z - x - Ey = z - Mx \tag{3.20}$$

$$\dot{e} = Ne + (NM + LC - MA)x + (G - MB)u - MFd \tag{3.21}$$

$$\dot{e} = Ne \tag{3.22}$$

$$MF = 0 \Leftrightarrow ECF = -F \tag{3.23}$$

$$\begin{aligned} NM + LC - MA &= (MA - KC)M - MA + LC = MAM - KCM - MA + LC \\ &= MAEC - KCM + KC + KCEC - MAEC \\ &= KCC(I + EC) - KCM = KCM - KCM = 0 \end{aligned} \tag{3.24}$$

The equation (3.21), can be written as equation (3.22), using the conditions (3.23) and (3.24). Condition in equation (3.23) results from the independence of the UIO convergence from the disturbance input, which is the definition of UIO. Using the necessary and sufficient condition for asymptotic stability of equation (3.21), with a quadratic Lyapunov function defined using a symmetric positive definite matrix $P$, the below conditions shall be satisfied:

$$N^T P + PN < 0 \tag{3.25}$$

Equation (3.25) imposes the condition of asymptotic stability for the quadratic Lyapunov function defined using $P$. Solution of this equation has the form given by equation (3.26), where $(CF)^+$ stands for the left inverse of $CF$.

$$E = -F(CF)^+ + Y\left(I - (CF)(CF)^+\right) \tag{3.26}$$

With the definitions of matrices $U$ and $V$ as given by the equations (3.27), the equation (3.26) can be written as in equation (3.28).

$$U = -F(CF)^{+}, V = I - (CF)(CF)^{+} \tag{3.27}$$

$$E = U + YV \tag{3.28}$$

Using these transformations the equation (3.25) can be formulated as an LMI in $\bar{Y} = PY$ and $\bar{K} = PK$ as given in equation (3.29)

$$\begin{aligned}((I+UC)A)^{T} P + P(I+UC)A + (VCA)^{T} \bar{Y}^{T} \\ + \bar{Y}(VCA) - C^{T}\bar{K}^{T} - \bar{K}C < 0\end{aligned} \tag{3.29}$$

After solving the LMI in equation (3.29), $Y$ and $K$ for the UIO can be computed using $P^{-1}\bar{Y}$ and $P^{-1}\bar{K}$ respectively. To estimate the unknown input, $d$ the equation (3.26) shall be used to formulate an equation where the $d$ appears linearly with the known quantities. The disturbance signal $h$ is formulated as $Fd$ and its estimate is represented using $\hat{h}$

$$E\dot{y} = EC\dot{x} = EC(Ax + Bu) + ECFd \tag{3.30}$$

$$= EC(Ax + Bu) - Fd \tag{3.31}$$

The estimated disturbance signal and error in its estimation can be written as

$$\hat{h} = Ky - E\dot{y} - (KC - ECA)\hat{x} + ECBu \tag{3.32}$$

$$h - \hat{h} = Fd - Ky + EC(Ax + Bu + Fd) + (KC - ECA)e - ECBu \tag{3.33}$$

$$= -(KC - ECA)e \tag{3.34}$$

As it can be seen, the error in the estimation of the disturbance is proportional to the error in the state estimation $e$. With $e \to 0$ would lead to $\hat{h} \to F\hat{d}$. Using the full column rank of $F$ and $\hat{d}$, the estimate of the actual disturbance signal acting on the plant can be computed as in equation (3.35)

$$\hat{d} = F^{-1}\hat{h} = F^{-1}(Ky - E\dot{y} - (KC - ECA)\hat{x} + ECBu) \tag{3.35}$$

#### Nonlinear dynamics

In case of Lipschitz nonlinearities in the system definition as in the equation (3.36), the Lipschitz bounds shall be used to formulate an LMI using the error

definitions in the equations (3.37) - (3.38), where the nonlinearity is represented by $f(x)$ satisfies the Lipschitz inequality $\|f(x)-f(\hat{x})\| \leq \gamma\|x(t)-\hat{x}(t)\|$.

$$\dot{x} = Ax + Bu + Mf(x) + Dd, \quad y = Cx, \tag{3.36}$$

By using the bounds on the nonlinearity, the similar procedure would lead to the equation (3.39), which contains additionally the effect of the nonlinearity entering through $\gamma$ compared to the equation (3.25).

$$e(t) = \hat{x} - x = z - x - Ey = z - Mx \tag{3.37}$$

$$\begin{aligned} \dot{e}(t) = Ne + (NM + LC - MA)x + (G - MB)u \\ +M(f(\hat{x}) - f(x)) - MDv \end{aligned} \tag{3.38}$$

$$N^T P + PN + \gamma PMM^T P + \gamma I < 0 \tag{3.39}$$

The procedure for LMI based synthesis of the UIO has been summarized as an algorithm and given below in Algorithm 1.

**Algorithm 1** Unknown Input Observer

**procedure** LMI METHOD
  **Input:** $u, y$
  $(CF)^+ = [(CF)^T CF]^{-1}(CF)^T$,
  $U = -F(CF)^+$
  $V = I - (CF)(CF)^+$
  choose $\gamma$
  solve $P$ from the linear matrix inequality:
  $\begin{pmatrix} X & X_{12} \\ X_{12}^T & -I \end{pmatrix} < 0$ with
  $X = ((I+UC)A)^T P + P(I+UC)A + (VCA)^T \bar{Y}^T + \bar{Y}(VCA) - C^T \bar{K}^T - \bar{K}C + \gamma I$
  $X_{12} = \sqrt{\gamma}[P(I+UC) + \bar{Y}(VC)]$
  compute $Y = P^{-1}\bar{Y}, \quad K = P^{-1}\bar{K}$
  **Output:Vector** $K$ **(SISO case)**
**end procedure**

### 3.3.2 Pole placement approach

The synthesis of the UIO using linear model can be performed using classical pole placement design. The following notations shall remain common: $\hat{x}(t)$ stands for

the state estimate, $e(t)$ stands for error in state estimation and $z(t)$ represents the states of full order dynamic observer. In order to avoid confusion in the observer design using LMI s, different notation shall be used for the observer dynamics as below, the matrices $F$, $T$, $K$ and $H$ shall be computed to achieve decoupling of the state estimation dynamics from the estimation of disturbances.

$$\dot{z} = Zz(t) + TBu(t) + Ky(t) \tag{3.40}$$
$$\hat{x}(t) = z(t) + Hy(t) \tag{3.41}$$
$$e(t) = x(t) - \hat{x}(t) \tag{3.42}$$

Observability of the pair $(C, A_1)$ shall be checked with $A_1$ defined in (3.48), as this will be used to place the poles of the observer. The error dynamics can be formulated in such a way that it is dependent only on $e(t)$:

$$\begin{aligned} \dot{e} = (A - HCA - K_1C)e(t) + (T - (I - HC))Bu(t) + \\ (F - (A - HCA - K_1C))z(t) + (HC - I)Fd(t) \\ + (K_2 - (A - HCA - K_1C)H)y(t) \end{aligned} \tag{3.43}$$

The observer matrix $K$ is composed as $K = K_1 + K_2$. If the relations hold good, then the UIO error dynamics depends only on the error. If the matrix $Z$ has stable eigenvalues with $(C, A_1)$ being detectable along with the rank condition $rank(CF) = rank(F)$ are the necessary and sufficient conditions for the UIO.

$$(HC - I)F = 0 \tag{3.44}$$
$$T = I - HC \tag{3.45}$$
$$Z = A - HCA - K_1C \tag{3.46}$$
$$K_2 = ZH \tag{3.47}$$
$$A_1 = A - F[(CF)^T CF]^{-1}(CF)^T CA \tag{3.48}$$

The dynamics of the observer depends on the matrix $K_1$ as seen in the equation (3.46). The matrix $K_1$ can be used to place the poles of the observer in the desired location. Estimation of the unknown input is given by equation (3.49). A detailed discussion on the classical design method for the UIO synthesis can found in [87]. The entire procedure has been explained using the algorithm given below in Algorithm 2.

$$\hat{d} = (CF)^+(\dot{y} - CA\hat{x} + CBu) \tag{3.49}$$

**Algorithm 2** Unknown Input Observer

**procedure** POLE PLACEMENT DESIGN METHOD
  **Input:** $u, y$
  **Assumption:** $rank(CF) = rank(F)$
  Compute the following observer matrices:
  $E = -F(CF)^{+}$
  with $(CF)^{+} = [(CF)^{T}CF]^{-1}(CF)^{T}$,
  find $L_1$ by solving Riccatti equations, such that $N = (I + EC)A - L_1C$ is Hurwitz
  calculate $G = (I + EC)B$ and $L = -NE + L_1$
  $\dot{\hat{x}} = A\hat{x} + Bu + Dd + L_1(y - C\hat{x}) - ECA(x - \hat{x})$
  $\dot{\tilde{x}} = \dot{x} - \dot{\hat{x}} = A\tilde{x} - L_1C\tilde{x} + ECA\tilde{x} = N\tilde{x}$
  compute $\hat{d} = (CF)^{+}(\dot{y} - CA\hat{x} + CBu)$
  **Output:Unknown Input** $d$
**end procedure**

### 3.3.3 Variants of unknown input observer

This section discusses the application of UIO for the design of torque observers for powertrain test benches. The initial step is to check for the existence conditions: relative degree and minimum phaseness condition. It requires a system approximation along with the selection of input and output vectors. The design is demonstrated here for observing the internal torque of the combustion engine but can be extended for powertrain test benches which are part of the validation data. The design of the internal engine torque observer assumes an approximation of the engine test bench as a two-mass oscillator system for the relevant frequency band of interest.

$$\begin{aligned} \dot{x}(t) &= Ax(t) + Bu(t) + Fd(t) \\ y(t) &= Cx(t) \end{aligned} \tag{3.50}$$

The following notation shall be used. $T_{shaft}$ refers to the shaft torque. $T_{ICE}$ and $T_{Dact}$ represent the torque acting on the engine and dynamometer inertia respectively. The speeds of the combustion engine and dynamometer are represented using $\omega_E$ and $\omega_D$ respectively. $J_E$ refers to the inertia of the combustion engine, $J_D$ is the inertia of the dynamometer, $c$ is the coupling stiffness and $b$ damping of the

**Table 3.1:** Variants of UIO for the engine test bench

| Variant | Inputs | Outputs |
|---|---|---|
| V2.1 | $T_{Dact}$ | $\omega_E$, $T_{shaft}$ |
| V2.2 | - | $\omega_E$, $\omega_D$, $T_{shaft}$ |
| V2.3 | $T_{Dact}$ | $\omega_E$, $\omega_D$ |

coupling shaft. Depending on the available measurements, different variants of the observer can be synthesized which is presented below.

#### Variant1 (V1): Estimation of $T_{UUT}$ using two measurement signals

The estimation of the unknown engine torque is done using $\omega_E$ and $T_{shaft}$ as measurement signals. The system description thereby involves only the combustion engine and therefore requires only the inertia of the combustion engine as parameter as given in equation (3.51). The state vector (scalar in this case) takes the form $x(t) = \begin{bmatrix} \omega_E \end{bmatrix}$

$$\dot{\omega}_E = (J_E)^{-1}\omega_E - (J_E)^{-1}T_{shaft}, y = \omega_E \tag{3.51}$$

#### Variant 2 (V2): Estimation of $T_{UUT}$ using three measurement signals

The variant V2 includes the coupling and the dynamometer in the system, enlarging the system boundary. Based on the configuration employed, the available measurement signals used for the observer can vary. The system is described by equation (3.50) with the state vector $x^T(t) = \begin{bmatrix} \Delta\phi & \omega_E & \omega_D \end{bmatrix}$ and system matrices are given by equation (3.52) respectively.

The Table 3.1 summarizes the configurations that differ based on the measurement signals used for estimation. Inputs and outputs here refer to the interfaces of the observer which are measurement signals. Methods developed in [91] can be used to estimate these parameters in closed loop operation using Error-In-Variables stochastic framework.

$$A = \begin{bmatrix} 0 & -1 & 1 \\ \frac{c}{J_E} & -\frac{b}{J_E} & \frac{b}{J_E} \\ -\frac{c}{J_D} & -\frac{b}{J_D} & \frac{b}{J_D} \end{bmatrix}, B = \begin{bmatrix} 0 \\ -\frac{1}{J_E} \\ 0 \end{bmatrix}, F = \begin{bmatrix} 0 \\ 0 \\ \frac{1}{J_D} \end{bmatrix}, \tag{3.52}$$

**Variant 2.1 (V2.1): Estimation of $T_{UUT}$ using $\omega_E$, $T_{Dact}$ and $T_{shaft}$**

This variant uses the dynamometer torque as input and the outputs of the UIO are engine speed and shaft torque.

$$C = \begin{bmatrix} 0 & 1 & 0 \\ 0 & 0 & 1 \\ c & -b & b \end{bmatrix} \tag{3.53}$$

**Variant 2.2 (V2.2): Estimation of $T_{UUT}$ using $\omega_E$, $\omega_D$ and $T_{shaft}$**

This variant does not use any input. But it uses engine and dynamometer speed as well as the shaft torque. The inputs acting on the system can only be torque sources acting on the inertia in the system. As only the shaft torque is used, which is result of the dynamic operation of the combustion engine, it is not suited as an input in the UIO design.

$$C = \begin{bmatrix} 0 & 0 & 1 \\ c & -b & b \end{bmatrix} \tag{3.54}$$

**Variant 2.3 (V2.3): Estimation of $T_{UUT}$ using $\omega_E$, $\omega_D$ and $T_{Dact}$**

This configuration does not require the measurement of shaft torque and is attractive from the cost viewpoint, as the extra investment on the shaft torque sensing is not required. The dynamometer torque is used as an input. The speeds at both the combustion engine inertia and the dynamometer inertia are used as outputs. It is also suitable for End-Of-Line testing environment at the engine production line.

$$C = \begin{bmatrix} 0 & 0 & 1 \\ 0 & 1 & 0 \end{bmatrix} \tag{3.55}$$

## 3.4 Estimator

Estimators filter the non-periodic mean value from the signal corrupted by harmonics and noise. It can be used for harmonically corrupted noise signals and is not restricted to torque, speed signals but signals such as acceleration can be also be processed. It comprises a fixed window-size low-pass filter (LPF) component and linear parameter variant (LPV) component. The task of the LPF component is to

estimate the mean-value from its input. The input of the LPF component contains the noisy signal without the harmonics. The harmonics that are estimated by the parameter variant component are removed from the noisy signal before it is fed to the LPF component. Hence the task of the LPF component is to estimate the mean value from the noisy signal. The structure employed for the estimator is shown in the Figure 3.2. The proposed structure offers flexibility in the choice of LPF realization, which can be exploited later in the implementation phase. Choice of LPF can be done taking advantage of the well-developed theory of digital filter design [92]. Thanks to the time triggered operation of the estimator, it does not require sampling based on a trigger from an incremental encoder as in CASMA approach [93]. The model used for the estimation of the mean and harmonic content is simple, parameterized only using the cutoff frequency of the low pass filter and the order of the required harmonic. As a consequence, robustness with respect to model parameters is not an issue.

Implementation of estimator requires the choice of a low pass filter component used to estimate the mean value of the signal. [85] uses Finite Impulse Response (FIR) filters along with Running Average filter, but this work uses an Infinite Impulse Response (IIR) Filter. The choice of IIR filter is motivated by its ability to meet specifications with lower filter order than corresponding FIR realizations. The IIR filter is also termed as a recursive filter as the output of the filter is feedback.

The choice of an FIR filter not only leads to a filter of higher order compared to IIR realizations but also lead to a comb-type gain frequency response [92], resulting from finite term approximation of the impulse response using windows. Further IIR filter can be designed by mapping the characteristics of analog filtering of the mean value signal to digital filter [92]. As there is no adaptation of neither the coefficients nor the order of the filter, stability issues due to the usage of IIR filters do not exist. One disadvantage of IIR filters is the nonlinear phase response, however, approximations such as Bessel filter can be used to obtain linear phase relationship, otherwise termed as constant group delay property [92]. Nevertheless, IIR filters have a better frequency response which sharper roll-offs and can be designed to be of minimum phase. IIR filters are suitable for applications insensitive to phase information, in case of filtering the mean value from the noisy signal. The bandwidth of the filter can be tuned to block out frequencies higher than the harmonics of interest in case of a harmonically corrupted signal.

### 3.4.1 Low pass filter component

As discussed, the LP component is realized as an Infinite Impulse Response (IIR) filter with a discrete time representation given by the equation (3.56). The corre-

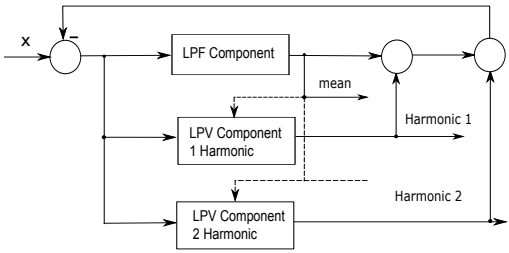


**Figure 3.2:** Structure of a (generic) harmonic estimator with the low pass filter as well as linear parameter varying component for the first and second harmonics

sponding Z-domain representation and the frequency response are given by equation (3.57).

$$y(k) = b_0 x(k) + ... + b_{N_x-1} x(k-N_x+1) - a_1 y(k-1) - ... - a_{N_y} y(k-N_y) \quad (3.56)$$

$$H(Z) = \frac{\sum_{i=0}^{N_x-1} b_i z^{-i}}{1+\sum_{k=1}^{N_y} a_k z^{-k}}, H(e^{j\omega}) = \frac{\sum_{i=0}^{N_x-1} b_i e^{-j\omega_i}}{1+\sum_{k=1}^{N_y} a_k e^{-j\omega_k}} \quad (3.57)$$

Any filter design method can be used to compute the LP filter. As solutions of linear differential equations involve exponentials with infinite durations, all analog filters are invariantly IIR. Hence analog filters can be for example designed which later can be transformed to the digital domain using the bilinear transformation. The equation (3.58) expresses the bilinear transformation pair for a sampling period $T_s$.

$$z = \frac{2+sT_s}{2-sT_s}, s = \frac{2(1-z^{-1})}{T_s(1+z^{-1})} \quad (3.58)$$

A first order IIR filter was chosen and direct form implementation was used as given by the equations (3.59) and (3.60). The equation (3.59) presents the discrete-time version and uses a simple structure with just a single pole with a unit steady-state gain. The value $k_0$ is the single design parameter which can be tuned to trade-off between the dynamics of the filter and the noise cancellation characteristics. The representation in continuous time is given by equation (3.60) with $\tau$

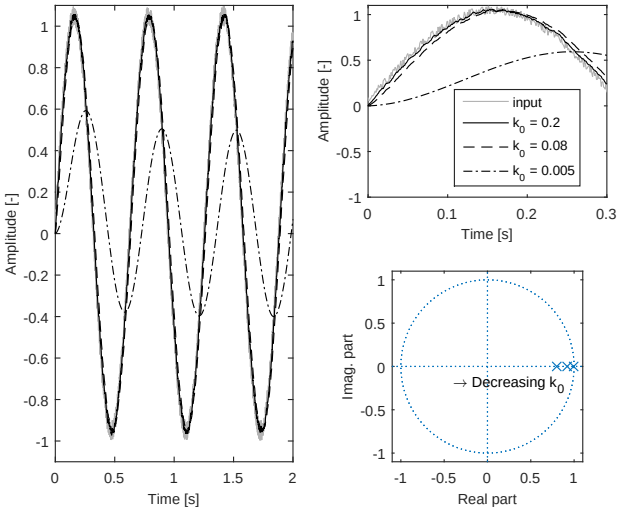


**Figure 3.3:** Dynamics of the low pass filter component in case of mean value estimation of a noisy sinusoidal signal

denoting the time constant of the filter. The equivalence between the parameters $k_0$ and $\tau$ can be derived using the transformation given in equation (3.58). The representation in continuous time is presented for better understanding and is used for stability analysis of the estimator along with the output regulation controller discussed in chapter 7.

$$LP(Z) = \frac{k_0}{Z - 1 + k_0} \tag{3.59}$$

$$LP(s) = \frac{\tau}{s + \tau} \tag{3.60}$$

A filter with better dynamics would have poor noise rejection and vice versa. This fact shall be illustrated with an example of noisy mono-frequent sinusoid being filtered by the LPF component. Figure 3.3 presents the result of parameter variation of $k_0$ that defines the dynamics of the estimator. Both time domain plots along with the location of the pole in the Z-plane is depicted. With decreasing value of $k_0$, the pole approaches the unit circle, which can be interpreted equivalently as an integrator in the continuous time. This behavior is reflected in the time

domain plot with the value of $k_0 = 0.005$ the output of the filter closely resembles an integrated input signal. One advantage of the smaller value of $k_0$ is better noise rejection but it suffers from slow dynamics. With an increasing value of $k_0$ (inversely proportional to $\tau$), the output better tracks the input, however, suffers from poor noise rejection.

This analysis in the simulation gives an insight into the design of the LPF component. The parameterization of the LPF component which trades-off between dynamics and noise rejection is performed at the test bench specifically based on the noise effects of the used measurement signal.

### 3.4.2 Linear parameter variant component

The core idea of the LPV component is to generate an orthogonal system for each set of signal harmonics. The second order generalized integrator (SOGI) presented in [94] can be represented in Laplace domain as shown in equation (3.61), with a resonant frequency at $\omega = 2\pi f$.

$$G(s) = k\frac{s}{s^2 + \omega^2} \tag{3.61}$$

The closed loop expressions involving the SOGI to obtain the corresponding direct and quadrature axis components with a gain of $k_d$ and $k_q$ from the error to the state of the direct and quadrature components respectively are shown in equations (3.62) and (3.63) respectively [94].

$$G_d(s) = \frac{k_d s - k_q \omega}{s^2 + k_d s + \omega^2 - \omega k_q} \tag{3.62}$$

$$G_q(s) = \frac{k_q s + \omega k_d}{s^2 + k_d s + \omega^2 - \omega k_q} \tag{3.63}$$

The expression $G_d$ is the transfer function from the input to the direct axis component and $G_q$ refers to the expression of the transfer from the input to quadrature component which is 90 degree phase shifted to the direct axis component. As it can be seen from the expressions, the value of the frequency corresponding to the

harmonic is required for estimating the amplitudes of the direct and quadrature axis components. This frequency is computed by the low pass filter component.

$$A = \begin{pmatrix} 0 & -\omega \\ \omega & 0 \end{pmatrix}, \; C = \begin{pmatrix} 1 & 0 \end{pmatrix} \tag{3.64}$$

$$(A - LC) = \begin{pmatrix} -k_d & -\omega \\ \omega - k_q & 0 \end{pmatrix} \tag{3.65}$$

The gain values in the expressions in equations (3.62) and (3.63) as computed assuming a constant value of $\omega$, to get expressions which are frequency dependent to enable its tuning under frequency varying situations. The gain computation uses pole placement expressions for the classical Luenberger observer. Let the system matrix be denoted by $A$, output matrix by $C$ with the expressions as shown in equation (3.64). As it can be seen in the expression for $C$, only the direct components are measured. The computation of eigenvalues of the observer are shown in equations (3.65-3.69).

$$(\lambda I - (A - LC)) = 0 \tag{3.66}$$

$$\begin{vmatrix} \lambda + k_d & \omega \\ -\omega + k_q & \lambda \end{vmatrix} = 0 \tag{3.67}$$

$$\lambda^2 + k_d\lambda - \omega k_q + \omega^2 = 0 \tag{3.68}$$

$$\lambda = \frac{-k_d \pm \sqrt{k_d^2 - 4(-k_q\omega + \omega^2)}}{2} \tag{3.69}$$

$$= \frac{-k_d}{2} \pm \frac{1}{2}\sqrt{k_d^2 - 4(-k_q\omega + \omega^2)} \tag{3.70}$$

Based on the internal model principle, as one tries to have the same frequency in the model as in the harmonics of the real system, the oscillatory modes of the model shall have the value of the harmonic frequency.

$$\begin{aligned} \frac{1}{2}\sqrt{k_d^2 - 4(\omega^2 - k_q\omega)} &= j\omega \\ k_d^2 - 4(\omega^2 - k_q\omega) &= -4\omega^2 \\ k_d^2 + 4k_q\omega &= 0 \end{aligned} \tag{3.71}$$

Let $k_d$ and $k_q$ be parameterized using single parameter $\alpha$ (which is the only degree of freedom).

$$k_d^2 + k_q^2 = \alpha \tag{3.72}$$

$$\alpha - k_q^2 + 4k_q\omega = 0$$

$$k_q = 2\omega \pm \sqrt{4\omega^2 + \alpha} \tag{3.73}$$

Equation (3.73) has two signs for the expression $k_q$ and can be reformulated as in equation (3.74). In order to arrive at the proper sign, the expression (3.69) shall be considered. The term in equation (3.74) is the square root term in equation (3.69) which shall lead to imaginary roots which requires a negative sign of the expression (3.74), hence negative sign is chosen in equation (3.73), resulting in an equation for tuning the gains.

$$\underbrace{-k_q\omega + \omega^2}_{\text{square term}} = -\omega^2 \mp \omega\sqrt{4\omega^2 + \alpha} \tag{3.74}$$

$$\lambda_{1,2} = \frac{-k_d \pm \sqrt{k_d^2 - 4(-k_q\omega + \omega^2)}}{2} \tag{3.75}$$

$$-k_q\omega + \omega^2 = -\omega^2 \mp \omega\sqrt{4\omega^2 + \alpha} \tag{3.76}$$

The tuning expressions for $k_d$ and $k_q$ are given by equations (3.78-3.79). If the second harmonic is to be estimated, the value of $\omega$ shall be doubled and the corresponding gains have to be computed online. Hence the ease of tuning the LPV component for the different harmonic components present in the signal is discussed.

$$\pm\omega\sqrt{4\omega^2 + \alpha} > \omega^2 \tag{3.77}$$

$$k_q = 2\omega - \sqrt{4\omega^2 + \alpha} \tag{3.78}$$

$$k_d = \sqrt{\alpha - k_q^2} \tag{3.79}$$

The harmonic estimator shall be used to estimate the mean values of speed and torque signals. The correlation between the mean value of the speed signal and the higher harmonics shall be used for speed estimation, this shall be presented in case of ICE mean speed and torque estimation. In case of 4-stroke engines with $z_{cyl}$ cylinders, the frequency of the dominant harmonic in Hz ($f_{mean}$) can be computed using the mean operating speed $n_{mean}$ as given in equation (3.80). The higher

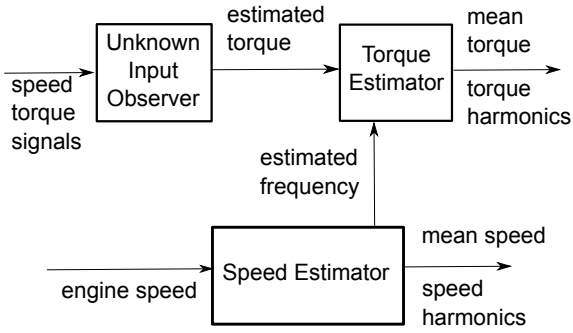


**Figure 3.4:** Proposed structure for the estimation of mean and harmonic torque values using the developed UIO and harmonic estimator

harmonics are multiple of the mean frequency $f_{mean}$. Based on the harmonic of interest, the matrix $A$ as in equation (3.64) of the LPV component can be extended for multiple components.

$$f_{mean} = (n_{mean} \times z_{cyl})/120 \tag{3.80}$$

However, the discussed correlation between mean value and harmonics does not exist for torque signals. In such case the harmonic frequency is computed from the mean speed and is used to estimate the unknown amplitude of the mean value and the harmonics of the torque signal. This is depicted in the structure of the UIO and estimator in Figure 3.4.

The model used for the estimation of the mean and harmonic content is parameterized only using the cutoff frequency of the low pass filter and the order of the required harmonic. As a consequence, robustness with respect to model parameters is not an issue. For deployment at the (industrial) test benches for rotatory energy converters, the observer shall be able to function in a noisy environment. It also requires implementation with a minimal memory and computation demand which are satisfied by the developed filtering techniques.

## 3.5 Validation of the developed Filtering Techniques

The proposed filtering techniques are validated using dynamic simulation models before implementation on the experimental test benches. Experimental validation is performed at ICE test bench with a 4-cylinder diesel ICE and hybrid powerpack

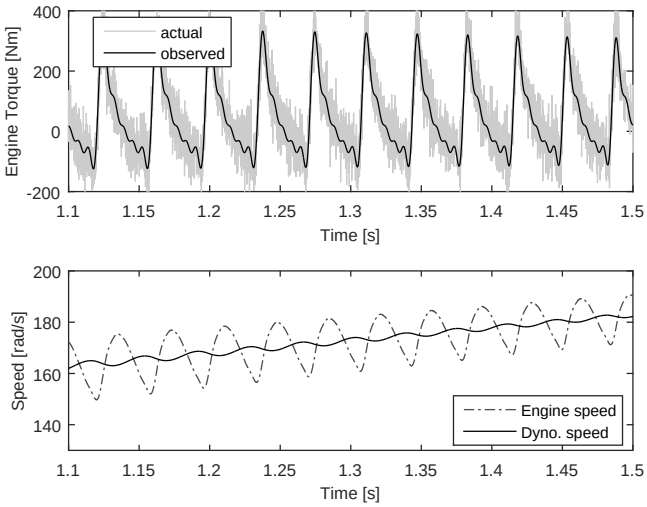


**Figure 3.5:** Estimated engine torque based on engine speed, dynamometer speed and dynamometer torque value in simulation using the 2-cylinder gasoline engine model

test benches with the CEA powertrain [95] coupled to an eddy current dynamometer. The developed filtering scheme as in Figure 3.4 is implemented on the real-time system with a sampling frequency of 1 kHz. The model used in the observer is parameterized using techniques presented in [91]. The manipulated variables in the model and the test bench are the dynamometer speed and the pedal value corresponding to the torque generated by the UUT. Torque acting on the inertia of the ICE and the dynamometer is denoted by $T_{ICE}$ and $T_{Dact}$ respectively. The speed of the inertia is represented by $\omega_E$ and $\omega_D$ respectively. The value of shaft torque is denoted using $T_{shaft}$. Quantities $J_E$ and $J_D$ are inertia of ICE and dynamometer respectively. The stiffness of the shaft is denoted by $c$, its damping is represented as $d$ and angular deflection be $\Delta\phi$.

The design of the internal engine torque observer for operation in the engine test bench assumes a two-mass oscillator system approximation for the relevant frequency band of interest. This assumption is validated using measurements and non-parametric identification techniques [91]. Figure 3.5 presents the results of validation of UIO Variant V2.3 (in table 3.1) using simulation. The engine torque is estimated using $\omega_E$, $\omega_D$ and $T_{Dact}$. To account for process noise in the simulation study, Gaussian white noise has been added to the combustion torque generated

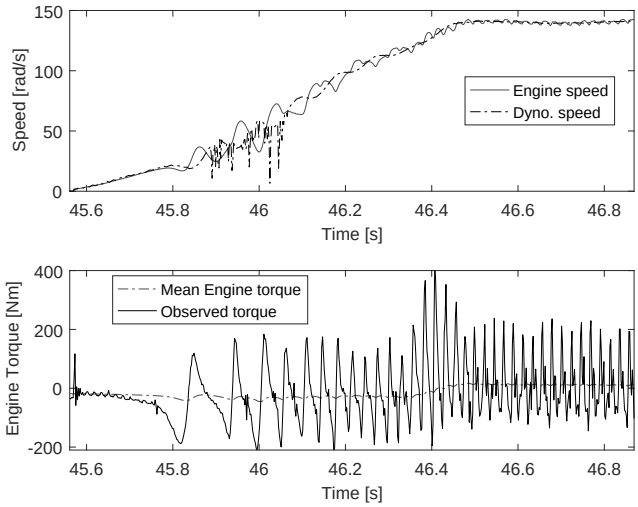


**Figure 3.6:** Estimated engine torque and its mean value based on engine speed and shaft torque measurements during start up of a 4-cylinder diesel engine at the engine test bench.

by the model. The speed of the engine is ramped using speed controller at the dynamometer and it can be seen that the internal torque of the ICE is recovered in the presence of noisy measurement signals. The rotational irregularity of the ICE visible in its speed signal is a measure of validity of the model. As the speed is ramped up the torque peaks in the ICE torque come closer due to higher ignition frequency associated with the higher engine speed.

Validation of the ICE at the experimental test bench shall be restricted to V1 (in table 3.1) due to the availability of the shaft torque measurement flange at the engine test bench for diagnostic purposes. One important event during the ICE operation is the start-up of the engine, which gains further importance in the engine is part of a hybrid powertrain due to start/stop operation.

Figure 3.6 displays the estimates obtained using the combination of UIO and estimator. The engine is started and operated at the idling speed. The distortions on the dynamometer speed signal are noise effects and do not influence the performance analysis as the signal is not being used by the filters. Both the dynamic estimated torque and its mean value are presented. The engine is ramped to a

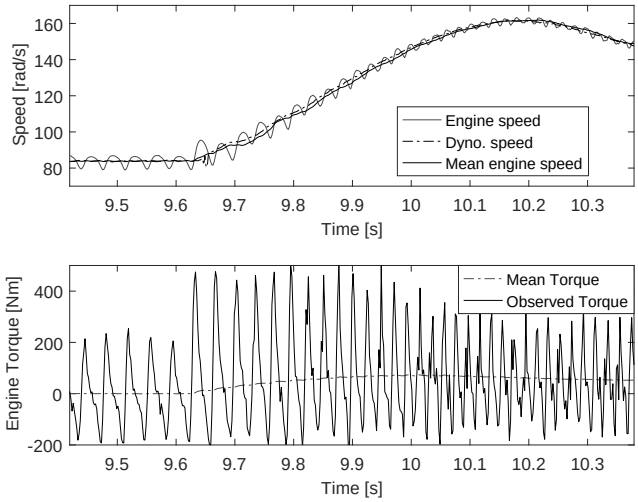


**Figure 3.7:** Mean value and dynamic estimates of the combustion engine torque and speed signals during transient operation of the 4-cylinder diesel engine at the engine test bench

speed higher than the idling speed using the dynamometer without employing the ICE starter motor. It can be seen that the observer reproduces not only the torque during firing of the engine but also estimates the torque during motoring of the ICE. Furthermore, the beginning of the combustion around 46.4 seconds can be observed with the high torque pulses. The ICE speed at this instant is the speed at which the injected fuel is ignited and the ICE is capable of accelerating to idling speed. It can also be seen that the mean torque is negative during motoring and positive during fired ICE operation.

The transient operation of the ICE speed is depicted in Figure 3.7. The ICE speeds with cyclic irregularity from measurements and its mean value from the estimator which closely follows the measured speed can be observed. In addition, the speed of the dynamometer is also displayed. During this speed transient, the pedal value demand to the engine is increased at 9.62 seconds to a mean engine torque value of 65 Nm. This results in higher mean value and dynamic torque from the ICE. After 10 seconds, the pedal request is reduced which is reflected by lower combustion torque both in its dynamic and mean values.

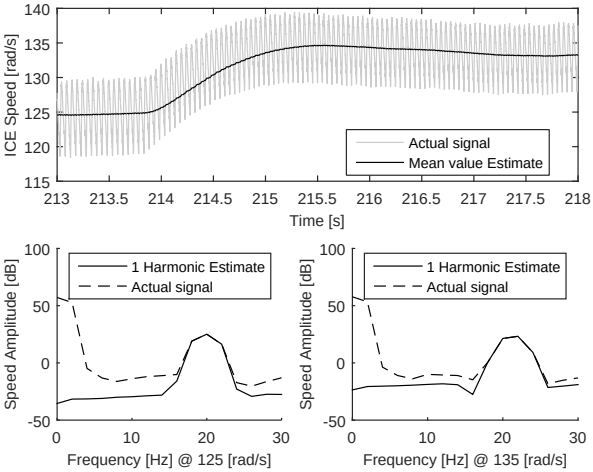


**Figure 3.8:** Mean value and harmonic estimates of the combustion engine speed signals during step speed change of the 2-cylinder gasoline engine at the powerpack test bench

The performance of the harmonic estimator in case of a 2-cylinder combustion engine is presented in Figure 3.8. A step change in speed is triggered at 213.8 seconds. The mean value estimate of the ICE speed signal tracks the actual speed signal. The plots at the bottom present the Welch spectral estimate of the harmonic estimate before and after the step change and the welch spectral estimates of the actual ICE speed signal is also displayed for comparison. The actual speed signal contains the power at zero frequency corresponding to the mean speed. Comparing the spectral estimates of the actual and first harmonic speed, it can be concluded that the power in the harmonic estimates reflects the signal power in the actual signal corresponding to the harmonic frequencies.

Estimation of the ETM speed signal is studied with a powerpack test bench, comprising of a 2-cylinder ICE and ETM coupled using a hydraulically actuatable friction clutch. The test bench is operated initially only with the ETM coupled to an eddy current dynamometer. Around 36 seconds, the clutch is closed and the ICE is ramped to speed. Due to the increased inertia and additional friction due to the ICE, a drop in the ETM speed signal can be observed. After the ICE start, the pedal value for torque request is provided to it. It can be seen in the speed signal that the oscillations due to ICE operation result in a more oscillatory signal, which is filtered using the mean speed estimator. It can be seen that the mean value signal

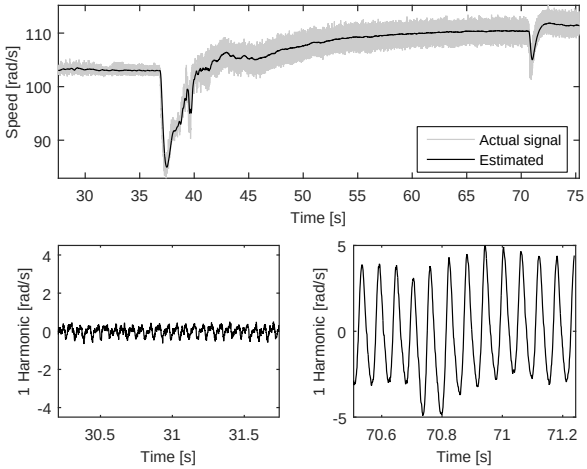


**Figure 3.9:** Mean value and estimates of the first harmonic of the electric machine speed with coupled and decoupled state of the 2-cylinder gasoline engine at the powerpack test bench

closely follows the oscillatory signal also during transients. In addition to the mean value estimation, the dominant harmonic of the speed signal is also estimated. As it can be seen the value of the first harmonic, which is the dominant one is nearly zero during operation with a decoupled ICE. After the ICE start, the value of the dominant harmonic is estimated and further, it also follows the speed transients.

The filtering techniques presented are not just restricted to energy converters for onboard /in-vehicle purpose. They can also be used for estimating shaft torque and also filtering torque generated by loading devices. The discussion of the results hitherto was limited to speed and torque signals of the ICE which shall be extended to torque measurements at the shaft.

Figure 3.10 presents the results of the filtering technique in case of torque signal from the measurement flange HBM T10F. The same scenario with the start-up of the 2-cylinder engine is considered. The top plot presents the actual torque measurements and the filtered mean value torque. In addition to the rejection of noise effects and the harmonics resulting from the operation of the 2-cylinder engine, the mean torque value follows the actual measurements during step changes and during transient operation.

The spectral representation displays the signal power in the first harmonic and second harmonics of the torque signal, computed from the first harmonic estimate. The signal power in the harmonics clearly follows the mean speed of operation depicted in Figure 3.9 due to the correlation between the spectral content of harmonics and the mean speed. The last row of plots show the estimated mean and harmonic torques in the time domain. Irrespective of the actual torque signal, both the mean value and the harmonics are estimated.

The trade-off between the dynamics of the LPF component presented in section 3.4.1 is investigated at the experimental setup and the results are presented in Figure 3.11. The combined structure of the UIO and the estimator as shown in Figure 3.4 is used to estimate the non-periodic mean value torque of the 4-cylinder gasoline engine. The engine test bench used for the investigation was operated with pedal value and dynamometer speed as set value signals. The resulting estimate of the mean value torque for different parameters of the LPF is shown in the top plot. The estimated torque tracks the set torque value commanded indirectly by the set value signals. As it can be seen in the top plot, the noise rejection depends on the value of $k_0$.

Though the mean value torque appears to be extremely noisy, a comparison of the estimated mean value with the UIO dynamic torque in the bottom right plot shows that the noise effects are negligible compared to the dynamic torque. The effect of the $k_0$ from equation (3.59) on the dynamics is presented in the bottom right plot. A behavior as presented in section 3.4.1 on the analysis of LPF parameterization can be observed. With a reduced value of $k_0$, the estimator better tracks the dynamic variations better than higher values of $k_0$. This is of specific interest for the realization of a controller based on the estimated mean torque values to ensure stable operation of the controller. In the scenario, with the considered parameterization a value of $k_0 = 0.08$ provides sufficient noise rejection and good tracking behavior.

The developed observer shall compute the dynamic torque over the bandwidth of interest. During ramp-up of the engine speed at the engine test bench, the spectrum of the engine torque signal corresponds to the mean speed of operation as given in equation 3.80. This fact is used for the investigation of the performance of the torque observer over the bandwidth of interest. The (mean) engine speed is linearly ramped from 1000 rpm to 1500 rpm over a time interval of 10 seconds using the commanded dynamometer speed. The plots in the first row of Figure 3.12 presents the variation of the speed over time. The plots in the bottom row present the corresponding observed dynamic torque over the same time interval for a pedal value of 15%.

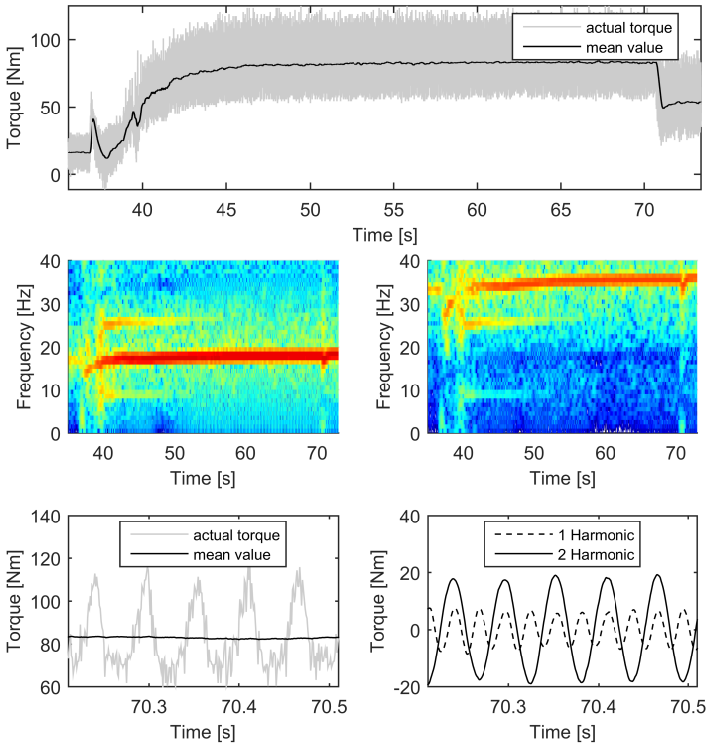


**Figure 3.10:** Mean value and harmonic estimates of the shaft torque signal during transient operation of the 2-cylinder gasoline engine at the powerpack test bench

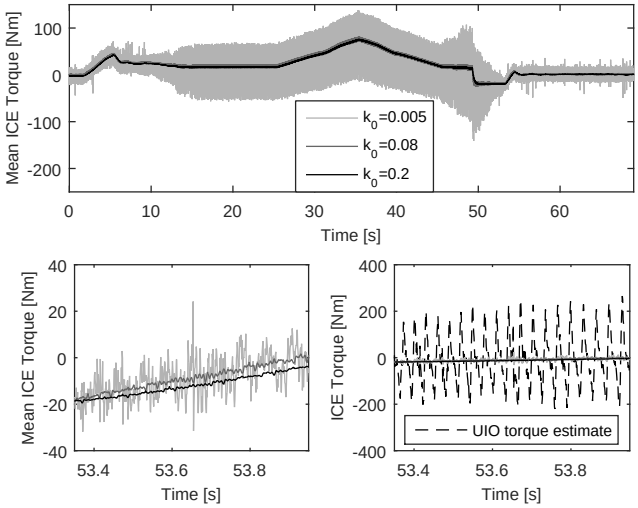


**Figure 3.11:** Dynamics of the low pass filter component for estimation of the ICE inner torque of the 4-cylinder diesel engine at the engine test bench

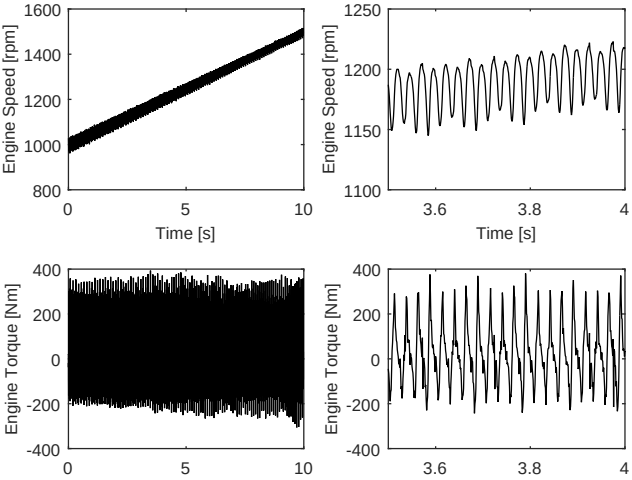


**Figure 3.12:** Time domain representation of the UIO dynamic engine torque estimates during speed ramp from 1000 rpm to 1500 rpm in 10 seconds of the 4-cylinder diesel engine at the engine test bench

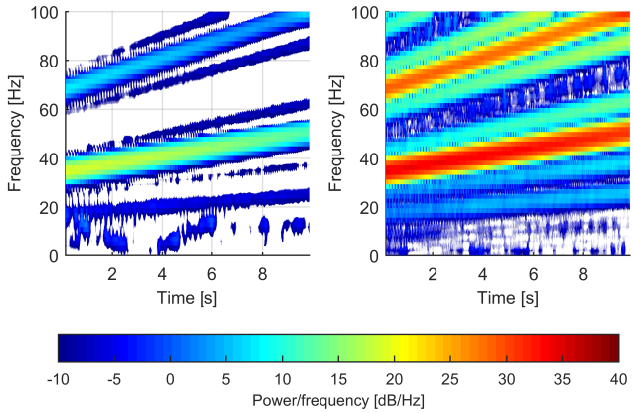


**Figure 3.13:** Spectral analysis of the engine speed and UIO ICE torque estimate during speed ramp from 1000 rpm to 1500 rpm in 10 seconds using the 4-cylinder diesel engine at the engine test bench

Figure 3.13 presents the spectrogram of the engine speed and the observed dynamic torque for the boundary conditions discussed in Figure 3.12. The spectral representation on the left and right side are of the engine speed and observed engine torque respectively. Power at the frequency ramps corresponding to the transient speed of operation can be clearly identified in both the spectral analysis of speed and torque values. Both the second and fourth harmonics corresponding to the speed transient have higher signal power in case of both the signals. The higher amplitude of the engine torque is reflected in the higher signal power in its spectral representation compared to that of the engine speed signal. The engine test bench is excited by the dominant harmonic of the engine torque during normal operation. The frequency of this excitation depends on the current engine operating speed. In addition, due to integration with real-time capable simulation models in the context of In-The-Loop test bench, additional frequency components can occur in the set value signals. Different architectures have been investigated ([74] and references therein) for the realization of such In-The-Loop test benches.

One commonly used architecture is a torque feedback from the test bench to the simulation model and speed command from the simulation model to the test bench. This architecture is realized at the test bench using torque measurements or observed inner torque and the commanded speed signal is realized using the dy-

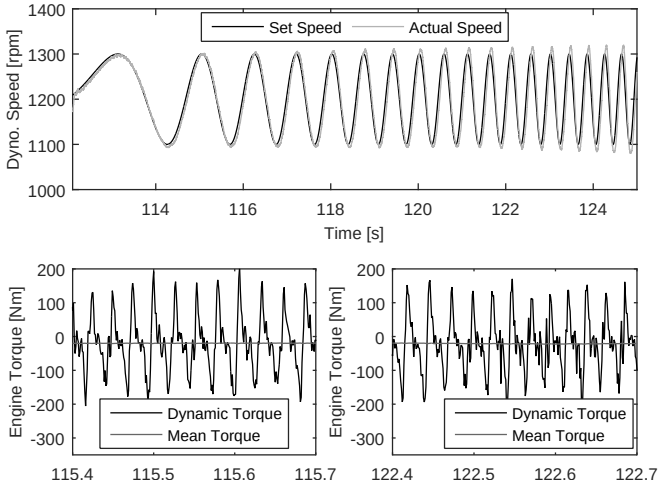


**Figure 3.14:** Analysis of the dynamic and mean value torque estimates of the 4-cylinder gasoline engine at the engine test bench with the superimposed swept sinusoidal signal on the dynamometer set speed value

namometer speed controller. Stationary and transient investigation of the observer does not involve additional excitations which can result from the In-The-Loop operation.

In order to study the performance under such boundary conditions, a chirp signal can be modulated on the set speed of the dynamometer. This investigation is performed with a motored engine with a linear chirp / swept sinusoidal of amplitude -/+ 100 rpm superposed on the mean dynamometer set speed of 1200 rpm. The generated engine torque depends on the ECU calibration and usually a function of the pedal value and operating speed. Due to the variation of the speed during this analysis, with a fixed pedal value there can be a variation of the dynamic torque generated by the engine, which is usually unknown and depends on factors such as engine temperature and condition of the after-treatment system. In order to avoid the influence of such effects, the investigation uses a zero pedal value or motored engine operation. During the motoring of a warm engine, the dynamic torque results from the inertial torque, gas torque due to compression and the friction torque. Further, the mean value of the torque during motoring operation can be determined by operating the engine at the dynamometer for the desired set speed value.

The set speed signal is shown in the top plot of Figure 3.14. The maximum rate of change of frequency of the chirp signal is bound by two factors. The absolute maximum frequency is given by the bandwidth of the simulation model as well as of the dynamometer speed controller. In addition, the dynamics of the controller has to be considered during the choice of the maximum rate of change of frequency. The investigation used a sweep from 5 Hz to 20 Hz in 20 seconds. The bottom plots present the dynamic and estimated mean torque values during two different time windows with corresponding frequency values resulting from the sinusoidal sweep. The observed dynamic torque does not show the influence of the additional swept sinusoidal modulation. This can be verified by the periodicity of the dynamic torque from the different time windows. Further, the mean value estimate coincides with the measured value of -20 Nm for the engine at an operating speed of 1200 rpm irrespective of the frequency variation of the modulated sinusoid.

The proposed approach for the estimation of dynamic, mean and harmonic components of a noisy oscillatory signal is computationally efficient. It does not require a choice of basis functions depending on the shape of combustion torque as in [72] and benefits from the lower order of IIR filters requiring lower order than equivalent FIR filters proposed in [85]. In summary, the experimental investigations demonstrate not only good performance in estimating the dynamic signals using UIO as well as noise rejection in computing the mean value but also good tracking of the harmonics.

## 3.6 Conclusion

This chapter discusses filtering methods for dynamic and non-periodic mean value as well as harmonic estimates of harmonically corrupted signals specific to automotive energy converters. By partitioning the inputs into known and unknown quantities, UIO has been developed. The approach differentiates between the inputs that are known and unknown quantities and employs a UIO.

UIO was designed in continuous-time, suitable discretization was chosen for testbed implementation based on the desired dynamics of the observer. Synthesis of the UIO can be performed using classical and LMI based approaches. In addition to the absence of restrictions due to regularity conditions, UIO design using LMI approach can deal with systems with Lipschitz nonlinearities. Such nonlinear behavior which can be observed in the sector dependent stiffness characteristics desired at certain test benches. The developed methods are additionally capable of reconstructing the systems state along with estimating the unknown inputs under operation with unknown inputs. The efficacy of the UIO was demonstrated using

simulations and experiments with a 4-cylinder diesel engine as well as a 2-cylinder gasoline engine.

An estimator was developed exploiting the harmonic dependencies of the signals especially in case of ICE resulting from the combustion process. The estimator employs a low pass filter and linear parameter varying component, which is tuned based on the mean operating speed. The method is not only restricted to combustion engines or speed signals but can also be employed for other reciprocating machines and systems corrupted by harmonically related components. As the estimator uses the information of the harmonics present in the signal, the presence of subharmonics poses a challenge. Nevertheless, for the studied applications this is not a major issue due to the operational symmetry in the processes generating the oscillatory signal. This was shown experimentally in case of an electric traction machine speed on a powerpack test bench and shaft torque measurements. The proposed method for estimating the non-periodic mean and the harmonics provides consistent estimates both during steady and transient operation.

## 4 Closed Loop Identification of Torsional Dynamics

This chapter deals with the aspects of system identification of torsional dynamics. System identification is a procedure of deriving a model of a system using measurement data. The core idea is based on the fact that any measured output as a consequence of applied excitations of a system is constituted by deterministic and stochastic components. The objective of the identification task is to separate the deterministic components from the stochastic influences to characterize the dynamics of the underlying system. Due to the reasons mentioned below, the identification techniques developed in this chapter shall focus on the characterization of torsional dynamics at experimental test benches.

- The identification process involves the excitation of the torsional powertrain system using excitation signals. The response resulting from the system is studied with the input signals to obtain a characterization of the system. In the case of automotive powertrains, such excitation process can be performed only in the development stages. The reason being, the excitation of the torsional powertrain integrated in the vehicle, can cause passenger discomfort and unexpected vehicle/powertrain behavior from the driver perspective. The element of surprise to the driver is due to the fact that the excitations are usually not triggered by the driver rather by the specific functionality and may lead to dangerous situations depending on the driver's skill and the driving situation where the excitation is initiated.
- Torsional system identification is of specific importance in the context of engine/powerpack test benches, where the characterization of the test bench dynamics is a prerequisite for its operation and also for the extension of its capabilities using simulation. This shall be further discussed in section 4.1.
- Non-availability of the vehicle to perform in-vehicle identification.

This chapter is organized as follows. Section 4.1 introduces the problem of identification of test benches and presents a review of the related literature. The measurement setup for identification along with the discussion on the used excitations and the applied identification methods are presented briefly in section 4.3. Section 4.4 describes the developed identification methods for engine and powerpack test benches as well as the measurement strategy employed. Validation of the developed methods using Monte Carlo simulations and experimental data are discussed in section 4.5. Section 4.6 finally concludes this chapter with use cases to demonstrate the practical significance of the developed identification techniques, followed by concluding remarks.


**(a)** Engine Test Bench

**(b)** Powerpack Test Bench

**Figure 4.1:** Schematic of the engine and powerpack test benches

## 4.1 Identification of Engine and Powerpack Test Benches

Test benches were traditionally employed for initial calibration/testing at different stationary operating points of the UUT. These procedures have been extended to transient maneuvers derived from/related to real-world driving scenarios. The basic mechanical structure of such a test bench consists of a UUT coupled to a loading machine (commonly referred to as dynamometer) by a flexible shaft.

With the increasing complexity of the development tasks coupled with shorter developmental cycles, flexible development environments that can emulate real-world driving scenarios is necessary. In-The-Loop environments offer the flexibility of combining both simulated dynamics of the process with the real components controlled in a test setup hence ideally suited for future powertrain development tasks. Engine and Powerpack-In-The-Loop test benches are experimental setups which are an extension of the Engine and Powerpack test bench with simulated dynamics.

A common prerequisite for both transient operation in case of stand-alone test benches and better transferability of real driving scenarios to In-The-Loop test benches is understanding of their dynamic behavior. One common bottom-up approach is to use parameters from the component data sheets to explain the test bench dynamics. This may lead to insufficient or misleading characterization due to the wrong parameterization as the integration of the UUT to the test bench requires among others mechanical adaptation. Further, measurement equipment contributes to influences that can be better identified using in-situ measurements. Test benches also exhibit a variation of behavior based on aging and loading related effects specifically in case of endurance run test benches. These effects can be monitored and countermeasures can be implemented by identification techniques at the corresponding test setups.

The terminologies engine and powerpack test benches shall be clarified before further discussion. Engine test bench refers to the test bench configuration with the ICE as the UUT mechanically coupled to the dynamometer. In the case of the powerpack test bench, additional powertrain components can be integrated with the test bench, which may not even be prime movers. The main difference here is the presence of additional inertia not stiffly coupled to the rotating masses of the engine and the dynamometer. In the case of hybridized powertrains in the parallel configuration, both the ICE and ETM can be physically coupled to the dynamometer. A powerpack test bench in case of a conventional powertrain may comprise of ICE along with the clutch and the transmission unit. Figure 4.1 depicts the schematic of both the test bench configurations with the coupling realized using shafts. The discussion in this study refers to the test benches of the described configuration. However, the identification techniques presented are applicable also to other configuration of test benches with stiff or non-stiff coupling between the UUT and the loading machine. The UUT need not be a prime mover and can be a powertrain component such as a transmission unit in the case of powerpack test benches.

## 4.2 Overview of related studies

In [96] test bench dynamics is identified by linear chirp with an unfired combustion engine in the frequency range 0 rad/s $\leq \omega \leq$ 3000 rad/s. The excitation was realized using the electric dynamometer torque with 10 kHz sampling frequency. The identification was restricted to the computation of the non-zero eigenfrequencies of the three inertial torsional oscillatory system approximation fitting the measured system response to the response from the model.

The approach in [97] identifies a Multiple Input Multiple Output (MIMO) model of the test bench for an input vector comprising of current input to the dynamometer and throttle input to the combustion engine, to the output vector consisting of the shaft torque and speed of the dynamometer. The excitation was realized using multi-sinusoidal signals at arbitrarily selected operating points. The excitation was performed by excitation of one input at a time, while the other input is maintained at its mean value using dynamometer current and ICE throttle signal. Identification of frequency responses used H1 spectral estimation. Parametric representation was obtained by fitting a rational transfer function with a delay element to measurement data. Effects such as leakage, input/output errors and transients were not considered. Both [96] and [97] use response fitting to identify parametric models. Besides, [96] employs excitations with a sampling frequency of 10 kHz,

whereas methods in this chapter use excitations with the sampling frequency of 1 kHz.

The procedure in [98] performs the identification in the closed loop operation. Broadband excitation of the system with a motored engine is performed using speed excitations. Further, the identification was carried out at different operating speeds to quantify nonlinearity. Convergence problem of the identification procedure is avoided using measurements from the motored operation of the engine. The measurement data is used for identification using direct closed loop identification with prediction error methods [99] dealing with the data as if they result from an open loop experiment. One prerequisite for the application of direct closed loop identification for obtaining consistent estimates is the selection of proper model structure [100]. Also, [98] does not present any physically motivated model selection. Further, the method does not identify the parameters of the test bench/driveline but only the eigenfrequency of the setup around different operating speeds.

Despite the well established theoretical background for linear system identification, methods of identification have not been exploited to identify the dynamics of the discussed experimental test setup. This chapter investigates different methods of non-parametric and parametric methods for identification of automotive test benches, not restricted to engine test benches alone. In addition, the developed methods can handle data resulting from closed loop operation and also consider the error in the input signals.

## 4.3 Measurement Setup and Identification Methods

This section presents the measurement setup used for the identification along with the methods employed for both non-parametric and parametric identification. The measurement setup is known as Error-In-Variables (EIV) setup, with noise entering both the input and output measurements.

### 4.3.1 Measurement setup

In an EIV measurement framework, disturbing noise sequences occur both in the input and output of the setup. In contrast, the Output Error (OE) Framework, used widely for time-domain identification approaches [100], assumes disturbing noise only at the output. The schematic of the EIV Framework is depicted in the Figure 4.2. The notation and further discussion of the framework are discussed below. Linear dynamic EIV modeling is relevant for applications requiring a better understanding of the underlying input-output relation of a process rather than making

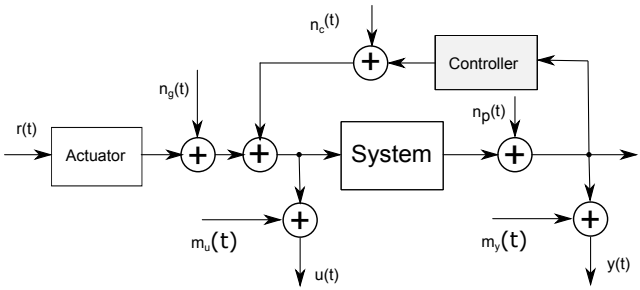


**Figure 4.2:** Schematic of the Error-In-Variables framework in closed loop configuration

an output prediction from the observations. In this work, it shall be assumed that the measurements of the input and output signals shall be synchronized.

In the stochastic EIV framework, identification of a parametric system and noise model is reported to be involved [101]. However, use of non-parametric noise model better handles the EIV problem setup. With assumptions of periodic signals [102] and known reference signal [103] it is reduced to a solvable problem using frequency domain methods and non-parametric noise models.

Engine and powerpack test benches are usually operated due to the integrating characteristics of the process with a speed control loop. Hence, the reference speed is controlled using the dynamometer, due to the dynamics of the controller the input has to be measured using speed sensors which are prone to noise and hence requires analysis using EIV framework. The experimental setup in the Figure 4.2 involves also a feedback loop. When the experimental setup includes feedback, the experiment turns out to be not completely informative, even if the input is persistently exciting. The presence of disturbing noise on the input measurements creates a systematic error in the identification results as shown in [104]. However, measurements under feedback conditions can be considered as a special case of the EIV problem. This equivalence between the EIV framework and the problem of closed loop identification using a known periodic reference signal shall be discussed.

Measurement data in time-domain from the interval $1 \leq t \leq N$ shall be defined by equation (4.1). The same notation for the limited duration data shall be

employed for frequency-domain data denoted by $Z^k$, with $k = 1, 2, ..., F$ frequencies. In comparison to the entries in $Z^N$, the entries in $Z^k$ contain $2F$ complex valued quantities corresponding to the measured input-output DFT spectra.

$$Z^N = \{u(1), y(1), ..., u(N), y(N)\} \tag{4.1}$$

$$Z^k = \{U(1), Y(1), ..., U(F), Y(F)\} \tag{4.2}$$

The corresponding input and output measurements of the true noise-free inputs $u_0(t)$ and outputs $y_0(t)$ in the time and frequency domain can be represented as in equations (4.3) and (4.4) respectively.

$$\begin{aligned} y(t) &= y_0(t) + n_y(t) \\ u(t) &= u_0(t) + n_u(t) \end{aligned} \tag{4.3}$$

The DFT spectra $U(k)$ and $Y(k)$ of the observed input and output signals are noisy replicas of the DFT spectra $U_0(k)$ and $Y_0(k)$ respectively.

$$\begin{aligned} Y(k) &= Y_0(k) + N_Y(k) \\ U(k) = U_0(k) + N_U(k), &\quad k = 1,\ 2,\ ...\ F \end{aligned} \tag{4.4}$$

The DFT spectra of the noise samples at the input and output are represented by $N_U(k) = DFT(n_u)$ and $N_Y(k) = DFT(n_y)$ respectively.

$$\sigma_U^2 = \mathbb{E}\{|N_U(k)|^2\}, \sigma_Y^2 = \mathbb{E}\{|N_Y(k)|^2\}, \sigma_{YU}^2 = \mathbb{E}\{N_Y(k)\overline{N_U(k)}\} \tag{4.5}$$

Non-parametric representation is restricted to frequency response function of the plant as well as the inputs and outputs, $G(j\omega_k), k = 1, 2...$ and (co-)variances of circular complex distributed noise with the representations as in equation (4.5) where $\sigma_U^2, \sigma_Y^2$ and $\sigma_{YU}^2$ denoting the input and output noise variances as well as covariance of the input-output noise assuming zero-mean Gaussian distribution respectively.

In case of periodic excitations in the EIV framework for operation in open loop, the expressions for non-parametric representation are given by equations (4.6)-(4.8) where $N_g(k)$, $N_p(k)$, $M_U(k)$ and $M_Y(k)$ are frequency domain representations of generator, process, input measurement and output measurement noise respectively. The time domain representations of reference signal, genera-

tor, process, input measurement and output measurement noise are given by $r(t)$, $n_g(t)$, $n_p(t)$, $m_u(t)$ and $m_y(t)$ respectively.

$$Y(k) = Y_0(k) + N_Y(k), U(k) = U_0(k) + N_U(k) \tag{4.6}$$

$$Y_0(k) = G_0(j\omega_k)U_0(k), U_0(k) = U_g(k) \tag{4.7}$$

$$N_Y(k) = G_0(j\omega_k)N_g(k) + N_p(k) + M_Y(k), N_U(k) = N_g(k) + M_U(k) \tag{4.8}$$

The corresponding expressions for closed loop operation with $R(k)$ denoting the frequency domain representation of the reference signal and assuming an ideal actuator is given by equations (4.9)-(4.11).

$$Y_0(k) = G_0(j\omega_k)U_0(k), U_0(k) = \frac{R(k)}{1 + G_0(j\omega_k)} \tag{4.9}$$

$$N_Y(k) = \frac{G_0(j\omega_k)N_g(k) + N_p(k)}{1 + G_0(j\omega_k)} + M_Y(k) \tag{4.10}$$

$$N_U(k) = \frac{N_g(k) - N_p(k)}{1 + G_0(j\omega_k)} + M_U(k) \tag{4.11}$$

Without loss of generality, the noise effects on the inputs and the outputs shall be represented using $n_u(t)$ and $n_y(t)$ respectively in a simplified notation. As it can be seen from equation (4.9)-(4.11), the case with generator noise, process noise, as well as input and output noise along with feedback, can be reformulated involving just the input and output noise with the knowledge of the reference signal which is periodic. This approach shall be used for both non-parametric (Local Polynomial Method) and parametric (Maximum Likelihood Method) estimation using the EIV framework.

### 4.3.2 Excitation signals

Linear Time-Invariant (LTI) systems have to be identified over a pre-defined frequency range. An optimal excitation signal shall have a flat spectrum in the frequency range of interest. A very primitive requirement on the excitation signal is the flexibility to impose a user-defined spectrum. A discussion on the characteristics of commonly used signals such as Pseudo Random Binary Sequence (PRBS), chirp and multi-sine signals with reference to identification experiments is discussed in [104], [100].

Excitation signals are subjected to design trade-offs such as time window-frequency resolution trade-off. Signals that exist over shorter time window have

wide frequency contents. An impulse in the time domain has a flat frequency spectrum. This trade-off also applies to stochastic signals in terms of Auto-Correlation Function (ACF) and the associated Power Spectral Density (PSD). Such trade-offs shall be discussed further for the multi-sine signal for a fixed root mean square signal amplitude.

For a multi-sine signal of a fixed Root Mean Square (RMS) value, there exists a trade-off between measurement time, Signal Noise Ration (SNR) and frequency resolution. Increasing the measurement time by appending multiple periods in the time domain, increases the frequency resolution resulting in more number of bins. Increasing the measurement time is generally disadvantageous both from measurement and data processing perspective unless explicitly desired. Assuming constant noise variance, the noise in the measurements gets distributed and the SNR of the measurement is improved. On the other hand, if the frequency resolution is increased, then the number of excited frequencies is increased. This results in a decreased amplitude of the corresponding spectral lines (under the assumption of constant RMS) which subsequently reduces the SNR.

In this work, PRBS and multi-sine signals shall be used as excitation signals. Swept sinusoidal signals are used to evaluate the notch filter parameterization in section 4.6 and for the validation of the UIO developed in chapter 3.

### 4.3.3 Non-parametric identification

Non-parametric identification methods identify the dynamic behavior of the system without employing a finite-dimensional parameter vector. Such methods are formulated both in time and frequency domain. Time domain methods include transient response analysis (impulse response and step response) and analysis using auto- and cross-correlation of the data sequences. Frequency domain techniques comprise of frequency analysis using correlation methods, Fourier analysis and spectral analysis [100]. The Fourier transform of the impulse response gives the frequency response function (FRF) of the system. Taking advantage of this equivalence relationship only frequency domain methods shall be investigated for non-parametric identification in this work.

#### Local Polynomial Method

This section presents the Local Polynomial Method (LPM) [104], an alternative to classical non-parametric identification approaches such as spectral analysis (SA) methods and Empirical Transfer Function Estimates (ETFE). LPM approximates both the plant model and the transient effects using the smooth functions

of the frequency. Such modeling using local polynomial approximations by the complex polynomial is done in a narrow band of frequency around the user specified frequency $k$. Estimation of the complex polynomial parameters is done from the measurements. [105] presents theoretical analysis supported by results from simulations and experiments showing LPM with two or more realizations better suppresses the noise transients than the classical spectral analysis methods for computing FRF estimates. The below section presents LPM for output noise and extends the discussion to the case with input and output noise and the case with feedback which can be applied for closed loop identification using the EIV framework as discussed in section 4.3.1.

$$Y(k) = G(\Omega_k)U(k) + T(\Omega_k) + V(k) \tag{4.12}$$

In case of an LTI system under excitation, the closed-form expression between the input and output DFT spectra is given by equation (4.12). This expression includes transient error $T(k)$ apart from the output of the system resulting from the input excitation, $V(k)$ quantifies noise effects on the measurements. Due to its generality, to be used for continuous time ordinary differential equation (ODE), discrete time ODE a generalized frequency variable $\Omega_k$ is introduced. In case of continuous time ODE $\Omega_k = j\omega_k$, whereas in case of discrete time ODE $\Omega_k = e^{-j\omega_k}$.

$$G(\Omega_{k+r}) = G(\Omega_k) + \sum_{s=1}^{R} g_s(k) r^s + O((\frac{r}{N})^{(R+1)}) \tag{4.13}$$

$$T(\Omega_{k+r}) = T(\Omega_k) + \sum_{s=1}^{R} t_s(k) r^s + N^{-\frac{1}{2}} O((\frac{r}{N})^{(R+1)}) \tag{4.14}$$

$$Y(k+r) = (G(\Omega_k) + \sum_{s=1}^{R} g_s(k) r^s) U(k+r) + T(\Omega_k) + \sum_{s=1}^{R} t_s(k) r^s \tag{4.15}$$

Using the information that $G(\Omega_k)$ and $T(\Omega_k)$ are rational forms in $\Omega_k$ and their smoothness over frequencies, estimates of the transfer function of the system can be computed. Equations (4.13) and (4.14) indicate the polynomial approximations of the system transfer function and the transient terms. The reason for the factor $N^{-1/2}$ in equation (4.14) is due to the residues that are approximated in the order of $O(N^{-1/2})$ [104]. The approximations are valid around local frequencies $\Omega_k$ in-

dexed using the variable $r = -n, -n+1, ..., n$. This approximation results in $2n+1$ equations for $2(R+1)$ unknowns is given by equation (4.15).

$$\Theta(k) = [G(\Omega_k)\ g_1(k)\ g_2(k)\ \dots\ g_R(k)\ T(\Omega_k)\ t_1(k)\ t_2(k)\ \dots\ t_R(k)] \tag{4.16}$$

$$Y(k) \approx \Phi(k)\Theta(k) \tag{4.17}$$

The $2(R+1)$ unknown coefficients are stacked in the parameter vector $\Theta$ given by equation (4.16). The set of equations can be written as in (4.17), where $Y(k)$ is given by equation (4.18).

$$Y(k) = \begin{bmatrix} . \\ . \\ Y(k+r) \\ . \\ . \end{bmatrix} \Phi(k) = \begin{bmatrix} & . & & . & . \\ & . & & . & . \\ \begin{bmatrix} 1 & r^1 & \dots & r^R \end{bmatrix} U(k+r) & & 1 & r^1 \dots r^R \\ & . & & . & . \\ & . & & . & . \end{bmatrix} \tag{4.18}$$

The parameter vector is then estimated in the least square sense as in equation (4.19)

$$\hat{\Theta} = (\Phi(k)^H \Phi(k))^{-1} \Phi(k) Y(k) \tag{4.19}$$

The covariance of the estimates is computed using the residue for the frequency $k+r$ as in equation (4.20) using which the variance of the FRF estimate using LPM can be computed as in equation (4.21) normalized by the number of degrees of freedom.

$$e(\Omega_{k+r}) = Y(k+r) - (G(\Omega_{k+r})U_{k+r} + T(\Omega_{k+r})) \tag{4.20}$$

$$\sigma^2(k) = \frac{1}{2n+1-6} \sum_{r=-n}^{n} |e(\Omega_{k+r})|^2 \tag{4.21}$$

In case of systems with (mild) nonlinearities, the approximation in equation (4.12) involves the DFT of nonlinear distortions. In such case, the best linear approximation at the central frequency k, can be computed using the local polynomial model as the measurement of the FRF at that frequency. This step is repeated every time for all DFT frequencies in the band of interest by shifting the sliding window over the DFT bins resulting in a local estimate of the FRF. Further covariance of the nonlinear distortions can also be computed [105].

As it can be seen, calculation of LPM approximation of FRF estimates is computationally intensive than other methods such as SA or ETFE. On the contrary,

the combination of information from multiple frequencies is inherent to LPM and hence averaging of data from multiple experiments as in spectral averaging is not necessary for obtaining smoother estimates over the frequency region of interest. For comparison and analysis of the methods, the interested reader is referred to [106]. An involved discussion on identification of nonlinear systems using LPM method employing the best linear approximation along with stochastic nonlinear distortions, multiple input and multiple output systems is presented in [105].

#### Noisy Input / Feedback case

In the case of noisy input measurements or input resulting from a feedback loop, the estimates can be biased if the input to the process is correlated with the process noise. Hence to avoid bias, the reference signal is required for the estimation of the FRF of the system.

Let $Z(k) = [Y(k)\ U(k)]^T$ denote the stacked version of output and input measurements. The FRF estimates of the reference to the input and reference to the output are denoted by $G_{ru}(\Omega_k)$ and $G_{ry}(\Omega_k)$ respectively. The noise on the input and output is represented by $V_Z(k) = [V_Y(k)\ V_U(k)]^T$. The system can be represented as in equation (4.22) with transient noise and system error on the output and input be jointly denoted by $T_{rz}(\Omega_k)$. With the suppression of the noise transients using the LPM method, a consistent estimate of the FRF $\hat{G}(\Omega_k)$ can be obtained using equation (4.23). The terms $\hat{G}_{ry}(\Omega_k)$ and $\hat{G}_{ru}(\Omega_k)$ can in turn be computed using LPM estimates or using spectral methods.

$$Z(k) = G_{rz}(\Omega_k)R(k) + V_Z(k) + T_{rz}(\Omega_k) \tag{4.22}$$

$$\hat{G}(\Omega_k) = \hat{G}_{ry}(\Omega_k)\hat{G}_{ru}^{-1}(\Omega_k) \tag{4.23}$$

Non-parametric identification provides a good insight into the dynamics of the process to be identified. For LTI systems, FRF measurement is an intermediate step that eases the process of subsequent parameter identification. A comparison of the spectral analysis method and Local Polynomial Method (LPM) on a theoretical perspective is presented in [106]. The discussion on LPM was limited to the study of linear dynamical systems, the method has been extended to nonlinearity by separating the response of the system to best linear approximation along with stochastic nonlinear distortions, multiple input and multiple output systems [105].

### 4.3.4 Parametric identification

The basic idea of parametric identification is to explain the input-output measurement data using approximations using a finite-dimensional vector entries known as parameters. In case of LTI system dynamics, the output of the system can be composed of a deterministic and stochastic component relying on the principle of superposition. In such case the model in an input($u(k)$)-output($y(k)$) setting can be written as in equation (4.24) where $q$ is the forward shift operator. With $G(q,\theta) = \sum_{k=1}^{\inf} g_\theta(k)q^{-k}$, $H(q,\theta) = 1 + \sum_{k=1}^{\inf} h_\theta(k)q^{-k}$, $f_e(.)$ is the probability distribution of the disturbance. Hence model corresponds to specification of the functions plant model $G$, noise model $H$ and $f_e$

$$y(k) = G(q,\theta)u(k) + H(q,\theta)e(k) \tag{4.24}$$

Provided the model of the system belongs to the set of model structures, search for the best parametric model among the set of candidate models can be viewed as a parameter estimation problem. Classical parametric identification methods require not only information on the model structure but also on the model order to solve the optimization problem for obtaining the parameter estimates. [107] presents a criterion that helps iteratively evaluate and select automatically the best model based on the given input-output data. The choice of model structure can be guided by two different philosophies [100].

- Flexible model structures: Use of flexible model sets without using knowledge of the internal structure of the process. Models of this structure are focused to mimic the input-output characteristics of the process.
- Physically motivated model structures: Physical insight can be used to reduce the parameter set to match what prior knowledge of the system. Usually, such models are formulated as continuous-time models. This approach is also usually termed as grey-box modeling approach [108].

As in [104], parametric identification uses optimization of a cost function to match the model and data. Both time-domain (Prediction Error Method) and frequency-domain (Maximum Likelihood Method) approaches shall be investigated for identification of engine and powerpack test bench dynamics. Time domain methods work with the sampled data from the experimental setup, whereas the initial step of the frequency domain methods is to determine the spectrum of the observations. The parametric methods discussed namely, Prediction Error Method and Maximum Likelihood Estimation used in this work handle the problem of noise modeling differently. This shall be discussed in the following section.

### Prediction Error Method (PEM)

PEM [100] are a class of time-domain methods to identify parametric models using minimization of an error criterion formulated in terms of prediction error. The key idea is that the models can be used for prediction of the outputs provided the inputs are known. The predicted value of $\hat{y}[k|k-1]$ uses the data $Z^N$ till time instant $k-1$ to predict the output at time $k$. The method is based on certain assumptions on the plant and noise model apart from assuming knowledge of noise statistics [100]:

- the plant model is stable
- the noise model is stable and invertible

The parametric model is a tuple $\{G(q), H(q), \text{pdf of e}\}$ composed of the parametric plant and noise model as well as the probability density function of the disturbances. The equation (4.25) represents the output $y(k)$ based on the input $u(k)$ and noise signals. The noise $v(k)$ acting on the output is modeled using Gaussian white noise $e(k)$ filtered by the noise transfer function $H(q)$ given by equation (4.26).

$$y(k) = G(q)u(k) + v(k) = G(q)u(k) + H(q)e(k) \tag{4.25}$$

$$v(k) = H(q)e(k) = \sum_{t=0}^{\infty} h(t)e(k-t) = e(k) + m(k-1) \tag{4.26}$$

$$m(k-1) = \hat{v}(k|k-1) = (H(q)) - 1)e(k) = (1 - H_{\text{inv}}(q))v(k) \tag{4.27}$$

With $e(k)$, the white noise sequence, the conditional expectation of $v(k)$ which is also the sample mean $m(k-1)$ up to time instant $k-1$ is given by equation (4.27), where $H_{\text{inv}}(q))$ denotes the inverse of the parametric noise model. The one-step ahead predictor for the output is given by equation (4.28).

$$\begin{aligned} \hat{y}(k|k-1) = E\{y(k)|Z_K\} &= G(q)u(k) + \hat{v}(k|k-1) \\ &= G(q)u(k) + (1 - H_{\text{inv}}(q))v(k) \\ &= H_{\text{inv}}(z)G(q)u(k) + (1 - H_{\text{inv}}(q))y(k) \end{aligned} \tag{4.28}$$

The infinite step-ahead prediction can be interpreted as the simulation of the process. The prediction error is for the output is given by equation (4.29). The theoretical one-step ahead predictor is the white-noise sequence also known as innovations, is the part of the output prediction that cannot be estimated from

past measurements. The term theoretical refers to the complete knowledge of the system, in such a case only noise realizations shall be the predictions.

$$\begin{aligned} y(k) - \hat{y}(k|k-1) &= -H_{\text{inv}}(q)G(q)u(k) + H_{\text{inv}}(q)y(k) \\ &= H_{\text{inv}}(q)(y(k) - G(q)u(k)) = H_{\text{inv}}(q)v(k) \\ &= e(k) \end{aligned} \tag{4.29}$$

Considering the parameterization of the plant and noise models, the predictor and the prediction-error is given by the equations (4.30) and (4.31) respectively.

$$\hat{y}(k|\theta, Z_{\text{K}}) = H_{\text{inv}}(\theta, q)G(\theta, z)u(k) + (1 - H_{\text{inv}}(\theta, q))y(k) \tag{4.30}$$

$$\epsilon(k, \theta) = y(k) - \hat{y}(k, \theta) \tag{4.31}$$

A cost function in equation (4.32) is defined using the some norm on the (weighted) prediction error (usually 2-norm) resulting in an optimization problem to estimate the parameters in equation (4.33).

$$\epsilon_F(k, \theta) = F(q)\epsilon(k, \theta) \quad \text{(weighted error)}$$

$$J(\theta, Z_K) = \frac{1}{K}\sum_{k=0}^{K-1} l(\epsilon_F(k, \theta)) \quad \text{typically} \quad l(\epsilon_F(k, \theta)) = \|\epsilon_F(k, \theta)\|_2 \tag{4.32}$$

Minimization of the prediction error results in a nonlinear optimization problem in case of models other than the ARX model structure. Using the ARMAX model structure, the problem turns out to be the pseudo-linear regression.

$$\hat{\theta} = \underset{\theta}{\operatorname{argmin}}\, J(\theta, Z_K) \tag{4.33}$$

A typical assumption on the measurement setup in the prediction error approach assumes that the disturbing noise occurs at the output, termed as OE framework. In addition, PEM is directed toward the identification of discrete-time models.

#### Maximum Likelihood Method (MLE)

MLE technique estimates the parameters such that the likelihood function is maximized. The likelihood function is a deterministic function of the parameters that quantifies the probability that the observations are high for the given set of parameters. In other words, the estimates are computed to make the observed data the most probable [35]. MLE is computationally intensive but offers asymptoti-

cally consistent and efficient estimates. However, the small sample performance of MLE may be inferior to that of other classical estimators. It offers flexibility to be formulated for frequency domain identification methods as discussed in [104].

MLE based parametric frequency domain identification methods require knowledge of the non-parametric noise model in the form of covariance estimates as a function of frequency. Assuming the noise on the inputs and outputs have zero mean, circular complex normally distributed and independent over frequencies with known covariance matrix, the Gaussian ML cost function [104] can be written as in equation (4.34). The term $e$ in the the expression refers to the equation error for all the frequencies $k = 1, ..., F$ is expressed in equation (4.35). The associated error covariance is given by equation (4.36). $Z(k) = [Y(k)\ U(k)]^T$ denotes the input and output measurements. Further assumptions include deterministic spectra for true excitation and response.

$$V_{ML}(\Theta, Z) = \sum_{k=1}^{F} \frac{|e(\Omega_k,\ \Theta,\ Z(k))|^2}{\sigma_e^2(\Omega_k,\ \Theta)} \tag{4.34}$$

$$\text{where, } e(\Omega_k,\ \Theta,\ Z(k)) = Y(k) - G(\Omega_k,\ \Theta)U(k) \tag{4.35}$$

$$\sigma_e^2(\Omega_k,\ \Theta) = \sigma_Y^2(k) + |G(\Omega_k,\ \Theta)|^2\sigma_U^2(k) - 2Re(\overline{G}(\Omega_k)\sigma_{YU}^2(k)) \tag{4.36}$$

An alternative expression for the ML cost function is expressed in equation (4.37). The ML cost function has an inherent weighting of the frequencies with a better SNR ratio. Frequency bands with better SNR are weighted more than the ones with lower SNR due to the effect of the inverse noise covariances in the ML cost function.

$$V_{ML}(\Theta, Z) = \sum_{k=1}^{F} |\varepsilon(\Omega_k,\ \Theta,\ Z(k))|^2, \quad \text{with } \varepsilon(\Omega_k,\ \Theta,\ Z(k)) = \frac{e(\Omega_k,\ \Theta,\ Z(k))}{\sigma_e(\Omega_k,\ \Theta)} \tag{4.37}$$

In practice in absence of knowledge of the noise covariance, noise characteristics are quantified using the sample mean and sample variance obtained from repeated measurements with multiple periods. Hence only estimates of the quantities to multiple periods of multi-sine excitations are available resulting in the sample maximum likelihood (SML) estimator which uses sample means and covariances. This results in the sample maximum likelihood estimator whose cost function is given by equation (4.38), with the corresponding equation error and error covariance given by equations (4.39) and (4.40) respectively. [109] presents the effect of replacing

the values of the covariance matrix by sample values for parametric estimations, concluding the resulting estimator is strongly consistent with the consistency and loss of efficiency as a function of the number of data sets available.

$$V_{SML}(\Theta, Z) = \sum_{k=1}^{F} \frac{|\hat{e}(\Omega_k,\ \Theta,\ \hat{Z}(k))|^2}{\hat{\sigma_e}^2(\Omega_k,\ \Theta)} \tag{4.38}$$

$$\text{where, } \hat{e}(\Omega_k,\ \Theta,\ \hat{Z}(k)) = \hat{Y}(k) - G(\Omega_k,\ \Theta)\hat{U}(k) \tag{4.39}$$

$$\sigma_e^2(\Omega_k,\ \Theta) = \hat{\sigma_Y}^2(k) + |G(\Omega_k,\ \Theta)|^2 \hat{\sigma_U}^2(k) - 2Re(\overline{G}(\Omega_k)\hat{\sigma_Y U}^2(k)) \tag{4.40}$$

Analysis of the asymptotic properties of this sample maximum likelihood estimator is presented in [105] and the equivalence between the SML and ML estimates has been discussed in [104]. From a practical viewpoint, due to increased measurement time in order to access low frequencies, the number of periods can be restricted to 2 [104]. If the non-parametric models are known apriori they can be directly used to estimate the parametric plant models. Else the initial step would be to identify the non-parametric noise model in the pre-processing stage. The computation of parametric estimates using the ML criterion is done using the Levenberg-Marquardt method due to the nonlinearity of the resulting optimization problem. [104] discusses different initialization strategies using estimates from the simple least squares method to initialization using subspace estimates.

#### Noise modeling: PEM and MLE Methods

The studied parametric identification methods differ in handling of the noise models. Inefficient and inconsistent estimates can result if the noise power spectrum cannot be described by the rational model of the chosen order [104]. This is an additional model selection problem apart from the model selection for the plant identification. Further, improper parameterization of the noise model affects the convergence region of the optimization problem [109]. Noise variances are as important quantities as FRF estimations [106]. Noise variance helps define uncertainty bounds on the estimated FRF and shall also be employed as a non-parametric weighting in the estimation of parametric models in case of unknown noise models.

In the parametric noise modeling approach, noise affecting the plant is modeled as filtered white noise parameterized by the filter coefficients. Using a parametric noise model, in the PEM framework both the plant and noise models are identified simultaneously which may lead to a complex numerical optimization

problem [100],[104]. In the case of the Maximum Likelihood (ML) method, non-parametric noise modeling is used.

The non-parametric noise representation in the frequency domain uses estimates of noise variance at different frequencies. The noise variances can be used for non-parametric weighting in the associated cost function, leading to a tractable optimization problem. Further using the approach, frequency bands with higher noise covariances and lower noise covariances contribute less and more to the ML cost function respectively. FRF estimates can be used for the choice of parametric transfer function models and also validate the estimated parametric models. Further, the computed spectra and the (co-)variances can be used to find good initial values for parametric estimates, avoiding convergence to a local minimum of the formulated optimization problem in case of parametric modeling.

#### Subspace Method

Subspace identification methods have its roots in the field of system theory, (numerical) linear algebra, specifically geometry and statistics [110]. They are non-iterative methods to directly identify LTI state space models and do not differentiate between multi-input, multi-output (MIMO) and single-input, single-output (SISO) systems. Further, from the numerical implementation viewpoint, subspace methods rely on QR decomposition and singular value decomposition. This results in stable implementations and avoiding problems of initialization as in the case of the classical methods relying on nonlinear optimization techniques. From the parameterization perspective, the method requires minimal effort with only an upper bound on the system order.

Subspace methods compute estimates of the states using input-output data employing projection techniques. From the state estimates the state space model is constructed using least squares techniques reducing the parameterization of the model to an upper bound to the order of the identified model. Equation (4.41) is the state space realization of an LTI system with state estimates denoted by $\hat{x} \in \mathscr{R}^n$, inputs denoted by $u \in \mathscr{R}^p$. The quantities $\eta$ and $\nu$ represent the noise realization on the states and output respectively. Equation (4.41) can be formulated as a

regression problem for the parameter vector defined by $\Theta \in \mathscr{R}^{(n+p)x(n+m)}$ with the structure given by $\Theta = \begin{bmatrix} A & B \\ C & D \end{bmatrix}$.

$$\begin{bmatrix} \hat{x}(t+1) \\ y(t) \end{bmatrix} = \begin{bmatrix} A & B \\ C & D \end{bmatrix} \begin{bmatrix} \hat{x}(t) \\ u(t) \end{bmatrix} + \begin{bmatrix} \eta(t) \\ \nu(t) \end{bmatrix} \tag{4.41}$$

$$rank \begin{bmatrix} \hat{x}(0) & \hat{x}(1) & \dots & \hat{x}(N-1) \\ u(0) & u(1) & \dots & u(N-1) \end{bmatrix} = n+m \tag{4.42}$$

In order for the regression problem to have a unique solution (independent row vectors) the rank condition mentioned in equation (4.42) have to be satisfied. Under this assumption, the value of $\Theta$ can be computed in the least squares sense as given by equation (4.43). Apart from the estimate of the state space representation, noise covariances and the initial condition of the system can also be computed.

$$\hat{\Theta} = \left( \sum_{t=0}^{N-1} \begin{bmatrix} \hat{x}(t+1) \\ y(t) \end{bmatrix} \begin{bmatrix} \hat{x}^T(t) & u^T(t) \end{bmatrix} \right) \left( \sum_{t=0}^{N-1} \begin{bmatrix} \hat{x}(t+1) \\ y(t) \end{bmatrix} \begin{bmatrix} \hat{x}^T(t) & u^T(t) \end{bmatrix} \right)^{-1} \tag{4.43}$$

The above section summarized the subspace identification method, a detailed discussion of the method can be found in [110], [111]. The subspace methods discussed here, are used for the identification of the three inertial and two inertial torsional system using the test bench measurements in chapters 5 and 8 respectively.

## 4.4 Identification of Engine and Powerpack Test Benches

This section begins with a brief introduction to the identification workflow, followed by the description of the developed non-parametric and parametric identification techniques. The identification methods involve the solution of a nonlinear optimization problem. As with any nonlinear optimization problem, the convergence and optimality depend on the initial values of the estimates or the optimization variables. The initialization of the identification algorithms is discussed in section 4.4.5. In order to facilitate the ease of understanding, the concepts shall be presented for the engine test benches first. They are extended to powerpack test benches in section 4.4.6.

### 4.4.1 Workflow for identification

In the identification workflow, different choices have to be performed right from the choice of the measurement setup, the design of excitation signals to the method of validation employed. The choice of the identification method is one of the important decisions. Before the identification is performed, the relevant frequency band shall be selected. An initial estimate of the relevant frequency range of the test bench can be obtained by performing run-down of the engine at the test bench. In the run-down procedure the Engine or the UUT is operated at a nominal speed and allowed to decelerate to a standstill with a closed throttle.

During the run-down process, the UUT runs through the critical speed of the test bench. This critical speed can be used to compute the eigenfrequency of the test setup. A valid frequency range would be from standstill to the frequency corresponding to the maximum speed of the engine. A better choice would be to restrict the maximum frequency to a value greater than the largest eigenfrequency from the run-down procedure. The value of 20 Hz is chosen as bandwidth of the excitations for the test bench measurements due to the trade-off between frequency resolution and dynamics of the system. Usually, beyond the largest eigenfrequency of the system, the dynamics is that of the isolation region of the rotational inertia-stiffness system. Hence it is not much value from an operation viewpoint. However, knowledge of critical speeds in case of test benches with multiple inertias can be used to compute better estimates based on weightings at the frequencies corresponding to the critical speeds using frequency domain methods. In the subsequent discussion, no frequency weighted identification is performed, rather generic identification of the frequency band which includes the eigenfrequency will be done.

Following the definition of the frequency range for identification, measurements are performed at the experimental setup. The strategy used for the measurement data acquisition is presented in section 4.4.2. Subsequently, parametric and non-parametric identification are discussed in section 4.4.3 and 4.4.4 respectively.

### 4.4.2 Measurement strategy

The procedure [98] requires torque measurements at the inertial elements, namely combustion engine and dynamometer. But the discussed methods do not require measurements or estimates of the combustion engine torque. PEM method uses PRBS signals as excitations whereas the MLE method employed multi-sinusoidal signal as excitation. In both cases, the reference speed signal to the dynamometer

was employed as excitation. During the design of excitation around the certain operating speed, the amplitude of the excitations signals such as multi-sinusoidal, chirp and PRBS has to be designed to avoid nonlinearity. One source of nonlinearity is the actuation signal from the controller to the dynamometer which saturates at the maximum value of the torque. The excitation amplitude should be designed to be high enough for sufficient excitation but low enough to avoid nonlinearity. Without knowledge of the controller, the limits of the command value of the dynamometer speed can be reduced to avoid saturation of the torque generated by the dynamometer during the identification experiments.

From the measurement data perspective, the measurement strategies for MLE estimation are classified into robust and fast methods based on [104]. The fast method uses data from a single experiment whereas robust method requires data from multiple experiments. The methods differ in how the FRF is computed. Under closed loop operation, the fast method uses LPM of the sample mean at the excited frequencies to compute FRF estimates from reference to input and from reference to output, using them to compute the indirect FRF estimate. The robust method computes FRF estimates using H0 estimation averaged over the experiments of the projected input-output DFT spectra on reference DFT spectra, along with covariances estimates. Table 4.1 summarizes the features of both the measurement strategies. Both methods shall be considered only for closed loop operation.

### 4.4.3 Non-parametric identification

As discussed in section 4.3, transient system errors lead to biased and increase the variability of the estimated FRF. Measurement during transient operation and in feedback is unavoidable from the perspective of the involved measurement time and effort. The system approximation (of the test bench) under closed loop operation in the presence of noise can be represented as in equation (4.44), where $H_U(\Omega_k)$ and $H_Y(\Omega_k)$ represent the transfer function from the error to the input and output respectively. The effects of transients on the system and the noise models are represented using $T_{Gu}(\Omega_k), T_{Gu}(\Omega_k)$ and $T_{Hy}(\Omega_k), T_{Hy}(\Omega_k)$ respectively.

$$\begin{bmatrix} Y(k) \\ U(k) \end{bmatrix} = \begin{bmatrix} G_{ry}(\Omega_k) \\ G_{ru}(\Omega_k) \end{bmatrix} R(k) + \begin{bmatrix} T_{Gy}(\Omega_k) \\ T_{Gu}(\Omega_k) \end{bmatrix} + \begin{bmatrix} H_Y(\Omega_k) E_Y(k) \\ H_U(\Omega_k) E_U(k) \end{bmatrix} + \begin{bmatrix} T_{Hy}(\Omega_k) \\ T_{Hu}(\Omega_k) \end{bmatrix} \tag{4.44}$$

The measurement strategy uses multi-sinusoidal signals with discrete frequency excitations as reference signals. The corresponding frequency response at the non-

**Table 4.1:** Summary of the measurement strategy for torsional system identification based on [104]

| | Robust Method | Fast Method |
|---|---|---|
| Measurement data | Single experiment with random phase multisines with more than 2 periods | Multiple experiments with full random orthogonal multisines with more than 2 periods |
| Transient Handling | Transient removal via LPM at non-excited lines resulting in sample mean and noise covariance estimates | LPM approximation of non-excited frequencies are used to remove transients |
| FRF Estimates | Computation of FRF using H0 estimates averaged over the experiments of the projected input-output DFT spectra on reference DFT spectra, along with covariances estimates | Local polynomial approximation applied to the sample means at the excited frequencies to compute FRF estimates from reference to input and from reference to output, later used to compute indirect FRF estimate |

excited frequencies is used to estimate the noise transients and the noise covariance. At the excited frequencies, the plant FRF is computed after removing the noise transients. Using the formulation in equation (4.44), the approach presented in 4.3.3 is applied to arrive at the system and noise FRF representations. The total covariance of the FRF estimates with the stochastic nonlinear distortions can be computed [104]. From the measurement data perspective, the measurement strategies robust and fast can be applied. In addition, to obtaining the FRF, the non-parametric identification also has other benefits which shall be presented.

#### Use of non-parametric identification: Choice of Parametric Model

From the form of the estimated FRF response, the number of poles and zeros of the transfer function can be estimated which can be used to determine the form of the denominator and numerator polynomials of the transfer function model. Thus the non-parametric model helps decide what form of approximation has to be used. It gives information about high frequency roll-off characteristics, phase shift and resonance peaks. Further, the order of the approximation required can be determined. This shall be shown with the test bench identification as a use case.

The estimated FRF using non-parametric identification of the dynamics between $\frac{\omega_D}{T_{Dact}}$ and $\frac{\omega_E}{T_{Dact}}$ is depicted in Figure 4.3. A multi-sine speed signal around the speed of 1500 rpm with a frequency band extending from 0 to 20 Hz was used as excitation. The response between the speed and torque at the dynamometer shows a notch and a resonant peak, whereas the ICE speed output with the dynamometer torque as input has only a resonant peak. The presence of a single resonant frequency requires approximation using 2-mass oscillator. In case of a test bench only with the internal combustion engine (ICE) coupled with the dynamometer through a shaft coupling, the equation (4.45) represents the transfer functions between dynamometer torque as input and speed of the dynamometer as output. The equation (4.46) represents the transfer function with dynamometer torque as input and engine speed as output.

$$\frac{\omega_D}{T_{Dact}} = \frac{J_{ICE}s^2 + ds + k}{J_{ICE}J_{dyno}s^3 + d(J_{ICE} + J_{dyno})s^2 + k(J_{ICE} + J_{dyno})s} \tag{4.45}$$

$$\frac{\omega_E}{T_{Dact}} = \frac{ds + k}{J_{ICE}J_{dyno}s^3 + d(J_{ICE} + J_{dyno})s^2 + k(J_{ICE} + J_{dyno})s} \tag{4.46}$$

This choice of the expressions is based on the observations from the identified frequency response functions from the test bench using non-parametric estimation

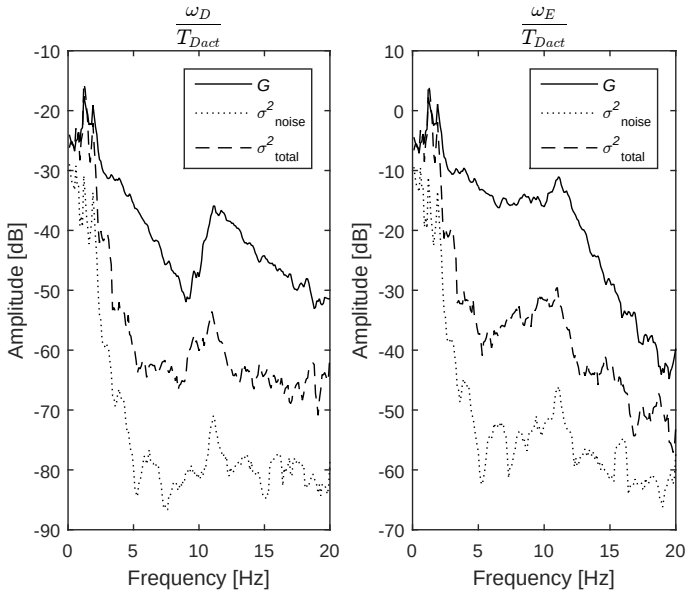


**Figure 4.3:** Non-parametric modeling of the engine test bench excited around mean speed of 1900 rpm using dynamometer set speed value

techniques. These expressions shall be used for formulating the model structures (ARMAX,ARX) for the identification of the test bench parameters.

#### Use of non-parametric identification: Weighting of SML Cost function

The estimates of the noise covariances from repeated measurements with multiple periods are used in the expression of the sample maximum likelihood estimator given by equation (4.47). As it can be seen the estimated covariances of the input noise ($\hat{\sigma}_U(k)$), output noise ($\hat{\sigma}_Y(k)$) and input-output noise ($\hat{\sigma}_Y U(k)$) is used in the formulation of the SML cost function.

$$V_{SML}(\Theta, Z) = \sum_{k=1}^{F} \frac{|\hat{e}(\Omega_k,\ \Theta,\ \hat{Z}(k))|^2}{\hat{\sigma_e}^2(\Omega_k,\ \Theta)} \tag{4.47}$$

$$\text{where, } \hat{e}(\Omega_k,\ \Theta,\ \hat{Z}(k)) = \hat{Y}(k) - G(\Omega_k,\ \Theta)\hat{U}(k) \tag{4.48}$$

$$\sigma_e^2(\Omega_k,\ \Theta) = \hat{\sigma}_Y^2(k) + |G(\Omega_k,\ \Theta)|^2\hat{\sigma}_U^2(k) - 2Re(\overline{G}(\Omega_k)\hat{\sigma}_Y U^2(k)) \tag{4.49}$$

### 4.4.4 Parametric identification

Parametric test bench identification uses the methods of prediction error method and the sample maximum likelihood procedure. Parametric Identification is performed using both the OE and EIV setup. PEM uses the OE setup and MLE method is based on the EIV framework. Both the approach identifies discrete-time models with data sampled with a frequency of 1 kHz. Euler forward rule is used as a method of discretization of the continuous time system. As the sampling frequency is higher than the eigenfrequency of the system use of Euler discretization does not lead to numerical instability for the stable test bench system in closed loop operation.

$$s \approx \frac{z-1}{T_s} \tag{4.50}$$

The discretization scheme can be expressed as a relationship presented in equation (4.50) between the continuous time and discrete time-frequency variable assuming constant values between the instants of discretization $kT_s < t \leq (k+1)T_s$. The following notations are used in the discussion, the speed of the inertia is represented using $\omega_E$ and $\omega_D$ respectively. $T_s$ stands for the sampling time of the measurements. The value of shaft torque is denoted using $T_{sh}$. Quantities $J_E$ and $J_D$ inertia of ICE and dynamometer respectively. The stiffness of the shaft is denoted by $c$ and its damping is represented as $d$.

### PEM Method

This work uses the PEM to identify discrete time models, the parameters of the system are computed using equivalence between continuous time and discrete time models. The discussion presents generic expressions for the general class of polynomial models as in [100], followed by its application for PEM based parametric identification of powerpack test benches.

Let $y(k)$ and $u(k)$ represent the output and input of a discrete time process in an equation error form with the error being modeled as moving average filtering of Gaussian white noise realization. The generic structure of the studied models can be written of the form given in equation (4.51) with the plant and noise models represented as $G(q,\theta)$ and $H(q,\theta)$ respectively. The quantity $\theta$ represents the parameter vector.

$$y(k) = G(q,\theta)u(k) + H(q,\theta)e(k) \tag{4.51}$$

$$y(k) = \frac{B(q)}{A(q)}u(k) + \frac{C(q)}{A(q)}e(k) = Gu(k) + He(k) \tag{4.52}$$

If the error in the equation (4.51) is modeled as moving average of white noise, then the system representation takes the form in equation (4.52) with polynomials $A(q) = 1 + a_1 q^{-1} + ... + a_{n_a} q^{-n_a}$ and $B(q) = b_1 + b_2 q^{-1} + ... + b_{n_b} q^{-n_b+1}$ along with $C(q) = 1 + c_1 q^{-1} + ... + c_{n_c} q^{-n_c}$. If the equation error is modeled as AR filtered the white-noise term $e(k)$, the ARMAX representation reduces to AutoRegressive process with eXogeneous inputs (ARX) model structure. The parameter reduces to $\theta = [a_1 a_2 ... a_{n_a} b_1 ... b_{n_b}]$, the ARX model can be written using the generic form with $C(q) = 1$.

ARMAX involves nonlinear regression problem which requires proper initialization. ARX model assumes the same denominator for plant and noise models reducing the problem to a linear regression problem. The torque balance at the combustion engine inertia can be written as in equation (4.53), with $T_{E\_int}$ rep-

resenting the internal combustion engine torque, where $s$ stands for the Laplace variable.

$$\omega_E(s) = \frac{1}{J_E s}(T_{E\_int}(s) - T_{sh}(s)) \tag{4.53}$$

$$\omega_E(s) = -\frac{1}{J_E s} T_{sh}(s) \tag{4.54}$$

$$\omega_E(k) = \omega_E(k-1) - \frac{T_s}{J_E} T_{sh}(k) \tag{4.55}$$

The combustion engine is operated around a certain operating speed in motored mode, in case of dynamic engine test bench without torque compensation schemes as in [112]. Hence the deterministic component of the model can be written as in equation (4.54), modeling the combustion torque as noise excitations. In such a case, an ARMAX model representation can be used. The discretized version of the deterministic component can be written as in equation (4.55), which results in the approximations of the form in the equation (4.56). The shaft torque oscillations are due to the torque oscillations of the combustion engine. Hence the noise spectrum of the shaft torque of the combustion engine and internal engine torque would have the same frequency content. As a result, the same denominator polynomial can be used for parametric approximations of the noise and plant model also validating the choice of an ARX model representation.

$$a_1 = -1, b_1 = -\frac{T_s}{J_E} \tag{4.56}$$

In order to identify the coupling characteristics, the shaft torque resulting from the engine operation at the test bench shall be considered as given by equation (4.57). The value $\Delta\omega = \omega_E - \omega_D$ represents the speed difference between the combustion engine and dynamometer speed. The discretized version is given by equation (4.58) which is used to identify the parameters as shown in equation (4.59).

$$T_{sh}(s) = -(\frac{c}{s} + d)\Delta\omega(s) \tag{4.57}$$

$$T_{sh}(k) - T_{sh}(k-1) = -(cT_s + d)\Delta\omega(k) - d\Delta\omega(k-1) \tag{4.58}$$

$$a_1 = -1, b_1 = -(cT_s + d), b_2 = -d \tag{4.59}$$

As discussed, the PEM is applied to identify the model parameters ignoring feedback, without considering input noise and without using the reference signal. Such a straightforward application of the PEM is termed as the direct approach to closed loop identification using PEM [99], [100].

### MLE Method

MLE requires a parametric model for the plant. The noise model in contrast to PEM is non-parametric which can be obtained from the LPM estimation presented in section 4.4.3 .The MLE procedure then reduces to computing the best approximation only of the plant model based on the input/output data and the estimated non-parametric models.

Let the parametric plant model be denoted by $G(\Omega_k, \theta)$ where $\theta$ stands for the parameters. The generic form of the parametric model is given by equation (4.60). Using the models and the chosen parametric representation, the parameters are computed using the defined MLE optimization criterion.

$$G(\Omega_k, \theta) = \frac{B_\theta(\Omega_k)}{A_\theta(\Omega_k)} = \frac{b_0 + b_1\Omega_k^{-1} + ... + b_{nb}\Omega_k^{-nb}}{a_0 + a_1\Omega_k^{-1} + ... + a_{na}n\Omega_k^{-na}} \tag{4.60}$$

MLE methods use the same system approximations resulting in the same expressions as in equation (4.53) and (4.57) for the inertial and coupling elements at the test bench. The deterministic component of the engine inertia is presented in equation (4.61), from which the engine inertia can be computed as in equation (4.62). Based on the approximations, the coefficients of $G(\Omega_k, \theta)$ for estimation of inertia is defined as $n_a = 1$, $n_b = 0$. Using the knowledge of the resonant frequency, the inertia of the dynamometer can be computed. The computation of the dynamometer inertia can also be used for PEM, using the knowledge of resonant frequency obtained from non-parametric identification. Using the shaft torque measurements and the speed difference between the inertia, the stiffness and the damping of the shaft can be computed as in equation (4.63) and (4.64). The corresponding set-

tings for identification of the coupling characteristics uses the definition $n_a = 1$, $n_b = 1$.

$$\omega_E(k) = -\frac{\frac{T_s}{J_E}}{1 - z^{-1}} T_{sh}(k) \tag{4.61}$$

$$J_E = \frac{T_s}{b_1}, J_D = \frac{c}{\omega_r^2 - \frac{c}{J_E}} \tag{4.62}$$

$$T_{sh}(k) = \frac{(d - T_s c) - dz^{-1}}{1 - z^{-1}} \Delta\omega(k) \tag{4.63}$$

$$c = \frac{(b_2 - b_1)}{T_s}, d = -b_2 \tag{4.64}$$

### 4.4.5 Initialization of the identification algorithm

Despite the linear modeling assumed in this work, the cost function of the optimization problems involved is usually nonlinear and non-convex (except ARX models). Hence the initial values used for the optimization based parametric identification methods namely Prediction Error Method (PEM) and Maximum Likelihood (ML) play an important role in the convergence to the global minimum. As the parametric models use physically motivated model structures, the natural way to initialize the parameters shall be using prior knowledge of the process. This prior knowledge may not available, hence this section discusses alternative methods to arrive at the initial values. Both the approaches PEM and MLE use damped Gauss-Newton method for optimization with corrections based on the Levenberg-Marquardt method in case of divergence of the cost function [113].

#### Prediction Error method

The initial value of the cost function in case of prediction error method done as follows [100]

- initial estimate of the plant transfer function ($\hat{A}(q)$ and $\hat{B}(q)$)is determined using four-stage instrumental variables (IV) algorithm.
- an estimate of the equation noise is computed as in equation (4.65), where q stands for the backward shift operator.

- determine initial estimates of $C(q)$ using the equation (4.66) after high-order AR approximation to compute $\hat{e}$ as estimates of ARX model with $\hat{v}$ as output and $\hat{e}$ as input using linear least squares approach.

$$\hat{v}(k) = \hat{A}(q)y(k) - \hat{B}(q)u(k) = C(q)e(k) \tag{4.65}$$
$$\hat{v}(k) = (C(q)-1)\hat{e}(k) + e(k) \tag{4.66}$$

#### Maximum Likelihood method

The cost function employed for the SML based Error-In-Variables estimation uses the cost function as given in equation (4.67). This expression is a reformulation of the equation (4.47) for a parametric transfer function representation $G(\Omega_k, \theta) = \frac{B_\theta(\Omega_k)}{A_\theta(\Omega_k)}$.

$$V_F(\theta, Z) = \frac{1}{F}\sum_{k=1}^{F} \frac{|A_\theta(\Omega_k)Y(k) - B_\theta(\Omega_k)Y(k)|^2}{\hat{\sigma}_Y^2(k)|A_\theta(\Omega_k)|^2 + \hat{\sigma}_U^2(k)|B_\theta(\Omega_k)|^2 - 2Re(\hat{\sigma}_{YU}^2(k)A_\theta(\Omega_k)\bar{B_\theta}(\Omega_k)} \tag{4.67}$$

It is nonlinear in parameters $\theta$ as they appear in both numerator and denominator polynomials. In order to generate initial values, the nonlinear cost function shall be modified such that the global minimum can be computed using numerical techniques such as singular value decomposition [104]. Such an approximation is expressed in equation (4.68). The cost function formulated in equation (4.68) leads to a weighted generalized total least squares problem, a much tractable problem.

$$V_F(\theta, Z) = \frac{\sum_{k=1}^{F} |A_\theta(\Omega_k)Y(k) - B_\theta(\Omega_k)Y(k)|^2}{\sum_{k=1}^{F} \hat{\sigma}_Y^2(k)|A_\theta(\Omega_k)|^2 + \hat{\sigma}_U^2(k)|B_\theta(\Omega_k)|^2 - 2Re(\hat{\sigma}_{YU}^2(k)A_\theta(\Omega_k)\bar{B_\theta}(\Omega_k)} \tag{4.68}$$

### 4.4.6 Identification of powerpack test benches

This section presents the extension of the identification method to test benches with multiple inertial components and associated couplings. The following notation shall be used. The quantities $J_i$ represent the moment of inertia of the $i^{th}$ inertia, the characteristics of the $j^{th}$ coupling is modeled using the stiffness $c_j$ and $d_j$ respectively. The shaft torque in the $k^{th}$ coupling is denoted by $T_{sh,k}$. The speed of the $m^{th}$ inertia is denoted by $\omega_m$.

In the case of powerpack test benches with multiple inertia different modes of operation are possible. In a speed controlled operation, speed control can be realized using any of the energy converters, other than the ICE as speed controlled operation of the ICE is difficult to realize. For the powerpack in Figure 4.1 speed control can be realized using the ETM or the dynamometer.

#### Non-parametric identification and validation using simulation

The non-parametric identification is based on the LPM method using the known reference signal. Non-parametric identification results using a simulation model of the powerpack test bench with speed controlled operation using the dynamometer has been shown in Figure 4.4. The computed FRF between the shaft torque at the second coupling ($T_{s2}$) and speed at the third inertia ($\omega_3$) is depicted. Multi-sinusoidal excitation of the dynamometer speed controller up to a frequency of 100 Hz was employed. The two eigenfrequencies of the setup around 20 Hz and 60 Hz along with the anti-resonant frequency at 41 Hz can be observed from the FRF. These values can be verified using the equations (4.69) and (4.70) approximately neglecting the damping effects. The values of inertia, stiffness parameters were selected as $J_1 = 0.244, J_2 = 0.144, J_3 = 0.306$ in $kgm^2$ and $k_1 = 6000, k_2 = 10000$ in $Nm/rad$.

$$\omega_{eigen}^4(J_1J_2J_3) \approxeq -k_1k_2(J_1 + J_2 + J_3) + (k_1J_2J_1 + (k_1 + k_2)J_2J_1 + k_1J_2J_3)\omega_{eigen}^2 \tag{4.69}$$

$$\omega_{notch}^2 \approxeq k_1(J_1 + J_2)/(J_1J_2) \tag{4.70}$$

This observation motivates a three inertial approximation for parametric identification. This step is essential as test setups may have a stiffer interconnection between the inertia requiring a two-inertial approximation in the operational frequency range or even finer discretization with more than three inertia in case of powerpack and more than two inertia in case of engine test benches [96]. On the similar lines as used to compute the FRF in Figure 4.4, the FRF between the dynamometer speed (as input) and the engine speed (as output) of the powerpack is presented in Figure 4.5. As in the previous case, the two eigenfrequencies of the setup around 20 Hz and 60 Hz are observable. The identification was performed using excitation around a mean speed of 2400 rpm with a non-zero pedal value. As the engine is not motored, the excitation of the engine at the first and second dominant harmonics from the 2-cylinder engine used in the simulation model at frequencies 40 Hz and 80 Hz can be observed in the noise and total covariance estimates.

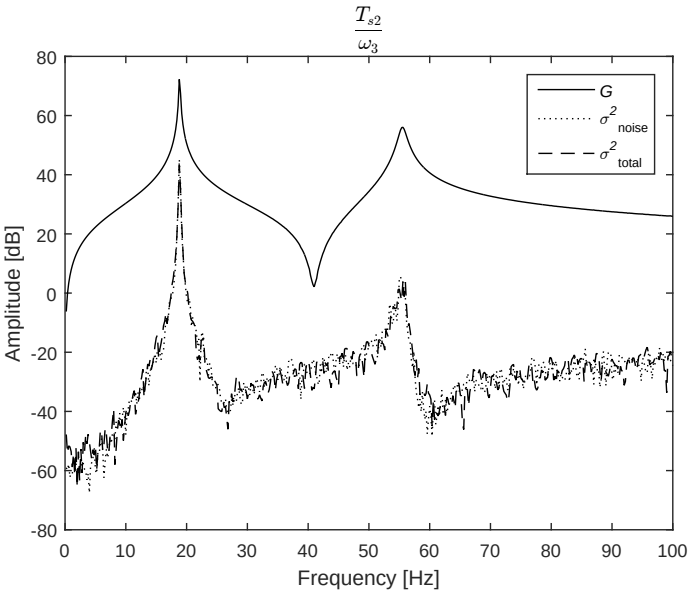


**Figure 4.4:** Non-parametric LPM identification of the powerpack test bench using simulation at a mean speed of 1500 rpm using a motored engine

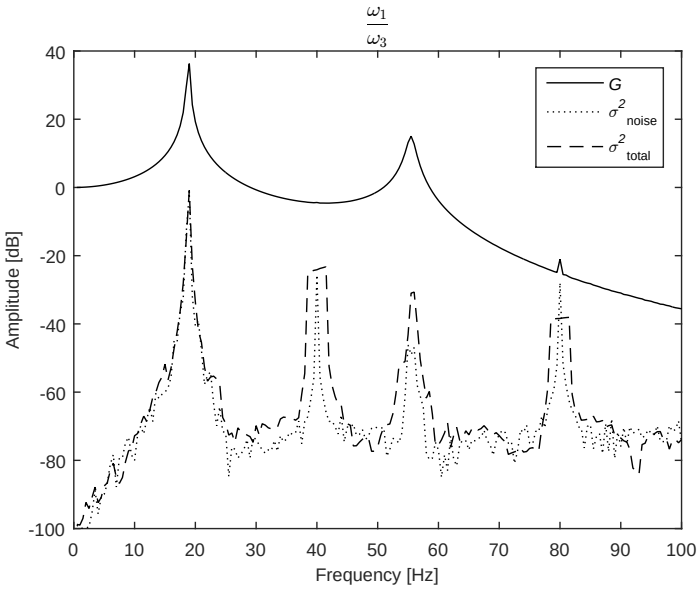


**Figure 4.5:** Non-parametric LPM identification of the powerpack test bench using simulation at a mean speed of 2400 rpm using a fired engine

Despite the excitations at the above-mentioned frequencies due to the engine operation, the FRF does not show any distortions and reflects the system behavior. The small distortion corresponding to the second harmonic at 80 Hz can be neglected as it is below -20 dB, a negligible value. It has to be noted that with higher pedal values and the corresponding higher dynamic engine torque, a distortion of the estimated FRF is possible. These distortions of the noise covariance function, if not handled properly would also affect the parametric estimates as the non-parametric noise covariances as weighting functions in the case of the MLE method. In the case of PEM method, one would have to deal with a higher order noise transfer function representation. This effect has been observed in the literature in case of PEM and has been termed as the convergence problem in computing the parametric estimated in [98]. Here, it has been shown that the effect is not limited to parametric but also observable in case of non-parametric identification. Nevertheless, one workaround to deal with this effect is to perform the identification both parametric and non-parametric with a motored engine.

#### Parametric identification using the iterative procedure

As discussed in the case of PEM and MLE, the identification of inertial component requires torque acting on the inertia. Torque transmitted by the shaft along with speed at both ends of the shaft is required for the identification of coupling parameters. In addition, there exist other possibilities for iterative identification in the case of three inertial test bench due to the possibility of speed control at different inertia. The discussion assumes that the first inertia is that of the ICE, the second and third inertia correspond to the ETM and the dynamometer respectively. Using the speeds $\omega_1$ and $\omega_2$ as well as the torque $T_{sh1}$ the coupling stiffness can be identified. As the inertia one is the ICE which is motored, using noise approximation of the drag torque along with its speed $\omega_1$ and the shaft torque $T_{sh1}$, $J_1$ can be computed. This procedure is repeated to identify $J_2$ and $k_2$. This procedure can also be used in case of speed control at the second inertia if the actuated torque at the second inertia is known, to identify $J_2$. The discussion of the results of this method using simulation with different noise power is done in section 4.5.1.

## 4.5 Validation

This section discusses the simulation and experimental validation of the developed identification techniques. The simulation employs a model of the test bench mechanics using component data sheets based on the configuration of the test bench. Analysis of the identification methods in simulation can be used to study their performance using different noise levels on the measurement signals. This is realized by adding noise to both speed and torque signals based on the SNR defined. The input-output signals are sampled uniformly with a sampling interval of 1 ms which is also used for experimental measurements. Experimental validation shall be limited to the engine test bench configuration.

### 4.5.1 Monte Carlo simulations

The Monte Carlo simulation results are listed in Table 4.2 and 4.3 where the mean and standard deviation of the estimated parameters along with their true value is presented. A Monte Carlo simulation of 100 realizations for the different noise levels defined by SNR was performed. In case of robust MLE method, each realization used 4 experiments, with each experiment has 4 periods.

Table 4.2 presents the results in case of a test bench with 2 inertia. It can be seen from the table that the OE based methods, ARX and ARMAX perform similarly in the presence of input noise and exhibit a bias in the estimation. Methods

**Table 4.2:** Results from Monte Carlo simulation of a two inertial test bench

| Method | SNR [dB] | | Stiffness $k$ [Nm/rad] | Inertia $J_E$ [kgm$^2$] |
|---|---|---|---|---|
| ARX | 30 | true value | 2260 | 0.12 |
| | | mean | 2266.20 | 0.12 |
| | | std | 0.2477 | 1e-5 |
| | 10 | true value | 2260 | 0.12 |
| | | mean | 1962.52 | 0.138 |
| | | std | 9.746 | 6e-4 |
| ARMAX | 30 | true value | 2260 | 0.12 |
| | | mean | 2266.21 | 0.12 |
| | | std | 0.2362 | 1e-5 |
| | 10 | true value | 2260 | 0.12 |
| | | mean | 1961.8 | 0.138 |
| | | std | 9.84 | 6e-4 |
| MLE Fast | 30 | true value | 2260 | 0.12 |
| | | mean | 2266.24 | 0.118 |
| | | std | 5.55 | 2e-4 |
| | 10 | true value | 2260 | 0.12 |
| | | mean | 2305.7 | 0.118 |
| | | std | 9.746 | 4e-4 |
| MLE Robust | 30 | true value | 2260 | 0.12 |
| | | mean | 2262.8 | 0.118 |
| | | std | 0.448 | 2e-5 |
| | 10 | true value | 2260 | 0.12 |
| | | mean | 2267.34 | 0.118 |
| | | std | 5.9 | 1e-4 |

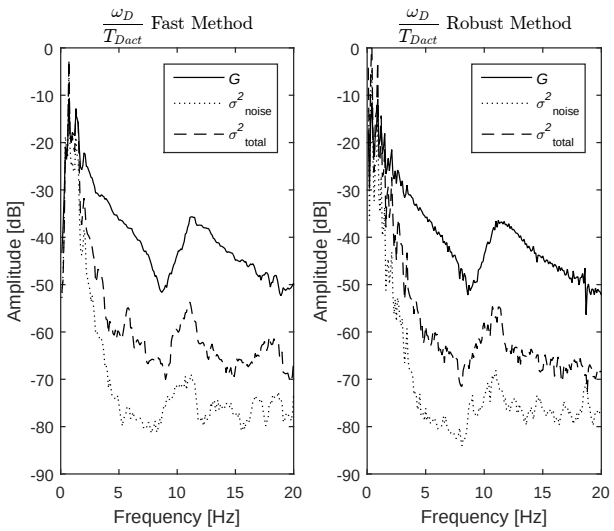


**Figure 4.6:** Comparison of robust and fast methods of non-parametric identification using LPM measured at 1500 rpm

based on EIV framework perform better than the OE based methods with the robust method providing the best results. Similar trends in the results can be seen in the Monte Carlo simulation analysis of the identification of test benches with 3 inertia listed in Table 4.3.

In the presence of noise, the MLE methods perform better than the OE based PEM identification. Further among the OE based methods, the performance of the ARX and ARMAX methods do not differ significantly. In the case of PEM, the ARX method uses linear regression techniques and is more attractive from the computational perspective than the ARMAX method. The smaller bias of the MLE parametric estimates in comparison to the PEM estimates in the presence of noise can be observed. Based on these observations, only the ARX and MLE methods shall be used for identification of the test bench from measurements.

### 4.5.2 Experimental validation

The test engine is a series-production, current generation 4-cylinder light-duty diesel engine, equipped with a common-rail injection system, cooled, high-pressure

**Table 4.3:** Results from Monte Carlo simulation of a three inertial test bench

| Method | | Stiffness $k_1$ [Nm/rad] | Inertia $J_1$ [kgm$^2$] | Stiffness $k_2$ [Nm/rad] | Inertia $J_2$ [kgm$^2$] | Stiffness $k_1$ [Nm/rad] | Inertia $J_1$ [kgm$^2$] | Stiffness $k_2$ [Nm/rad] | Inertia $J_2$ [kgm$^2$] |
|---|---|---|---|---|---|---|---|---|---|
| | | SNR 30 dB | | | | SNR 10 dB | | | |
| ARX | true value | 500 | 0.244 | 9000 | 0.144 | 500 | 0.244 | 9000 | 0.144 |
| | mean | 500.24 | 0.244 | 9240.3 | 0.145 | 501.9 | 0.357 | 9049.43 | 0.111 |
| | std | 8e-13 | 5e-16 | 2e-11 | 2e-17 | 7e-13 | 1e-16 | 2e-11 | 8e-17 |
| ARMAX | true value | 500 | 0.244 | 9000 | 0.144 | 500 | 0.244 | 9000 | 0.144 |
| | mean | 500.24 | 0.244 | 9240.3 | 0.146 | 501.9 | 0.357 | 9049.43 | 0.111 |
| | std | 8e-13 | 5e-17 | 2e-11 | 2e-16 | 7e-13 | 2e-16 | 2e-11 | 9e-17 |
| MLE Robust | true value | 500 | 0.244 | 9000 | 0.144 | 500 | 0.244 | 9000 | 0.144 |
| | mean | 500.3 | 0.245 | 9031.4 | 0.145 | 500.22 | 0.244 | 9038.41 | 0.1436 |
| | std | 7e-13 | 2e-16 | 2e-11 | 9e-17 | 6e-3 | 1.7e-4 | 8e-2 | 1e-4 |
| MLE Fast | true value | 500 | 0.244 | 9000 | 0.144 | 500 | 0.244 | 9000 | 0.144 |
| | mean | 500.6 | 0.248 | 9033.1 | 0.143 | 501.9 | 0.249 | 9049.43 | 0.145 |
| | std | 2e-4 | 1e-05 | 0.67 | 1e-4 | 9e-3 | 3e-05 | 3.433 | 3e-4 |

exhaust gas recirculation and a variable geometry turbine. The engine is operated using an induction machine as a dynamometer. The coupling between the engine and the dynamometer is realized using a flexible shaft. As discussed in section 4.5.1 only ARX and MLE approaches are studied using test bench measurements.

Non-parametric identification of the test bench torsional dynamics was performed using fast and robust methods. The fast method uses 2 periods of multi-sinusoidal excitation whereas the robust method uses 5 realizations of multi-sinusoidal excitations with 2 periods each. The measurements were repeated at speeds 1500, 1900 and 2200 rpm with a motored engine. The maximum amplitude of the excitations was limited to 50 rpm around the mean speed to avoid the nonlinear operation of the speed controller.

Figure 4.6 presents the results of the identification using measurements around the speed of 1500 rpm. The identified transfer function between the actual value of the dynamometer torque and the speed of the dynamometer at the engine test bed for the whole frequency range of the excitations is presented in the figure. The form of the identified transfer function is similar to the transfer behavior between actuated torque and speed of a controlled two inertial system. It shall be noted that the shaft torque measurements have not been used for the identification. By comparison of the fast and robust methods, it can be concluded that the robust method has a better separation between the plant transfer function and the identified noise models than the fast method. The eigenfrequency of the setup at 12.5 Hz and anti-resonant frequency at 9.8 Hz can be observed.

The applicability of the developed identification methods for different realizations of the engine test bench shall be discussed. Figure 4.7 presents the identified FRF using LPM and robust measurement strategy from two different engine test benches. The FRF presented corresponds to the transfer function with dynamometer torque as input and shaft torque as the output. The form of both the FRFs shows the behavior of the two inertial torsional oscillatory systems. The corresponding eigenfrequencies of 10.8 Hz and 11.2 Hz, followed by the respective isolation regions corresponding to the torsional spring can be seen.

To study the influence of operating points on the identification results, LPM identification using fast method was performed around the speeds 1500, 1900 and 2200 rpm with the motored engine and the results of the identified transfer function are presented in Figure 4.8. The measurement data used for this identification was the set and actual dynamometer speeds, without any torque measurements at the test setup. As it can be seen, the anti-resonant frequency around 9 Hz and

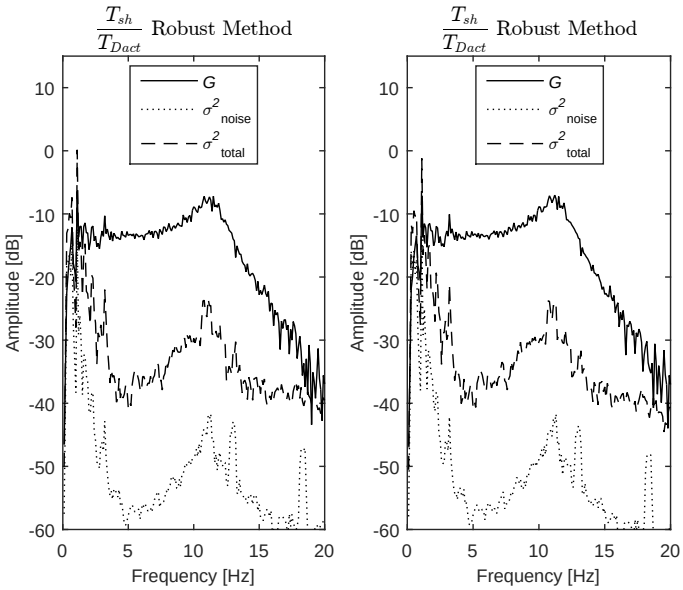


**Figure 4.7:** Comparison of robust non-parametric identification using LPM of engine test benches measured at 2400 rpm using motored engine

**Table 4.4:** Identified parameters from the engine test bench

| **Quantity** | **ARX Method** | **MLE Method** |
|---|---|---|
| ICE Inertia $[kgm^2]$ | 0.222 | 0.270 |
| Shaft Stiffness $[Nm/rad]$ | 805.89 | 831.31 |
| Dynamometer Inertia $[kgm^2]$ | 0.387 | 0.341 |

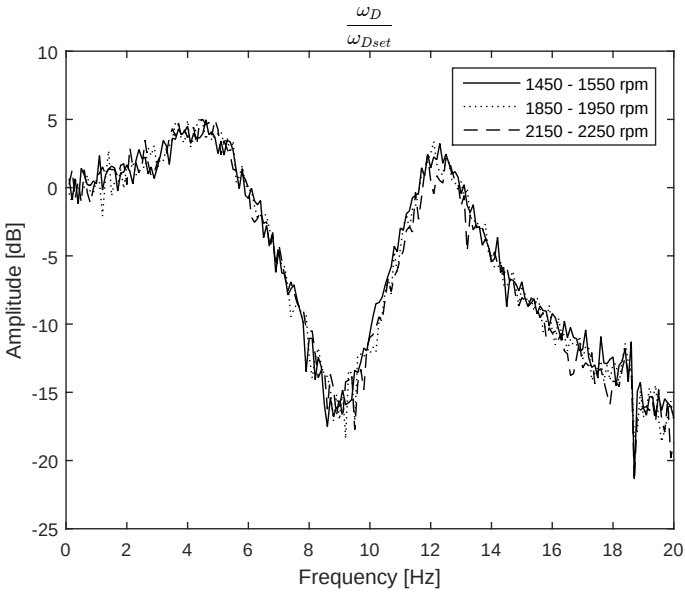


**Figure 4.8:** Non-parametric LPM identification of transfer function between set and actual dynamometer speed of the engine test bench

**Table 4.5:** Identified parameters from the engine test bench at various speeds

| Quantity | Fast Method | Robust Method |
|---|---|---|
| Operating Speed 1500 $rpm$ | | |
| ICE Inertia $[kgm^2]$ | 0.2731 | 0.276 |
| Shaft Stiffness $[Nm/rad]$ | 839.56 | 831.31 |
| Operating Speed 1800 $rpm$ | | |
| ICE Inertia $[kgm^2]$ | 0.2739 | 0.2715 |
| Shaft Stiffness $[Nm/rad]$ | 847.82 | 838.51 |
| Operating Speed 2200 $rpm$ | | |
| ICE Inertia $[kgm^2]$ | 0.2791 | 0.2754 |
| Shaft Stiffness $[Nm/rad]$ | 851.02 | 848.13 |

the eigenfrequency around 12.5 Hz show very little variations over the different speeds.

Table 4.4 presents the results of parametric identification. The measurement data for ARX model identification uses PRBS excitations with a maximum amplitude of 20 rpm around the mean speeds. The results of identification in Table 4.4 are from measurements around a mean speed of 1500 rpm and motored engine of the PEM ARX and MLE fast method. The values of the ICE and dynamometer inertia identified using the MLE method are close to the computed values from CAD data and dynamometer data from the manufacturer respectively. One advantage of the ARX identification is the linear regression based computation, which can be implemented on the test bench for real-time computation though it provides less accurate estimates when compared to the MLE method.

Due to these reasons, a further experimental study of the parametric identification using MLE shall be extended to different operating speeds of the engine test bench. The results of MLE identification for fast and robust methods at different operation speed is tabulated in Table 4.5. Both the identified shaft stiffness values lie in the range provided by the manufacturer between 800 - 850 Nm/rad. Subsequently, the experimental validation is also carried out at another engine test bench with a stiffer coupling validating the identification method at different test benches. The identified results in this case which agree well with the manufacturer data are listed in Table 4.6.

In summary, the MLE method provides better estimates than PEM in the presence of noise effects. The robust MLE method using additional data performs

**Table 4.6:** Identified parameters from the engine test bench with stiffer coupling

| Quantity | Fast Method | Robust Method |
|---|---|---|
| Operating Speed 1500 $rpm$ | | |
| ICE Inertia $[kgm^2]$ | 0.2878 | 0.2974 |
| Shaft Stiffness $[Nm/rad]$ | 1512.9 | 1570.0 |
| Operating Speed 1800 $rpm$ | | |
| ICE Inertia $[kgm^2]$ | 0.2801 | 0.299 |
| Shaft Stiffness $[Nm/rad]$ | 1577.6 | 1550.3 |
| Operating Speed 2200 $rpm$ | | |
| ICE Inertia $[kgm^2]$ | 0.2768 | 0.301 |
| Shaft Stiffness $[Nm/rad]$ | 1535.7 | 1516.4 |

marginally better than MLE using a fast measurement strategy. Among the OE framework methods, the ARX is attractive due to the reduced complexity in computing the parameters.

## 4.6 Evaluation

This section demonstrates the relevance of developed identification methods. With the presented methods, identification can be performed for engine and powerpack test benches during commissioning and also reconfiguration. In commissioning phase the identified model can be used to tune the speed controller in the testbed using loop-shaping procedures. In addition, identification in the reconfiguration phase helps to tune notch filters to suppress excitation of resonant frequencies during In-The-Loop operation.

### 4.6.1 Use case 1: Implementation of notch filter

With the knowledge of the eigenfrequency of the test bench, filters can be designed to avoid its excitation. Conventional powertrains with combustion engines are operated at the test bench at speeds above the idling speed with the test bench eigenfrequency sufficiently ($\sqrt{2}$ times) away from the frequency corresponding to the idling speed of the engine. Combustion engines with start/stop functionality or which is constituent of a hybrid powertrain operation of the test bench at the entire speed range from zero speed to the maximum speed of the engine is essential. With the introduction of In-The-Loop operation, the spectra of the externally computed

set value can include components in the eigenfrequency. Specifically, in the case of Engine-In-The-Loop operation, the commanded speed signal which is computed by the model based on the load conditions can excite the test bench eigenfrequency due to model instability. Under such operation, the excitation of the test bench eigenfrequency shall be avoided.

One approach is to enable mechanical redesign of the test bench for the increased bandwidth of operation along with a redesign of the controller by extension using disturbance rejection scheme [112]. A simpler but sub-optimal (optimality with respect to reproducibility of realistic powertrain behavior at the test bench) approach would be to employ a notch filter to suppress energy in the excitation signal around the eigenfrequency of the test bench. The parameterization of the notch filter requires resonant frequency and Q-factor. The resonant frequency can be identified directly using non-parametric methods or indirectly using parametric methods.

The identified eigenfrequency was used to implement a notch filter to avoid excitations of the eigenfrequency at the test bench with the 4-cylinder diesel engine. The results using a chirp excitation from 0 Hz to 20 Hz of the dynamometer set speed around a mean speed of 1200 rpm at the engine test bench is presented in Figure 4.9. The engine was motored during the experiment. The top plot presents the shaft torque signal during normal operation. The increased amplitude of excitations around the eigenfrequency is noticeable. With the implementation of the notch filter, the excitations around the eigenfrequency are damped. The resulting shaft torque oscillations can be observed in the bottom plot.

### 4.6.2 Use case 2: Parametrization of observer

The inner engine torque in case of the internal combustion engine results from the pressure variations in the combustion chamber without the effects of friction torque and other parasitic torque demand from the auxiliary devices. The inner ICE torque is used for control and diagnosis purposes as presented in section 3.2. Considering packaging, cost and durability reason torque sensing devices cannot be used for its measurement. Chapter 3 presents a method to estimate the engine torque as an unknown input to the dynamic system and uses the theory of Unknown Input Observers (UIO) with a proportional structure. The variant of the UIO with the ICE as the system requires the measurements of ICE speed and shaft torque as well as the ICE inertia as a parameter. The parametric identification methods described in this work can be used to estimate the ICE inertia.

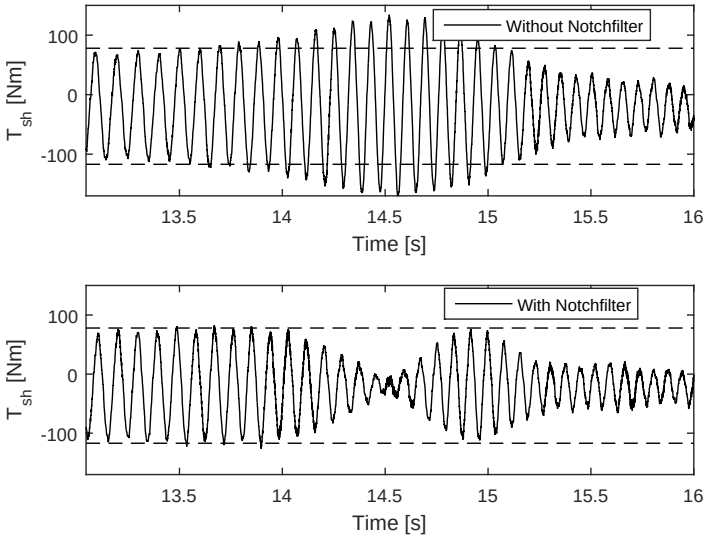


**Figure 4.9:** Reduction of shaft torque amplitude with a notch filter at the engine test bench

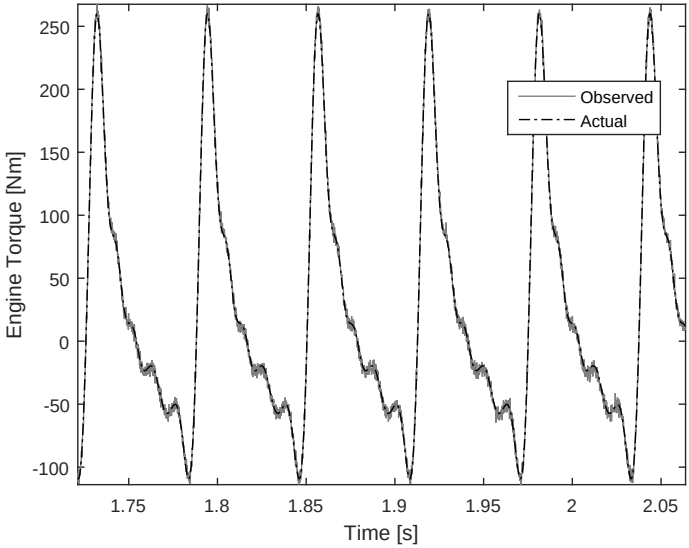


**Figure 4.10:** Estimation of engine torque using observer in simulation

As the inner engine torque requires additional measurement equipment and effort, simulation result shall be used for demonstration. The designed UIO observer in the simulation is parameterized with the engine inertia. Figure 4.10 presents the actual and the observed engine torque of the 2-cylinder gasoline engine from the CEA powertrain during operation at speed of 1000 rpm and mean torque value of 60 Nm. As it can be seen, the observed torque using the parameterized UIO is close to the actual torque generated by the combustion engine.

## 4.7 Conclusion

In this chapter, the non-parametric and parametric identification of test bench dynamics using different methods and model structures within a closed loop environment have been presented. Non-parametric identification was used to gain an initial idea of the process dynamics. In addition, non-parametric models are used for arriving at a choice for the parametric model. This is of specific interest in case of direct closed loop identification using PEM to obtain consistent parameter estimates. It can also be used to determine weights in case of sample

maximum likelihood estimation. Local Polynomial Method was used to identify the non-parametric model in an EIV stochastic framework.

The flexibility of the developed identification methods based on the available measurement signals was demonstrated. This was done by test bench identification only using the speed signal as excitations and measurements. The methods were able to deal with errors also in the input signals in an EIV framework using periodic reference signals. Nonlinear behavior of the test benches was analyzed by identification at different operating speeds with the motored engine. Though no nonlinearity was observed, the methods can be used to handle mild non-linearities if any.

The developed methods are studied using Monte Carlo simulations with different noise levels. In the case of PEM, the ARX model approximation provided good results as in the case of ARMAX approximations requiring only linear regression solutions. Further, the MLE method additionally provides a noise model in addition to the identified parameters and better estimates than the ARX method. Further validation of the non-parametric and parametric methods was performed on a dynamical test bench with a motored combustion engine. The evaluation of the developed identification methods was done using two exemplary use cases.

## 5 Adaptive Filtering based Active Vibration Reduction Controller

This chapter approaches the active torsional vibration reduction problem as an active noise control (ANC) problem, proposing solutions using adaptive filtering techniques. Adaptive filter based ANC uses the output signal and a signal correlated with the disturbance to realize ANC. In ANC jargon, the term primary refers to the noise source and secondary refers to the anti-noise generator. From the torsional vibration perspective, the ICE is the primary source and the ETM which generates the compensation torque serves as the secondary source. In contrast to the (robust) output feedback control approaches discussed in chapter 6, adaptive filtering based compensation techniques do not require a model of the process provided the primary and secondary source locations coincide. In case of presence of secondary path dynamics between the actuator which realizes the control action and the output signal, knowledge of the secondary path dynamics is necessary which can be identified using techniques discussed in chapter 4. The novel aspects of the approach discussed in this chapter are listed below:

- Application of Conjugate Gradient (CG) method based adaption procedure for ANC in torsional powertrains
- Implementation of the adaptive filtering based controller without measurement of a reference signal
- Pretuning of adaptive filter weights for improved convergence

The aspects listed above can be broadly classified into algorithmic features and features based on physical insight into the problem. The algorithmic feature involves the use of the CG method. Instead of the commonly employed stochastic descent approach, CG method has been used thanks to faster convergence and reduced computational complexity. The other two aspects are based on the physics of the active torsional vibration problem. The frequency of the disturbance signal acting on the system, the ICE torque pulsations have a frequency corresponding to its mean speed as given in equation (3.80). With the knowledge of the mean ICE speed, a signal with similar spectral characteristics as the disturbance signal can be generated. This signal which is correlated to the external disturbance signal which is the ICE torque and can be used as the reference signal instead of using additional instrumentation to measure a suitable reference signal.

In case of ICE operation, certain events such as start/stop occur frequently due to wide acceptance of start/stop systems to avoid idling phase of the engine. In addition, prediction of such start/stop events with high probability during certain scenarios such as a stop at a traffic light due to the red signal is possible. Provided

the information about the signaling of the traffic light and the distance to the traffic light is available, the start of the ICE can be predicted with high accuracy. In such a situation, with a warm engine, the idling speed to which the engine shall be restarted is known and can be used to pretune the adaptive filter weights. It has to be noted that the adaptive filter to compensate for the torsional oscillations is activated only after the idling speed is reached. This avoids the unnecessary intervention of the engine start-up process which involves calibration from emission and comfort viewpoints. Apart from the above list, subspace methods are used to identify the secondary path transfer function which allows for IIR based realization of the transfer function rather than FIR based realization when using adaptive filtering techniques for secondary path identification. The FIR based filters are used to avoid stability issues during adaptation of the filter weights.

This Chapter is organized as follows. Section 5.1 presents the active noise control approach to active vibration reduction. Section 5.2 introduces the algorithms used for filter weight adaption and subsequently discusses the solution methods to adapt the filter coefficients. The developed adaptive controller along with its structure and the generation of the reference signal is discussed in section 5.3. This section also presents the offline identification of the secondary path transfer function at the experimental test bench. Validation of the developed controller using simulations and experimental investigations of the controller performance is done in section 5.4. Finally section 5.5 concludes this chapter.

## 5.1 Active Noise Control (ANC)

This section discusses the ANC approach for torsional vibration reduction in automotive powertrains after introduction to the feedforward and feedback ANC approaches. Adaptive filters will be used to realize the ANC algorithm. ANC cancels the primary noise using an anti-noise signal of equal amplitude and opposite phase based on the principle of superposition [65]. The active torsional vibration reduction problem is a single channel ANC problem. According to [65] a single channel ANC system comprises of a single reference sensor, single secondary source and signal error sensor in addition to the adaptation algorithm. As opposed to this configuration, multi-channel ANC systems use several secondary sources, error sensors and possibly several reference sensors.

The Wiener filter defines a solution to the linear filtering problem in the mean-square error sense. This solution represents the minimum point of the error response surface, which is a plot of the mean square value of the error with respect to the tunable filter weights of the linear filter. However, this statistical approach

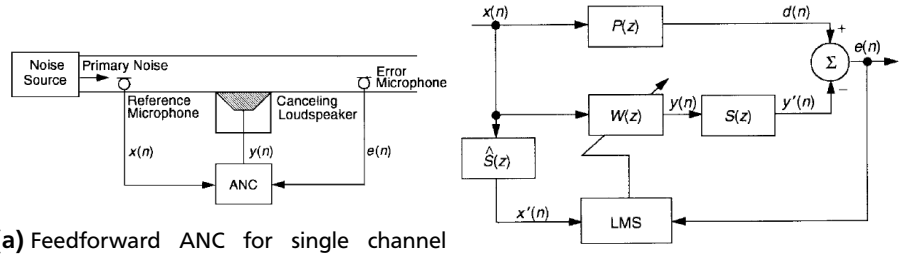


**(a)** Feedforward ANC for single channel acoustic noise cancellation

**(b)** Block diagram of the feedforward ANC using FxLMS algorithm

**Figure 5.1:** Schematic of the single-channel broad-band feedforward ANC system and its block diagram realized using FxLMS algorithm [65]

to the linear filtering problem assumes knowledge of statistical parameters such as mean and correlation function. Provided these statistical characteristics are known a-priori during the design, the Wiener filter represents the optimal design with the minimal mean-square error.

Due to the impracticality of the underlying assumptions and the non-stationarity of the associated signals adaptive filters have gained importance. The term adaptation refers to the update of the filter weights (starting with an initialization) during operation for satisfactory performance without complete knowledge of the relevant signal characteristics. Using recursive updates the Wiener solution or its time-varying counterpart the Kalman filter solution is approached subject to non-stationarity using the finite amount of data available. Variety of adaptive algorithms exist both in the time domain and frequency domain.

In this Chapter, time domain adaptive filters for FIR structures of least mean square and recursive least squares family shall be studied in the context of active noise control for torsional oscillation reduction in automotive powertrains. The feedforward scheme for single-channel ANC system is depicted in Figure 5.1. The depiction in Figure 5.1a presents the schematic of the ANC system. It requires both the reference signal and the error signal for its operation. Hence the implementation requires sensing of both the reference and the error signal along with an actuator to introduce the anti-noise signal. The associated block diagram representation in discrete time domain representation is shown in Figure 5.1b. The block diagram representation uses the Least Mean Square (LMS) algorithm for the adaptation procedure of the filter denoted using $W(z)$. $P(z)$ denotes the plant transfer function and $S(z)$ the secondary path transfer function respectively. The filtering

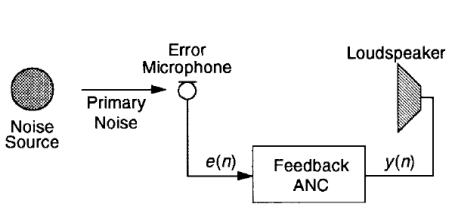


**(a)** Feedback ANC for single channel acoustic noise cancellation

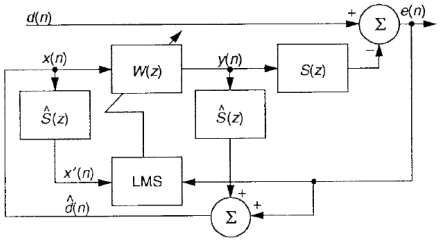


**(b)** Block diagram of the feedback ANC using FxLMS algorithm

**Figure 5.2:** Schematic of the single-channel broad-band feedback ANC system and its block diagram realized using FxLMS algorithm [65]

of the reference signal $x(n)$ by the estimate of the secondary path transfer function $\hat{S}(z)$ is performed to account for the secondary path transfer characteristics. Both LMS method and secondary path effects are discussed in section 5.3.

$$x(k) \equiv \hat{d}(k) = e(k) + \sum_{m=0}^{M-1} \hat{s}_m y(k-m) \tag{5.1}$$

$$X(z) \equiv \hat{D}(z) = E(z) + \hat{S}(z)Y(z) \tag{5.2}$$

Figure 5.2 presents the schematic and block diagram realization of a single channel feedback ANC system. The notation used is the same as in Figure 5.1. From a generic perspective, feedback ANC systems have been discussed in [65]. The common approach is to generate the reference signal based on the adaptive filter output and the error signal as given by the equations (5.1) or (5.2) in the time domain and frequency domain. Hence the basic idea is to estimate the primary noise based on the measured adaptive filter output and the measured error signal. Alternatively approaches based on Internal Model Control to generate the reference signal generation [114] have been also investigated. The approach in this study generates the reference signal based on the physics of the problem only using the measurements, without using the output of the adaptive filter. The generation of the reference signal is presented in section 5.3.2. As the reference signal is not measured, the developed scheme can also be interpreted as a feedback ANC system.

After the introduction of the schemes employed, the formulation of the active torsional vibration reduction as an adaptive ANC problem shall be done. Let $x(k)$

represent signal correlated with the disturbance acting on the system. $d(k)$ stands for the primary disturbance. The quantity $e(k) = d(k) - y(k)$ shall quantify the residual error signal. The output of the ANC used to cancel the disturbances shall be denoted using $y(k)$. $r(k)$ is the reference signal that is correlated with the disturbance signal. The objective of the ANC algorithm shall be to reduce the formulated error signal to zero as in equation (5.3), which can be interpreted as perfect cancellation based on the principle of superposition of two out of phase signals. To maintain consistency, all signals are assumed to be represented in the discrete time domain with time index k. Further, as the discussion is restricted to real-valued signals, the Hermitian operation denoted by $^H$ can be interpreted as $^T$ without loss of generality.

$$e(k) \stackrel{!}{=} 0 \tag{5.3}$$

## 5.2 Algorithms for Adaptive Filtering

Adaptive digital filters are often used to form an internal model of the response of the physical system under control [35]. A direct application of the adaptive filters to active control is mainly associated with the generation of an inverse response to oscillatory inputs. The adaptive filters considered in this work, have a fixed structure with the ability to adapt their parameters/filter weights online. The adaptation rule can be written in a generic form as in equation (5.4), which represents that the filter weights $w$ are adapted over the iteration variable $k$, depending on the chosen update rule denoted by $g$, with $e$ representing the error between the actual and desired signal characteristics. The adaptation algorithm used in this work employs linear updates.

$$w(k+1) = f(w(k), e, g) \tag{5.4}$$

### 5.2.1 Least mean square algorithm and variants

Since its introduction in [115] for adaptive control and in [116] for active noise control LMS algorithm has been widely applied due to its simplicity. The LMS algorithm was conceived as an approximate recursive solution to a stochastic least-squares problem. Assuming no knowledge of the signal statistics, neither the quantities $R = E\{u(k)u^H(k)\}$ denoting the input correlation matrix as well as

$p = E\{u(k)y(k)\}$ representing the cross-correlation vector between the input vector denoted by $u(k)$ and the scalar output represented by $y(k)$, nor the gradient of the error function can be computed. The LMS algorithm searches for weights along the direction of the negative instantaneous gradient given by $u^H(k)e(k)$ in the expression (5.5). The quantity $\mu$ is the learning rate. The error estimate $e(k)$ takes the form given by equation (5.6).

$$w(n+1) = w(k) + \mu u^H(k)e(k) \tag{5.5}$$

$$e(k) = d(k) - u^H(k)w(k) \tag{5.6}$$

#### Normalized LMS (NLMS)

With a higher amplitude of the input vector, the LMS filter suffers from gradient noise amplification problem [35]. As a solution to this problem, normalization using the squared Euclidean norm of the input vector at the current iteration is employed leading to normalized LMS (NLMS) filter. [35] discusses the NLMS based on the principle of minimal disturbance, which requires a change of the filter weights in a minimal fashion, subject to the constraints imposed on the output updates. In order to avoid numerical issues with very small input vectors regularization as shown in equation (5.7) can be employed with $\epsilon$, a small positive constant. The implementation in this work ensures a non-zero denominator to avoid the numerical issues. The normalization renders the adaptation of constant dimensionless and time-varying. [35] shows that the weight update of NLMS can be interpreted as the minimum-norm least-squares solution of an underdetermined problem.

$$\mu = \frac{\tilde{\mu}}{||u(k), 2||^2 + \epsilon} \tag{5.7}$$

#### Filtered LMS (FxLMS)

FxLMS is an extension of the LMS structure for systems which have a forward or secondary path. The secondary path represents the transfer path from the output of the adaptive filter to the desired signal used for adaptation. The introduction of the secondary-path transfer function into a controller with the standard LMS algorithm can cause instability [117]. This is due to the misalignment of the signals due to the presence of the secondary path and requires compensation. FxLMS first proposed in [118], uses an identical filter with the same transfer characteristics to weigh the update of the LMS algorithm. As the inverse of the transfer path may

necessarily not exist, this approach has gained wide acceptance over the use of inverse of the secondary path to cancel its effects. The usage of the NLMS method along with the secondary path transfer function leads to FxNLMS algorithm.

### 5.2.2 Recursive least squares algorithm

In simple terms, Recursive Least Squares (RLS) method is an extension of least squares to design adaptive filters. Despite its simplicity, variants of the LMS algorithm require an increased number of iterations to converge sufficiently close to the optimal solution once in its neighborhood. RLS method tries to achieve faster convergence at the expense of computational complexity during the iterations [35]. It can be interpreted as the LMS algorithm with the step size parameter $\mu$ replaced by the inverse of the input correlation matrix, a deterministic quantity. The computation of filter weights of RLS algorithm is an extension of the deterministic minimum square error solution expressed as in equation (5.8) computed in a recursive fashion [119], where $R$ is the deterministic correlation matrix and $p$ the correlation vector between the input signal and the desired response.

$$w(k) = R^{-1}(k)p(k) \tag{5.8}$$

### 5.2.3 Solution methods

LMS algorithm is realized using gradient descent, minimizing the local quadratic approximation of the error along the direction of the negative gradient. Such a minimization problem can be equivalently approached as a solution to a linear equation as given in equation (5.9). This viewpoint offers new possibilities to employ other methods to solve the linear system for the realization of adaptive filters.

The solution to a set of linear algebraic equations is common to many fields of science. The methods to solve such a system of equations can be broadly classified into direct methods and iterative methods [120]. Direct methods try to solve the set of equations exactly, whereas iterative methods try to approximate the solution to a certain degree of accuracy. There exist a wide variety of iterative and non-iterative methods for the solution of a system of linear equations. The discussion is restricted to iterative methods for the solution of linear equations.

This section gives an overview of the most common methods to motivate the selection of an appropriate algorithm for solving the adaptive filtering problem. Starting with an initial guess, iterative methods gradually approach the solution of

the system. Let $Ax = b$ with $A \in R^{n \times n}$ and $b \in R^n$ represent the system of equations whose solution $x \in R^n$ is of interest. The section briefly presents the methods for an involved discussion on the analysis and convergence properties the interested reader is referred to [120], [121].

#### Jacobi method

Jacobi method is an algorithm for determining the solutions of a diagonally dominant system of linear equations. The matrix A is split as $A = D + R$ with $D$ denoting a diagonal matrix and $R$ representing the remainder. The solution is computed iteratively as $x_{k+1} = D^{-1}(b - Rx_k)$. The steps involved are summarized in the algorithm 3.

**Algorithm 3** Jacobi Method

Initialize : **b, A,** $x^{(0)}$, $k_{max}$, $\epsilon$
$k = 0, \delta = 100 \times \epsilon$
While$[(\delta > \epsilon)\ AND\ (k < k_{max})]$
    For i =1:n
    $x_{Ni} = x_i + \left(\frac{r_i}{a_{ii}}\right)$
    End For
    $\delta = \frac{\|r\|}{\|b\|}$
    $x = x_N, k = k + 1$
End While

#### Gradient descent (GD) method

Gradient Descent (GD) method is a method to solve in an indirect fashion a system of linear equations modeling the problem as the minimization of linear least squares problem. This fact is presented by the equation (5.9). The core idea is to travel in search of the solutions in the direction of the negative gradient with a predefined step size. The direction is denoted by $d_k$ and the step size be denoted using $\alpha_k$. The expression for $d_k$ and $\alpha_k$ is given in the equation (5.10) and (5.11) respectively. It has to be noted that denominator in the equation (5.11) is a

scalar. With the values of $d_k$ and $\alpha_k$ the next iterate of the solution is computed as $x_{k+1} = x_k + \alpha_k d_k$.

$$Ax = b \leftrightarrow x = \text{argmin}(\frac{1}{2}||Ax - b||_2) \tag{5.9}$$

$$d_k = b - Ax_k \tag{5.10}$$

$$\alpha_k = \frac{d_k^T d_k}{d_k^T A d_k} \tag{5.11}$$

#### Newton method

Newton method is primarily used to solve a system of nonlinear equations. The method exhibits local quadratic convergence. It can be also used to solve the linear system of equations without requiring globalization techniques as in the case of nonlinear systems as given by equations (5.12) and (5.13).

$$x_{k+1} = x_k - \frac{f(x_k)}{f'(x_k)} \text{ with } f(x) = Ax - b \tag{5.12}$$

$$x_{k+1} = x_k - \frac{(Ax_k - b)}{A} \tag{5.13}$$

#### Conjugate gradient (CG) method

Conjugate Gradient is an iterative method which solves the equation $Ax = b$ by searching over the Krylov subspace $\mathscr{K}_j$ for $x_j$ such that the residual $r_j = b - Ax_j$ is orthogonal to $K_j$. Krylov subspace is a sequence of nested subspaces ($\mathscr{K}_0$) as in equation (5.16). The jth Krylov subspace $\mathscr{K}_j$ is a linear combination of $b, Ab, ..., A^{j-1}b$. The computational procedure of the CG method is summarized in the algorithm 4.

$$\mathscr{K}_0 = \{0\} \tag{5.14}$$

$$\mathscr{K}_k = span\{b, Ab, ...A^{k-1}b\}, k \geq 1 \tag{5.15}$$

$$\mathscr{K}_0 \subseteq \mathscr{K}_1 \subseteq \mathscr{K}_2 \subseteq ... \tag{5.16}$$

Convergence analysis of the presented algorithms has been theoretically investigated [120],[122]. This section discusses the convergence from a practical perspective with exemplary use cases. The use cases consider a linear system $Ax = b$. The first use case analyzes the convergence of the solution methods for randomly

**Algorithm 4** Conjugate Gradient Method

1: Choose the initial approximation $x_0(e.g.\ 0)$
2: $r_0 = p_0 = b - Ax_0$
3: For i=0,1...,n-2
4: $\quad \alpha_i = \frac{p_i^T r_i}{p_i^T A p_i}$
5: $\quad x_{i+1} = x_i + \alpha_i p_i$
6: $\quad r_{i+1} = r_i - \alpha_i A p_i$
7: $\quad$ If $r_{i+1} \times r_i < \epsilon$ break
8: $\quad \beta_i = \frac{r_{i+1}^T r_{i+1}}{r_i^T r_i}$
9: $\quad p_{i+1} = r_{i+1} + \beta_i p_i$
10: End For

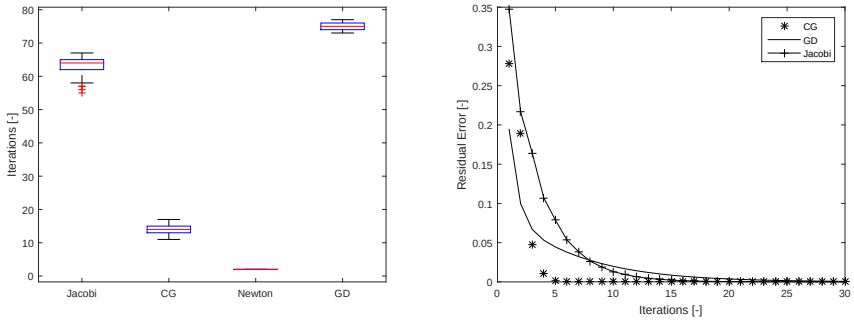


**(a)** Comparison of Iterations **(b)** Error over Iterations

**Figure 5.3:** Comparison of iterative solution methods for linear system of equations

generated b vectors. The second use case presents the number of iterations required for the methods to converge to a value below a predefined tolerance value in a deterministic setting with a fixed $A$ matrix and $b$ vector.

Figure 5.3 presents a comparison of the different iterative methods with a square matrix $A$ as given by equation (5.18) and a vector $b$. The residual vector $r(i)$ (of the $i^{th}$ iteration) is computed using the equation (5.17) with the norm interpreted as 2-norm of the vector. The quantity $x(i)$ refers to the solution obtained at the $i^{th}$ iteration of the system. The plot in figure 5.3a compares the number of iterations required to achieve a tolerance value of $1e^{-5}$ between the $i^{th}$ and $(i+1)^{th}$ iteration for the given matrix A but randomly generated vectors $b$. The number of

iterations required to converge within the given tolerance is depicted as box plots for the discussed solution methods starting with a zero initial value for vector $x$. The Newton method outperforms all other methods but involves the inversion of the matrix $A$. Based on the data of the current iteration in case of adaptive filters this inversion can be difficult in case of an ill-conditioned data. The Jacobi and GD method require roughly the same number of iterations, whereas the CG method converges faster than these two methods.

$$r(i) = \frac{||x(i) - x_{true}||}{||x_{true}||} \tag{5.17}$$

$$A = \begin{bmatrix} 3 & -2 & -1 \\ -2 & 4 & 2 \\ -1 & 0 & 5 \end{bmatrix} \tag{5.18}$$

$$b = \begin{bmatrix} 3 & -2 & -1 \end{bmatrix}^T \tag{5.19}$$

Figure 5.3b presents the dynamics of the residue (with the norm of the residue interpreted as the distance of the current solution iterate with the actual solution) given by equation (5.17) for the $A$ matrix and $b$ vector given by equations (5.18) and (5.19) respectively. Due to the additional computational complexity of inverting the system matrix associated with the Newton method, it is not considered for the comparison. The CG method converges to a value closer to the actual value with a fewer number of iterations than the other methods.

It has to be noted that the choice of $A$ matrix and $b$ vector in the above study was random. The analysis was repeated with other initializations of the solution vector for the methods CG, GD and Jacobi with a similar conclusion as presented. The validity of the above argument in a theoretical perspective can be understood due to the global behavior of the solution to the linear system provided its existence is guaranteed.

From the above discussion, it can be concluded that the CG method offers advantages in convergence speed compared to the other methods without requiring complex operations such as matrix inversion. Hence the LMS method which is usually implemented with (stochastic) gradient descent will be implemented using the CG method termed as FxNLMS CG, which shall be the focus of the discussion in section 5.3.3.

## 5.3 Development of Adaptive Filtering based Vibration Controller

This section discusses the development of the adaptive filter based active vibration controller. Beginning with the structure of the controller, the section proceeds to discuss the physically motivated generation of a reference signal. Followed by which the realization of the adaptive filtering algorithms is discussed. The advantages arising from the pretuning of the adaptive filters is presented. The section concludes with a discussion on the identification of the secondary path transfer function.

### 5.3.1 Structure of the controller

Figure 5.4 depicts the structure of the active vibration reduction controller. The only input to the controller is the ETM speed denoted by $n_{ETM}$ whose mean value $n_{ETM,mean}$ and the harmonics are computed by the estimator, as given in chapter 3. The signal $n_{ETM,mean}$ is used by the reference signal generator to compute the reference signal. The identified model of the secondary path is denoted by $S'(z)$ and the secondary path is represented by $S(z)$. The adaptation schemes for the first harmonic leaky FxNLMS and RLS have been represented (the case $i = 1$). Further, the extendability of the scheme to multiple harmonics (the cases $i = 2...L$ where L stands for the harmonic to be reduced) has also been depicted. The structure has been presented for multiple reference signals, however, the implementation only uses single reference signal as discussed in the single channel ANC from section 5.1. The computed set value compensation torque denoted by $T_{EM,set}$ is fed to the ETM. The error signal is computed from the measured ETM speed and the estimated mean value. The factorization map can be used for calibration for powertrain variants with different maximum available torque-speed characteristics of the ETM. This feature is used for the realization of unidirectional compensation torque either in generator or motor operation of the ETM and is discussed in section 5.4.4.

### 5.3.2 Reference signal generator

The source of disturbance is the combustion engine, an ideal reference signal would be the dynamic torque (and not just the non-periodic component) generated by the combustion engine. Such an approach is only feasible in a simulation environment and was used for the initial development of the vibration controller using simulations. Torque sensing using measurement flanges is difficult in practice as it is expensive, sensitive to temperature and leads to an error in the case of shaft bending making it difficult to realize the controller using the ICE torque as the reference

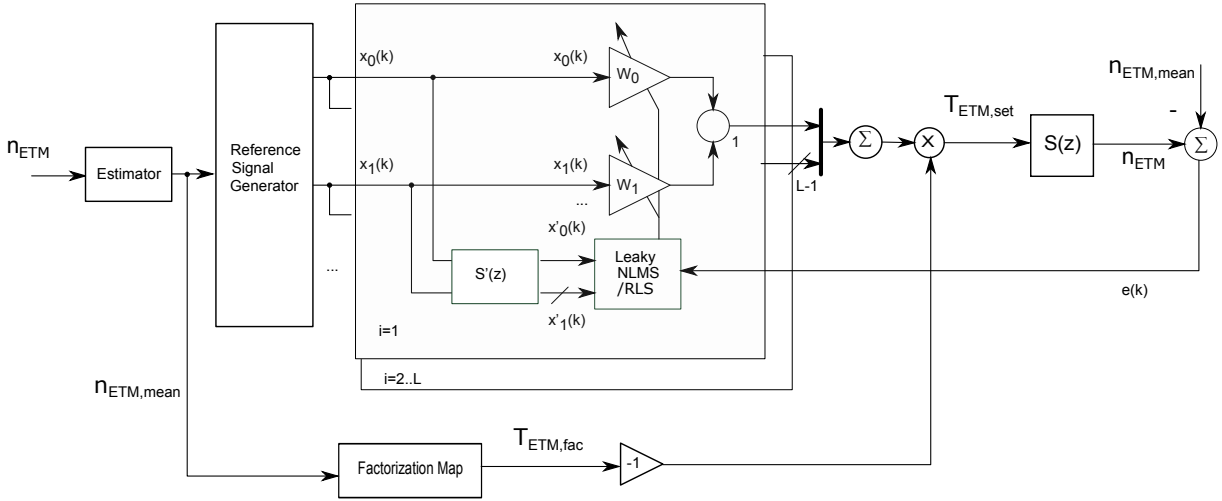


**Figure 5.4:** Structure of the adaptive filtering based active vibration reduction controller

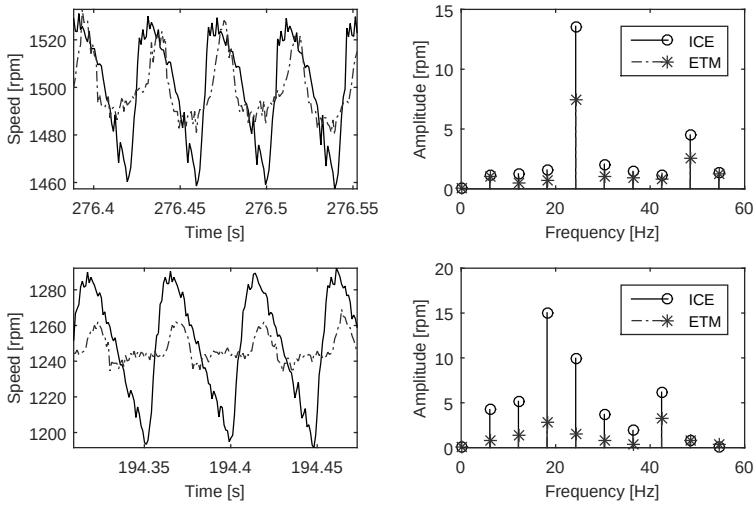


**Figure 5.5:** Time domain and FFT representation of the ICE and ETM speeds at mean speed of 1500 rpm and 1240 rpm

signal. The other alternative for the realization of the vibration reduction controller based on feedforward control would require sensing of the ICE speed in addition to the ETM speed. Further, the use of the ICE speed signal for control places requirements on its quality. Due to the additional cost and complexities, only the ETM speed shall be used for vibration control. But the signal correlated to the disturbance is generated online.

As it can be seen in the Figure 5.5, the first harmonic is the dominant order which shall be eliminated using active compensation. The plots in the first row present the correlation at 1500 rpm. The plots in the bottom row present the same effect at 1240 rpm. In case of the depiction around the speed of 1240 rpm, the leakage effects due to the employed rectangular window can be seen due to the fact that not a complete period of the ETM speed signal is used for the FFT computation which is the case in the plots of the top row.

The dominant harmonics of an inline four stroke engine equals $n_{cyl}/2$ where $n_{cyl}$ stands for the number of cylinders. In case of V 90 and V 60 engine configuration, the dominant harmonics is $n_{cyl}/2$ and $n_{cyl}/4$ respectively. This equivalence is used to formulate the reference signal whose frequency corresponds to the non-

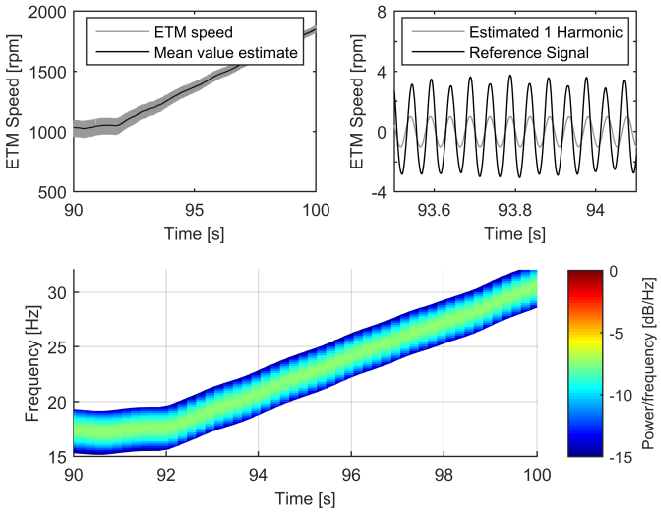


**Figure 5.6:** Time and frequency domain analysis of the reference signal generation during a speed ramp from 1000 rpm to 2000 rpm in 10 seconds

periodic mean value component of the ETM speed. The estimated mean value can be used to generate the reference signal $r(k)$ with only the first harmonic as in equation (5.20), where $\omega_1$ corresponds to the non-periodic component. The sinusoidal with twice the frequency corresponds to the second harmonic of oscillation. The reference signal can be also formulated to include the second harmonic as in equation (5.21).

$$x(k) = r_1(k) = cos(\omega_1 k) \tag{5.20}$$

$$x(k) = r_2(k) = cos(\omega_1 k) + cos(2\omega_1 k) \tag{5.21}$$

An alternative approach would be to use the harmonic content computed by the harmonic estimator as a reference signal. The inherent problem with such an approach is that when the compensation torque is set to higher values the resultant would be a lower amplitude of the corresponding harmonic component. This can be amplified to obtain the required amplitude. Another workaround would be to use the harmonic which shall not be compensated to generate the reference signal. In case of first harmonic elimination, the second harmonic signal shall be used to generate a subharmonic corresponding to the frequency of the first harmonic.

Figure 5.6 presents the generated reference signal using the estimated mean value of the ETM speed in time and frequency domain during speed transient from 1000 rpm to 2000 rpm in 10 seconds. The top left plot presents the actual ETM speed value and the estimated mean value. The mean value estimate follows the speed transients and is used for the computation of the reference signal. The generated reference signal and the estimated first harmonic is presented in the top right plot. As it can be seen both the signals have the same phase relationship in the presented time window. In addition, the reference signal resembles a unit amplitude version of the first harmonic, this fact can be used alternatively to generate the reference signal from the estimated first harmonic. The spectrogram plot of the generated reference signal is depicted in the bottom plot. As given by the equation (3.80), the frequency content of the reference signal follows the ETM speed transient.

An advantage of the reference signal generator is the absence of feedback effects. In the general ANC framework, the reference signal along with the error signal is used to generate the anti-noise signal to cancel the effect of noise. The anti-noise output to the actuator can corrupt the reference signal leading to coupling from the control actuator to the reference sensor [65].

Even with the introduction of the second harmonic, the vibration reduction controller remains narrow band, with bands centered around the first and second harmonics. [19] presents a feedforward controller based on the pulsed operation of the EM to reduce torsional oscillations. In the case of stiff powertrain, the triggering of the pulses was done in reference to the ICE spark timing. However, for operation with a flexible connection between the ICE and EM would require elaborate calibration of the delay with reference to the ignition timing. Further such an offline calibration approach could not take care variation over the operation and transient effects. An interesting feature of the strategy is to employ unidirectional pulses rather than positive and negative torques for vibration reduction. This feature shall also be demonstrated using the developed controller.

### 5.3.3 Realization of adaptive algorithms for active vibration control

After the presentation of the variants of adaptive filters, this section discusses topics specific to the implementation of the adaptation schemes.

#### Stochastic gradient descent

Adaptive LMS is usually realized as a member of the class of (stochastic) steepest descent algorithms. It uses an instantaneous estimate of the gradient based on

a single sample of error. The gradient descent approach can be viewed as a solution method for the system of linear equations modeling it as minimizing a (differentiable) quadratic objective function as in equation (5.22).

$$w_{GD}(k+1) = w_{GD}(k) - \mu \nabla \xi(k) \tag{5.22}$$

$$w_{SGD}(k+1) = w_{SGD}(k) - \mu \hat{\nabla} \xi(k) \tag{5.23}$$

The quantity $w_{GD}(k)$ stands for the kth-iterate of the gradient descent method. $\nabla \xi(k)$ stands for gradient (which here is represented as variant over iterations) and $\mu$ represents the step-size. This procedure of approximating the value of gradient stochastically as in equation (5.23) using the current estimate is termed as Stochastic Gradient Descent (SGD). Using a quadratic approximation of the error surface $\epsilon = d - w'x$, the approximation of the gradient can be computed as in equation (5.24). The corresponding weight updates $w_{SGD}(k)$ can be expressed as in equation (5.25).

$$\hat{\nabla} \xi(k) = \frac{\partial e^2}{\partial w} = 2\epsilon \frac{\partial e}{\partial w} = 2e(-x) \tag{5.24}$$

$$w_{SGD}(k+1) = w_{SGD}(k) + 2\mu e(k)x(k) \tag{5.25}$$

Due to the advantages of the leakage factor and normalization, the implementation is extended to leaky normalized FxLMS.

### Conjugate gradient method

Instead of searching in the direction of the negative gradient (or) negative residue $r_j$, conjugate gradient method performs a search in the direction such that the subsequent search directions are A-orthogonal. Alternatively, CG method can be viewed as an energy minimizing algorithm, minimizing $E(x) = 0.5x^T Ax - x^T$ on the growing Krylov subspaces [120]. The application of the CG method to adaptive transversal filters is reported in [123]. In line to the discussion on CG method to solve a linear system of equations, the matrix $A$ becomes the correlation matrix of the input data and $b$ is the cross-correlation vector between the input data and the desired response $d(k)$. The RLS and second-order methods such as Newton-based LMS require computation or an estimate of the inverse of the correlation matrix. In case the correlation matrix loses the property of positive definiteness, the algorithms diverge [115]. CG does not have this restriction as it approximates $A^{-1}b$ by $x_j$ with residual $b - Ax_j$ in the Krylov subspace $\mathscr{K}_j$ [120].

### 5.3.4 Pretuning of adaptive filters

Pretuning of the adaptive filters offers the potential to accelerate the convergence of the filter coefficients. The convergence is of practical importance, as the speed of convergence of the filter determines both the effectiveness of the controller and its dynamics. In this section, the basic idea behind the pretuning of filter weights shall be demonstrated using simulations which shall later be implemented at the experimental test bench in section 5.4.3.

As the convergence shall be quantifiable, a system identification setting shall be used for the investigation. At the first iteration, the filter weight initialization is performed. Let $W_o$ denote the initial value of the first filter weight. Three different initializations are done, the first one initializes the filter weight to the actual value which is known during this investigation thanks to the system identification setting. The second and third initialization schemes are initialized with two times and five times of the actual filter weight respectively. The initialization and the subsequent convergence of the filter weight can be seen in Figure 5.7a. The farther the initialization places the weight of the filters from the final value, the more time it requires to converge.

Pretuning methods can be employed irrespective of the realization of the adaptive filters. It has to be noted that in order to demonstrate this fact, the gradient descent method is used in the simulation study and experimental investigations use the CG method, is discussed in section 5.4. The plot 5.7b presents the convergence over the iterations with the mean squared error (MSE) as a metric. It is worth mentioning, that the convergence here refers to the convergence in mean, which allows small variations around the optimal value and the convergence shall be uniform with respect to the iterations. The closer the initial value is to the actual value, the lesser is the time required to convergence to the optimal MSE value.

### 5.3.5 Identification of secondary path

Power transfer from the source (ICE/ETM) to the wheels is realized using torsional powertrain constituted by components such as clutches, gearbox and driveshafts. The variation of the system dynamics occurs due to the decoupling of the powertrain components while declutching during normal operation or due to wear of the components. Active vibration is only possible with an existing torsional coupling of ICE and ETM through the clutch in the CEA powertrain, further component wear is not part of this study. In order to develop the methods in a simulation environment, an analytical expression of two mass damper is employed. This facilitated the

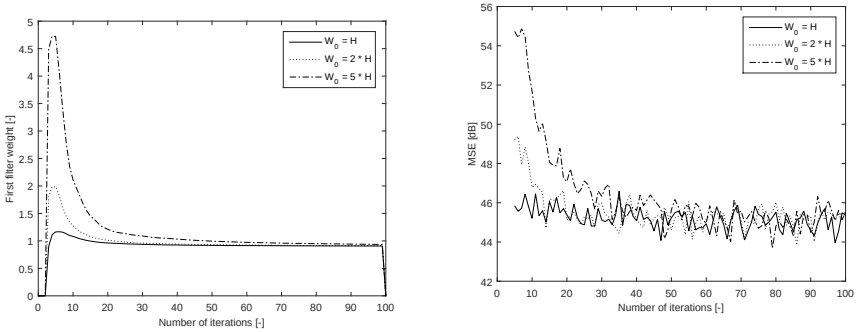


**(a)** Filter weight variation over iterations

**(b)** Mean Squared Error as measure of fit over iterations

**Figure 5.7:** Comparison of filter weight pretuning with Mean Squared Error (MSE) as measure of fit over iterations

development of the controller in the initial phase of controller development before the implementation of the powertrain components. At the experimental test bench, implementation of the adaptive filter requires identification of the secondary path transfer characteristics. The modeling of the secondary path shall be restricted to linear time-invariant models as this study is restricted to the class of linear filter based adaptive filtering. Such identification techniques are commonly used in the field of structural analysis. Modal analysis, a common approach in the vibrational analysis of mechanical systems employs linear identification techniques [124].

The paper [115] discusses the sensitivity of the FxLMS algorithm, with respect to variations in the estimation of the secondary path transfer function and concludes that the effect on the sensitivity to be low. This offers an opportunity to use offline modeling to estimate the secondary path transfer function rather than performing an online adaptation. Further, online estimation of the secondary path exhibits difficulties in regard to the prerequisite of persistent excitation during powertrain operation. With white noise excitation, in the absence of output noise, the best model of the unknown system realized using an FIR filter with N coefficients coincides with the N coefficients of the system's impulse response [119].

Prediction Error Methods are well-established for identification of a broad family of parametric models in an Output-Error stochastic Framework. However, in the case of MIMO systems in state space representation, full parameterization of the state space would introduce a large number of parameters. Hence difficulty arises

in constructing a numerically robust canonical realization of the state space representation. The identification of the multi-inertia torsional system is done using subspace methods, which shall be discussed further.

The subspace identification procedure was introduced in section 4.3.4. [110] present a more elaborate description of both the theory and details of numerical implementation. From the perspective of implementation, the non-iterative nature of the subspace identification for offline identification is a better choice than the classical iterative parametric optimization techniques. Further, iterative optimization based methods applied for system identification can lead to local convergence with an increased model order in the presence of lightly damped modes [125]. In case of identification of dynamics of the mechanical structure, such modes are trivial especially with the increasing influx of lightweight constructions.

The condition of the persistence of excitation was introduced as a pre-requisite for obtaining consistent estimates [100]. A persistent excitation contains sufficiently many distinct frequencies in the identification bandwidth. Measurements obtained using an input that is persistently exciting is informative for an open-loop experiment. In the application of adaptive filtering techniques for system identification, assumptions of persistent excitation are satisfied in case of white-noise excitation. In case of adaptive torsional vibrations reduction, the secondary path is the transfer function between the actual torque of the electric machine to its speed. Persistent excitation, in this case, translates to excitation of the bandwidth during operation which is not possible without degrading passenger comfort.

Though in this study, secondary path identification is restricted to (offline) identification at the powertrain test bench. This is no limitation of the method but is motivated by the non-availability of a vehicle with the powertrain and the required interfaces for identification, such as fast access to the torque of the electric traction machine. Provided the above-mentioned requirements are met, an offline identification of the secondary path in the vehicle can be performed possibly at the end of the production line due to reasons such as passenger comfort as discussed before.

### 5.3.6 Offline identification at powerpack test bench

Owing to its advantages such as inherent separability of the periodic excitations and random disturbances, periodic inputs are employed. The periodicity of the output signal enables a direct way to handle noise effects, as the deterministic part of the output of the system with periodic stationary excitation is stationary. PRBS excitation was used, since its implementation in comparison to other signals with

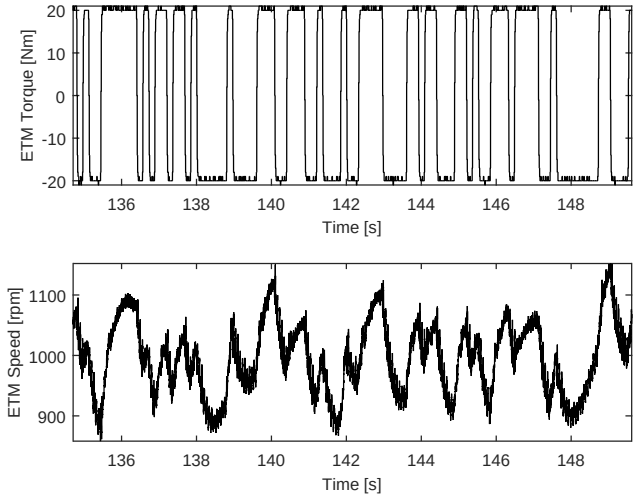


**Figure 5.8:** PRBS torque excitations and speed measurements at the experimental setup with a motored ICE around a mean speed of 1000 rpm

periodic realizations requires minimal data transfer to the torque or current controller of the electric traction machine, as opposed to other periodic counterparts like multi-sine or swept-sine signals. The PRBS excitation using the electric traction machine torque requires a transfer of data to the inverter at instants of the jump between the minimum and maximum torque levels.

The identification is performed at the powerpack test bench with the speed of operation being controlled by the eddy current dynamometer. Further, the torsional system is excited using torque from the electric traction machine and the combustion engine is motored. Motoring operation of the combustion engine avoids additional high amplitude periodic excitation of the torsional system due to the combustion process. The (residual) torque due to friction and compression effects in the motoring operation is accounted for in the noise model which depends on the operating speed. PRBS torque excitations around a speed of 1000 rpm and the corresponding measured ETM speed can be seen in Figure 5.8. During the identification experiment, the speed controller of the eddy current dynamometer was tuned so that its disturbance rejection properties do not influence the speed oscillations. This is to ensure that the identification experiment is conducted in open loop operation. If this is not desired, the algorithm for subspace identification

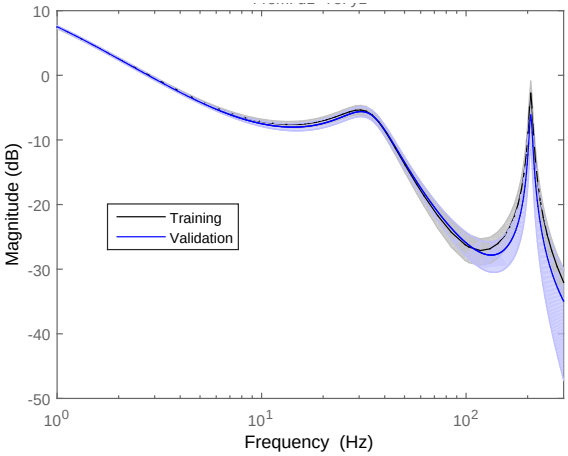


**Figure 5.9:** Identification result of the secondary path dynamics presented using training and validation data

shall be able to handle closed loop data, else methods developed in for closed loop identification in chapter 4 can be employed.

The dataset was partitioned into identification and validation sets. The torsional dynamics computed from the training and validation datasets at 1000 rpm using the subspace method is depicted in Figure 5.9. It can be seen that the identified models from the training and validation are close to each other. Further, the two non-zero eigenfrequencies of the test bench which can be approximated as three inertial torsional vibration system can be inferred from the bode representation. In addition, the linearity of the system over operating speeds was also studied by performing the identification at different speeds. A discrete version of this model is used by the adaptive filtering based controller as a secondary path transfer function.

## 5.4 Validation of the Controller

The validation of the developed control strategy was performed on the powerpack test bench available at the Institute for Internal Combustion Engines and Powertrain Systems, TU Darmstadt. The experimental bench is depicted in Figure 2.6 was presented in section 2.4. Experimental validation of the developed methods is performed both in stationary and transient operation. Identification of

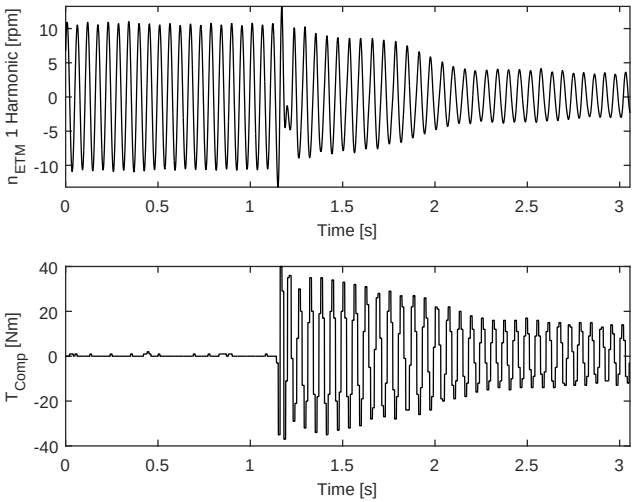


**Figure 5.10:** Active vibration reduction in stationary operation using FxNLMS CG adaptive filter

the secondary path transfer function shall be presented followed by validation of the developed controllers.

### 5.4.1 Stationary operation

In this section, the experimental validation of the adaptive controllers at constant speed operation shall be studied at 1100 rpm and constant torque of 40 Nm. Figure 5.10 displays the compensation torque and the achieved vibration reduction for the CG based FxNLMS controller. Due to the lower computational complexity, eleven filter weights were used for adaptation. In addition, the presence of initial transients during switching on the controller can be seen around 1.25 seconds.

Vibration reduction achieved using RLS filtering at the same ICE operating point is depicted in Figure 5.11. With the real-time processor and other computational loads remaining the same, RLS method can be realized by only two filter weights as opposed to eleven in case of FxNLMS. Though the transients are absent, the convergence of the RLS filter is slower than FxNLMS. This is due to the availability of two adaptation coefficients to compensate for the process variability. Accounting for the cyclic variations in the combustion process, a value of 0.9

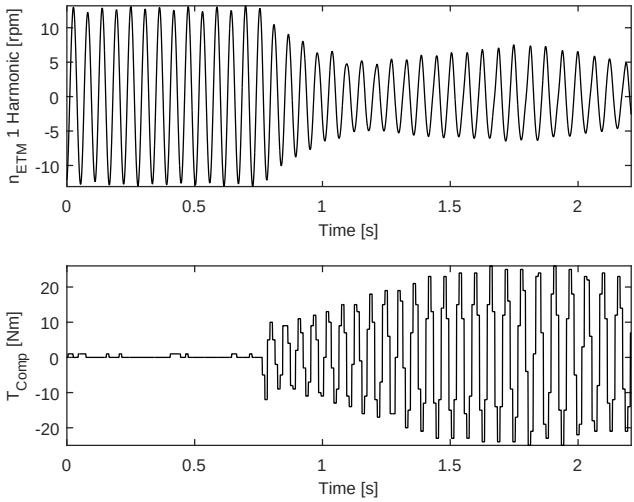


**Figure 5.11:** Active vibration reduction in stationary operation using RLS adaptive filter

was used for the forgetting factor $\lambda_f$. As it can be seen from the study at stationary operation speed, the FxNLMS achieves similar vibration reduction as that of RLS based adaptive filtering controller. Similar effects were observed at the experimental setup for step changes in the combustion engine torque at stationary speeds.

### 5.4.2 Transient operation

This section discusses the performance of the developed controllers during speed transients. The ICE and ETM are accelerated from 1100 rpm to 2000 rpm in 7 seconds operated at 2000 rpm and ramped from 2000 rpm to 1100 rpm in 7 seconds at constant ICE torque of 60 Nm. The described test maneuver was repeated with and without the controller for comparison purposes. The same test conditions were used to evaluate the performance of FxNLMS and RLS adaptive filters. Spectrogram of the ETM speed is used to quantify the vibration reduction. This ensures an evaluation without using the estimator discussed in section 3.4.

Figure 5.12 presents the results of transient operation with FxNLMS CG adaptive filtering controller. The spectrogram representation till 40 seconds is without the controller and from 20 to 40 seconds is with the controller compensation. The

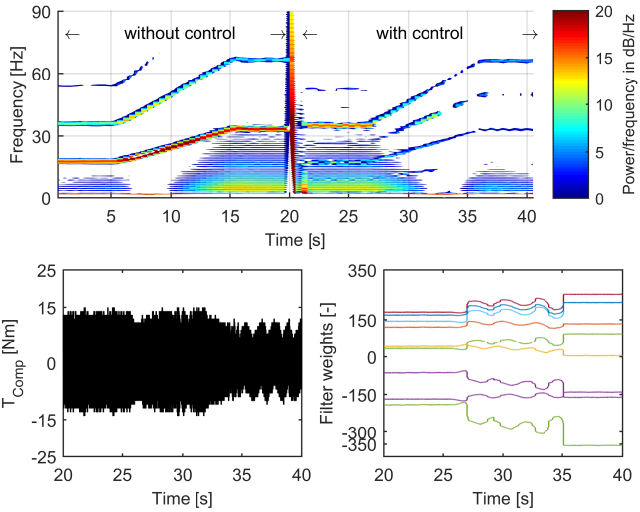


**Figure 5.12:** Active vibration reduction in transient operation using FxNLMS CG adaptive filter

vibration energy in the different orders can be observed. As the vibration controller is activated, the reduction in vibration energy in the ETM speed corresponding to the operation speed can be clearly observed in the ramps between 18 and 33.3 Hz, which corresponds to the first order. In addition to the ETM speed, the compensation torque and the filter weights computed by the controller have been presented. In comparison with the results from the stationary operation, dynamics due to activating the controllers is absent. The convergence of the filter weights during stationary operation at 1100 rpm and 2000 rpm can be observed. Despite the oscillations of the filter weights, vibration reduction is realized during the speed ramps. As discussed in section 5.3 the control action is designed to reduce only the first harmonic, this is reflected in the experimental results. However, there is a marginal increase in vibration energy in the 1.5th order. Vibration energy in the 1.5th order can be reduced by generating a reference using $r_{1.5}(k)$ analogous to equations (5.20 and 5.21), if it is undesired. The frequencies corresponding to the 1.5th order do not have high sensitivity to human perception of vibrations and can be effectively reduced using supplementary passive measures as in powertrains with 3-cylinder engine currently in series production.

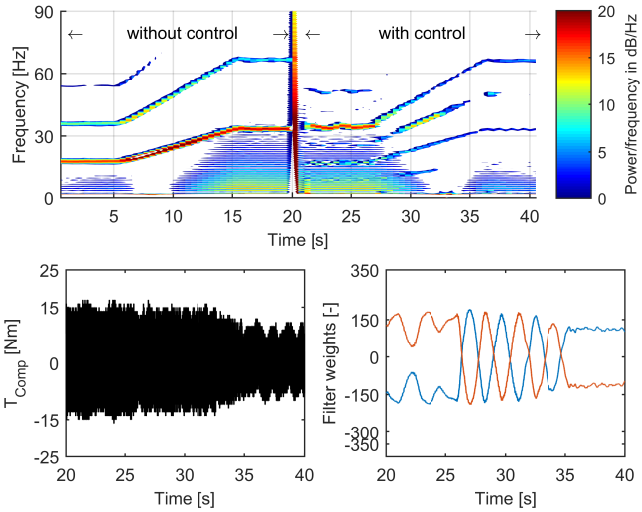


**Figure 5.13:** Active vibration reduction in transient operation using RLS adaptive filter

Evaluation of the performance of RLS adaptive filtering controller can be seen in Figure 5.13. The reduction in vibration energy corresponding to the first harmonic can be seen. Further RLS method uses similar compensation torque amplitudes as in FxNLMS CG method. The oscillation of filter weights is due to lower variability of the two filter weights available for adaptation. These oscillations increase during the speed ramps. One possibility to avoid these oscillations is to use additional filter weights which is not possible due to the increased computational demand. In comparison to the FxNLMS CG control, the RLS adaptive filtering controller performs slightly worse during the ramps as observable in the spectrogram of the ETM speed. It can be concluded that FxNLMS achieves similar or better vibration reduction with reduced computational demand and shall be studied further.

### 5.4.3 Pretuning of adaptation methods

Active compensation methods are usually required only in certain operating regimes due to excessive undesirable effects in such regions. Typical operation regimes of the compensation techniques in case of automotive powertrains are low speed and high torque operational regions. Further energy consumption and lim-

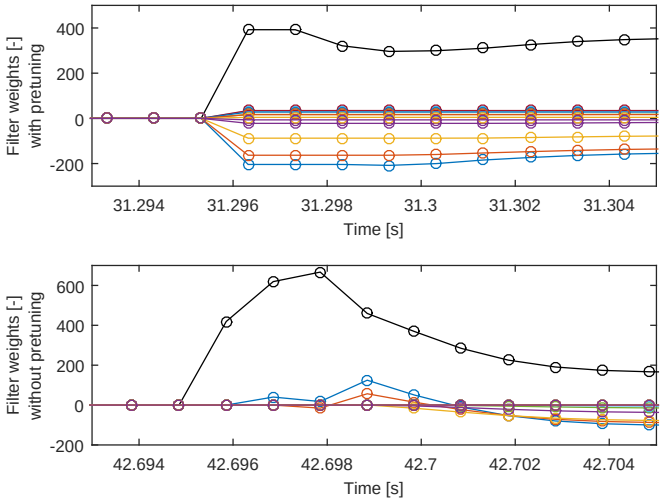


**Figure 5.14:** Convergence of the filter weights using pretuning using FxNLMS CG adaptive filter

ited onboard energy availability also place a restriction on the continuous activation of such methods. In case of active torsional vibration reduction, it is also found to be subjectively effective in lower operating speeds with higher mean torque values [19]. As the active torque compensation methods shall be activated intermittently, the adaptive filter weights shall be pretuned for the particular operating regions. The optimal pretuned weights can be determined by evaluation in the powerpack test setup.

Figure 5.14 presents the effect of pretuning adaptive filter weights. The top and bottom plots display the adaptation of the weights when the controller is switched on for vibration reduction around a mean ICE speed of 1000 rpm with and without pretuning of the filter weights respectively. As it can be seen, the pretuned filter weights which are initialized to their respective operational speed dependent values convergence faster than the weights in case of normal operation. This offers a possibility for pretuning filter weights using lookup tables with the speed of operation as the independent variable. Further, this helps to avoid transients while switching on FxNLMS CG controller as it can be seen in Figure 5.10.

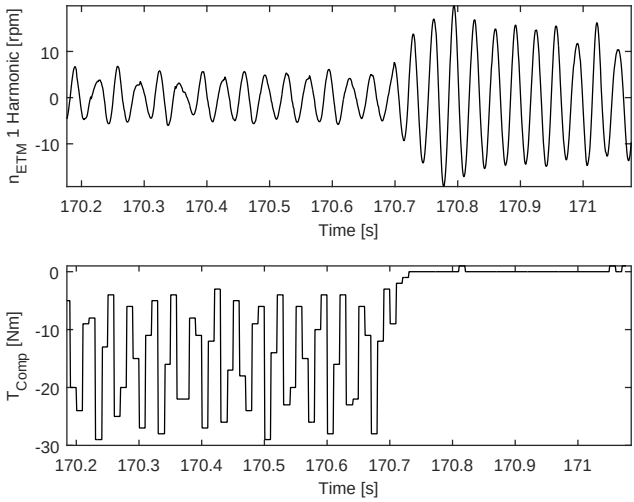


**Figure 5.15:** Active vibration reduction using unidirectional torque in generator operation

Dependency on the process parameters is of special interest during re-start of a warm engine using the ETM. As with the cold engine, a repeatable torque generation during start-up is difficult to achieve from the perspective of combustion stability. A similar argument applies during speed transients, making pretuning of filter weights due to the non-repeatable combustion process and also from the perspective of parameterization (calibration) as it has to be performed for different possible speed transients along with the difficulty to detect or predict such transient operation.

### 5.4.4 Unidirectional compensation torque

The previous discussion imposed constraints neither in amplitude nor in the rate of change of the compensation torque. This section shall present vibration reduction in the presence of amplitude restrictions on the ETM compensation torque. The restriction is limited to the sign of the compensation torque, in other words, the ETM compensation is restricted to motor or generator operation. This feature is of practical interest from an energetic perspective. In case of low battery charge, generator operation of the ETM is desired to maintain the level of State of Charge (SOC). In addition to this generator operation, the ETM shall be used for vibration

reduction without discharging the battery by operating with negative compensation torque. Figure 5.15 displays vibration reduction achieved using negative torque, in other words operating the ETM in generator mode. It can be seen in the presence of the adaptive filtering based ANC, the desired reduction in the first harmonic of the ETM speed signal (till 170.7 seconds) is achieved.

## 5.5 Conclusion

This chapter presented adaptive filtering techniques for ANC of torsional powertrain systems. A promising feature of the adaptive algorithms is that other than the secondary path function, no additional approximation of the system is required for the realization of the adaptive controllers. The secondary path function can be identified by employing system identification techniques. In contrast to the iterative methods used for adaption, non-iterative subspace method is used for offline identification of the secondary path dynamics. The identification procedure required excitation of the system with pre-defined excitation signals. These excitations were realized at the powerpack test bench to identify a model of the secondary transfer path.

Realizations of adaptive filtering methods for torsional vibration reduction employ an additional triggering signal derived from the engine speed signal [66]. Taking advantage of the periodic nature of the combustion engine oscillations which are proportional to the mean value of the engine speed, the requirement for the additional sensor has been eliminated. FxNLMS algorithm using conjugate gradient search is developed and is found to achieve performance comparable to RLS algorithm, with reduced computational effort.

Due to comfort and energy consumption reasons, active vibration reduction is realized as an on-demand system. The operating speeds at which the compensation is activated can be pretuned during the calibration phase. Using prediction information about the future driving velocities and the corresponding engine speed pretuning of the adaptive filter weights for the specific speed has been performed. Such a pretuning procedure is advantageous for computationally demanding methods. Besides, the realization of ANC using unidirectional compensation torque was also realized. Experimental investigation of the developed ANC demonstrated the effectiveness of the developed controller in stationary and transient operation.

# 6 Output Feedback Control for Active Vibration Reduction Controller

In this chapter, the active torsional vibration reduction is approached as an (robust) output feedback control problem. The output fed back is the ETM speed signal and the robustness shall be guaranteed against uncertainties in the model of the torsional powertrain used for control synthesis. The control synthesis is performed using $H_\infty/H_2$ and $\mu$ synthesis methods. An approach for constraining the amplitude of the compensation torque that can be calibrated online is developed. The performance of the controller is studied using simulation and at the experiment setup with real powertrain components.

## 6.1 Introduction

One of the main contributions of this chapter is the ability to consider parameter variation of the model used to synthesize the controller. Apart from the application of the theory of robust control, the approach is also of practical interest. Handling of the shorter development cycles and the increasing number of variants is one of the challenges faced by automotive development. One solution to the problem is to use a platform based development approach. Platform-based automotive development requires standardization and modularization of the components. One such platform approach is the Modularer Querbaukasten (MQB) platform from Volkswagen AG. It offers advantages such as standardization of position as well as measures, better competitiveness, and exploitation of synergy between development and production [126].

The approach when applied to hybrid powertrain units, could be extended to combine the ICE of different power levels, using different fuels with the ETM module based on the desired hybrid topology. Hence components with different characteristics such as a hybrid powertrain with a 3-cylinder engine and 4-cylinder engine could be coupled to the same ETM. From the perspective of torsional dynamics, this would lead to hybrid powertrains with ICE inertia varying in a range spanned by the inertia of the 3-cylinder ICE and the 4-cylinder ICE respectively. A similar variation of the inertia of the ETM and stiffness characteristics of the coupling is also conceivable.

The use of robust control approach offers the ability to synthesize and calibrate controllers for different combinations of ICE, ETM and the coupling between them. The key idea behind the approach is to model the different variants of the powertrain components along with their particular characteristics as uncertainties around a certain mean value. There are different philosophical approaches to the

synthesis of controllers to ensure robustness [127] such as worst-case design, average design and probabilistic robust design. This work tackles the robust control synthesis problem using the worst-case design as done in most of the control literature. This decision is based on both practical and computational considerations. From the practical perspective, the controller shall guarantee a performance level of the closed loop system for all possible values of the uncertainty. In addition, as only linear dynamics with uncertain model parameters are considered, the resulting Linear Matrix Inequality (LMI) optimization problems are solvable directly or using relaxation or multiplier based approaches [128], [90], [129].

Besides ensuring robustness, the reduction of the control effort required is realized in the context of multi-objective optimization by using minimization of the $\mathscr{H}_2$ norm along with the $\mathscr{H}_\infty$ norm. The weighting of the objectives can be tuned by the weighting factors using scalarization approach to solve a multi-objective problem. However, change of the weights requires the solution of the multi-objective LMI problem to be recomputed. In case of torsional vibration reduction, due to derating of the ETM or due to the integration with the energy management strategy of the hybrid powertrain, the desired torque (which is the control action) used for vibration reduction shall be tunable. The online solution of the scalarized multi-objective LMI problem for different compensation torque amplitudes is not possible currently from the computational perspective. The approach presented in this chapter offers an alternative termed as the amplitude modulation acting on the computed control effort of the output feedback controller to tune the actuation command during operation. This is another key contribution of the chapter, apart from the robust controller synthesis.

The outline of this chapter is as follows. Section 6.2 introduces the notions of robustness and uncertainty considered. Section 6.3 presents the theoretical results and method of control synthesis using solution to LMI problems. The validation of the developed controllers is presented in section 6.4, followed by concluding remarks in section 6.5.

## 6.2 Robust Control Approach

Robustness of a control system refers to its ability to maintain stability and adequate performance in the face of uncertainties. In other words, it is a property of the closed loop control system to exhibit behavior similar to the nominal plant for a class of plants sufficiently close to the nominal plant [90], [130], [128].

### Uncertainty characterization

The term uncertainty refers to the discrepancies or errors between assumed models (the approximation of the system dynamics) and reality. Uncertainties in physical systems may arise due to the following reasons [90].

- Unmodeled dynamics: unmodeled (usually high-frequency) dynamics, neglected nonlinearities in the modeling, effects of deliberate reduced-order nominal models treating the neglected dynamics as uncertainty.
- Time variance: time variance of dynamics of linear models may arise due to neglected nonlinearities or change in operating conditions (set-point dependent dynamics)
- Actuators and sensor dynamics: deviations of the sensor and actuator dynamics from their nominal approximations shall be detrimental to stability specifically with high gain feedback control.
- Environmental influences: system-parameter variations due to environmental changes and/or over its lifetime.
- Manufacturing variance: deviations from nominal dynamics may also be due to manufacturing tolerance.

The mechanism used to express the considered uncertainty shall be termed as a representation of uncertainty. Commonly encountered uncertainty descriptions can be categorized based on their form [130]:

- Structured uncertainty: Uncertainty in the value of constant or time-varying parameters of the system model
- Unstructured uncertainty: Uncertainty of neglecting higher order dynamics of the system including nonlinear effects (which are neglected for linearized control synthesis)

In general, the uncertainty of both structured and unstructured types occur in the problem. Mathematical categorization of the uncertainty classes can be classified into two broad classes, constituted by norm-bounded uncertainties and uncertainties satisfying integral quadratic constraints (IQC). Uncertainty representation using IQC are more generic and have been showed to encompass uncertainties with norm-bound constraints [90], [130]. This study considers the uncertainty of parameters within a range which can be expressed as bounds on the nominal value of the parameters. Hence the focus shall be on norm bounded uncertainty. The

methods presented however are applicable to both structured and unstructured uncertainty.

Boundedness of uncertainty can be on the level of the system parameter as in equation (6.1) which considers the variation $\Delta$ of the parameter value over time or in its frequency domain characterization in case of LTI systems as in equation (6.1 - 6.2).

$$||\Delta(t)|| \leq \delta_t \quad \forall t \geq 0 \tag{6.1}$$

$$||\Delta(j\omega)|| \leq \delta_\omega \quad \forall \bar{\omega_l} \leq \omega \leq \bar{\omega_u} \tag{6.2}$$

Equation (6.1) represents the variation of a time-varying parameter which is bounded in its absolute value (by the value $\delta_t$). Uncertainty in certain frequency ranges $\omega \in [\bar{\omega_l}, \bar{\omega_u}]$ of a transfer function is represented as in equation (6.2) is bounded by $\delta_\omega$. Other descriptions of uncertainty based on norm bounds can be based on their type such as constant, time-varying and nonlinear uncertainties exist.

The uncertainties irrespective of their type shall be organized in a standardized notation using the Linear Fractional Transformation (LFT). In such case, the generic uncertainty block $\Delta$ would have the following structure (6.3) with $\sum_{i=1}^{s} r_i + \sum_{j=1}^{f} m_j = n$, which means that the number of full blocks of the form $\Delta$ represented by $\Delta_1, \Delta_2 ... \Delta_f$, which correspond to dynamic / unstructured uncertainty and the scalar blocks represented by $\delta_1, \delta_2 ... \delta_s$ with $\delta$ shall be equal to the size of the combined structured uncertainty block $\Delta$.

$$\Delta = \text{diag}[\delta_1 I_{r1}, ..., \delta_s I_{rs}, \Delta_1, ..., \Delta_f] \quad \text{with} \quad \delta_i \in C, \Delta_j \in C_{m_j \times m_j} \tag{6.3}$$

This chapter deals only with constant uncertainties which enter the system model as parameters. This requires tools to handle structured uncertainty but the methods are also applicable for unstructured uncertainty using LFT representation.

### Uncertainty modeling using Linear Fractional Transformation (LFT)

LFT standardizes block diagram representations for feedback control as well as robust control analysis and synthesis. For systems with both dynamical and parametric uncertainty, it is a general representation of uncertainty.

**Definition 6.1.** LFT : For a complex block matrix M partitioned as given by expressions (6.4). Let the domains of mappings be defined as $D_1 \subset C^{p_1 \times q_1}$ and

$D_2 \subset C^{p_2 \times q_2}$. The maps of the linear fractional transformation (LFT) is defined as in equations (6.5) and (6.6) respectively.

Let be a complex matrix (also termed as coefficient matrix) partitioned as in equation (6.4). Let $\Delta_l \subset C^{q_2 \times q_2}$ and $\Delta_u \subset C^{q_1 \times p_1}$ be complex matrices. Then the lower LFT is formally defined with respect to $\Delta_l$ as the map, $\mathscr{F}_l(M, \Delta_l) : C^{p_2 \times q_2} \mapsto C^{p_1 \times q_1}$ with $\mathscr{F}_l(M, \Delta_l)$ given by equation (6.5). In similar lines the upper LFT is defined respect to $\Delta_u$ as the map, $\mathscr{F}_u(M, \Delta_u) : C^{q_1 \times p_1} \mapsto C^{p_2 \times q_2}$ with $\mathscr{F}_u(M, \Delta_u)$ given by equation (6.6).

$$M = \begin{bmatrix} M_{11} & M_{12} \\ M_{21} & M_{22} \end{bmatrix} \in C^{(p_1+p_2)\times(q_1+q_2)} \tag{6.4}$$

$$\mathscr{F}_l(M, \Delta_l) := M_{11} + M_{12}\Delta_l(I - M_{22}\Delta_l)^{-1}M_{21} \tag{6.5}$$

$$\mathscr{F}_u(M, \Delta_u) := M_{22} + M_{21}\Delta_u(I - M_{11}\Delta_u)^{-1}M_{12} \tag{6.6}$$

As it can be inferred from equations (6.5) and (6.6), the existence of the inverses is a necessary condition for the well-undefinedness of the LFT. LFTs enjoy properties that allow their manipulation similar to state space representations [131].

One such fundamental property with regard to linear systems is that the interconnections of LFTs are again LFT. Further, the inverse of an LFT exists which is also an LFT [131]. Construction of LFT in case of state space parametric uncertainty shall be discussed in case of mass-spring-damper system defined in the benchmark problem 6.3.2 as in [132].

LFT is not restricted to constant uncertain parameters, models with time-varying affine or polynomial parameter dependencies can also be transformed exactly to an LFT representation. In addition, the generic nature of LFTs, enable a transformation of complex and diverse robustness questions in control to specific algebraic problems [90]. The uncertainties considered in this study will be studied using their corresponding LFT representations. Interested readers could refer to literature [130], [90].

#### Robustness characterization

In the presence of uncertainty, it is essential to understand the notions of stability and performance specifications before introducing tools to study them. This

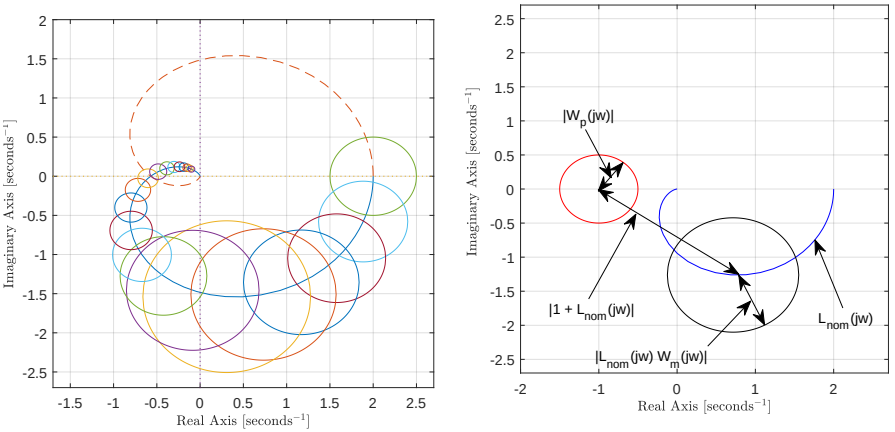


**(a)** Uncertainty characterizations of the nominal plant using Nyquist plot [134]

**(b)** Graphical representation of the stability and performance notions using Nyquist plot

**Figure 6.1:** Graphical representation of the plant uncertainty and stability as well as performance notions using Nyquist plot

section gives an overview of the required notions. Followed by which one of the fundamental results of robust control, the small gain theorem is presented. For ease of understanding, SISO LTI systems shall be studied with the aid of pictorial representations without loss of generality. The extension of these notions to MIMO system is handled in [133], [128].

The discussion uses a plant with uncertainty as given in equation (6.7) with $G_{nom}$ denoting the nominal plant model and $\Delta$ the uncertainty which is bounded in value by a parameter $\gamma$. Let $K$ denote the controller that stabilizes the system in closed loop operation. The expressions for the (open) loop transfer ($L_{nom}$), sensitivity ($S$) and complementary sensitivity ($T$) transfer functions are given in equation (6.8).

$$G(s) \in \{G_{nom}(s) + \Delta \,|\, \|\Delta\| \leq \gamma\} \tag{6.7}$$

$$L_{nom} = G_{nom}K, S = \frac{1}{1 + G_{nom}K} = \frac{1}{1 + L_{nom}}, T = \frac{G_{nom}K}{1 + G_{nom}K} = \frac{L_{nom}}{1 + L_{nom}} \tag{6.8}$$

Robustness characterizations can be viewed as extensions to the classical frequency response metrics such as gain and phase margin. In the case of SISO systems, the stability and robustness properties can be quantified using inequalities [128]. A pictorial characterization of dynamic/ unstructured uncertainty using the Nyquist diagram is given in Figure 6.1a. The colored circles centered on the Nyquist curve of the nominal system at the different frequencies have a radius corresponding to the magnitude of the uncertainty at the respective frequencies. The weighting functions $W_p$ and $W_m$ represent performance objectives and model uncertainty respectively.

- *Nominal stability*: if $K$ internally stabilizes the nominal model $G_{nom}$. It indicates the stability of the closed loop system with its exact knowledge. Pictorially, nominal stability can be quantified using the nominal blue curve and the point (-1,0) of the complex plane based on Nyquist stability condition.
- *Nominal performance (NP)*: if the performance objectives are satisfied for the nominal plant $G_{nom}$. Nominal performance indicates the satisfaction of performance specifications of the closed loop system when the plant is known exactly.

$$NP : ||W_p S|| < 1 \iff ||W_p|| < ||1 + L_{nom}|| \quad \forall \omega \tag{6.9}$$

  Graphically this requires no intersection of the blue curve in Figure 6.1b with the red circle of size $|W_p|$ (absolute value is used as norm as it each frequency the weighting function returns a scalar) around the point (-1,0).

- *Robust stability (RS)*: if $K$ internally stabilizes every plant belong to a class of uncertain plants / considered uncertainty set. Robust stability quantifies the stability of the closed loop system when there is uncertainty in the plant model.

$$RS : ||W_m T|| < 1 \quad \forall \omega \tag{6.10}$$

  This can be quantified by applying Nyquist condition on the black ball at the different frequencies of the Figure 6.1b and the point (-1,0) of the complex plane.

- *Robust performance (RP)*: if the performance objectives are satisfied for every plant belonging to the class of uncertain plants / considered uncertainty set.

$$RP : ||W_p S|| + ||W_m T|| < 1 \quad \forall \omega \tag{6.11}$$

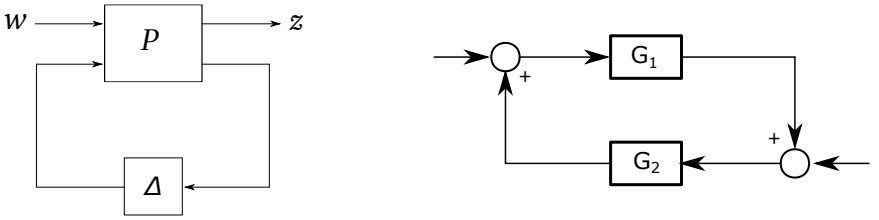


**(a)** System and uncertainty interconnection structure

**(b)** Small gain theorem

**Figure 6.2:** System - Uncertainty interconnection structure and Small gain theorem

Pictorially, this requires no intersection between the red and black balls in the Figure 6.1b.

Small gain theorem is one of the fundamental tools in robust control theory. It is a sufficient condition that can be used to analyze the stability of interconnections as shown in Figure 6.2a. The condition holds also if the controller $K$ is replaced by the uncertainties pulled out of the system (for example using LFT).

*Theorem* 6.1. Small gain theorem : Let $G_1$ and $G_2$ be (possibly nonlinear) stable systems with finite input-output gains (induced norms) represented by $\gamma_1$ and $\gamma_2$ respectively. If $\gamma_1\gamma_2 < 1$ then the closed loop depicted in Figure 6.2b consisting of $G_1$ and $G_2$ is stable.

For the system representation in Figure 6.2a, this would require that equations (6.12) and (6.13) hold, with the norm being a suitable induced norm based on the signals considered.

$$||P||.||\Delta|| < 1 \tag{6.12}$$

$$\text{with } ||\Delta|| < \alpha \rightarrow ||P|| < \frac{1}{\alpha} \tag{6.13}$$

## 6.3 Theory and Controller design

This section addresses a brief overview of the methods of robust control theory that shall be used for controller synthesis. Since the original formulation of $\mathscr{H}_\infty$ optimal

control theory in an input-output setting [135], various solutions have been investigated. [136] presents a solution to the $\mathcal{H}_\infty$ synthesis problem by unique stabilizing positive definite solutions to two algebraic Ricatti equations and their joint spectral radius less than the square of the $\mathcal{H}_\infty$ norm of the closed loop transfer function. Ricatti equation based solution to $\mathcal{H}_\infty$ problem requires rank conditions on the plant, [137] and [138] arrived at the use of Riccati inequalities in the effort to remove these conditions, which are very similar to the approach using Linear Matrix Inequalities (LMI).

### 6.3.1 Robust control - an Linear Matrix Inequality (LMI) approach

LMI approach to the robust control problems without restrictions on the plant was presented in [139]. An additional advantage of the LMI approach is its ability to handle multi-objective control synthesis as a mixed control problem using the Lyapunov shaping paradigm [140], [141]. The approach makes the mixed control problem numerically tractable by requiring the different specifications are satisfied by a single closed loop Lyapunov function. Though it introduces conservatism in the synthesis, the approach exploits the available degrees of freedom to produce controllers of reasonable order. Before discussing the synthesis of the controllers, some standard results in $\mathcal{H}_\infty$ and $\mathcal{H}_2$ control theory shall be presented.

The robust control techniques that shall be employed for control synthesis are $\mathcal{H}_\infty$ control, $\mathcal{H}_\infty$ / $\mathcal{H}_2$ control and $\mu$ synthesis in an output feedback setting. Definition of the required norms and their computations based on LMI conditions shall be introduced first. Two main methods of synthesis for $\mathcal{H}_\infty$ based control design exists, namely method based on solution to Ricatti equations and method using solution to LMI. The Ricatti solution does not offer flexibility to impose additional requirements on the controller synthesis, which can be exploited using LMI synthesis [140].

#### $\mathcal{H}_\infty$ Control [90], [142]

$\mathcal{H}_\infty$ norm represents the maximum value of the frequency response in the SISO case. For a stable transfer function $G$, $\mathcal{H}_\infty$ norm is given by equation (6.14) where $\bar{\sigma}$ denotes the maximum singular value. It can be interpreted as a generalization of the frequency domain performance specifications of classical control.

$$\| G \|_\infty = \sup_{\omega \in R} \bar{\sigma}(G(j\omega)) \tag{6.14}$$

Using the Bounded Real Lemma, [139] shows the $\mathscr{H}_\infty$ norm of a continuous time transfer function $G(s) = D + C(sI - A)^{-1}B$ is upper bounded by $\gamma$ if and only if there exists a positive definite solution $K$ to the LMI given by equation (6.15):

$$\begin{bmatrix} A^TK + KA & KB & C^T \\ B^TK & -\gamma^2 I & D^T \\ C & D & -I \end{bmatrix} \prec 0 \tag{6.15}$$

### $\mathscr{H}_2$ Control [90], [142]

Let $G$ be a transfer function with all its poles on the open left complex plane, its $\mathscr{H}_2$ norm is given by equation (6.16). It is a measure of performance to guarantee small asymptotic variance against white noise inputs or small energy of outputs for impulse inputs. In case of a multiple input single output system, $\mathscr{H}_2$ norm evaluates to the energy-to-peak gain [90].

$$\|G(j\omega)\|_2 = \left( \frac{1}{2\pi} \int_{-\infty}^{\infty} \text{trace}[G(j\omega)G(j\omega)^*] d\omega \right)^{\frac{1}{2}} \tag{6.16}$$

For a continuous time transfer function representation $G(s) = D + C(sI - A)^{-1}B$ with Hurwitz $A$ and $D = 0$, the bound $\|G(j\omega)\|_2 < \gamma$, is equivalent to the existence of positive definite $K$ satisfying the set of LMIs given by equation (6.17)

$$\begin{bmatrix} A^TK + KA & KB \\ B^TK & -\gamma I \end{bmatrix} \prec 0, \tag{6.17}$$
$$\begin{bmatrix} K & C^T \\ C & Z \end{bmatrix} \succ 0, \text{trace}(Z) \prec \gamma$$

#### Output feedback synthesis

The generic setting of the output feedback shall be presented followed by the LMI conditions. LMI based approach has been adopted due to the regularity conditions associated with the Ricatti-based solutions [139]. Subsequently, output feedback approach to both $\mathscr{H}_\infty$ and $\mathscr{H}_2$ control shall be presented, followed by a discussion on $\mu$ synthesis.

### Output Feedback Controller

The controller in this chapter uses static output feedback and does not require online tracking of harmonics or parameters. Output feedback controller is a dynamical system with the measurements being the input ($u$) and the output ($y$) being the control signals. It can be expressed as in equation (6.18).

$$\dot{x}_c = A_c x_c + B_c y, u = C_c x_c \tag{6.18}$$

The open loop system and controller are presented by equation (6.19) and (6.20) respectively. The presentation is limited to zero feedthrough term in the controller, for LMI conditions with non-zero direct feedthrough term in the controller the interested reader is referred to [140] and references therein.

$$\begin{bmatrix} \dot{x}_c \\ z \\ y \end{bmatrix} = \begin{bmatrix} A & B_w & B_u \\ C_e & D_{ew} & D_{eu} \\ C_y & D_{yw} & 0 \end{bmatrix} \begin{bmatrix} x \\ w \\ u \end{bmatrix} \tag{6.19}$$

$$\begin{bmatrix} \dot{x}_c \\ u \end{bmatrix} = \begin{bmatrix} A_c & B_c \\ C_c & 0 \end{bmatrix} \begin{bmatrix} x_c \\ y \end{bmatrix} \tag{6.20}$$

The below discussion uses the variables $z$ for the channels whose $\mathscr{H}_\infty$ and $\mathscr{H}_2$ performance are considered. This does not impose a restriction that the channels for the different performance specifications are the same. In other words, $z$ can be written as $z = \{z_\infty, z_2\}$.

### $\mathscr{H}_\infty$ synthesis [90], [142]

If there exists a solution $(\eta, X, Y, \hat{A}, \hat{B}, \hat{C})$ for the LMI given by equation (6.21) with $\mathscr{F} = YA + A^T Y + \hat{B} C_y + C_y^T \hat{B}^T + \hat{C}^T B_u^T$ and $\mathscr{L} = B_w^T Y + D_{yw}^T \hat{B}^T$, then there exists

a controller defined by the matrices $(A_c, B_c, C_c)$ which ensures that the $\mathscr{H}_\infty$ norm of the transfer from $z$ to $w$ defined as $\| T_{wz} \|_\infty$ is bounded by $\eta$.

$$\begin{aligned} &\text{minimize} \quad \eta \quad \text{subject to} \\ &\begin{bmatrix} X & I \\ I & Y \end{bmatrix} \succ 0 \\ &\begin{bmatrix} AX + B_u\hat{C} + XA^T + \hat{C}^T B_u^T & * & * & * \\ A^T + \hat{A} & \mathscr{F} & * & * \\ B_w^T & \mathscr{L} & -I & * \\ C_e X + D_{eu}\hat{C} & C_e & D_{ew} & -\eta I \end{bmatrix} \prec 0 \end{aligned} \tag{6.21}$$

$*$ stands for symmetric completion of the LMIs. From the solution of the LMI given by equation (6.21), the controller matrices $(A_c, B_c, C_c)$ can be computed from the expressions in equation (6.22).

$$\begin{aligned} NM^T &= I - YX \\ \hat{A} &= NA_cM^T + NB_cC_yX + YB_uC_cM^T + YAX \\ \hat{B} &= NB_c \\ \hat{C} &= C_cM^T \end{aligned} \tag{6.22}$$

**$\mathscr{H}_2$ synthesis [90], [142]**

$$\begin{aligned} &\text{minimize} \quad \zeta \quad \text{subject to} \quad \text{trace(W)} < \zeta \\ &\begin{bmatrix} AX + B_u\hat{C} + XA^T + \hat{C}B_u^T & * & * \\ A + \hat{A}^T & \mathscr{M} & * \\ B_w & B_w^T Y + D_{yw}^T \hat{B}^T & -I \end{bmatrix} \succ 0 \\ &\begin{bmatrix} W & * & * \\ XC_e^T + \hat{C}^T D_{eu} & X & I \\ C_e{}^T & I & Y \end{bmatrix} \prec 0 \end{aligned} \tag{6.23}$$

If there exists a solution $(\zeta, X, Y, \hat{A}, \hat{B}, \hat{C})$ for the LMI given by equation (6.23) with $\mathscr{M} = YQ + \hat{B}C_y + A^TY + C_y^T\hat{B}$, then there exists a controller defined by the

matrices $(A_c, B_c, C_c)$ which ensures that the $\mathscr{H}_2$ norm of the transfer from $z$ to $w$ defined as $\|T(j\omega)_{zw}\|_2$ is bounded by $\zeta$. Using the solution $(\zeta, X, Y, \hat{A}, \hat{B}, \hat{C})$ and the equality $NM^T = I - XY$ and the expressions in equation (6.22) the controller matrices for output feedback synthesis can be computed.

### $\mathscr{H}_\infty$ / $\mathscr{H}_2$ control [90], [142]

In practice, multi-objectives have to be satisfied by the synthesized controllers, one such case being the minimization of $\mathscr{H}_2$ norm (not exceeding $\zeta$) is to reduce the control effort while maintaining the achieved $\mathscr{H}_\infty$ norm to handle disturbance rejection (lesser than $\eta$). Mathematically, this problem can be formulated as in equation (6.24) where $\mathscr{A}$ stands for the closed loop system which is required to have roots in the open left half complex plane.

$$\sigma(\mathscr{A}) \subset \mathbf{C}^-, \quad \| G_{\mathscr{A}} \|_\infty < \eta, \quad \|G_{\mathscr{A}}\|_2 < \zeta \tag{6.24}$$

To handle such multi-objective problems, [141] proposes an approach using a common Lyapunov function to specify the closed loop objectives, transforming the controller synthesis to a convex optimization problem. One drawback of the approach is that it introduces conservatism due to the employed common Lyapunov function. This translates for the output feedback case to require the solutions of equation (6.21) and (6.23) being satisfied simultaneously, from which the controller matrices can be computed using equation (6.22). The $\mathscr{H}_\infty$ and $\mathscr{H}_2$ norms of the closed loop system defined on the corresponding signals are denoted by $\| G_{\mathscr{A}} \|_\infty$ and $\|G_{\mathscr{A}}\|_2$ respectively.

In addition to the discussed combination involving $\mathscr{H}_\infty$ and $\mathscr{H}_2$ norms, regional constraints on the location of the closed loop poles/characteristic roots can be imposed. Pole placement constraints exploit the well-understood relation between the transient response of a linear system and the location of its poles [143]. This requires a definition of regions of desirable pole locations using LMIs. An LMI region $\mathscr{R}$ in the complex plane is defined as in equation (6.25) with real matrices $L = L^T$ and $M$.

$$\mathscr{R} = \{z \in \mathscr{C} : L + zM + z^* M^T \prec 0\} \tag{6.25}$$

[144] presents a theorem to define LMI conditions to restrict the poles of the closed loop (with system matrix $A$) within the LMI region defined by equation (6.25).

This requires the existence of a symmetric matrix $P$ such that the LMI defined by equation (6.26) hold, where $\otimes$ is the Kronecker product of matrices.

$$L \otimes P + M \otimes (AP) + M^T \otimes (PA^T) \prec 0 \tag{6.26}$$

**Structured singular value (SSV) [133]**

SSV is a matrix function denoted by $\mu$. It is an analysis tool for the robust performance of the system. It gives a measure of the smallest structured $\Delta$ (set of block diagonal matrices) that causes instability of the feedback loop connecting $\Delta$ and the matrix $M \in C^{n\times n}$ [131]. The definition of $\mu$ is given by the equation (6.27).

$$\mu_{\Delta}(M) = \frac{1}{\min\{\bar{\sigma}(\Delta) : \det(I - M\Delta) = 0\}} \tag{6.27}$$

$$\rho(M) \leq \mu(M) \leq \bar{\sigma}(M) \tag{6.28}$$

For a defined uncertainty set, if the condition given by $\mu < 1$ is satisfied for normalized uncertainty $||\Delta||_{\infty} < 1$, then the robust performance can be concluded [131]. In [129] it is shown that an exact computation of $\mu$ with respect to real and mixed uncertainty sets is an NP hard problem. Hence usually bounds on $\mu$ is computed with the approximations using scalings as shown in equation (6.29). The scalings of lower bound are unitary matrices, $\mathscr{U} = \{U \in \Delta : UU^H = I\}$. Upper bound scalings $\mathscr{D} = \{\text{diag}(d_1 I_{m1}, ...d_{F-1} I_{mF-1}, I_{mF}) : d_i \in \mathscr{R}, d_i > 0\}$ are diagonal matrices that commute with block structure of the uncertainty definition.

$$\max_{U\in\mathscr{U}} \rho(MU) \leq \mu(M) \leq \max_{D\in\mathscr{D}} \bar{\sigma}(DMD^{-1}) \tag{6.29}$$

**$\mu$ synthesis [133]**

$\mu$ synthesis is the problem of minimizing $\mu$ as a function of a free parameter, usually the controller in case of $\mu$ based control synthesis. This is done by minimization of the peak value of $\mu$, SSV of the robust performance problem with respect to the uncertainty set over frequencies. Since there is no direct method to compute a $\mu$-optimal controller, a heuristic method known as DK-iteration or scalings/controller-iteration is widely applied [145]. The scalings referred to D, in the upper bound in equation (6.29) are used to better approximate the computed $\mu$. The procedure involves iterations computing controllers in the synthesis (K step) with constant D values associated with the scaled $\mu$ upper bound and evaluating $\mu$

over the D scalings with a constant controller. The procedure can be summarized as in equation (6.30) with $G$ and $K$ denoting the system and the controller respectively. The DK-synthesis routine in MATLAB Robust Control Toolbox was used for controller synthesis.

$$\inf_{K(s)} \sup_{\omega \in \mathbf{R}} \mu[M(G,K)(j\omega)] \tag{6.30}$$

The formulation of the robust synthesis problem is completed by definition of the weighting functions on the output/performance $W_p$ and the input $W_u$ respectively. The choice of the weighting function on the output directly influences the performance of the controller and the actuator limits can be defined using the input weighting function. The performance weighting function is a second order high pass filter of the form given by equation (6.31) with gains $A$ and $Q$ such that $A > Q$ and $\omega$ denotes the frequency above which the vibration reduction is active. $n$ stands for the order of the high pass filter determining the slope of the rising edge. Another conceivable form for $W_p$ would be a bandpass filter, however, the synthesized controller shall be active up to 2000 rpm which implicitly defines bandpass without introducing complexity in the synthesis. For the same reason, $W_u$ was chosen to have a constant value.

$$W_p = \frac{(\frac{1}{Q^{1/n}} \cdot s + \omega)^n}{(s + \omega \cdot A^{1/n})^n} \tag{6.31}$$

The discussion above is a direct application of the theory of robust control. The section below presents an extension based on the physical insight of the problem at hand. In order to be able to compare the performance of the synthesized controllers, the controller using $\mathscr{H}_\infty$ / $\mathscr{H}_2$ control and $\mu$ synthesis shall be reduced to an order of 5.

### 6.3.2 Application to the robust control benchmark problem

This section applies the theory discussed in section 6.3.1 employing the system used in the robust control benchmark problem proposed in [146] as an example. The uncertainty enters the model through the uncertainty in its fixed parameters. A pictorial representation of the system is given by Figure 6.3a. The masses are represented by $m_1$ and $m_2$ respectively. The stiffness and damping characteristics of the spring are denoted by $k$ and $b$. The masses and the stiffness of the spring are subjected to uncertainty. The effect of uncertainty on the system can be seen in

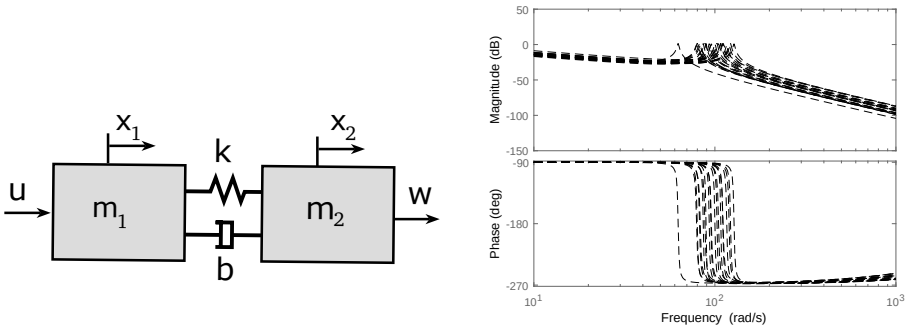


**(a)** System proposed in the benchmark problem

**(b)** Frequency domain representation of the uncertain system

**Figure 6.3:** Graphic representation of the system proposed in the benchmark problem along with its frequency domain representation

the frequency domain representation given in Figure 6.3b. The nominal system is given by the equations (6.32) and (6.33).

$$\begin{bmatrix} \dot{x}_1 \\ \dot{x}_2 \\ \dot{x}_3 \\ \dot{x}_4 \end{bmatrix} = \begin{bmatrix} 0 & 0 & 1 & 0 \\ 0 & 0 & 0 & 1 \\ -\frac{k}{m_1} & \frac{k}{m_1} & -\frac{b}{m_1} & \frac{b}{m_1} \\ \frac{k}{m_2} & -\frac{k}{m_2} & \frac{b}{m_2} & -\frac{b}{m_2} \end{bmatrix} \begin{bmatrix} x_1 \\ x_2 \\ x_3 \\ x_4 \end{bmatrix} + \begin{bmatrix} 0 \\ 0 \\ \frac{1}{m_1} \\ 0 \end{bmatrix} u \tag{6.32}$$

$$y = \begin{bmatrix} 0 & 1 & 0 & 0 \end{bmatrix} \begin{bmatrix} x_1 \\ x_2 \\ x_3 \\ x_4 \end{bmatrix} \tag{6.33}$$

The parametric uncertainties of the model are

$$m_1 = m_{10} + \alpha_1 \delta_1 \quad \text{with} \quad |\delta_1| \leq 1 \tag{6.34}$$

$$m_2 = m_{20} + \alpha_2 \delta_2 \quad \text{with} \quad |\delta_2| \leq 1 \tag{6.35}$$

$$k = k_0 + \alpha_3 \delta_3 \quad \text{with} \quad |\delta_3| \leq 1 \tag{6.36}$$

$$(m_{10} + \alpha_1 \delta_1)\ddot{x}_1 = m_{10}\ddot{x}_1 + \alpha_1 \delta_1 \ddot{x}_1 = u - f \tag{6.37}$$

with $w_1 = \delta_1 z_1$ and $z_1 = \ddot{x}_1$, it can be rewritten as

$$m_{20}\ddot{x}_2 + \alpha_2 w_2 = f \tag{6.38}$$

$$f = k_0(x_1 - x_2) + \alpha_3 w_3 \tag{6.39}$$

where

$$\begin{bmatrix} w_1 \\ w_2 \\ w_3 \end{bmatrix} = \begin{bmatrix} \delta_1 & & \\ & \delta_2 & \\ & & \delta_3 \end{bmatrix} \begin{bmatrix} z_1 \\ z_2 \\ z_3 \end{bmatrix} = \begin{bmatrix} \delta_1 & & \\ & \delta_2 & \\ & & \delta_3 \end{bmatrix} \begin{bmatrix} \ddot{x}_1 \\ \ddot{x}_2 \\ x_1 - x_2 \end{bmatrix} \tag{6.40}$$

The LFT of the system shall be formulated as in [132]. Using the notation $\dot{x}_1 = x_3$, $\dot{x}_2 = x_4$ and using equations (6.38), (6.39), and (6.40),the state space model for the fixed, LTI part of the uncertain system with state equation

$$\begin{bmatrix} \dot{x}_1 \\ \dot{x}_2 \\ \dot{x}_3 \\ \dot{x}_4 \end{bmatrix} = \begin{bmatrix} 0 & 0 & 1 & 0 \\ 0 & 0 & 0 & 1 \\ -\frac{k_0}{m_{10}} & \frac{k_0}{m_{10}} & -\frac{b}{m_{10}} & \frac{b}{m_{10}} \\ \frac{k_0}{m_{20}} & -\frac{k_0}{m_{20}} & \frac{b}{m_{20}} & -\frac{b}{m_{20}} \end{bmatrix} \begin{bmatrix} x_1 \\ x_2 \\ x_3 \\ x_4 \end{bmatrix} + \tag{6.41}$$

$$\begin{bmatrix} 0 & 0 & 0 \\ 0 & 0 & 0 \\ -\frac{\alpha_1}{m_{10}} & 0 & -\frac{\alpha_3}{m_{10}} \\ 0 & -\frac{\alpha_2}{m_{20}} & \frac{\alpha_3}{m_{20}} \end{bmatrix} \begin{bmatrix} w_1 \\ w_2 \\ w_3 \end{bmatrix} + \begin{bmatrix} 0 \\ 0 \\ \frac{1}{m_{10}} \\ 0 \end{bmatrix} u$$

$$\begin{bmatrix} z_1 \\ z_2 \\ z_3 \end{bmatrix} = \begin{bmatrix} -\frac{k_0}{m_{10}} & \frac{k_0}{m_{10}} & -\frac{b}{m_{10}} & \frac{b}{m_{10}} \\ -\frac{k_0}{m_{20}} & \frac{k_0}{m_{20}} & \frac{b}{m_{20}} & -\frac{b}{m_{20}} \\ 1 & -1 & 0 & 0 \end{bmatrix} \begin{bmatrix} x_1 \\ x_2 \\ x_3 \\ x_4 \end{bmatrix} + \tag{6.42}$$

$$\begin{bmatrix} -\frac{\alpha_1}{m_{10}} & 0 & -\frac{\alpha_3}{m_{10}} \\ 0 & -\frac{\alpha_2}{m_{20}} & \frac{\alpha_3}{m_{20}} \\ 0 & 0 & 0 \end{bmatrix} \begin{bmatrix} w_1 \\ w_2 \\ w_3 \end{bmatrix} + \begin{bmatrix} \frac{1}{m_{10}} \\ 0 \\ 0 \end{bmatrix} u$$

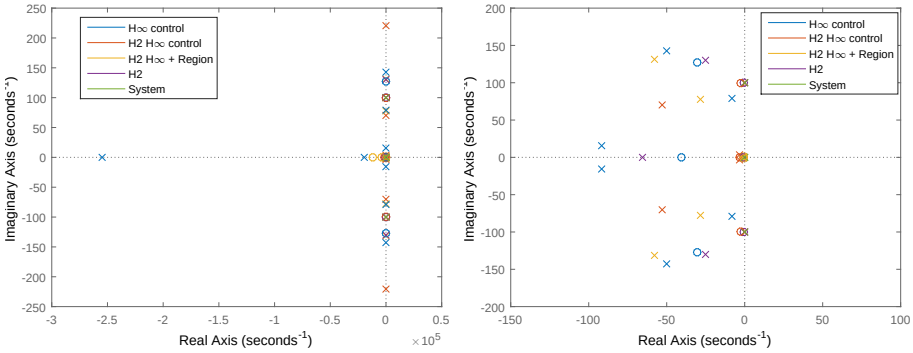


**(a)** Normal view **(b)** Enlarged view

**Figure 6.4:** Pole zero location of the closed loop and open loop systems

**Table 6.1:** Comparison of $\mathscr{H}_\infty$ and $\mathscr{H}_2$ norms

| $\mathscr{H}_\infty$ norm weight | $\mathscr{H}_2$ weight | Computed $\mathscr{H}_\infty$ norm | Computed $\mathscr{H}_2$ norm |
|---|---|---|---|
| 1 | 1 | 0.1 ($\leq$ 0.1) | 1.39 ($\leq$ 3) |
| 1 | 1 (+ Region) | 0.7236 | 20.3103 |
| 0.1 | 1 | 1.8133 | 1.1255 |

$w = \Delta z$, where $\Delta = \text{diag}(\delta_1, \delta_2, \delta_3)$. In a more compact form, it reduces to

$$\dot{x} = Ax + B_w w + B_u u \tag{6.43}$$
$$z = C_z x + D_{zw} w + D_{zu} u \tag{6.44}$$
$$y = C_y x + + D_{yw} w \tag{6.45}$$

The representation in the equations (6.43) - (6.45) shall be used to demonstrate $\mathscr{H}_\infty$, $\mathscr{H}_\infty$ / $\mathscr{H}_2$ and $\mathscr{H}_\infty$ / $\mathscr{H}_2$ with pole placement constraints. Figure 6.4 presents the location of the poles of the closed loop system with the different controllers. One important observation is that the pole locations using the regional pole constraints have shifted poles of the closed loop system within an angle of $\pi/4$ measured from the imaginary axis as seen in Figure 6.4b. In addition, all the controllers shift the poles of the damped oscillatory system from the imaginary axis avoiding marginal stability. Table 6.1 presents the results of the corresponding norms with mixed $\mathscr{H}_2/\mathscr{H}_\infty$ control of the benchmark problem.

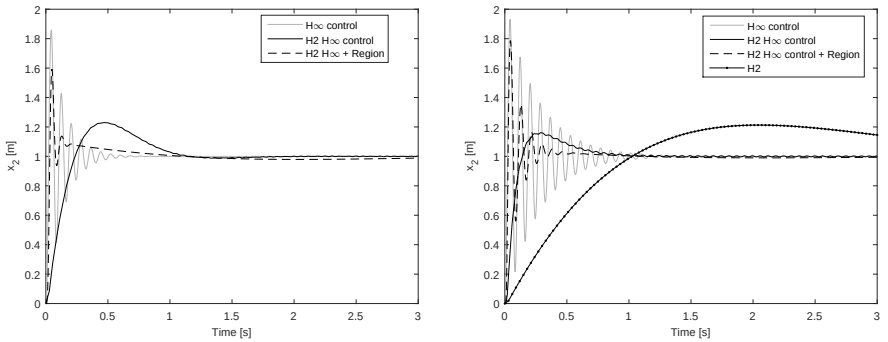


**(a)** Time response to a step of the nominal system

**(b)** Time response to a step of one realization of the uncertain system

**Figure 6.5:** Time domain responses of the closed loop system from the benchmark problem for unit step input

The responses to a step input to change the position of the second mass is depicted in Figure 6.5. Figure 6.5a presents the response of the nominal system, whereas the image 6.5b depicts the response from a realization of the uncertain system with values within the range used for control synthesis. The responses with $\mathscr{H}_2$ and $\mathscr{H}_2$ with regional pole constraints have well damped response as expected due to the location of closed loop poles presented in Figure 6.4. The above analysis presents the stability and better performance of the $\mathscr{H}_\infty$ / $\mathscr{H}_2$ controller for the benchmark problem, this controller shall be investigated in case of the active vibration reduction problem.

### 6.3.3 Modeling of the CEA powertrain

To study the torsional vibration phenomenon, the powertrain is discretized into finite-dimensional torsional inertial-spring-damper system [16]. The degree of discretization, in other words, the number of degrees of freedom of the discretized system depends on the vibration effects under study [68]. Effects such as shuffle arise due to abrupt load changes or change in drive torque exciting the first drivetrain mode requiring a simpler model with the inertia of the drive unit and the vehicle mass coupled by a powertrain dependent stiffness. On the other hand, transmission noise such as rattle from unloaded gears, whine due to transmission error and dynamic mesh forces from loaded gears in kHz range require finer dis-

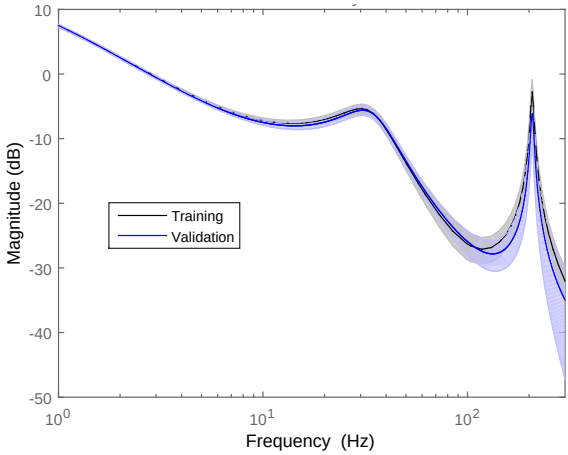


**Figure 6.6:** Identified model using data from the experimental setup

cretization of the model. The vibration effect of interest is in the range of engine operating speeds from idling speed to 2000 rpm. Depending on the engine configuration this range translates to a frequency band of 16.67 - 33.33 Hz or 25 - 50 Hz in case of 2-cylinder and 3-cylinder engines respectively. Employing models with eigenfrequencies outside the above-discussed bandwidth increases the complexity of the model without additional benefits.

From a control synthesis perspective, the dynamics of the powertrain can be modeled as a three inertial torsional oscillatory system. The three inertia represent the combustion engine which is the source of vibration, the electric machine used to attenuate the disturbances and the remaining powertrain. Validation of the three inertial approximation assumption for the frequency domain of interest is performed by system identification. Identification is performed at the experimental test bench depicted in Figure 2.6.

$$\begin{aligned} \dot{x}(t) &= Ax(t) + Bu(t) + Dw(t) \\ y(t) &= Cx(t) \end{aligned} \tag{6.46}$$

Model identification is performed at the powertrain test bench with the speed of operation being controlled by the Eddy current dynamometer. Pseudo Random Binary Sequences (PRBS) signal is used for torque excitations realized using ETM, whereas the ICE is motored at a mean speed of 1000 rpm. Subspace method is

used to identify models from training and validation datasets. The identification procedure is presented in detail in [147]. The two non-zero eigenfrequencies of the test bench corresponding to the three mass oscillator system approximation can be seen from the amplitude spectrum of the bode representation in Figure 6.6. The test setup reproduces similar conditions as in the vehicle by emulating the torsional dynamics of a powertrain with DMF. Using this study, the three mass oscillator approximation of the system has been validated. Subsequently, this model of the system with uncertainty shall be used to synthesize the active vibration reduction controller using robust control techniques.

$$A = \begin{bmatrix} -\frac{b_1}{j_1} & -\frac{k_1}{j_1} & \frac{b_1}{j_1} & 0 & 0 \\ 1 & 0 & -1 & 0 & 0 \\ \frac{b_1}{j_2} & \frac{k_1}{j_2} & -\frac{b_1+b_2}{j_2} & -\frac{k_2}{j_2} & \frac{b_2}{j_2} \\ 0 & 0 & 1 & 0 & -1 \\ 0 & 0 & \frac{b_2}{j_3} & \frac{k_2}{j_3} & -\frac{b_2}{j_3} \end{bmatrix} \tag{6.47}$$

$$B = \begin{bmatrix} 0 \\ 0 \\ \frac{1}{j_2} \\ 0 \\ 0 \end{bmatrix}, D = \begin{bmatrix} \frac{1}{j_1} \\ 0 \\ 0 \\ 0 \\ 0 \end{bmatrix}, C = \begin{bmatrix} 0 & 0 & 1 & 0 & 0 \end{bmatrix} \tag{6.48}$$

The state space representation of the model is given by equation (6.46) with $x = \begin{bmatrix} \omega_1 & \triangle\phi_1 & \omega_2 & \triangle\phi_2 & \omega_3 \end{bmatrix}^T$, $y = \omega_2$. $w$ stands for disturbance input which is the periodic ICE torque excitation and ETM torque $u$ is the actuator input. The inertia of the masses are represented by $j_1$, $j_2$ and $j_3$ respectively. Stiffness and damping of the interconnections are denoted by $k$ and $b$ respectively. The uncertainty considered is from parameter uncertainty of the powertrain components namely the inertia, stiffness and damping parameters.

An uncertainty value of 30% is used for the stiffness and damping coefficients of the shafts. As the $j_3$ accounts for the inertia of the remaining powertrain and vehicle no uncertainty is assumed, as the parameter variations are negligible when compared to inertia associated with the vehicle. The inertia $j_1$ and $j_2$ are parameterized with an uncertainty of 30%. Apart from unknown parameter values of the powertrain components, the uncertainty bounds can also be used to model bounded nonlinearities by embedding them using uncertain linear models. The uncertain system is represented using Linear Fractional Transformation (LFT) which is also used in computing $\mu$ (discussed in section 6.3.1) to characterize robustness and performance of linear feedback interconnections.

Other approaches to formulate uncertainty descriptions instead of using bounds on the parameters can be to use, the covariance bounds on the estimated frequency response using subspace methods to define dynamic uncertainty over the frequency domain. Alternatively, identification over different operation speeds as in Figure 8.5 can be used to define uncertainty bounds on model parameters.

### 6.3.4 Online limits on ETM compensation torque

Minimizing the $\mathscr{H}_2$ norm using the multi-objective approach reduces the control effort maintaining the disturbance rejection objective [140]. However, it is subjected to the trade-off between the achievable reduction of control effort and the desired level of vibration reduction which is inherent to the multi-objective control problem. Tuning the weights on the different objectives offers an alternative, but this requires solving the multi-objective LMI problem which cannot be done online during the control execution.

This section presents a physically motivated alternative to $\mathscr{H}_2$ control specific to the problem of vibration attenuation. This alternative approach shall be termed actuation amplitude modulation. As the goal is to reduce the dominant harmonic, the actuation signal to the ETM to be expected of the same frequency as only linearized dynamics is considered. In case of presence of multiple sinusoids in the signal due to nonlinearities or other effects, the estimator discussed in chapter 3 can be used to split the sinusoids and then apply the amplitude modulation to the individual sinusoidal components. Hence the discussion will be restricted to mono-frequent sinusoidal signals.

The core idea of amplitude modulation is the normalization of the signal to the appropriate amplitude without introducing phase shift. This involves computing the harmonic amplitude of the signal from the controller. This harmonic filtering uses the estimator presented in section 3.4. Hence the discussion in this section will be brief. Estimation of the direct ($d$) and quadrature ($q$) components of the torque command is estimated using a low pass filter along with a second order generalized integrator (SOGI) [94]. The expression of the SOGI which is given by equation (6.49), has a resonant frequency at $\omega = 2\pi f$. This resonant frequency shall be tuned to the harmonic to be estimated. The frequency of the harmonic is estimated from the corresponding speed signal using the relation between the speed signal and its harmonic content. Since the frequency of the engine torque disturbances depends on the current engine operating speed and the engine configuration, the torque to compensate the disturbances shall also have the same spectral characteristics.

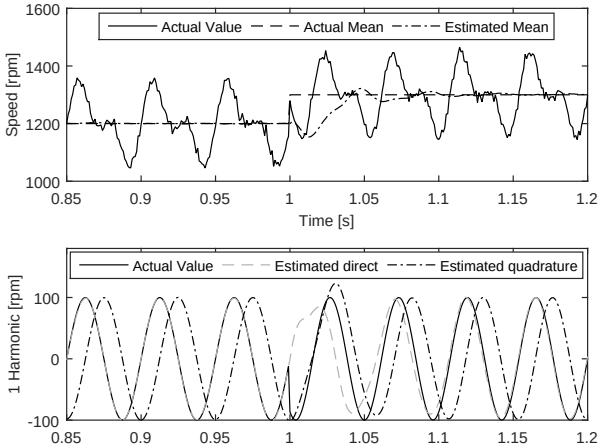


**Figure 6.7:** Analysis of the harmonic estimation in simulation

The frequency of the dominant harmonic in case of inline 4-stroke engines with $z_{cyl}$ cylinders with an operating speed of $n_{ICE}$ (in rpm) is given by equation (6.50). The value of the current operating speed is computed with a low pass filter given by equation (6.51) with a time-constant $\tau$. It can be seen that the low pass filter has a steady state gain of one, converging to the steady state value of the input signal. Figure 6.7 presents the results of harmonic decomposition of a noisy speed signal with multiple harmonics from the simulations. The noisy signal was generated as the sum of constant value denoted by $c$ (in rpm) and the first 2 harmonics with the frequency of the first harmonic given by $f_1 = c \times 30/\pi$. The first harmonic has a constant amplitude of 100 rpm.

$$G(s) = k\frac{s}{s^2 + \omega^2} \tag{6.49}$$

$$f = (n_{ICE} \times z_{cyl})/120 \tag{6.50}$$

$$F(s) = \frac{\tau}{s + \tau} \tag{6.51}$$

At t = 1 second the constant (mean) value of the signal jumps from 1200 rpm to 1300 rpm. The first plot displays the actual signal along with actual mean and estimated mean values. It can be seen that the estimate of the mean value after the step change reaches the actual mean value in 50 ms. A similar convergence behavior is observed with the estimation of the first harmonic. The plot below

presents the estimated and actual value of the first harmonic. Both the direct ($d$) and quadrature ($q$) estimates of the first harmonic signal are depicted. The direct component estimate is synchronous with the first harmonic, the quadrature component is 90 ° phase shifted with respect to the direct component. After the step change in the input signal and the corresponding harmonics, the estimate of the harmonics also converges to their true values at around 60 ms.

The values of the estimated $d$ and $q$ component of the harmonics can be used to compute $u_{amp}$ and $u_{nom}$ as shown in equations (6.54) and (6.55) respectively. The quantity $u_{amp}$ denote the unknown amplitude of the actuation signal from the controller. As the signals are sinusoids, with the knowledge of the instantaneous values of phase and quadrature components can be used to compute the amplitude of the signal. The desired value of the amplitude of the actuation signal is denoted by $A_{set}$. This method does not require computation over sliding windows to compute the harmonic content of the signal. Alternatively computing online a frequency transformation and using the amplitude of the dominant harmonic can be seen as an alternative approach, but involves frequency domain transformation and additional computational effort.

$$u_d(t) = A\sin(\omega t) \tag{6.52}$$

$$u_q(t) = A\cos(\omega t) \tag{6.53}$$

$$u_{amp} = \sqrt{(u_d(t)^2 + u_q(t)^2)} \tag{6.54}$$

$$u_{nom} = \frac{A_{set}}{u_{amp}} u(t) \tag{6.55}$$

In addition to being able to change the amplitude of the compensation torque, this method can be used to change the mean value of the compensation torque. Presence of mean value of the compensation torque injects additional positive or negative torque into the powertrain. This is of interest from the battery energy management perspective and offers the flexibility of operating the ETM in motor or generator mode. With a lower state of charge in the battery, the ETM can be operated in generator mode with active torque compensation and in motor mode with compensation in case of higher battery state of charge. Such a shifting of the mean value can be commanded by the energy management system as described in [61], without influencing the performance of the active compensation method.

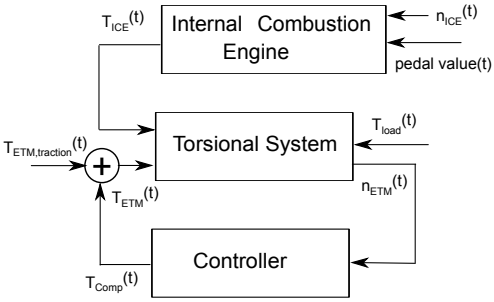


**Figure 6.8:** Structure of the output feedback active vibration reduction controller

### 6.3.5 Structure of the controller

The structure of the developed output feedback controller is depicted in Figure 6.8, with the time domain signals denoted by $t$. The ETM speed signal denoted by $n_{ETM}$ is used as an input to the controller. The commanded compensation torque $T_{Comp}$ is realized by the ETM along with the ETM torque command for the traction demand denoted by $T_{ETM,traction}$. The torsional system depicted refers to the complete powertrain with the different inertia and coupling elements from the engine inertia to the wheel along with the equivalent vehicle inertia. The load on the powertrain is denoted by $T_{load}$. The disturbance acting on the system results from the oscillatory combustion engine torque $T_{ICE}$ which is a function of engine speed $n_{ICE}$ and pedal value or torque command to the engine. The structure in Figure 6.8 is also used for the simulation study of the developed vibration controller.

## 6.4 Validation of the Controller

This section discusses the results of the implemented vibration reduction controller using simulations and at the experimental setup. The experimental setup is the powerpack unit from the CEA-Powertrain comprising of the 2-cylinder ICE coupled to the ETM through a hydraulically actuated clutch [19]. The experimental setup is shown in Figure 2.6 is operated with torque as the command signal for the ICE as well as the ETM and speed for the eddy current dynamometer. Using this mode of operation, rotational irregularity around a mean speed value is created by the ICE torque command.

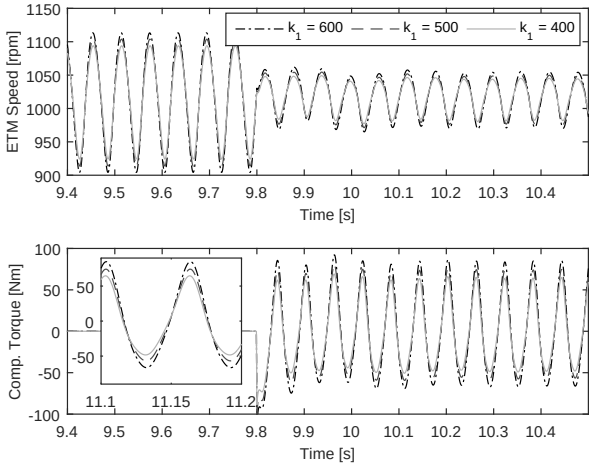


**Figure 6.9:** Results of the active vibration reduction controller at stationary operation using $\mathscr{H}_\infty/\mathscr{H}_2$ controller

The goal of vibration reduction will be examined using the torque value computed by the controller. The ETM speed which serves as input to the output feedback control schemes shall be used to evaluate the achieved vibration reduction. Experimental validation of the developed controllers is performed both in stationary and transient operation. In order to better depict the performance of the developed controllers, both the amplitude of oscillations with and without the controller of the ETM speed signal shall be presented along with the required compensation torque used to realize the achieved reduction in oscillations.

### 6.4.1 Simulation

The simulation model has the structure presented in Figure 6.8 and was parameterized by using test bench measurements of the 2-cylinder ICE [36]. The simulation model offers a possibility to test the robustness of the vibration reduction controller with different parameterization. Figure 6.9 shows the simulation results with various stiffness for the coupling (between 400 and 600 Nm/rad) between the ICE and ETM around an operation speed of 1000 rpm and mean ICE torque of 40 Nm. The speed of the ETM is shown in the top plot. It can be observed that the amplitude of the speed oscillations is higher with a stiffer coupling. The controller is turned on at 9.8 seconds. The used controller was synthesized using $\mathscr{H}_\infty$ / $\mathscr{H}_2$

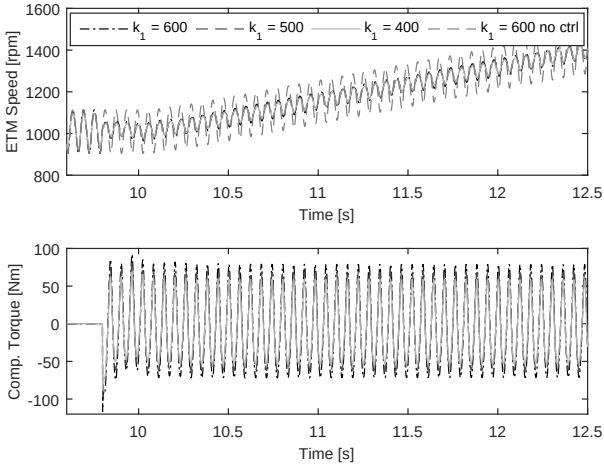


**Figure 6.10:** Results of the active vibration reduction controller using $\mathscr{H}_\infty/\mathscr{H}_2$ controller with transient operation 1000 to 1800 rpm in 10 seconds

with equal weighting of the performance objectives. After the controller activation, oscillations of the ETM speed is reduced. The transients due to the activation of the controller decay faster and the controller operates in a steady state to compensate the torque pulsations. Further, the higher compensation torque required for compensation in case of stiffer powertrains can be seen in the enlarged view of the second plot. Additionally, a small phase shift between the compensation torque for the varied parameterization can also be seen.

Figure 6.10 presents the results from the simulation of the developed controller during transient operation with a speed ramp from 1000 rpm to 1800 rpm in 10 seconds. The ETM speed signal for the different shaft stiffness values as earlier are depicted along with the ETM speed signal without any controller action. It can be observed that irrespective of the actual value of the shaft stiffness (in the parameter range used for control synthesis), the controller is able to realize the desired vibration reduction. The compensation torque required thereby is around -/+ 60 Nm for a mean ICE torque amplitude of 40 Nm. The values of the compensation torque required for the same level of vibration reduction, quantified using the amplitude of ETM speed oscillations are higher for a higher value of shaft stiffness. This can be explained due to the higher shaft torque as a result of higher stiffness value, subsequently requiring a higher ETM torque amplitude for compensation.

### 6.4.2 Experimental validation

**Stationary operation**

Figure 6.11 presents the results of the $\mathscr{H}_\infty$ / $\mathscr{H}_2$ controller action at stationary speed of 1450 rpm. The controller is activated at 109.5 seconds. A reduction in the amplitude of ETM speed oscillations can be observed. There is also a decrease in the mean speed signal of the ETM at the test bench. This is due to two reasons. The first reason is the torque oscillation between +15 Nm and -34 Nm, which has a negative mean value leading to a deceleration of the torsional system. The eddy current dynamometer at the test bench cannot motor the powertrain and hence compensate for the decrease in ETM speed. In addition, the controller bandwidth was parameterized in a way that it does not interfere in the high-frequency intervention of the active vibration controller. Due to the non-zero mean ETM compensation torque, the shaft torque measurement $T_{s2}$ at the test bench is changed after compensation as shown in the third plot of Figure 6.11. This is due to the effect of the test setup configuration which has to be differentiated from the effect of the controller. In summary, the activation of the controller leads to vibration reduction.

Before a discussion of the results of vibration reduction with amplitude modulation, the study of amplitude modulation is performed at the test setup. Figure 6.12 displays the functionality of the torque modulation during a speed transient between 1720 rpm and 1780 rpm in 0.2 seconds. The ETM speed signal is presented in the second plot in the figure. The compensation torque computed from the controller is displayed in the first plot as the actual torque. The estimated harmonic content of the compensation torque is presented as the estimated harmonic torque in the figure. The harmonic torque does not contain noise effects of the actual torque from the controller.

With the use of amplitude modulation, the modulated torque between -50 and +50 Nm has been computed online which can be seen in the figure. It can be concluded that the amplitude modulation is able to achieve compensation torque in the desired amplitude range without phase distortion during operation of the controller. It has to be noted that this feature has been achieved without modifying the weighting of the $\mathscr{H}_\infty$ / $\mathscr{H}_2$ objectives offline by solving the LMI problem.

The results of the vibration reduction using amplitude modulation is shown in Figure 6.13. The controller is activated at 99.35 seconds at a stationary speed of 1440 rpm. The compensation torque achieved using amplitude modulation was between -25 Nm and +25 Nm. The reduction in the ETM speed oscillations after

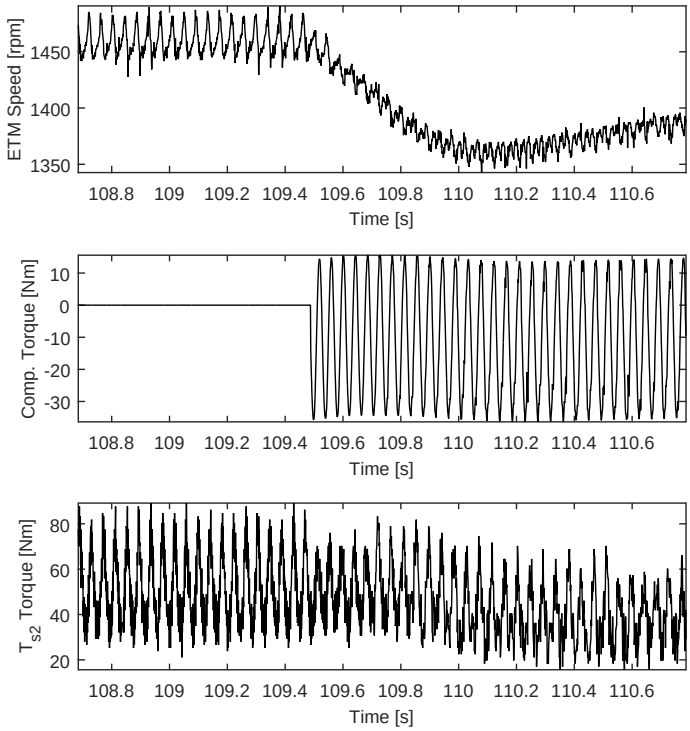


**Figure 6.11:** Results of the active vibration reduction controller during stationary speed at the experimental setup : $\mathscr{H}_\infty / \mathscr{H}_2$ controller

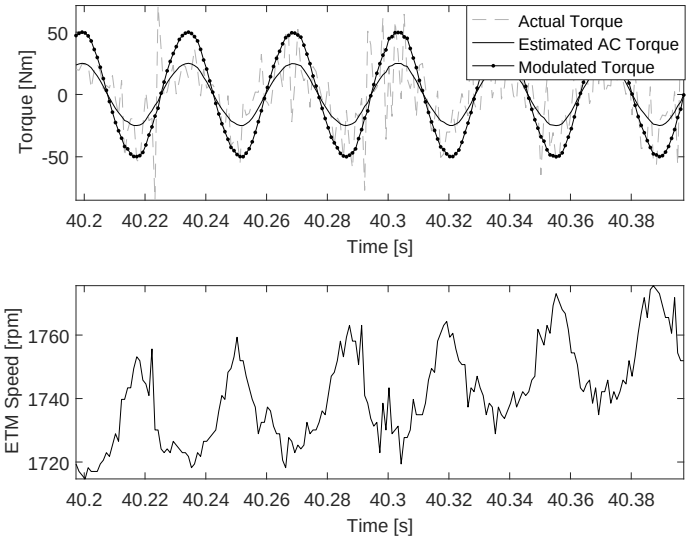


**Figure 6.12:** Validation of the amplitude modulation functionality at the experimental setup

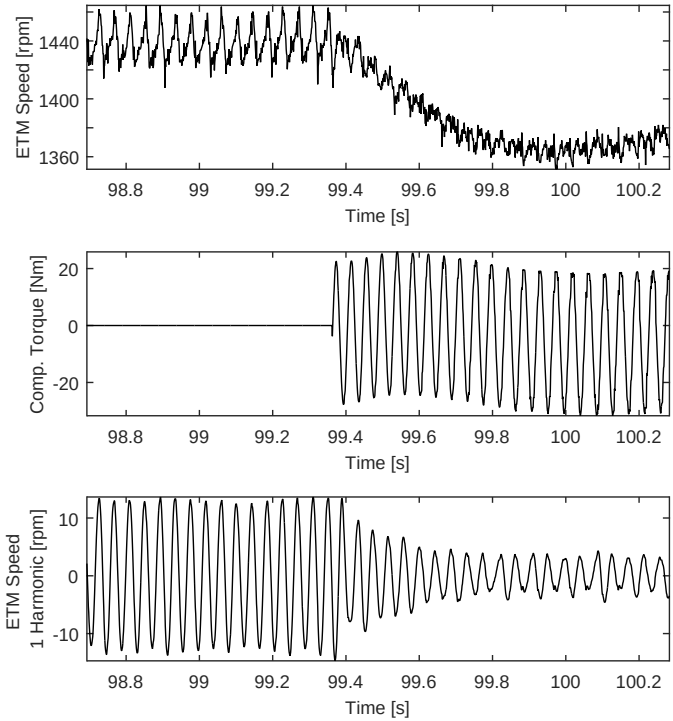


**Figure 6.13:** Results of the active vibration reduction controller during stationary speed at the experimental setup with amplitude modulation : $\mathscr{H}_\infty/\mathscr{H}_2$ Controller

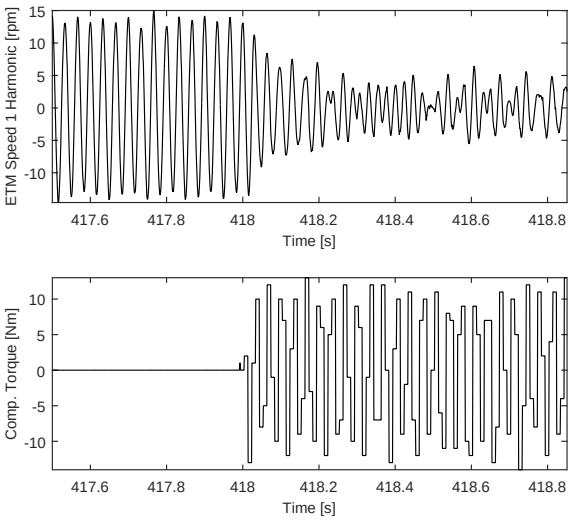


**Figure 6.14:** Results of the active vibration reduction controller during stationary speed at the experimental setup with amplitude modulation : $\mu$ controller

the activation of the controller can be observed. In comparison to Figure 6.11 the decrease in ETM mean speed is lesser because of the zero mean value of the compensation torque due to the amplitude modulation. Nevertheless, an effect of the test setup leading to a decrease in the ETM mean speed due to the action of the eddy current dynamometer is visible.

One possible way to avoid misinterpretation of the results from the influence of test setup is to use the harmonic content of the ETM speed signal for validation, as the eddy current dynamometer does not have the necessary dynamics to influence the harmonic content of the signal. This has been done by using the estimated first harmonic of the ETM speed signal displayed in the third plot of Figure 6.13. The amplitude of the first harmonic before activation was around 15 rpm is reduced to 5 rpm after activation of the controller. Modulation of the compensation torque can be used irrespective of the underlying controller. The discussion of vibration reduction with amplitude modulation shall be presented for the $\mu$ controller. The analysis is performed at the test setup at a stationary speed of 1800 rpm and 40 Nm mean torque of the ICE. After activation of the controller at 418 seconds, a

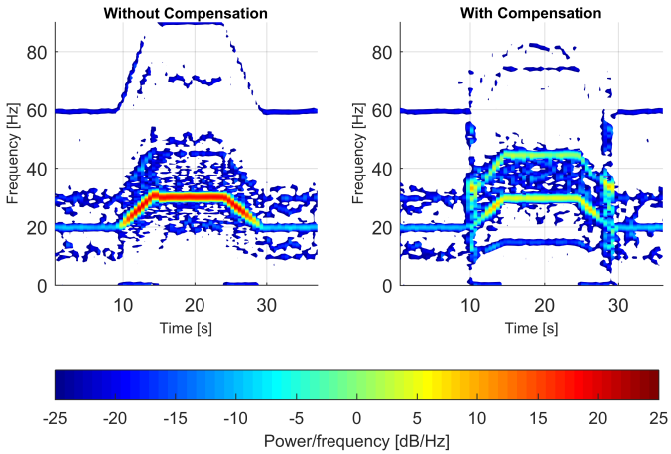


**Figure 6.15:** Spectrogram representation of the active vibration reduction controller in transient operation : $\mathscr{H}_\infty/\mathscr{H}_2$ controller

reduction in the amplitude of the first harmonic oscillation can be achieved with a compensation torque of amplitude 15 Nm. This shows the performance of the $\mu$ synthesis controller for active vibration reduction.

### Transient operation

The transient operation is realized using speed ramps of different slopes with constant mean torque demand of 40 Nm from the ICE. Along with time domain analysis, evaluation of the vibration suppression shall be performed using a comparison of the vibration energy associated with the harmonics in the ETM speed signal with and without compensation torque using a spectrogram representation. Comparison of oscillation amplitudes with and without compensation of the warm engine avoids misinterpretation of the reduction in torque excitation amplitude with an increase in speed as resulting from the compensation torque. The validation results during transient operation of the $\mathscr{H}_\infty/\mathscr{H}_2$ and $\mu$ controller with compensation amplitude of +/-25 Nm are presented. In both cases, a transient speed profile from 1200 to 1800 rpm in 5 seconds is realized at the test setup. Results of the $\mu$ controller performance during transient operation is displayed in Figure 6.16. Similar to the results of the $\mathscr{H}_\infty/\mathscr{H}_2$ controller, a small increase in the vibration energy of multiples of the 1.5th harmonic can be seen. But this increase is below

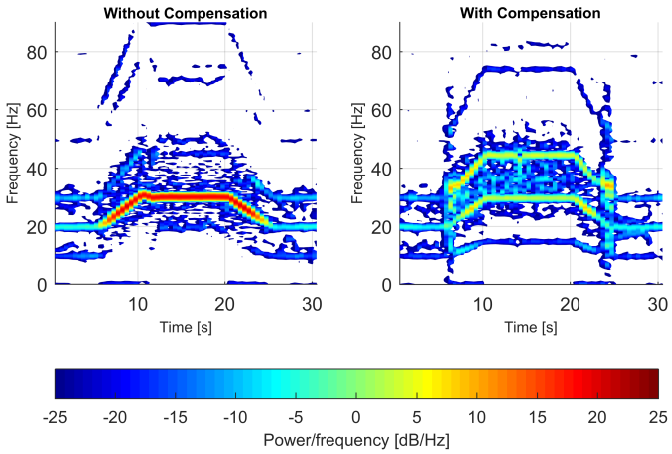


**Figure 6.16:** Spectrogram representation of the active vibration reduction controller in transient operation : $\mu$ controller

the level of the reduced first harmonic vibration and can be neglected. There is no observable performance degradation during positive and negative ramps as well as during the transition from ramps to steady speed operation and vice versa.

The effect of active vibration reduction during transient operation in the time domain is presented in Figure 6.17. As it was presented from the spectral representation, the time domain analysis also shows the realized reduction in vibration energy after activation of the controller. A compensation torque between -25 Nm and +25 Nm was achieved with amplitude modulation. The corresponding ETM speed signal during the speed transient is also presented. For better visualization of the speed signals with and without compensation, is offset by -40 rpm. As it can be observed, the ETM speed oscillations with compensation using the $\mu$ controller are reduced in comparison to the same signal without compensation.

## 6.5 Conclusion

This chapter presented an output feedback controller to generate the compensation torque to reduce the effect of pulsating torque resulting from the ICE operation. Robust control techniques were used to synthesize the controllers yielding

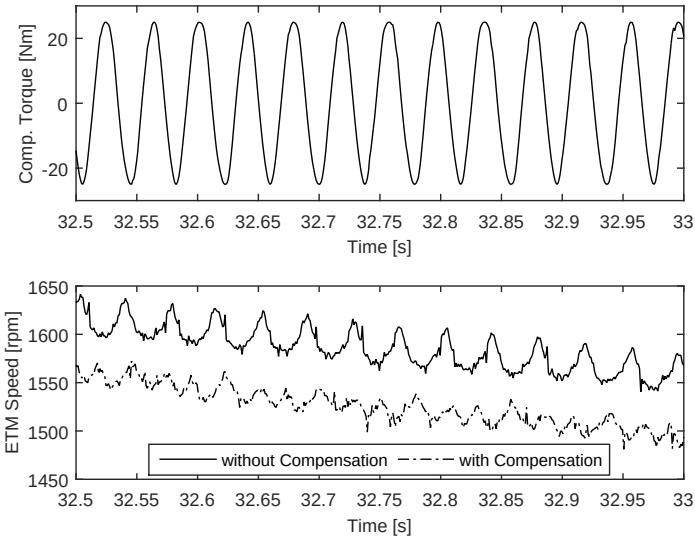


**Figure 6.17:** Results of the active vibration reduction controller in transient operation : $\mu$ controller

guaranteed stability and performance at the cost of an increased modeling effort and some design-induced degree of conservatism. The output feedback controllers do not require online tracking of harmonics or parameters and only the measured ETM speed signal as the input. The developed output feedback controllers are shown to realize vibration reduction in the presence of uncertainty introduced in the simulation model.

A direct application of robust control theory was not able to modify the limits on the maximum torque employed for vibration reduction during operation. The presented amplitude modulation technique was able to realize vibration reduction with constrained amplitude range for the compensation torque which can be calibrated during operation. Furthermore, experimental validation at the powerpack test bench shows promising results both in stationary and transient operation.

## 7 Adaptive Regulation based Active Vibration Reduction Controller

From the control perspective, the objective of the active torsional vibration reduction controller is to reduce multi-sinusoidal disturbances from the output of a stable system. The disturbance signal (which in the case of active vibration reduction is the ICE torque) with multiple harmonics can be compensated using narrow-band speed-adaptive disturbance rejection schemes. Depending on the ICE variant (3- or 4-cylinders) the harmonic to be rejected can vary. The frequency of the engine torque disturbances is a factor of the current engine operating speed and the engine configuration. In case of inline 4-stroke engines with $z_{cyl}$ cylinders, the frequency in Hz ($f$) of interest can be computed using equation (7.1) in terms of ($n$), the engine operating speed (in rpm).

$$f = (n \times z_{cyl})/120 \tag{7.1}$$

One method would be to approach the vibration reduction problem as an output regulation problem which would be the objective pursued in this chapter. Output regulation deals with asymptotic tracking of prescribed reference signals and/or asymptotic rejection of disturbances at the output of a dynamical system. In this chapter, we solve the active vibration reduction problem using harmonic rejection approach. One peculiar feature of the torsional vibration reduction problem is that the ICE which is torque source also introduces the disturbance into the system. In other words, due to the inherent nature of the internal combustion process, the ICE torque comprises of the desired mean value torque and harmonic disturbances that shall be attenuated. An output regulation based approach to the problem would require the errors to be regulated to zero shall be restricted to the harmonic content without affecting the non-periodic mean torque value.

The developed control strategy suppresses the effect of ICE torque pulsations of the dominant harmonics. The controller uses a real-time estimation of the harmonic content by spectral decomposition of the ETM speed signal, and controller design is transformed into a problem of the synthesis of an output regulation controller. The estimation of the harmonics is performed online using an adaptive disturbance estimation algorithm. The controller to reduce the harmonic content is designed to be a velocity-feedback controller to introduce damping in the system.

This chapter is organized as follows. Section 7.1 introduces the output regulation problem along with the theoretical results. The developed adaptive output regulation controller along with its structure and the generation of the adaptive disturbance estimates are discussed in section 7.2. The validation of the developed

controller using simulations and experimental investigation is presented in section 7.3. The section 7.4 presents the concluding remarks.

## 7.1 Output regulation

In this section, we discuss the controller developed for active torsional vibration reduction. The controller shall reject the time-varying oscillations using a disturbance rejection controller. This can be viewed as an output regulation based disturbance rejection approach. An overview of the historical development of the output regulation approach and recent developments have been documented in [148], [79] and [149]. The difference of such a controller to conventional tracking and disturbance rejection problems is that the class of reference signals and disturbances consists of solutions of some autonomous system known as exosystem. The term exosystem refers to the external disturbance generator. In the case of ICE-induced torsional vibrations, the ICE is the exosystem and the system being studied is the torsional powertrain. The persistent signals from the exosystem which are either reference signals and/or disturbances are termed exosignals.

One key result of the research in the field of output regulation [150], [151] and [60] is the internal model principle which proposes the formulation of an internal model. The exact asymptotic regulation requires the internal model of the dynamics of the disturbance generating exosystem to be a part of the controller that stabilizes the system. This leads to a structure of the controller with the replicated copy of the exosystem that generates the considered reference signals /disturbance and the stabilizing controller. This structure shall be studied for constant frequency disturbances and later extended for disturbance signals with time-varying frequencies.

Given the plant and the internal model, the output regulation problem reduces to design a controller for the aggregated system such that the error goes to zero. Let us consider an aggregated system and error definition given by equations (7.2 - 7.3) and (7.4) respectively. The error signal $e$ is a linear combination of the states $x$ and the disturbances $w$. The matrix $A$ is the system matrix, $B$ is the input matrix and the matrix $P$ is the matrix through which the disturbances affect the state, hence termed as disturbance input matrix. The matrix $S$ defines the dynamics of the exosystem generating the disturbances. In order to generate persistent disturbances, the matrix $S$ has imaginary eigenvalues, also known as neutral stability. The distur-

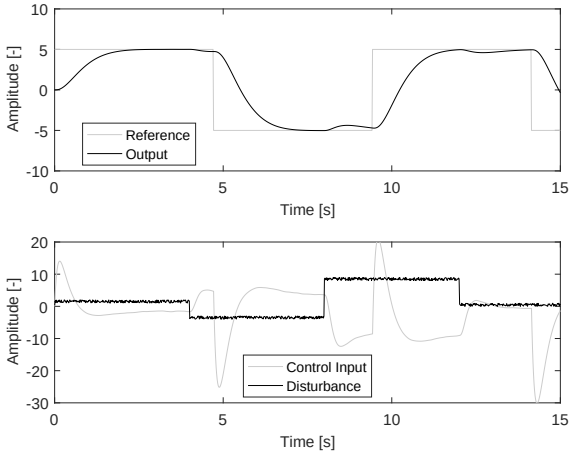


**Figure 7.1:** Output regulation in the presence of harmonic disturbance, with the output following the reference

bance is generated by a linear exogenous system which is neutrally stable. Neutral stability ensures that a persistent disturbance is imposed on the system.

$$\dot{x}(t) = Ax(t) + Bu(t) + Pw(t) \tag{7.2}$$

$$\dot{w}(t) = Sw(t) \tag{7.3}$$

$$e(t) = Cx(t) - Qw(t) \tag{7.4}$$

If the trajectory to be tracked and the disturbances that are to be rejected are not directly measurable, they shall be generated online as per the internal model principle using feedback schemes [60]. This feedback scheme to estimate the exogenous inputs shall be termed as the adaptive disturbance observer. The discussion assumes exact knowledge of the plant and exosystem models. The full-information regulation problem deals with the synthesis of the feedback controller, which uses the complete state information. The output feedback regulation assumes that only the output is available as a measurement. In this case, the goal is to find a dynamic controller given by equation (7.5). The quantity $e$ is the formulated error signal

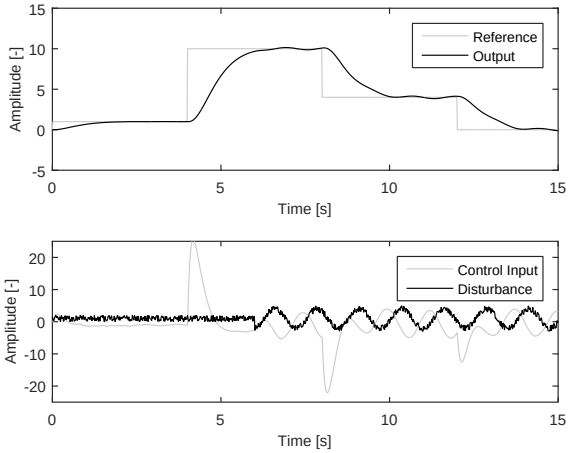


**Figure 7.2:** Output regulation in the presence of harmonic disturbance, with the output following the reference

which is the input to the system. The states of the controller are denoted by $\xi$ and input represented by $u$.

$$\begin{aligned}\dot{\xi}(t) &= F\xi(t) + Ge(t)\\ u(t) &= H\xi(t)\end{aligned} \tag{7.5}$$

*Theorem* 7.1. [60] Let $(A,B)$ be stabilizable and the pair $\begin{bmatrix}A & P\\ 0 & S\end{bmatrix}, (-C \quad Q)$ detectable. The controller, which solves the error feedback regulation problem exists if and only if there exist $\Pi$ and $\Gamma$ of appropriate dimensions such that the equations (7.6) and (7.7) hold.

$$\Pi S = A\Pi + P + B\Gamma \tag{7.6}$$

$$0 = C\Pi + Q \tag{7.7}$$

The equations given by (7.6) and (7.7) are known as regulator equations. The solution to the equations is used to construct the controller. The output regulation shall be presented with constant disturbances with noise effects followed by sinu-

soidal disturbances with Gaussian white noise. The case with constant disturbances can be handled using PI controller, where as the case with sinusoidal disturbance is of interest to the active vibration reduction controller. This demonstration serves to present the ability of output regulation to handle different disturbance signals using a generic method. Hence the underlying system and method of solution of the regulator equations shall not discussed. The interested reader is referred to [60].

The performance of the output regulation controller in case of constant disturbance is depicted in Figure 7.1. The top section of the plot presents the reference signal and the output signal that tracks the reference signal irrespective of the presence of the disturbances. The reference signal contains step changes which are tracked well by the output signal. The bottom section of the plot shows the piecewise constant disturbance signal and the control action. From the control action, the response of the controller to changes in the disturbance signal and the changes in the reference signal can be observed. As mentioned before, a similar control action can be achieved by integral action of the controller which compensates for the constant disturbances. The ability of the controller to handle other disturbance signals makes the method of output regulation attractive, one such case involving harmonic disturbances of constant frequency and amplitude shall be presented next.

Figure 7.2 presents an example of the achieved control action. The disturbance until 6 seconds is just noise, after 6 seconds the noise is modulated on a sinusoidal signal as it can be seen in the bottom plot. With the knowledge of the exogenous signal and the plant, the regulation is achieved by rejecting the disturbances as it can be seen by the tracking of the reference signal by the output. The detectability property can be without loss of generality be formulated as detectability of $(A, C)$ [60]. Together with the assumptions, the solvability of the regulator equations can be interpreted as observer based controller design with the observer for $(x, w)$. This observer based control approach shall be used to realize the adaptive output regulation vibration controller.

The disturbance attenuation problem is separated into the problems of frequency estimation and disturbance suppression. The adaptive disturbance observer estimates the harmonic content of the ETM speed signal under stationary and transient operation. In order to completely attenuate the oscillations with varying frequency, a suitable internal model of the oscillatory signal dynamics is essential. In addition to the adaptive observer, this would require a dynamic feedback control tuned to the respective harmonic frequency to achieve complete disturbance attenuation. The goal is to achieve the desired reduction over the frequency band with

a static feedback gain using the harmonic estimates from the designed observer. The disturbance observer requires only information about the frequencies which shall be estimated online. The controller does not require parameters of the plant as it indirectly influences the setting of the controller parameters, the proportional and integral gain in the case of PI controller or derivative gain of the PD controller. The complete suppression refers to complete attenuation of the harmonic estimates of the ETM speed signal without changing its (non-periodic) mean value. Further, a complete suppression of the harmonics is not desired due to practical considerations.

Complete attenuation requires higher compensation torque levels due to the higher peak pressure of modern combustion engines. Hence, in addition to meeting the traction demand, the ETM must maintain a suitable reserve for active damping. Such a calibration of the powertrain would lead to a negative impact from the perspective of driving dynamics available from the ETM, specifically at low speeds, where the vibration reduction is desired. Further, complete attenuation of the disturbances would require higher power demand, leading to problems of a reduced electric range of the hybridized powertrain. In addition, the state of the energy storage system (battery) shall also be considered, as the energy for active vibration reduction is drawn from the onboard electrical energy storage system.

## 7.2 Controller Development

This section begins with a discussion of the adaptive disturbance observer. Subsequently, the controller used for disturbance rejection along with its structure is presented.

### 7.2.1 Adaptive disturbance observer

The adaptive disturbance observer serves to estimate the harmonics of the signal and hence serves as a measure of disturbances acting on the system. It differs from a classical observer as it does not contain the copy of the system, rather uses an internal model to estimate the harmonics. Further, the observer shall adapt online according to the operating speed to generate the appropriate disturbance signal. The frequency of the harmonic components in the speed and torque signals correspond to the ignition frequency. The adaptive disturbance observer uses the estimation technique section 3.4 on the ETM speed signal to obtain its harmonic components which serve as an estimate of the disturbance acting on the system. Hence the explanation in this section can be skipped by the reader without loss of continuity.

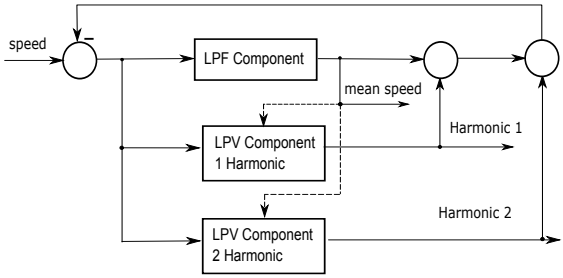


**Figure 7.3:** Structure of the adaptive disturbance observer

The adaptive disturbance observer generates an orthogonal system for each set of signal harmonics. This is performed employing a second order generalized integrator (SOGI) [94]. A prerequisite to compute direct ($d$) and quadrature ($q$) components of correct amplitude, the center frequency of SOGI should be equal to the signal frequency. This would be obtained from the LPF component in the observer structure presented in section 3.4, exploiting the fact that the frequency of the harmonics is related to the value of the non-periodic mean value component. The generation of an orthogonal system is also used in phase-locked-loops to detect the phase of the mean value with respect to the corresponding rotating harmonic frame. In addition, to the estimation of the disturbance on the system, the disturbance observer output can also be used to quantify the achieved vibration reduction.

The observer operates on the ETM speed and has a Low Pass filter (LPF) component and Linear Parameter Varying (LPV) component. Figure 7.3 displays the structure of the adaptive disturbance observer. The adaption of the observer to the current operating speed is done by the LPV component. The LPF component estimates the mean value which is equivalent to the frequency to which the LPV component shall be tuned to filter the harmonic components.

$$n(t) = n_{dc} + a_{1H}sin((n_{dc}/60)t) + a_{2H}sin((n_{dc}/30)t) \tag{7.8}$$

Figure 7.4 shows the performance of the disturbance observer during step changes in speed. The input to the disturbance observer is a noisy signal with a mean value ($n_{dc}$ in rpm) and multiple harmonics as given in equation (7.8). The quantities $a_{1H}$ and $a_{2H}$ stand for the first and second harmonics of the signal with frequencies of the mean value of the signal which are set to 100 rpm and 70 rpm respectively. The signal with an initial mean value of 1200 rpm undergoes a step change at 1.1

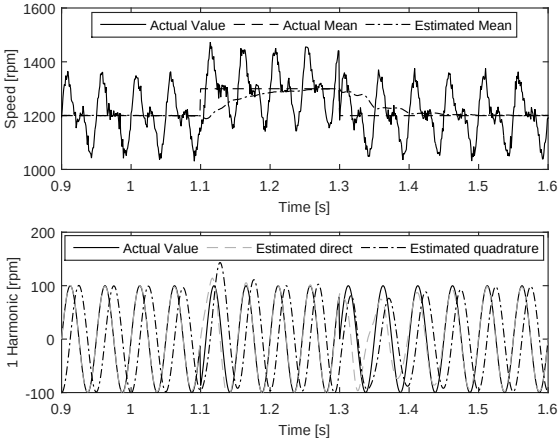


**Figure 7.4:** Performance of the adaptive disturbance observer computing the mean value and the first harmonic during step changes in speed

seconds to 1300 rpm and at 1.3 seconds from 1300 rpm to 1200 rpm. During both steps, the disturbance observer estimates the mean value signal in 0.1 seconds after the step change. The dynamics of the observer is governed by the low pass filter time constant parameter. As the mean value filtering involves only linear dynamics, the tradeoff between the speed of response and noise filtering exists. The presented results are with a time constant value of 0.05 seconds. The top plot shows the results of the mean value estimation. It includes the actual signal value, the actual mean value, and the estimated mean value. In addition to the mean value estimation, the results of the estimation of the first harmonic are also presented. The bottom plot displays the actual first harmonic along with the estimated direct and quadrature components of the first harmonic. As expected the direct component estimate is synchronous with the actual value of the first harmonic and is phase shifted by 90° to the estimate of the quadrature component. In the case of the mean value and the harmonic components, it can be observed that after the step changes, the estimation converges to the actual value of the harmonic estimate.

### 7.2.2 Controller

In order for ease of implementation and calibration, the controller is realized as PI/PD controller. Further, these controllers are widely accepted by field control engineers who would perform calibration of such controllers. The choices of PI

and PD controller are physically motivated, this shall be illustrated with a simple model followed by application to the system studied.

As the system is oscillatory a simple model would be mass-spring-damper-system whose speed response to an input torque is given by (7.9). The parameters $j$, $b$ and $k$ stand for inertia, damping and stiffness respectively. Using a negative feedback of the speed signal and the input torque as the control signal, the closed loop response of the system using PI and PD controllers are given by (7.10) and (7.11) respectively. The parameters $K_p$, $K_i$ and $K_d$ are the gains of the proportional, integral and derivative components respectively. As it can be seen in both the cases the damping of the system is improved. Furthermore, the PI controller stiffens the system, whereas the addition of the PD controller is equivalent to increasing the inertia of the system. As a complete attenuation of the disturbance is not desired as discussed in section 7.1, the implementation uses a PD controller.

$$G = \frac{s}{js^2 + bs + k} \tag{7.9}$$

$$G_{PI} = \frac{K_p s + K_i}{js^2 + (b + K_p)s + (k + K_i)} \tag{7.10}$$

$$G_{PD} = \frac{K_d s^2 + K_p s}{(j + K_d)s^2 + (b + K_p)s + k} \tag{7.11}$$

### 7.2.3 Structure of the controller

Figure 7.6 presents the structure of the developed controller which computes the required compensation torque based on the measured ETM speed signal. The estimates of the harmonic content of the ETM speed $\omega_{1H}$ and $\omega_{2H}$ are computed using the adaptive disturbance observer. The controllers for each harmonic use the estimated harmonic values and compute the required compensation torque. The amplitude modulation is used to shift the mean value of the compensation torque by $T_{mean1H}$ and $T_{mean2H}$. The modulated compensation torque corresponding to the different harmonics ($T_{Comp1H}$ and $T_{Comp2H}$) is used to compute the actual compensation torque.

The crux of the amplitude modulation is to change the mean value of the signal and the amplitude of the harmonic content of the signal without introducing a time delay. This is performed using the harmonic filtering of the signal. In the case of the vibration controller, based on the desired harmonic cancellation the compensation torque shall contain power in the corresponding frequencies. For further discussion

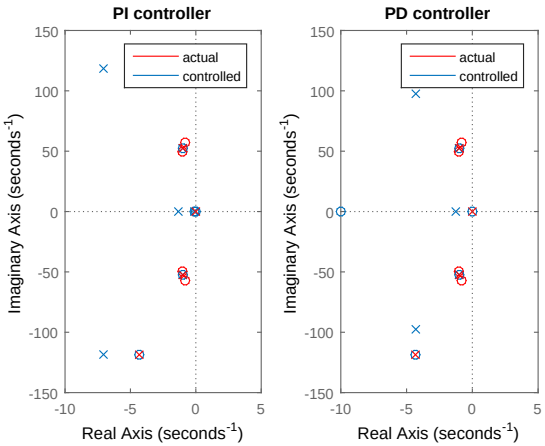


**Figure 7.5:** Pole zero locations of the actual system and the system with PI and PD controllers

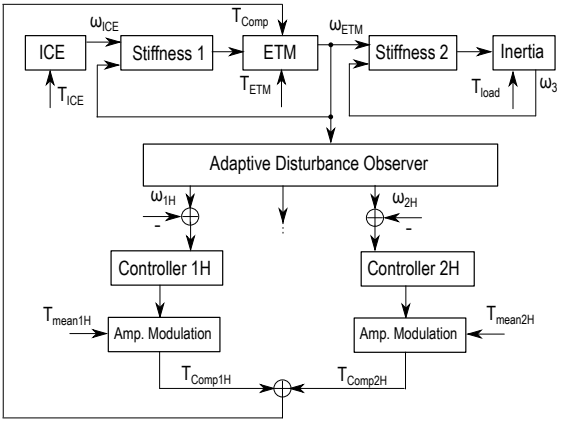


**Figure 7.6:** Structure of the active torsional vibration reduction controller based on adaptive output regulation and simulation model

on amplitude modulation applied to the compensation torque value refer to section 6.3.4.

## 7.3 Validation of the Controller

In this section, we discuss both the results from the simulation study and the experiments. In order to show the applicability of the developed controller for different engine configurations, the simulation study uses a 3-cylinder engine, whereas the experimental evaluation of the controller was performed on the powerpack test bench with a 2-cylinder combustion engine.

### 7.3.1 Simulation

Here, we discuss the simulation results with the 3-cylinder engine model. The simulation model has a structure as shown in Figure 7.6 using a model of the powerpack test bench in speed controlled operation. The torsional dynamics of the CEA powertrain is represented using a three inertia torsional mass-spring-damper system. The ICE, ETM and the rest of the powertrain are represented by their inertia reflected on the engine side. The ICE torque oscillations are modeled using test bench measurements [19], to represent the speed dependent oscillation frequency with the corresponding amplitude.

Figure 7.7 shows the result of the vibration controller operation around a mean speed of 1250 rpm and mean ICE torque value of 40 Nm. The plots in the first row are present of the speed at the ETM and the compensation torque. The compensation is activated at 10 seconds. After the initial transients due to activation, a torque amplitude of 47 Nm is used for compensation. The reduced oscillations of the ETM speed can be seen after the activation of the controller action. The FFT value of ETM speed with and without compensation are presented for comparison. The FFT representations in the bottom plot show the amplitude of oscillations in the 1.5 th (31 Hz) and 3 rd (62 Hz) order corresponding to the operating speed. After controller activation, the oscillations in the dominant order are reduced to half its actual value without any change in the oscillations of the other order.

Results from the transient operation of the developed controller during speed ramp from 1000 rpm to 2000 rpm in 5 seconds is presented in Figure 7.8. The plot shows the result for the first second after activation of the speed ramp and the controller. After the initial switching transients, the controller realizes the desired vibration reduction which can be seen in the reduced amplitude of the ETM speed oscillations.

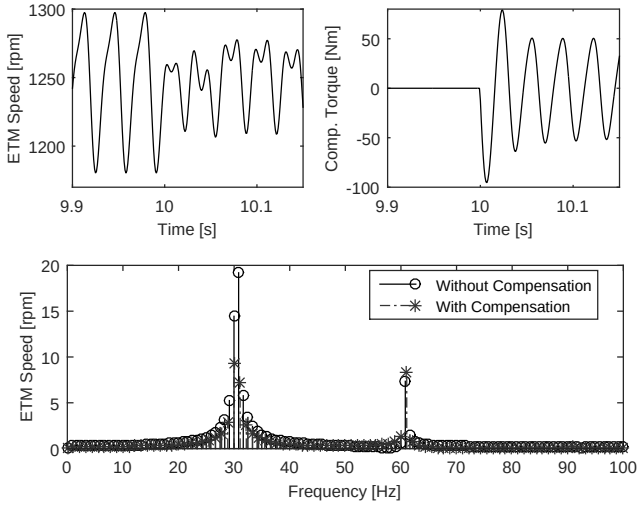


**Figure 7.7:** Performance of the active torsional vibration reduction in simulations at a mean ETM speed of around 1200 rpm

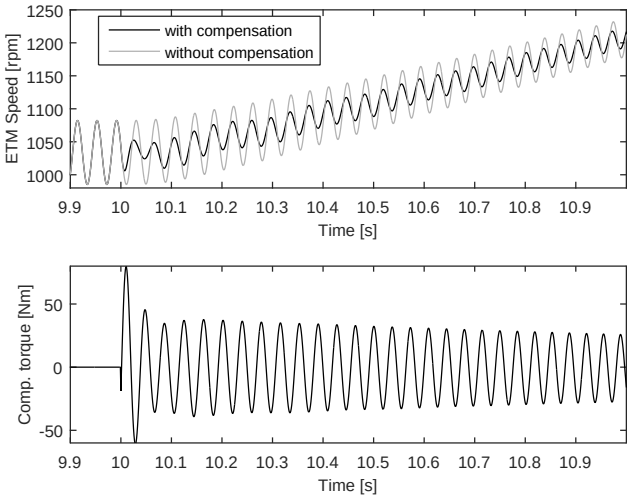


**Figure 7.8:** Performance of the active torsional vibration reduction in simulations under transient conditions 1000 to 1800 rpm in 5 seconds

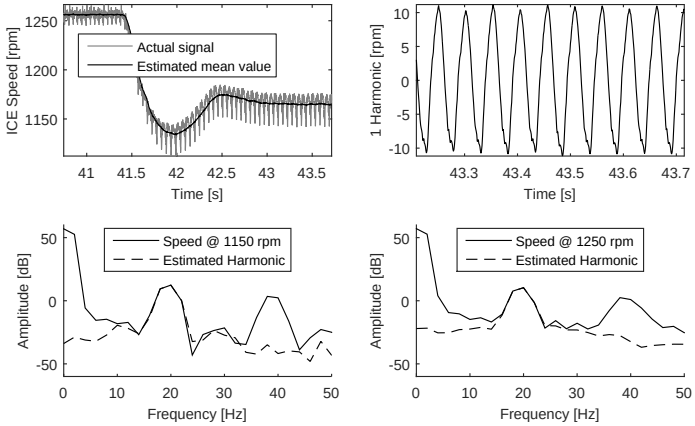


**Figure 7.9:** Performance of the adaptive disturbance observer at the experimental setup

### 7.3.2 Experimental validation

The CEA powertrain [95] is used as the experimental setup. The computed compensation torque is realized using an electric traction machine, which is flanged on the crankshaft axis, separated by a hydraulically operated friction clutch. The compensation strategy was executed on dSPACE ds1005 platform, the computed set-value torque for the electric machine is transferred to the electric traction machine inverter using an analog signal. The use of analog signals reduces communication delays compared to set value command using CAN bus. The sampling frequency of the controller was set to 1 kHz. The ETM and the dynamometer are operated in torque and speed control mode respectively. The set value for the ICE is the pedal value, which is used to realize the torque based on the ECU calibration. Figure 7.9 presents the performance of the adaptive disturbance observer using measurements from the powerpack test bench. The ICE is operated at a mean engine speed of 1250 rpm with a pedal value of 10% up to 41.5 seconds. Following the step change in speed and pedal value at 1150 rpm, 10% is realized using the automation system. The top left plot presents the speed of the combustion engine. Higher pedal value at 1150 rpm reflects in the increased amplitude of the speed oscillations at 1150 rpm. The plots at the bottom row present the welch spectral estimate at the operating speeds of 1150 and 1250 rpm respectively. In addition to

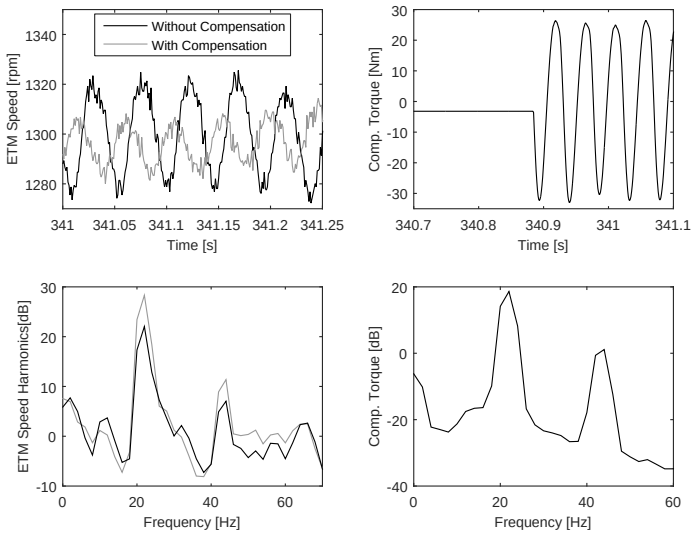


**Figure 7.10:** Experimental validation of the active vibration reduction controller in stationary operation at 1300 rpm ICE speed, 50 Nm ICE torque

the spectral representation of the speed signal, the spectrum of the estimated first harmonic is displayed.

As it can be seen, the estimation matches the actual signal at the first harmonic of the speeds around 19 Hz and 20 Hz for the operating speeds of 1150 and 1250 rpm respectively. The lower value of speed oscillations at 1250 rpm is reflected in the amplitude of the spectral estimate at the corresponding speed. In addition, the time domain representation of the first harmonic estimate at 1150 rpm is depicted. The top left plot displays both the actual signal and the estimated mean value of the ICE speed. It can be observed that the mean value tracks the actual signal irrespective of the configuration of the test bench (with/without the ICE). In addition to the first harmonic, higher harmonics can also be estimated using the disturbance observer.

### Stationary operation

The performance of the vibration controller at constant speeds is studied using bidirectional and unidirectional compensation torque. The unidirectional compen-

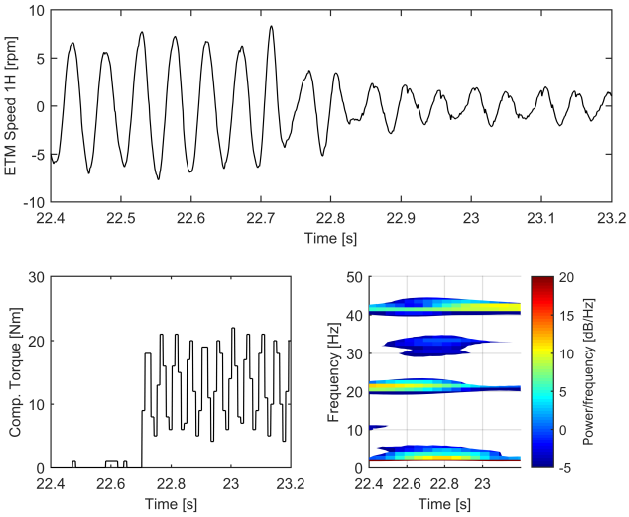


**Figure 7.11:** Experimental validation of the active vibration reduction controller in stationary operation at 1250 rpm ICE speed, 30 Nm ICE torque using unidirectional compensation torque

sation torque is realized using amplitude modulation. In both cases, the amplitude of oscillations of the ETM speed shall be used to quantify the effect of vibration reduction. In addition, the compensation torque used and the Welch spectral estimates of the ETM speed and the compensation shall also be discussed.

Figure 7.10 displays the results of vibration reduction around a mean ICE speed and ICE torque of 1300 rpm and 50 Nm respectively. The top left plot presents the effect of reduction with and without the compensation torque. The amplitude of oscillations is reduced with the activation of the controller at 340.9 seconds. The vibration controller in this case, targets both the first and the second harmonics. This can be seen in the presence of the harmonic content around 22 Hz and 44 Hz corresponding to the first and second harmonic associated with the operational speed. The effect of the harmonic reduction can also be seen in the frequency domain representation of the ETM speed at the respective frequencies corresponding to the amplitude of the harmonic torque at the corresponding frequencies.

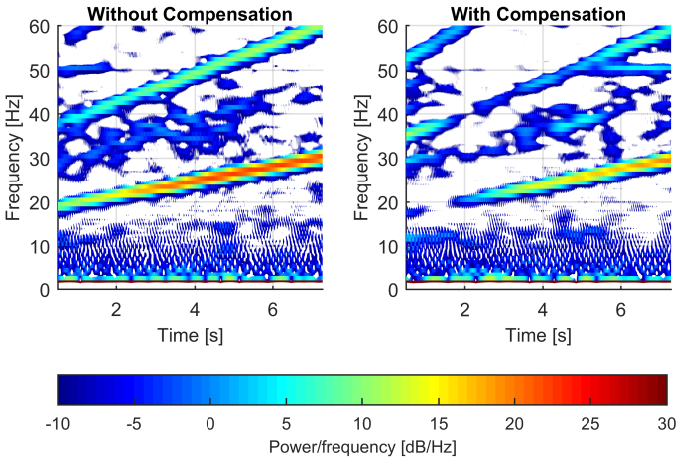


**Figure 7.12:** Experimental validation of the active vibration reduction controller in transient operation with 40 Nm ICE torque with speed transient 1200 rpm to 1800 rpm in 6 seconds

Figure 7.11 displays the effect of unidirectional compensation torque. The experiment is performed at a mean ICE speed of 1250 rpm and mean ICE torque of 30 Nm. The filtered first harmonic of the ETM speed signal from the disturbance observer and the compensation torque is presented. The compensation is activated at 22.69 seconds with a maximum amplitude of 23 Nm targeting only the first harmonic oscillation. The commanded control input to the ETM is periodic with the frequency of the harmonic to be eliminated. The reduction in the first harmonic after the compensation can be seen in the harmonic amplitude represented in the time domain. In addition, the achieved vibration reduction can be seen in the spectrogram representation of the ETM speed signal shown in the bottom right plot.

### Transient operation

This section presents the performance of the developed controller during speed transients. The powerpack comprising of the ICE and ETM is accelerated from 1200 rpm to 1800 rpm in 6 seconds at constant ICE torque of 40 Nm. This transient speed maneuver was executed with and without the controller. The speed transient corresponds to linear frequency ramp from 20 Hz to 30 Hz. Fig. 7.12 presents the result

of the experimental investigation. Spectrogram estimates of the ETM speed signal without and with compensation are displayed for comparison. During the speed transient without the controller, the power corresponding to the first and second harmonic can be observed. In the case of operation with an activated controller, the signal power in the corresponding frequencies has been reduced due to the control action. As a result of the control action, vibration energy corresponding to the 1.5th and third harmonic increases marginally. This fact does not have a negative impact due to the lower power signal power corresponding to these harmonics and lesser human sensitivity at these higher frequencies.

Summarizing, the torsional vibration reduction achieved in the simulation is also demonstrated at the experimental setup both in stationary and transient operation.

## 7.4 Conclusion

This chapter proposed a harmonic controller to attenuate multi-tonal disturbances using the method of output regulation. The source of the disturbance in the flexible powertrain is the ICE and the ETM serves as the actuator to reduce the torsional oscillations.

The adaptive disturbance observer estimates the mean value and the harmonic content of the ETM speed signal. The controller uses these estimates to realize the corresponding compensation torque. The harmonic correlation between the mean value of the ETM speed signal and its harmonics is used by the observer to compute the spectral components. The parameter-variant nature of the disturbances is handled directly by the LPV component of the disturbance observer.

The observer is augmented with controllers for every harmonic to generate the compensation torque. Physically motivated tuning of the controller parameters aids the calibration of the compensation of the respective harmonics. The developed controller scheme was studied using simulations in stationary and transient operation. Experimental validation on the powerpack test bench shows promising results both in stationary and transient operation.

## 8 Delayed Torque Feedback for Active Torsional Vibration Reduction

This chapter proposes a controller for active vibration reduction by the feedback of the estimated torque transmitted from the ICE to the ETM by the torsional coupling. In order to retain drivability, the mean torque value shall not be changed. Hence only feedback of the harmonic component is done aiming at the cancellation of the corresponding harmonic components without affecting the mean torque value. The solution to the problem requires estimation of the harmonic component that shall be canceled and a feedback mechanism to realize the cancellation.

Despite its simplicity, the controller faces challenges in implementation due to the time-delay effects involved. Delays may result from computations involved, communication of the compensation torque command to the current controller of the ETM inverter for realization and also delay associated with the realization of the commanded torque. Stabilization of the control scheme shall be performed by introduction of an additional delay in the lightly damped oscillatory system, studying the system using the model of time-delay system of the retarded type. None of the approaches in the literature regarding active torsional vibration reduction considers the effect of delays in the realization of the compensation torque, making it a unique contribution of the approach presented in this chapter.

The problem of stability due to time delay was mentioned as one of the issues that have to be solved to realize the harmonic shaft feedback based vibration reduction. In the field of systems theory, different notions of stability have been investigated. Stability in this chapter refers to a stable operation of the controller realizing vibration reduction. This abstract notion shall be first concretized with a practical example. The example involves the torsional vibration reduction at the experimental test setup realized using estimates of the shaft torque harmonics. Figure 8.1 presents the implementation of the feedback using estimated shaft torque without accounting for the delay effects. The instability due to the control action can be seen with higher amplitude speed oscillations and the phase relation between the speed signals. The periodicity of the compensation torque which correlates with the operating point can be seen in the ETM and ICE speed, leading to the conclusion that the problem could be due to phase mismatch resulting from the delays in the system.

The outline of this chapter is as follows. Section 8.1 presents the theoretical results and method of control synthesis. The validation of the developed controllers is presented in Section 8.2, followed by concluding remarks in Section 8.3.

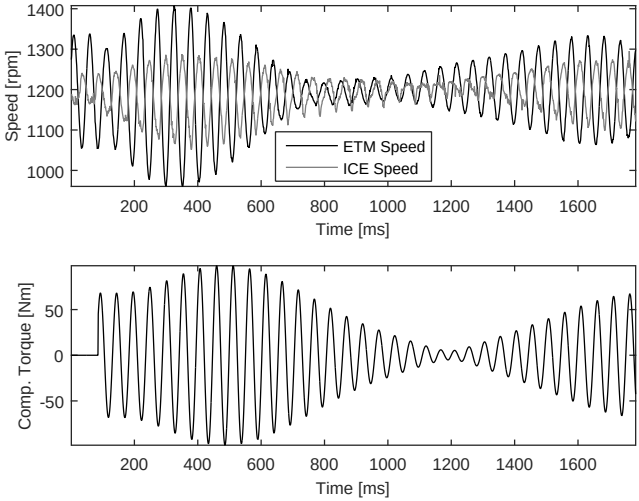


**Figure 8.1:** Instability of the active torsional vibration reduction using shaft torque feedback

## 8.1 Theory and Controller Design

In this section, we discuss the modeling of the flexible powertrain followed by identification using test bench measurements. Finally, the estimator to filter the harmonics of the estimator torque is introduced followed by the structure of the controller and its stability analysis.

### 8.1.1 System model and identification

The torsional system of interest, involving the inertia of the ICE and the ETM as well as the shaft coupling is depicted in Figure 8.2. The torsional dynamics is modeled as a linear dynamical system with 2 degree-of-freedom. This assumption is validated using non-parametric identification at the experimental test bench in Chapter 4. Equations (8.1 - 8.3) presents the dynamics where $\omega_{ICE} = \dot{\varphi}_{ICE}$ and $\omega_{ETM} = \dot{\varphi}_{ETM}$ represents the speed of the inertia. The quantities $J_{ICE}$ and $J_{ETM}$ represent the inertia of the ICE and ETM respectively. The characteristics of the coupling are denoted by the stiffness $c$ and damping $d$ parameters. The torque acting on the ETM inertia is represented by $T_2$, as opposed to $T_{ICE}$, since it is a resultant of the ETM torque and the torque from the shaft connecting the ETM to the rest of the

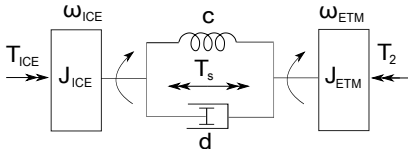


**Figure 8.2:** Torsional system used in the delayed torque compensation

powertrain. The torque transmitted through the coupling is denoted by $T_s$. Let the torsional deflection between the inertia be denoted by $\Delta\varphi = \varphi_{ICE} - \varphi_{ETM}$.

$$J_{ICE}\dot{\omega}_{ICE} = T_{ICE} - T_s \tag{8.1}$$

$$J_{ETM}\dot{\omega}_{ETM} = T_{ETM} + T_s \tag{8.2}$$

$$T_s = c(\varphi_{ICE} - \varphi_{ETM}) + d(\omega_{ICE} - \omega_{ETM}) \tag{8.3}$$

Identification was performed using subspace methods at the test bench without eddy current dynamometer as the system of interest is only the powerpack. Pseudo Random Binary Sequence(PRBS) speed excitations with a motored engine were used to avoid torque oscillations from the fired engine. The sample time for data acquisition was 1 ms.

Subspace identification methods offer an alternative to input-output model based methods specifically for Multiple Input and Multiple Output (MIMO) systems as there is no general linear input-output parametrization for MIMO systems. Subspace methods employ robust non-iterative numerical methods for obtaining the estimates. Due to the integrating nature of the process, identification has to be performed in closed loop operation. The basic problem with identification using closed loop data is the correlation between the unmeasurable noise and the input. One approach to avoid this correlation is to use pre-estimation, to separate input and past noise as presented in [152] termed canonical correlation analysis (CCA) method. [153] presents a method known as Subspace ARX (SSARX), that combines CCA and ARX, using a high order ARX model to obtain the initial estimates. This SSARX approach is used for identification of the torsional dynamics in closed loop operation.

PRBS excitations of the set ETM speed used for the identification around an operating speed of 1170 rpm is displayed in Figure 8.3. The response to these excitations which is the resulting ICE speed is also presented. The bottom plot of Figure 8.3 presents an enlarged view of the top plot of the same figure. Together

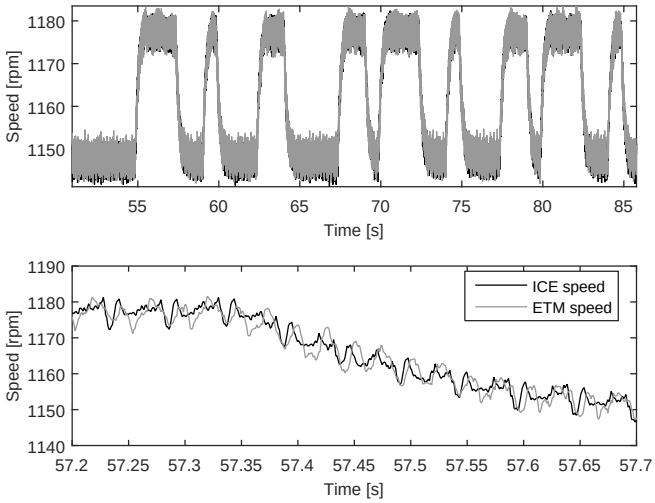


**Figure 8.3:** PRBS Excitations of the CEA powerpack unit at the test bench

the ETM and ICE speeds over the defined time window form the dataset used for identification.

Figure 8.4 presents the results of the identified torsional dynamics around 1000 rpm with the ETM. The identified resonance frequency around 120 Hz of the training measurements matches with the value from the validation dataset. Alternatively, parametric methods can be used to identify the stiffness and inertia parameters of the torsional system as in Chapter 4. Identification experiments were conducted at different operating speeds and the results are presented in Figure 8.5. It can be inferred that irrespective of the operating speed around which the measurement was performed, the eigenfrequency lies between 100 - 150 Hz. The stiffness parameter of the coupling between the inertia is computed using the identified eigenfrequency and the known inertia parameters of the machines using equation (8.4). With a minimal inertia of the machines of 0.1 $kgm^2$ the quantity $\frac{J_{ICE}J_{ETM}}{J_{ETM}+J_{ICE}}$ would have a value lesser than 0.1, reducing the sensitivity of the parameterized shaft stiffness of the identified eigenfrequency values. Further additional

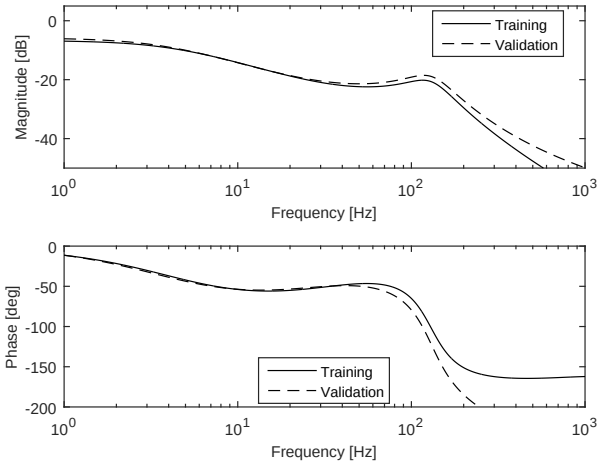


**Figure 8.4:** Identified torsional dynamics of the CEA powerpack using PRBS speed excitations. The models obtained from training and validation data around an operating speed of 1000 rpm is presented.

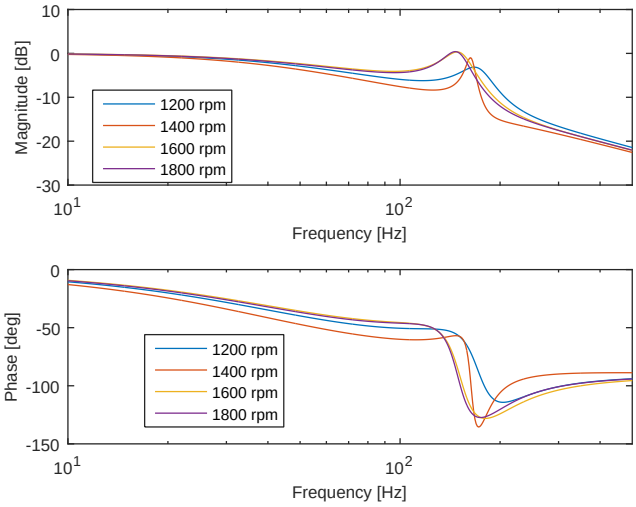


**Figure 8.5:** Identified dynamics between the ETM and ICE speed around different operating speeds

phase delay resulting from the improper parameterization of the shaft stiffness can be compensated using the time delay introduced.

$$\omega^2 = c(\frac{1}{J_{ICE}} + \frac{1}{J_{ETM}}) \tag{8.4}$$

Correlation analysis based methods for identifying delay effects in case of linear time-invariant systems have been developed. In case of transient operation of the active vibration reduction, such approximations are conservative hence an explicit identification of the delay effect is not performed for different speed and torque transients. In order to gain an idea of the actuation time delay, delay in the torque dynamics at the test bench was identified to be around 2 ms at different stationary speeds for a torque amplitude of 50 Nm. Instead of relying on extensive delay identification, a stable operation of the controller was realized using prior information from the stability analysis performing controller calibration for stable operation at the test setup. The sources of delays have been listed below.

- Computation delays associated with the real-time system arising from finite sampling frequencies
- Time delay for the realization of torque or corresponding current components of the dynamometer inclusive of dead-time of the power electronic devices, dependent on their switching frequency [1]
- Communication delay between the real-time systems as well as between real-time system and low-level controllers or actuation units. Low-level controllers comprise set-point controllers both of the dynamometer and Unit Under Test. In the case of dynamometer current and flux control constitute low-level controllers. In case of an ICE as Unit Under Test, the low-level controller refers to all the control units that are involved in the realization of the torque request demanded by the torque control structure of the Engine ECU. [2]
- Communication delay between real-time system and measurement devices

### 8.1.2 Estimator

Realization of the torque feedback control requires an estimate of the shaft torque harmonics. The shaft torque estimate is computed indirectly using an estimate of the torsional deflection angle $\Delta\varphi$ and the computed stiffness parameter from identification experiments. Alternatively, if the torque measurements of the shaft

connecting the ETM to the rest of the powertrain in the vehicle is available, estimates of the torque acting on the ETM from the ICE can be directly computed using unknown input observers as in section 3.4. In the context of the test bench, this would translate to the availability of torque measurements of the shaft connecting the ETM with the eddy current dynamometer.

The equation (8.5) presents the indirect computation of the shaft torque estimate. As both the quantities $\omega_{ICE}$ and $\omega_{ETM}$ within the integral oscillate with the same frequency around the mean speed value, the integral estimate does not exhibit any drift. One approach to avoid drift if any, would be to use the first harmonic estimate of the speeds in the equation (8.5) to compute the first harmonic shaft torque estimate $\hat{T}_{s1H}$ using the estimator presented in chapter 3.4. Nevertheless, the presence of a drift does not affect the designed controller, as only the first harmonic of the estimate $\hat{T}_{s1H}$ will be used.

$$\hat{T}_s = \hat{c} \int (\omega_{ICE} - \omega_{ETM}) dt \tag{8.5}$$

The functionality of the discussed estimated method is presented in Figure 8.6. The estimation of the shaft torque and its first harmonic along with the corresponding speed signals during a constant speed operation around 1430 rpm is presented. An estimated value of clutch stiffness of 1200 $Nm/rad$ was used. During time instances at which the $\omega_{ICE}$ leads $\omega_{ETM}$, a positive gradient of the estimated shaft torque can be observed. At instances during which $\omega_{ETM}$ leads $\omega_{ICE}$, a negative gradient of the shaft torque estimate can be seen. The estimation process does not introduce any in the estimated quantities can be seen. The first harmonic shaft torque with an amplitude of 20 Nm is estimated, using a harmonic estimator, which has been discussed in section 3.4.

To help the understanding, the functionality of the harmonic estimator shall be discussed with ICE speed signal. The result of the estimation of the non-periodic mean value of the ICE speed signal during a step change in speed is depicted in Figure 8.7. The top plot presents the actual and estimated mean value of the ICE speed. The estimated mean value follows the actual step change in speed. In addition, the welch spectral estimate of the actual speed signal is compared to the estimated first harmonic showing a good match of their magnitude before the step change in speed.

As already mentioned the estimated first harmonic of the speed signal can be used to evaluate the integral in equation (8.5) for the first harmonic computing

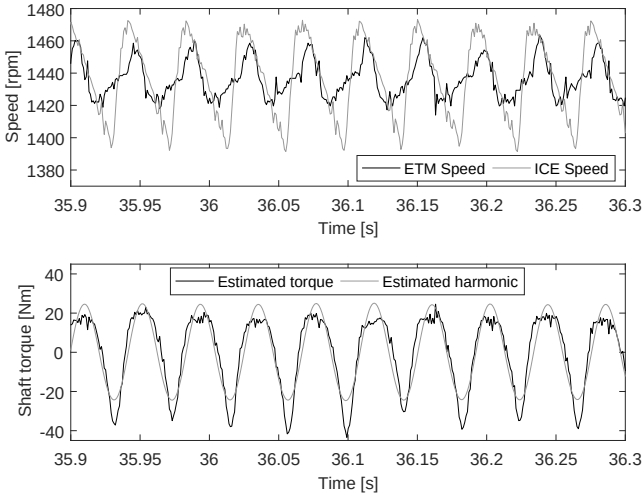


**Figure 8.6:** Estimation of the shaft torque and its dominant harmonic under constant speed operation using the ICE and ETM speed signals

the first harmonic shaft torque estimate directly, a method to eliminate drift, if any. The periodogram estimate of the first harmonic estimate depicted follows the actual speed as the frequency of the first harmonic oscillation are proportional to the mean value signal. The estimated harmonic components shall be used in section 8.2 to quantify the effect of vibration reduction. The discussed estimator was used to estimate the first harmonic of the estimated shaft torque given in equation (8.5), tracking the dominant harmonic.

### 8.1.3 Structure of the controller

Figure 8.8 depicts the structure of the developed controller which computes the compensation torque based on the measured speed signals. With the shaft torque harmonic estimates and using the frequency separation of the estimates as in section 8.1.2, the control action can be computed separately for each estimate. The controller contains a gain factor for tuning the torque request and time delay element to ensure stability. The shift of mean value of the compensation torque by $T_{mean1H}$ and $T_{mean2H}$ to realize unidirectional compensation torque is realized by amplitude modulation. Finally, compensation torque corresponding to the different harmonics ($T_{Comp1H}$ and $T_{Comp2H}$) is summed to obtain the actual compensation

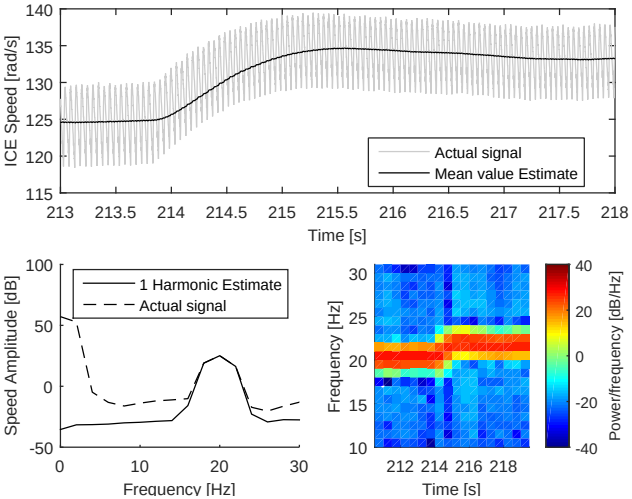


**Figure 8.7:** Estimation of the non-periodic mean value and the harmonic components of the ICE speed signal during a step change in speed.

torque. Apart from the controller, Figure 8.8 also presents the three inertia torsional model of the powertrain used in the simulation analysis of the developed controller. The ICE, ETM and the rest of the powertrain are represented as the inertia with the associated stiffness of the couplings.

The controller for each harmonic comprises of a gain $k$ to tune the amplitude of the compensation torque and a delay $\delta$ element to ensure stability. Due to the simple model and few known parameters, the robustness of the controller can be ensured. Stability analysis provides upper and lower bounds for the value of the delays discussed in section 8.1.4. The ability to tune gain $k$ during calibration at the experimental setup introduces a measure of robustness against uncertainty in the estimated stiffness parameter. This is due to the fact that both the stiffness parameter and the gain $k$ enter the computation of the compensation torque in a similar fashion. The clutch between the ICE and the ETM in the studied CEA powertrain was found to be constant over the operating speed/deflection range using the discussed identification method. If a DMF or multi-stage torsional damper is employed, the value of stiffness varies over the torsional angle would require a tuning of the controller gain to account for the stiffness variation. Amplitude modulation changes the mean value and the amplitude of the harmonic content of

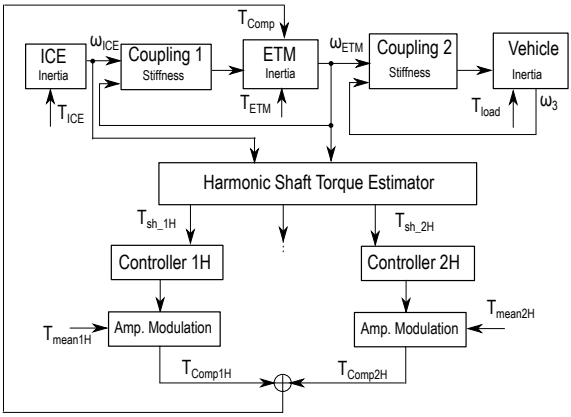


**Figure 8.8:** Structure of the active torsional vibration reduction controller based on delayed shaft torque feedback and simulation model.

the compensation torque without introducing a time delay. It has been presented in section 6.3.4.

### 8.1.4 Stability analysis

From a theoretical perspective, shaft torque harmonic feedback for active vibration reduction can be modeled as output feedback of a damped oscillatory system. The oscillatory system is the torsional powerpack discussed in section 8.1.1. This problem can be modeled as stabilization of the system given in equation (8.6) by a static output feedback $u(t) = -ky(t-\tau)$, where $k$ is the controller gain defined in section 8.1.3, $b$ indicating damping in the system, $\kappa$ denoting system gain and $\tau$ is the delay time.

$$\frac{Y(\lambda)}{U(\lambda)} = \frac{\kappa}{\lambda^2 + \lambda b\omega + \omega^2} \tag{8.6}$$

As the delay appears in the feedback path, stability analysis involves the study of (exponential) stability of the null solution of the linear damped oscillatory time-delay system of retarded type [154]. Eigenvalue based methods and time-domain methods are the two main categories of methods available for the stability analysis of time-delay systems. Eigenvalue based methods use necessary and sufficient

conditions hence are not conservative as compared to the use of a tractable form of Lyapunov functional depending on finitely many parameters in case of time-domain methods. As the study involves analysis of a linear system, eigenvalue based method/characteristic root analysis shall be used.

The study of delayed systems involves the study of functional differential equations (or) delay-differential equations. A differential equation defined on a finite dimensional space assumes discrete vectors as initial conditions. On the contrary initial condition for the delay-differential equation (generally referred to as functional differential equation), is the function segment represented by $\phi \in \mathscr{C}([-\tau_m, 0], \mathbf{R}^{n\times n})$, which is an element in Banach space of continuous functions mapping the interval $[-\tau_m, 0]$ into $\mathbf{R}^{n\times n}$ with the supremum norm, $\|.\|_s$ [155]. The functional differential equation can be formulated as an abstract ODE on function space $X := \mathbb{C}^n \times \mathscr{L}([-\tau, 0], \mathscr{C}^n)$ given by equation (8.7) - (8.11). Equation (8.11) defines the function spaces where the inputs, outputs and states live.

$$\frac{dz}{dt} = \mathscr{A}z(t) + \mathscr{B}u(t) \tag{8.7}$$

$$y(t) = \mathscr{C}z(t) + Du(t) \tag{8.8}$$

$$\mathscr{D}(\mathscr{A}) = z = (z_0, z_1) \in X : z_1 \in \mathscr{C}^1([-\tau, 0], \mathbb{C}^n), z_0 = z_1(0-), \tag{8.9}$$

$$\mathscr{A}z = (A_0 z_0 + \sum_{i=1}^{m} A_i z_1(-\tau), z_1'), z \in \mathscr{D}(\mathscr{A}) \tag{8.10}$$

$$\mathscr{B}\xi = (B\xi, 0) \in \mathscr{C}^m, \mathscr{C}z = Cz_0, z = (z_0, z_1) \in X \tag{8.11}$$

This abstract ordinary differential equation on the function space given by equations (8.7) - (8.11) is equivalent to the finite dimensional functional differential equation given by equation (8.12) [154], [155], with matrices $A_0$ and $A_k$ representing the delay-free and delayed system matrices obtained by the discretization of the operator $\mathscr{A}$ as given by equation (8.10).

Linear time-delayed system of retarded type can be described by the delay-differential equation (8.12), with $x(t) \in \mathbf{R}^n$ denoting the system state at time t, $\tau_i, t = 1, ..., m$ are the time-delays in the system and $A_k \in \mathbf{R}^{n\times n}$ representing the system matrices with real coefficients. Further, it has been shown ([154]) the infinite dimensional eigenvalue problem corresponding to the system (8.7) is equivalent to the finite dimensional eigenvalue problem corresponding to the system (8.12). This equivalence is represented in equation (8.13).

$$\dot{x}(t) = A_0 x(t) + \sum_{k=1}^{m} A_k x(t-\tau_k) \tag{8.12}$$

$$(\lambda I - \mathscr{A})u = 0 \Longleftrightarrow (\lambda I - A_0 - \sum_{k=1}^{m} A_k e^{-\lambda\tau_k})v = 0 \tag{8.13}$$

Using this fact, the characteristic roots of the infinite dimensional problem is computed using the nonlinear finite dimensional eigenvalue problem.

$$\Delta(\lambda) = \lambda I - A_0 - \sum_{k=1}^{m} A_k e^{-\lambda\tau_k} = 0 \tag{8.14}$$

$$\Delta(\lambda)v = 0, \lambda \in \mathbf{C}, v \in \mathbf{C}^n, v \neq 0 \tag{8.15}$$

The characteristic equation corresponding to the system (8.12) is given by equation (8.14). The equation (8.14) can be seen as solution of the nonlinear eigenvalue problem formulated in equation (8.15).

The equation (8.14) which is a quasi-polynomial has infinitely many roots in the complex left half-plane but a finite number of roots in the right half plane [154]. Hence the problem of finding the number of characteristic roots on any right half plane, defined by $\mathscr{C} = \{\lambda \in \mathbf{C} | \mathscr{R}(\lambda) \geq 0\}$ is well posed. The asymptotic behaviour of the solutions of the equation (8.12) is exponentially stable if all the characteristic roots are in the open left half plane. In other words, if the spectral abscissa $\mathscr{C}$ is strictly negative. The time delays in this study are point-wise or discrete, which indicates limited selective memory effect in the system. tem is lightly damped, in order to demonstrate the method of stabilization using delays, an undamped oscillatory system is considered.

$$A_\tau = \begin{bmatrix} -\frac{d_1}{J_1} & -\frac{c_1}{J_1} & \frac{d_1}{J_1} \\ 1 & 0 & -1 \\ \frac{d_1}{J_2} & \frac{c_1}{J_2} & -\frac{d_1}{J_2} \end{bmatrix} B_\tau = \begin{bmatrix} 0 \\ 0 \\ \frac{1}{J_2} \end{bmatrix} C_\tau = \begin{bmatrix} 1 \\ 0 \\ 0 \end{bmatrix}^T \tag{8.16}$$

The stability analysis is performed numerically to compute the upper and lower limit of delay values for stabilization. The numerical procedure does not suffer from robustness issues, as the goal is to compute range values of a nonempty interval to realize stable operation. For the torsional system under study, the matrix $A_0 = 0$ and the other system matrices corresponding to the delay are given by equation

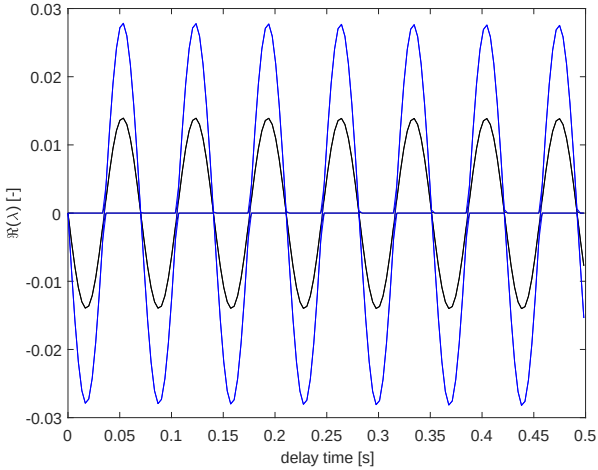


**Figure 8.9:** Compute rightmost characteristic root of the quasi-polynomial with respect to variation in the delay parameter. The computation is performed for controller gain value of $k = 1$ and $k = 0.5$ represented with blue and black lines.

(8.16) where the state vector is given by $x = \begin{bmatrix} \omega_1 & \triangle\phi_1 & \omega_2 \end{bmatrix}^T$ and the output is $y = \omega_2$.

Replacing the matrix $A_k$ with $A_\tau - B_\tau k C_\tau$ in equation (8.14), the characteristic quasi-polynomial of the system can be formulated. Using this formulation, the method developed in [156] is used to compute the rightmost characteristic roots as a function of the delay parameter.

Figure 8.9 presents the results of the computation for gain value of $k = 1$ and $k = 0.5$ represented with blue and black lines respectively. Any value of delay which causes the value of $\mathscr{R}(\lambda)$ to lie above zero, would lead to an unstable system. It can be noted that the values of delay leading to instability does not depend on the value of controller gain, as the stability depends only on the out-of-phase synchronization of the control action (compensation torque) to the output variable (ETM speed). In summary, stability analysis gives a range of delay values that lead to a stable disturbance rejection.

Figure 8.10 depicts the results of the computation of the characteristic roots for two exemplary delay values from stable and unstable regions with the control

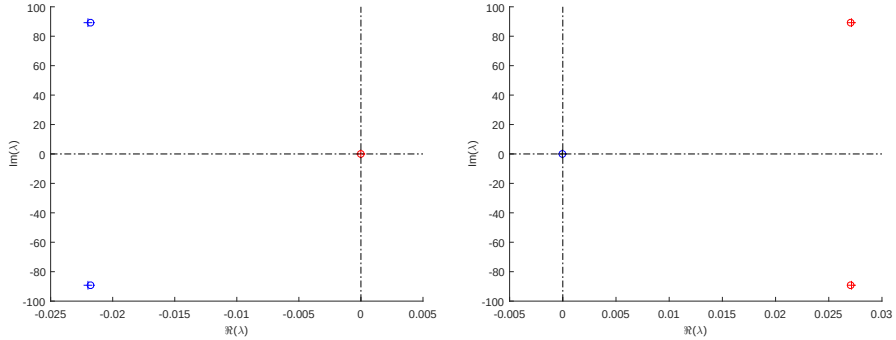


**(a)** Roots in stable region for $\tau = 0.025$ **(b)** Roots in unstable region for $\tau = 0.05$

**Figure 8.10:** Computed characteristic roots for a gain value k = 1 for delay values of 0.025 and 0.05 seconds. The circles indicate the approximation of the roots whereas the corrected roots are denoted by plus sign.

gain $k = 1$. The choice of the roots for which the depiction is made is chosen from the stability regions shown in Figure 8.9. It can be seen that the delay values of 0.025 and 0.05 correspond to stable and unstable operation. In the case of both the plots, the circles indicate the approximation used for the root computation and the plus indicates shows the corrected value of the roots computed by Newton's method. The method used to compute the initial approximation is based on the discretization scheme developed in [156] and references therein. The coloring scheme used in the plot is as follows. Blue indicates leftmost or stable whereas red is used to indicate rightmost or unstable roots. The plot 8.10a presents the location of the characteristic roots which are in the left half plane corresponding to the stable delay value of 0.025 seconds. The location of the unstable roots corresponding to the delay value of 0.05 seconds is shown in the plot 8.10b.

With this prior knowledge about the delay based stability region, parameterization of the controller for a stable operation was carried out at the test setup. As a model of the ICE torque with a phase shift between the harmonic content and the mean torque value is not available. The parametrization of the delay values at different speeds is performed at the test bench. Table 8.1 presents the delay values for the shift of the compensation torque to realize stable operation of the vibration reduction controller over the operational speed range of 1000 - 2000 rpm. These values are implemented as a lookup table with the mean value of the speed as an input.

**Table 8.1:** Delay value parametrization for shift of compensation torque

| Speed range [rpm] | Delay value [ms] |
|---|---|
| 1000 - 1390 | 15 |
| 1400 - 1590 | 10 |
| 1600 - 1690 | 4 |
| 1700 - 2000 | 2 |

## 8.2 Validation of the Controller

The developed controller is validated using dynamic simulation models before implementation on the experimental test bench. Both simulation and experimental validation shall be studied using the CEA powertrain with 3-cylinder and 2-cylinder engines respectively. The ICE and the ETM speeds serve as input to the controller and evaluation of the realized vibration reduction is done using the ETM speed signal.

### 8.2.1 Simulation

The dynamics of the CEA powertrain is modeled as a three inertia torsional mass-spring-damper system. The inertias represent the combustion engine which is the source of vibration, the electric traction machine used to attenuate the torsional oscillations and the rest of the powertrain respectively. The dynamic inner torque generated by the combustion engine is a prerequisite for the investigation of vibration reduction using dynamic simulations. The modeling and parameterization of the combustion engine are performed as in [36]. In contrast to the 2-cylinder engine used in the experimental validation, simulation analysis uses a 3-cylinder combustion engine. the only change required thereby is the tuning of the estimator to compute 1.5th harmonic instead of the first harmonic, hence showing the applicability of the vibration reduction controller to different engine configurations.

Figure 8.11 presents the results of vibration reduction during an operation about the mean speed of around 1200 rpm. The vibration controller is turned on at 10 seconds. Both the speed profiles with and without the controller action is displayed. As it can be seen after the initial transients due to switching on of the controller, the amplitude of ETM speed oscillations is reduced. The controller was implemented to act against the first dominant harmonic which in case of the 3-cylinder engine at 1200 rpm corresponds to 30 Hz. The evaluation of vibration reduction performance in the frequency domain is presented in Figure 8.14. The

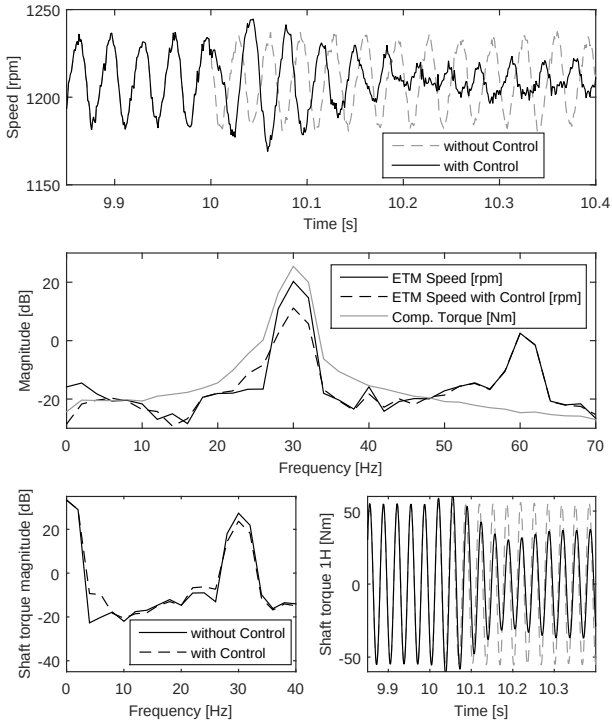


**Figure 8.11:** Performance of the active vibration reduction controller in simulation during stationary operation around a mean speed of 1200 rpm in case of 3-cylinder engine

welch estimate of the power spectral density of the mean value-free ETM speed and compensation torque is presented. The presence of higher power at the first and second harmonics corresponding to the 1.5 and 3 times of the operation speed in Hz can be observed. In the presence of the compensation torque, the power of the first harmonic is reduced without affecting the second harmonic. The reduction is achieved by compensation torque corresponding to the first harmonic. Further, the estimated shaft torque harmonic which is used for feedback is presented in the bottom row the figure. Both time domain and frequency domain representations are presented. After activation of the controller, the reduction in the first harmonic amplitude of the shaft torque can be observed.

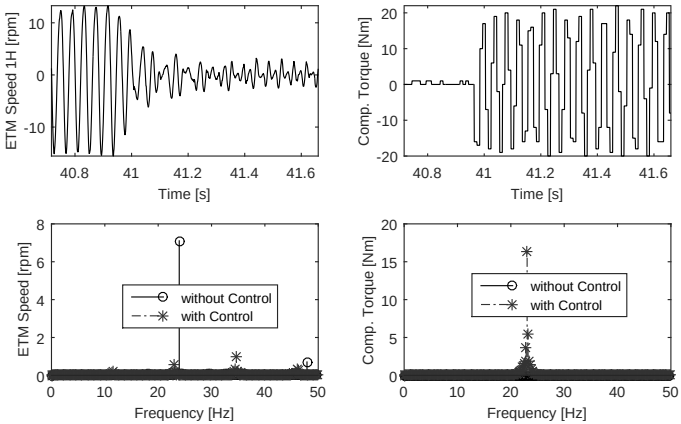


**Figure 8.12:** Experimental validation of the active vibration reduction controller in stationary operation at 1400 rpm ICE speed, 30 Nm ICE mean torque using bidirectional compensation torque.

## 8.2.2 Experimental validation

Experimental validation of the developed methods is performed both in stationary and transient operation along with unidirectional torque compensation using the setup shown in Figure 2.6. Stationary operation refers to operation at a constant speed. The experimental setup is operated with torque as a command signal for the ICE as well as the ETM. The eddy current dynamometer is operated in speed control mode. The compensation torque request to the ETM is sent using analog signals. The actual estimated torque by the ETM is available as a CAN signal with a sampling frequency of 100 Hz. The automation system and the active vibration reduction controller are implemented using dSPACE ds1005 real-time system with a sampling frequency of 1 kHz.

### Stationary operation

Stationary operation refers to constant speed operation using which two scenarios involving controller activation and change in pedal value during constant speed operation shall be studied. In both cases, the FFT of the mean value-free ETM speed signal shall be used to evaluate the controller performance. In addition, the performance of the controller using unidirectional compensation torque is

investigated. Unidirectional torque compensation involves compensation using either motor (positive compensation torque) and generator (negative compensation torque) of the ETM. This feature is practically motivated from the perspective of hybrid vehicle energy management. The generator operation of the ETM can be effectively exploited along with a load point shift of the ICE to charge the battery with the activated vibration reduction controller. Unidirectional torque compensation is realized using a change of the mean value of the compensation torque without affecting its harmonic content. This method of changing the mean value is done using the presented method of torque amplitude modulation.

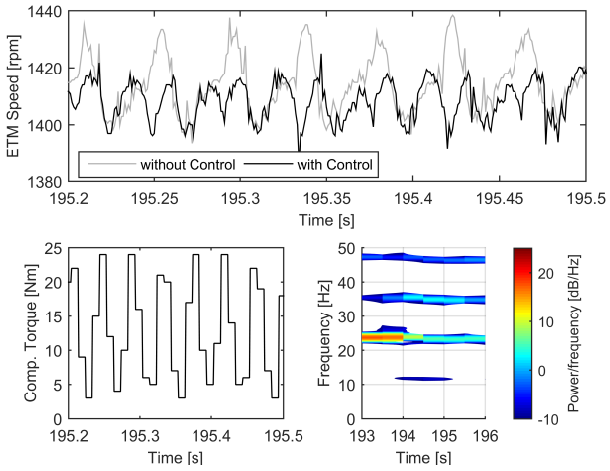


**Figure 8.13:** Experimental validation of the active vibration reduction controller in stationary operation at 1420 rpm ICE speed, 30 Nm ICE mean torque using unidirectional compensation torque.

Figure 8.12 presents the results of the controller performance around a speed value of 1400 rpm. The controller is activated at 40.9 seconds resulting in reduced oscillations of the ETM speed signal. The plots on the right side present the time and the frequency domain representations of the compensation torque. The discrete jumps in the compensation torque signal are due to the sampling of the CAN bus system used to send the actual ETM torque. The torque amplitude used for compensation is 16.3 Nm. The time domain filtered the harmonic content of the ETM speed signal is displayed in the top left plot. The amplitude of the dominant harmonic of the ETM speed signal is reduced after controller activation. The control input signal to the ETM shows periodicity with a frequency corresponding to

the first harmonic associated with the operating speed. The performance of the

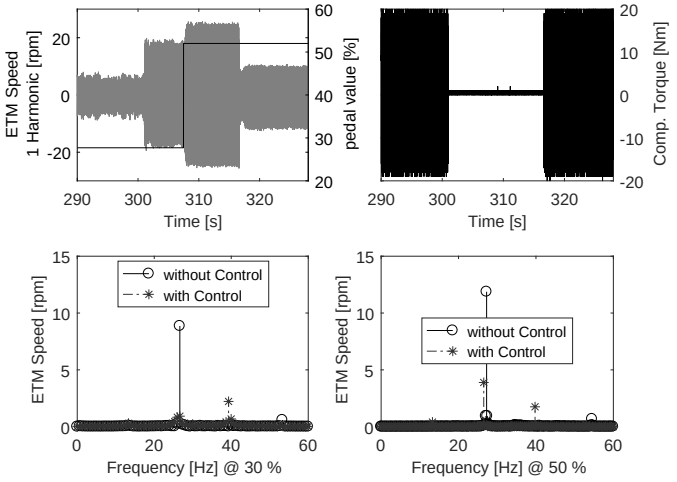


**Figure 8.14:** Experimental validation of the active vibration reduction controller in stationary operation at 1600 rpm ICE speed during a step change in ICE pedal value from 52% to 27%.

controller using positive compensation torque is shown in Figure 8.13. The shift of the mean value of the compensation torque without affecting its harmonic content was used to realize the actual compensation torque. With the compensation torque, the oscillations of the ETM speed value is reduced maintaining the mean ETM speed. The spectrogram representation of the ETM speed signal is displayed in the bottom right plot with the controller activation done at 194 seconds. In the absence of the controller, the power in the different harmonics corresponding to the mean operating frequency of 23.33 Hz can be observed. After activation of the controller, the signal power in the dominant harmonic is reduced along with a small increase in the power of the 0.5th harmonic.

The result of the controller operation in presence of step change in the ICE torque value triggered using step change in the ICE pedal value is depicted in Figure 8.14. The top plots present the conditions of the investigation performed at a mean ETM speed of 1600 rpm. The controller is activated in two phases, the first phase of activation is until 301 seconds and the second activation is after 316 seconds. At 307 seconds a step change in the ICE torque is realized using step change in pedal value to 52% from 27% corresponding to torque value change

from 20 Nm to 40 Nm. The FFT plot in the bottom left and bottom right display the frequency content of the first harmonic content at lower and higher ICE torque values respectively. The difference in the amplitude of the torque value is reflected in the different amplitude of the harmonic content. With the activated controller irrespective of the torque value, the compensation torque realizes a reduction in the oscillation amplitude. The reason for the larger amplitude of the ETM speed signal first harmonic at higher pedal value is due to the use of the same compensation torque amplitude despite the increased amplitude of the disturbance amplitude. This is due to the higher ICE mean torque value of 40 Nm corresponding to a pedal value of 52% compared to ICE mean torque of 20 Nm with a pedal value of 27%.

### Transient operation

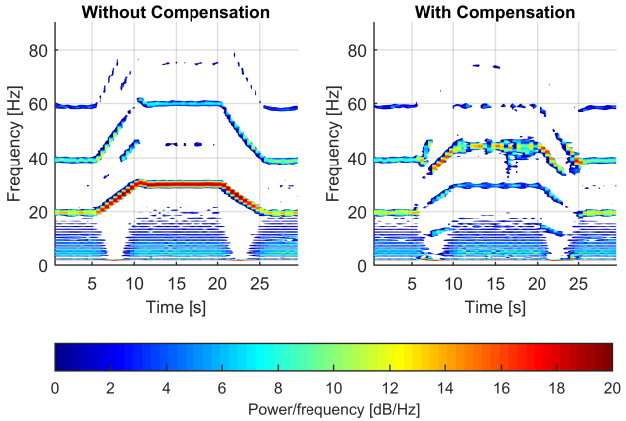


**Figure 8.15:** Experimental validation of the active vibration reduction controller in transient operation with 40 Nm ICE torque with speed transient 1200 rpm to 1800 rpm in 5 seconds.

This section discusses the performance of the developed controller in the presence of speed transients. The ICE and ETM are ramped from a mean speed value of 1200 to 1800 rpm in 3 seconds and operated at a constant speed of 1800 rpm and followed by a deceleration from 1800 to 1200 rpm. During the speed transient, the ICE is operated with a constant set torque value of 40 Nm. The speed transient is realized at the test setup using the eddy current dynamometer.

Figure 8.15 presents the result in the form of spectrogram representation of the ETM speed. The controller is deactivated till 15 seconds followed by an activation during similar speed transients. The speed transient corresponds to linear frequency ramp in the frequency range from 20 Hz to 30 Hz. The spectrogram estimates of the ETM speed signal without and with compensation are displayed for comparison. In the absence of compensation torque, the higher the power corresponding to the first and second harmonic of the ETM speed can be seen. With the activated controller the power of the ETM signal in the respective frequency range has been reduced along with a marginal increase of 1.5th harmonic. The compensation torque for the transient operation was set to -/+ 25 Nm. This small amplitude does not have a negative impact due to the lower power signal power corresponding to these harmonics and lesser human sensitivity at these higher frequencies as in [5].

Summing up, the efficacy of the proposed active vibration reduction controller is demonstrated using simulation analysis and experimental evaluations.

## 8.3 Conclusion

An approach based on delayed shaft feedback is presented for the realization of active torsional vibration reduction in hybridized powertrains. The estimation of the oscillatory shaft torque between the ICE and the ETM is performed by the speed measurements at the ICE and the ETM. This estimated shaft torque is separated into (non-periodic) mean value and the harmonic components using harmonic filtering. This harmonic filtering uses the torsional angle between the ICE and the ETM requiring the stiffness of the shaft coupling to compute the torque harmonics. Identification methods have presented to estimate the shaft stiffness. The filtered harmonic content is fed back to compensate for the torsional oscillations. However, time delays in the system pose a challenge to stable controller operation using the approach.

Stability of the vibration reduction controller requires out-of-phase synchronization with the oscillatory shaft torque. The damped oscillatory system approximation of the torsional powertrain is used for the stability analysis. The stability analysis involves the study of characteristic root location of the linear retarded delay dynamical system. The analysis shows that based on the resonant frequency of the powertrain, limits on time delay to ensure a stable operation can be computed. The realization of the stable controller is done using the introduction of additional delays between the compensation torque computed by the controller and the set torque command sent to the ETM inverter. The developed controller

was studied in simulation before validation at the experimental setup. Using amplitude modulation, both the amplitude of the compensation torque and its mean value can be varied during operation. This approach was used to realize unidirectional compensation torque, which is desirable from an energy management perspective. Experiments at the powerpack test bench using the CEA powertrain demonstrated good performance of the developed controller both in stationary and transient conditions.

# 9 Summary and Outlook

The goal of this thesis is to develop methods for estimation and control for active reduction of combustion engine-induced torsional oscillations in automotive powertrains. The work in this thesis is split into two major sections. The first section deals with signal estimation and model identification, whereas the second section focuses on the development of control methods. This chapter summarizes the work presented in the other chapters to provide the complete overview along with directions of future work.

## 9.1 Scientific Contribution

Main challenges for the development of torsional vibration damper systems arise from powertrain units with higher torque pulsations due to boosting and downsizing and increasing customer demand for more comfort. The passive torsional vibration reduction solutions are based on the modification of the properties (inertia/stiffness) of the torsional powertrain system. The introduction of tuned mass dampers with centrifugal pendulum absorbers (CPA), enable order specific vibration attenuation. However, with the increasing adoption of turbo/supercharging technology together with improving the power-to-volume ratio of the combustion engines, these measures become increasingly ineffective [22] over the entire operating spectrum of the powertrain, motivating the development of active vibration control methods. The goal of the thesis is the development of estimation methods and controllers for ICE-induced torsional vibration in automotive powertrains.

Besides passive measures, active methods offer an interesting alternative for torsional vibration reduction specifically in hybrid powertrains. In the lines of the Dual Mass Flywheel (DMF), the electric machine used for generation of the compensation torque acts as a secondary inertia. As a result, the compensation torque acts against the torque filtered through the DMF-similar setup of the ICE, damped clutch and the electric machine. This leads to a reduction of torque amplitude up to 10 times the value of torque required directly at the crankshaft [52]. This serves as a motivation for the development of active torsional vibration reduction methods.

The developed estimation methods were able to compute system properties (parameter estimation) and to determine the amplitude and frequency spectrum (signal estimation) of the excitation signals. Owing to the generic nature of the developed estimation methods, they can be also used for estimation of torsional systems at experimental test benches which is of increased practical interest. The

developed system identification methods are capable of both parametric or non-parametric characterization of the torsional system (powertrain or test bench). Apart from being used to characterize the system (as in case of modal analysis), the system properties such as stiffness parameter can be applied to calibrate the developed controllers.

Due to the additional costs and complexity, not all vibration quantities can be measured using sensory arrangements. One typical example is the oscillatory combustion engine torque which is the primary source of torsional excitation. The signal estimation techniques developed, compute the ICE torque and the harmonic estimates along with its mean value of speed and shaft torque signals. Besides, being useful for the characterization of the vibration they have been employed to realize control actions. Two classes of estimators have been synthesized. One class models the quantity to be estimated as an unknown signal and uses the measured signals for its estimation. This class known as unknown input observers are used to estimate the oscillatory combustion engine torque. The other class, termed estimators perform a harmonic separation of the input signal. Its realization uses a low pass filtering component (LPF) and a linear parameter varying (LPV) component. The LPF filters the mean value of the noisy signal devoid of harmonic content. The harmonics are filtered using the LPV component which is based on the correlation between the harmonic frequencies and the mean value of the oscillatory signal. The developed estimator can be used to estimate harmonic components of the torsional vibration signals such as speed and torque signals as demonstrated using experimental validation.

Active vibration reduction is achieved by the compensation torque generated by the Electric Traction Machine (ETM) to reduce the effect of pulsating torque resulting from the ICE operation. Active measures offer the additional flexibility of on-demand activation and can be effectively used to supplement passive measures. The tuning of measures such as CPA requires close interaction between powertrain construction and damper design [13] for exploitation of its potential. Active methods offer an attractive post-design solution. The effectiveness of active vibration reduction methods in case of non-stiff powertrains depends on the applied control functionality. This work presented different control schemes for the realization of active vibration reduction.

A common approach was employed to develop the controllers. The problem of torsional vibration reduction was handled in an abstract manner, irrespective of the components involved and their actuation dynamics. The influence of the components and their dynamics were handled separately by using the methodology of potential analysis. This step of abstraction, enabled the development of vibration

controllers based on the problem setting using different control methods. Furthermore, the controllers have been analyzed using simulations and validated on the experimental setup, demonstrating the desired torsional vibration reduction.

The novelties of each control scheme have been presented in the introduction section of the respective chapters. Hence an effort to compare the different control methods shall be done here after a brief introduction of the methods. The adaptive filter based controller uses a generic procedure to adapt the weights to realize a suitable out of phase signal for vibration cancellation. The output feedback controller does not require an online estimation of signal characteristics but generates the compensation torque using a fixed parameter feedback gain. The output regulation controller adapts itself to the current frequency of operation enabling vibration reduction using PI/PD controllers in tandem with the adaptive disturbance observer. The shaft torque feedback uses a delayed shaft torque estimate to realize active vibration reduction.

The developed controllers are based on different control methods with inherent advantages. Hence a direct comparison of the control schemes cannot be made. However, they can be compared from the perspective of torsional vibration reduction. Table 9.1 presents a comparison of the developed controllers. The criteria used for the comparison shall be presented along with the features specific to the controllers.

The first criterion considers the model assumptions required to synthesize the controller and the signals that are used in the realization of the controller. From the perspective of signals required, all the controllers except the shaft torque feedback control require the ETM speed signal only. The shaft torque feedback uses the ICE speed signal in addition to the ETM speed signal to estimate the shaft torque harmonics. However, the shaft torque feedback control requires minimal assumptions about the system. The need for the shaft stiffness parameter presented in section 8.1.2 is to compute the shaft torque using the estimated angular deflection. The output feedback control approach uses the system model along with the uncertainty definition to synthesize the controller. The adaptive filtering approach also requires a model of the secondary path and hence model of the torsional powertrain system. The adaptive regulation method uses the harmonic content of the ETM speed and hence requires no additional assumptions on the system.

The criterion implementation depends on among others the computational demand of the control method for computation of the compensation torque. The adaptive control schemes involve more computations than the fixed parameter

**Table 9.1:** Comparison of the developed active vibration reduction controllers

| Criteria | Adaptive Filtering | Output Feedback | Adaptive Regulation | Shaft Torque Feedback |
|---|---|---|---|---|
| Signals/Model | - | - | + | 0 |
| Implementation | - | 0 | + | + |
| Adaptability | ++ | + | ++ | 0 |
| Robustness | + | ++ | + | 0 |

feedback schemes. The most computationally intensive among the developed controllers is the adaptive filtering controller. This was the reason for the analysis of different solution methods and the selection of the Conjugate Gradient method for efficient computation. The reason behind the computational demand, in this case, is the computation of the adaptive filter weights. The adaptive output regulation uses the estimator for adaption to the current value of the harmonic content. This tracking of the harmonic amplitude along with the PI/PD controller is used to realize the control action. The output feedback uses fixed parameter feedback with the feedback gains computed using LMI. The computation demand associated with this scheme depends on the order of the synthesized output feedback control. The computational complexity of the shaft torque feedback arises only from the estimator used to compute the shaft torque harmonics. Once the harmonics are computed, they have to be shifted with the stabilizing delay and multiplied with a gain value to generate the compensation torque.

The generic applicability of the controllers for different engine configurations was demonstrated. This was done by using a 2-cylinder engine at the experimental test bench and 3-cylinder engine in the simulations. Further with the help of amplitude modulation, the generated compensation torque can be tuned for different ETM torque levels. Adaptability refers to the ability of the control scheme to be applied for different ICE and different ETM, which generates the compensation torque and also to adapt to system variations over time. The adaptive controller based on adaptive filtering and adaptive output regulation fair well with respect to adaptability. The output feedback controller due to its robustness properties (by design) can also handle plant variations provided the variations are in the class of uncertainties considered during the controller synthesis.

As the output feedback control methods are synthesized using methods of robust control, they exhibit robustness properties with respect to system variations.

The robustness of the shaft torque controller is a function of the used control gain and the stiffness parameter of the shaft coupling. If these parameters are tuned properly, the shaft torque feedback can cope with the variations in the system properties. In the case of system variations, the adaptive schemes can cope with them due to the adaptation of the computed control action. In the case of the adaptive filtering controller, the coefficients of the filter vary to compute the required control action in the presence of system variations.

### 9.1.1 Performance Assessment

Before presenting the inference of this thesis, a performance assessment of the formulated objectives shall be performed. Figure 9.1 presents the performance of the vibration reduction controller using the estimated quantities under stationary operation. The ETM speed signal is presented as a measure of torsional vibration. The Combustion Engine Assist (CEA) powerpack is operated at 1800 rpm with the ICE. The speed oscillations at the higher speed of 1800 are relatively less. As the operational speed is reduced to around 1200 rpm, with the same ICE pedal value, the speed oscillations increase which leads to component fatigue and passenger discomfort.

With the activation of the active vibration reduction controller at 242.5 seconds, the ETM speed oscillations reduce. It is noteworthy to mention, the controller did not use amplitude modulation. It can be observed that the torque amplitude required for compensation in steady state is -/+ 20 Nm. Such operation leads to consumption benefits if the lower operation speed limit of the ICE can be reduced further with the help of active vibration reduction methods. It can be concluded that the desired active vibration reduction is achieved.

### 9.1.2 Inference

It has been shown in this thesis that active vibration reduction can be used as an effective measure to reduce torsional vibration reduction. The implementation of the vibration reduction controller can be based on different control approaches based on the available signals and knowledge of the system. Irrespective of the control approach used for its realization, the underlying torsional powertrain system should be analyzed apriori to the implementation of the controller. If the compensation torque generation source is coupled supercritical to the inertia in the main (motive) torque transmission path of the ICE, the realization of active compensation would require higher torque amplitudes. The reason for this is the operation of the

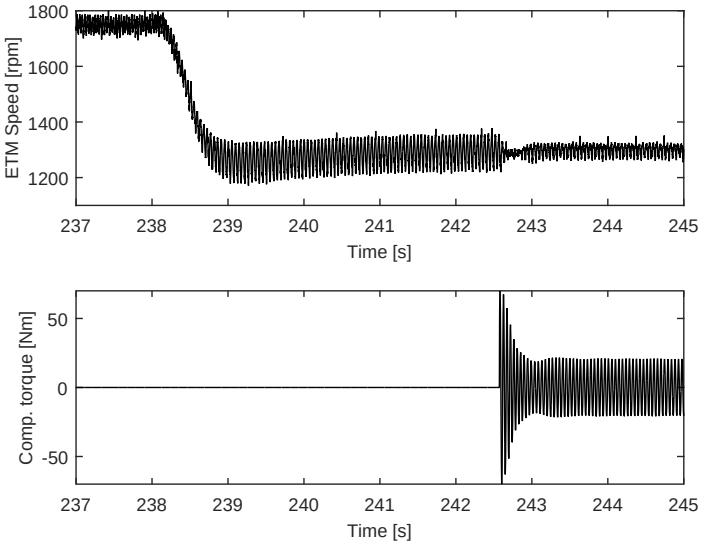


**Figure 9.1:** Performance of the active vibration reduction controller

coupling in the isolation region, resulting in higher torque amplitudes and higher power demand from the electrical energy source.

Additionally, using the architecture developed, the vibration reduction controller can be integrated with the hybrid vehicle Energy Management (EM). This modular integration approach uses a frequency based control allocation, facilitating an independent development of the EM and active vibration reduction controllers. The proposed harmonic efficiency characterization can be used to benchmark different combinations of active and passive vibration reduction measures to chose the optimal system for specific boundary conditions.

## 9.2 Outlook

Focus on quasi-semi-active systems (in the line of suspension systems) emulating parameter modification of the torsional stiffness using the electric traction machine is an open question. The term quasi has been used as it uses energy/command signal for switching between the different available characteristics. In contrast, a (complete) semi-active method would switch between different available stiffness characteristics of torsional spring or between different centrifugal pendulum

masses. Such designs, pose challenges with respect to the packaging demands associated with powertrains. However, they offer potential to supplement active/-passive torsional vibration reduction measures.

The focus of active vibration reduction was on the torque transfer path to final drive. The effect/advantages for accessory devices can be studied in future work. The experimental investigations were restricted to the test setup. An in-vehicle implementation and subjective calibration for passenger comfort are still open.

In addition to being used for the realization of the controllers and quantification of the achieved vibration reduction, the applicability of the developed signal estimation techniques has been demonstrated at experimental test benches. The developed mean value and harmonic estimation along with the torsional dynamics identification is an important contribution towards the development of Plug-and-Play Engine-In-The-Loop test benches.

## Bibliography


[1] T. Pauer; H. Yilmaz; J. Zumbrägel; W. Wiese; P. Rogler and E. Schünemann. *The New Generation Bosch Gasoline Direct Injection Systems*. In: *38. Internationales Wiener Motorensymposium*. 2017.

[2] K. Nakata and R. Shimizu. *Toyota's New Combustion Technology for High Engine Thermal Efficiency and High Engine Output Performance*. In: *37. Internationales Wiener Motorensymposium*. 2016.

[3] J. B. Heywood. *Internal Combustion Engine Fundamentals*. McGraw-Hill Book Company, New York, 1988. ISBN: 978-0070286375.

[4] M. Zink and M. Hausner. *LuK Kupplungssysteme und Torsionsdämpfer Schlüsselelemente für effiziente Antriebsstränge*. In: *Schaeffler Symposium*. 2010.

[5] *ISO 2631-1:1997/Amd 1:2010 - Mechanical vibration and shock — Evaluation of human exposure to whole-body vibration — Part 1: General requirements AMENDMENT 1*. In: *ISO/TC 108/SC 4 Human exposure to mechanical vibration and shock* (2010).

[6] H. Friedl. *Trends in gasoline powertrain technology for high performance and low emission*. In: *The International Congress of Automotive and Road Transport Engineering*. 2017.

[7] EUROPEAN COMMISSION. *Roadmap to a Single European Transport Area – Towards a competitive and resource efficient transport system*. In: *White Paper*. 2011.

[8] M. Wirth; L. Bartsch; S. Ploumen and C. Weber. *In a Hybridized Future with Alternative Fuels: Is the SI Engine the Winning Concept?* In: *SIA POWERTRAIN*. 2015.

[9] H. Faust. *Powertrain Systems of the Future*. In: *Solving the Powertrain Puzzle, 10th Schaeffler Symposium 2014*. Schaeffler. DOI: https://doi.org/10.1007/978-3-658-06430-3.

[10] C. O. Griebel; F. Rabenstein; M. Klüting; F. Kessler; J. Kretschmer and E. Hockgeiger. *The Full-Hybrid Powertrain of the new BMW ActiveHybrid 5*. In: *20. Aachen Colloquium Automobile and Engine Technology*. 2011.

[11] L. Eriksson and L. Nielsen. *Modeling and Control of Engines and Drivelines*. John Wiley & Sons, 2014. ISBN: 978-1118479995.

[12] M. Wacker. *Einfluss von Drehungleichfoermigkeiten auf die Zahnradlebensdauer in Fahrzeuggetrieben*. Dissertation. Institut fuer Maschinenelemente, Universitaet Stuttgart, 2013. ISBN: 978-3936100457.

[13] A. Kooy. *Isolation is the Key : The evolution of the centrifugal pendulum-type absorber not only for DMF*. In: *Solving the Powertrain Puzzle, 10th Schaeffler Symposium 2014*. Schaeffler. DOI: https://doi.org/10.1007/978-3-658-06430-3.

[14] J. Kroll; A. Kooy and R. Seebacher. *Land in Sicht? Torsionsschwingungsdämpfung für zukünftige Motoren*. In: *Schaeffler Symposium*. 2010.

[15] R. Golloch. *Downsizing bei Verbrennungsmotoren*. Springer, 2005. ISBN: 978-3540238836.

[16] R. Fischer; F. Küçükay; G. Jürgens; R. Najork and B. Pollak. *The Automotive Transmission Book*. Springer, 2015. ISBN: 978-3319052625.

[17] E. Kirchner. *Innovative Machine Components II*. In: *TU Darmstadt, Lecture Summer Semester*. 2018.

[18] R. S. Vadamalu; C. Beidl; G. Hohenberg and K. Muehlbauer. *Active Torsional Vibration Reduction: Potential Analysis and Controller Development for a Belt Driven 48 V System*. In: *Springer Automotive and Engine Technology* (2019).

[19] D. Buch. *Aktive Beruhigung verbrennungsmotorisch erregter Drehschwingungen im hybriden Fahrzeugantriebsstrang*. Dissertation. Institut fuer Verbrennungskraftmaschinen und Fahrzeugantriebe, TU Darmstadt, 2016.

[20] P. Hofmann. *Hybridfahrzeuge*. Springer, 2014. ISBN: 978-3709117804.

[21] H. Naunheimer; B. Bertsche and G. Lechner. *Fahrzeuggetriebe Grundlagen, Auswahl, Auslegung und Konstruktion*. Springer, 2007. ISBN: 978-3540306252.

[22] A. Kooy; A. Gillmann; J. Jäckel and M. Bosse. *ZMS - Nicht Neues ?* In: *LuK Symposium*. 2002.

[23] P. Zeller. *Handbuch Fahrzeugakustik*. Springer, 2012. ISBN: 978-3834886576.

[24] E. Köhler and R. Flierl. *Verbrennungsmotoren Motormechanik, Berechnung und Auslegung des Hubkolbenmotors*. Vieweg+Teubner Verlag, 2011. ISBN: 978-3834814869.

[25] W. Reik. *Torsionsschwingungsisolation im Antriebsstrang Ein Wertungsversuch*. In: *Torsionsschwingungen im Antriebsstrang, 4. Internationales LuK Symposium, Baden-Baden*. 1990.

[26] H. Dresig and A. Fidlin. *Schwingungen mechanischer Antriebssysteme*. Springer, 2014. ISBN: 978-3642241178.

[27] F. Küçükay. *Dynamik der Zahnradgetriebe*. Springer, 1987. ISBN: 978-3540171119.

[28] A. Fidlin and R. Seebacher. *DMF simulation techniques – Finding the needle in the haystack*. In: *Schaeffler Symposium*. 2006.

[29] M. Mitschke and H. Wallentowitz. *Dynamik der Kraftfahrzeuge*. 4. Auflage. Springer, 2004.

[30] A. Albers and D. Herbst. *Chatter - Causes and Solutions*. In: *6. LuK Symposium 1998*.

[31] K. Küpper; B. Serebrennikov and G. Göppert. *Software for automized transmissions - Intelligent driving*. In: *LuK Symposium 2006*.

[32] A. Albers. *Fortschritte beim ZMS–Geräuschkomfort für moderne Kraftfahrzeuge*. In: *LuK Symposium 1994*.

[33] M. Zink and M. Hausner. *Das Fliehkraftpendel : Anwendung, Leistung und Grenzen drehzahladaptiver Tilger*. In: Springer Automotive Media. DOI: https://doi.org/10.1007/BF03222092.

[34] M. Harrison. *Vehicle Refinement Controlling Noise and Vibration in Road Vehicles*. Butterworth-Heinemann, 2004. ISBN: 978-0080474755.

[35] S. Haykin. *Adaptive Filter Theory*. Prentice Hall, 2013. ISBN: 978-0132671453.

[36] T. Hu. *Development of a simulation model of torsional vibrations of internal combustion engines*. Master thesis. TU Darmstadt, 2014.

[37] T. Melz. *Grundlagen der Adaptronik*. In: *TU Darmstadt, Lecture Winter Semester*. 2017.

[38] Schaeffler Automotive Aftermarket GmbH & Co. KG. *LuK clutch course : Introduction to clutch technology for cars and LCVs*. In: 2015.

[39] W. Reik; R. Seebacher and A. Kooy. *Dual Mass Flywheel*. In: *LuK Symposium*. 1998.

[40] J. C. Depp. *Einfluss des Kurbelwellen-Startergenerators auf das Schwingungsverhalten des Verbrennungsmotors*. In: *Systemanalyse in der KFZ-Antriebstechnik, Haus der Technik Band 6*. Expert-Verlag, 2001.

[41] *Valeo 4 KKIT Product Description*. http://www.4kkit.de/. Accessed: 2018-09-25.

[42] Schaeffler Automotive Aftermarket GmbH & Co. KG. *Dual Mass Flywheel - Technology / Failure Diagnosis, Special Tool / User Instructions*. In: 2016.

[43] ZF Friedrichshafen AG. *Clutch Systems For passenger cars up to 1,000 Nm*. In: (2017).

[44] R. von Dahlen; J.W. van der Vecht; M. Geilen; U. Schreiber. *Abstimmung von Drehschwingungsdämpfern – Modellierung und Simulation*. In: *Systemanalyse in der KFZ-Antriebstechnik V*. Expert-Verlag, 2009.

[45] M. Schnurr. *Entwicklung zum superweitwinkel - ZMS*. In: *4. LuK Symposium 1994*.

[46] R. Markert. *Rotordynamik, Skript zur Vorlesung, 1. Auflage*. In: *Fachbereich Mechanik, TU Darmstadt*. 2003.

[47] A. Slibar and K. Desoyer. *Zur Erzielung optimaler Wirkung bei Pendel-Schwingungstilgern*. In: *Ingenieur-Archiv XXII. Band*. 1954.

[48] D. E. Newland. *Nonlinear Aspects of the Performance of Centrifugal Pendulum Vibration Absorbers*. In: *Journal of Engineering for Industry* (1964), pp. 257–263. DOI: 10.1115/1.3670529.

[49] A. G. Haddow and S. W. Shaw. *Centrifugal Pendulum Vibration Absorbers: An Experimental and Theoretical Investigation*. In: *Nonlinear Dynamics* 34.3 (2003), pp. 293–307. ISSN: 1573-269X. DOI: 10.1023/B:NODY.0000013509.51299.c0.

[50] A. Wedin. *Reduction of Vibrations in Engines using Centrifugal Pendulum Vibration Absorbers*. Master thesis. Chalmers University of Technology, Department of Product and Production Development, 2011.

[51] K. Küpper; R. Seebacher and O. Werner. *Think Systems - Software by LuK*. In: *LuK Symposium 2002*.

[52] M. Dilzer; D. Reitz; W. Ruder and U. Wagner. *Eine Idee. viele Anwendungen: Weiterentwicklung des Hybridmoduls von Schaeffler*. In: *Schaeffler Symposium*. 2014.

[53] J. Wang; P. Liu; J. Hicks-Garner; E. Sherman; S. Soukiazian; M. Verbrugge; H. Tataria; J. Musser and P. Finamore. *Cycle-life model for graphite-LiFePO4 cells*. In: *Journal of Power Sources* 196.8 (2011), pp. 3942–3948. ISSN: 0378-7753. DOI: https://doi.org/10.1016/j.jpowsour.2010.11.134.

[54] P. Micheau and P. Coirault. *A Harmonic Controller of Engine Speed Oscillations for Hybrid Vehicles*. In: *IFAC Proceedings Volumes* 38.1 (2005). 16th IFAC World Congress, pp. 19–24. ISSN: 1474-6670. DOI: https://doi.org/10.3182/20050703-6-CZ-1902.01891.

[55] M. Njeh; S. Cauet; P. Coirault and P. Martin. *H∞ control strategy of motor torque ripple in hybrid electric vehicles: an experimental study*. In: *Control Theory & Applications, IET*. Vol. 5. 2011, pp. 131–144.

[56] M. Njeh; S. Cauet and P. Coirault. *Control strategy of speed pulsations on hybrid powertrains*. In: *Advances in Hybrid Powertrains, IFP*. 2008.

[57] S. Tnani; P. Coirault and G Champenois. *Novel control strategy of torque pulsations on a hybrid vehicle*. In: *Proceedings of the Institution of Mechanical Engineers, Part D: Journal of Automobile Engineering* 220.10 (2006), pp. 1437–1444. DOI: 10.1243/09544070JAUTO169.

[58] A. T. Zaremba and R. I. Davis. *Control design for active engine damping using a starter/alternator*. In: *Proceedings of the 2000 American Control Conference. ACC (IEEE Cat. No.00CH36334)*. Vol. 3. 2000, 2043–2047 vol.3. DOI: 10.1109/ACC.2000.879560.

[59] S. Cauet; P. Coirault and M. Njeh. *Diesel engine torque ripple reduction through LPV control in hybrid electric vehicle powertrain: Experimental results*. In: *Control Engineering Practice* 21.12 (2013), pp. 1830–1840. ISSN: 0967-0661. DOI: https://doi.org/10.1016/j.conengprac.2013.03.005.

[60] B. A. Francis and W. M. Wonham. *The internal model principle of control theory*. In: *Automatica* 12.5 (1976), pp. 457–465. ISSN: 0005-1098. DOI: https://doi.org/10.1016/0005-1098(76)90006-6.

[61] R. S. Vadamalu and C. Beidl. *MPC for Active Torsional Vibration Reduction of Hybrid Electric Powertrains*. In: *IFAC-PapersOnLine* 49.11 (2016). 8th IFAC Symposium on Advances in Automotive Control AAC 2016, pp. 756–761. ISSN: 2405-8963. DOI: https://doi.org/10.1016/j.ifacol.2016.08.110.

[62] M. Beuschel; M. Rau and D. Schroder. *Adaptive damping of torque pulsation using a starter generator-opportunities and boundaries*. In: *IEEE Industry Applications Conference*. Vol. 3. 2000. DOI: 10.1109/IAS.2000.882068.

[63] R. I. Davis and R. D. Lorenz. *Engine torque ripple cancellation with an integrated starter alternator in a hybrid electric vehicle: implementation and control*. In: *IEEE Transactions on Industry Applications* 39.6 (2003), pp. 1765–1774. ISSN: 0093-9994. DOI: 10.1109/TIA.2003.818972.

[64] A. Tareilus; H. D. Endres; A. Oflaz and H. J. Schneider. *Aktive Schwingungsdaempfung im Antriebsstrang von Hybridfahrzeugen*. In: *VDI Fachtagung Schwingungen in Antrieben*. 2011.

[65] S. M. Kuo and D. R. Morgan. *Active noise control: a tutorial review*. In: *Proceedings of the IEEE* 87.6 (1999), pp. 943–973. ISSN: 0018-9219. DOI: 10.1109/5.763310.

[66] M. Kauba; J. Millitzer; D. Mayer and H. Hanselka. *Multi-channel narrowband Filtered-x-Least-Mean-Square algorithm with reduced calculation complexity*. In: *5th ECCOMAS Thematic Conference on Smart Structures and Materials* (2011).

[67] J. B. Rawlings; D. Q. Mayne and M. Diehl. *Model Predictive Control: Theory, Computation, and Design, 2nd Edition*. Nob Hill Publishing, 2018. ISBN: 978-0975937709.

[68] T. Wellmann; K. Govindswamy; E. Braun and K. Wolff. *Aspects of Driveline Integration for Optimized Vehicle NVH Characteristics*. In: *SAE Technical Paper* (2007). DOI: https://doi.org/10.4271/2007-01-2246.

[69] U. Konigorski. *Modelbildung und Simulation*. In: *TU Darmstadt, Lecture Summer Semester*. 2015.

[70] M. Willimowski and R. Isermann. *A Time Domain Based Diagnostic System for Misfire Detection in Spark-Ignition Engines by Exhaust-Gas Pressure Analysis*. In: *SAE 2000 World Congress*. SAE International, 2000. DOI: https://doi.org/10.4271/2000-01-0366.

[71] R. Isermann. *Engine Modeling and Control*. Springer, 2014. ISBN: 978-3642399343.

[72] S. Helm; M. Kozek and S. Jakubek. *Combustion Torque Estimation and Misfire Detection for Calibration of Combustion Engines by Parametric Kalman Filtering*. In: *IEEE Transactions on Industrial Electronics* 59.11 (2012), pp. 4326–4337. ISSN: 0278-0046. DOI: 10.1109/TIE.2012.2193855.

[73] M. Pettersson and L. Nielsen. *Gear shifting by engine control*. In: *IEEE Transactions on Control Systems Technology* 8.3 (2000), pp. 495–507. ISSN: 1063-6536. DOI: 10.1109/87.845880.

[74] M. Bier. *Hardware-In-the-Loop-Motorprüfstand zur Entwicklung hybrider Antriebsstraenge*. Dissertation. Institut fuer Verbrennungskraftmaschinen und Fahrzeugantriebe, TU Darmstadt, 2017.

[75] J. Franco; M. A. Franchek and K. Grigoriadis. *Real-time brake torque estimation for internal combustion engines*. In: *Mechanical Systems and Signal Processing* 22.2 (2008), pp. 338–361. ISSN: 0888-3270. DOI: https://doi.org/10.1016/j.ymssp.2007.08.002.

[76] A. Radke and Z. Gao. *A survey of state and disturbance observers for practitioners*. In: *2006 American Control Conference*. 2006. DOI: 10.1109/ACC.2006.1657545.

[77] D. S. Laila and E. Grunbacher. *Discrete-time nonlinear observer and output feedback design for a combustion engine test bench*. In: *2008 47th IEEE Conference on Decision and Control*. 2008, pp. 5718–5723. DOI: 10.1109/CDC.2008.4738943.

[78] G. Reale; P. Ortner and L. del Re. *Nonlinear observers for closed-loop control of a combustion engine test bench*. In: *2009 American Control Conference*. 2009, pp. 4648–4653. DOI: 10.1109/ACC.2009.5160109.

[79] A. Isidori. *Nonlinear Control Systems*. Springer, 1995. ISBN: 978-1-84628-615-5.

[80] E. Gruenbacher and L. del Re. *Adaptive Mean Value Engine Torque Estimation on Engine Test Benches*. In: *CACS International Automatic Control Conference*. 2007.

[81] J. Na; A. S. Chen; G. Herrmann; R. Burke and C. Brace. *Vehicle Engine Torque Estimation via Unknown Input Observer and Adaptive Parameter Estimation*. In: *IEEE Transactions on Vehicular Technology* 67.1 (2018), pp. 409–422. ISSN: 0018-9545. DOI: 10.1109/TVT.2017.2737440.

[82] A. Stotsky and I. Kolmanovsky. *Application of input estimation techniques to charge estimation and control in automotive engines*. In: *Control Engineering Practice* 10.12 (2002), pp. 1371–1383. ISSN: 0967-0661. DOI: https://doi.org/10.1016/S0967-0661(02)00101-6.

[83] J. Chauvin; G. Corde; P. Moulin; M. Castagne; N. Petit and P. Rouchon. *Real-time combustion torque estimation on a diesel engine test bench using time-varying Kalman filtering*. In: *2004 43rd IEEE Conference on Decision and Control (CDC) (IEEE Cat. No.04CH37601)*. Vol. 2. 2004, pp. 1688–1694. DOI: 10.1109/CDC.2004.1430287.

[84] J. Chauvin; G. Corde; N. Petit and P. Rouchon. *Periodic input estimation for linear periodic systems: Automotive engine applications*. In: *Automatica* 43.6 (2007), pp. 971–980. ISSN: 0005-1098. DOI: https://doi.org/10.1016/j.automatica.2006.12.012.

[85] W. Sun; J. Shen; K. Wang and M. Jin. *Motor Control Application of Fixed-Sampling-Interval and Fixed-Depth Moving Average Filters*. In: *IEEE Transactions on Industry Applications* 52.2 (2016), pp. 1831–1841. ISSN: 0093-9994. DOI: 10.1109/TIA.2015.2487452.

[86] Y. W. Kim; G. Rizzoni and Y.-Y. Wang. *Design of an IC Engine Torque Estimator Using Unknown Input Observer*. In: *European Control Conference* (1996).

[87] J. Chen; R. Patton and H.-Y. Zhang. *Design of unknown input observers and robust fault detection filters*. In: *International Journal of Control*. Vol. 63. 2007, pp. 85–105.

[88] D. S. Laila and E. Gruenbacher. *Nonlinear output feedback and periodic disturbance attenuation for setpoint tracking of a combustion engine test bench*. In: *Automatica* 64 (2016), pp. 29–36. ISSN: 0005-1098. DOI: https://doi.org/10.1016/j.automatica.2015.10.054.

[89] S. Boyd; L. El Ghaoui; E. Feron and V. Balakrishnan. *Linear Matrix Inequalities in System and Control Theory*. Society for Industrial and Applied Mathematics, 1994. DOI: 10.1137/1.9781611970777.

[90] C. Scherer and S. Weiland. *Linear Matrix Inequalities in Control,* 2015.

[91] R. S. Vadamalu and C. Beidl. *Closed Loop Identification of Engine and Powerpack Test Benches, under review*. 2018.

[92] J. G. Proakis and D. K. Manolakis. *Digital Signal Processing, 4th Edition*. Pearson New International Edition, 2014. ISBN: 978-0131873742.

[93] M. Schmidt and J. Achim-Kessel. *CASMA-crank angle synchronous moving average filtering*. In: 2 (1999), pp. 1339–1340. ISSN: 0743-1619. DOI: 10.1109/ACC.1999.783585.

[94] M. Ciobotaru; R. Teodorescu and F. Blaabjerg. *A new single-phase PLL structure based on second order generalized integrator*. In: *2006 37th IEEE Power Electronics Specialists Conference*. 2006, pp. 1–6. DOI: 10.1109/pesc.2006.1711988.

[95] C. Beidl; D. Buch; G. Hohenberg; C. Bacher; J. Hammer and A. Kufferath. *Effizienter E-Fahrzeugantrieb mit dem kompakten CEA-Konzept – Combustion Engine Assist*. In: *Der Antrieb von morgen*. 2012.

[96] C. Westermayer; R. Priesner; M. Kozek and R. Bauer. *High Dynamic Torque Control for Industrial Engine Test Beds*. In: *IEEE Transactions on Industrial Electronics* 60.9 (2013), pp. 3877–3888. ISSN: 0278-0046. DOI: 10.1109/TIE.2012.2206338.

[97] A. Lamara; P. Lanusse; A. Charlet; D. Nelson Gruel; G. Colin; A. Lesobre; A. Oustaloup and Y. Chamaillard. *High Dynamic Engine-Dynamometer Identification and Control*. In: *IFAC Proceedings Volumes* 47.3 (2014). 19th IFAC World Congress, pp. 5217–5222. ISSN: 1474-6670. DOI: https://doi.org/10.3182/20140824-6-ZA-1003.01141.

[98] P. Langthaler and L. del Re. *IDENTIFICATION OF DRIVELINE PARAMETERS USING AN AUGMENTED NONLINEAR MODEL*. In: *IFAC Proceedings Volumes* 38.1 (2005). 16th IFAC World Congress, pp. 31–36. ISSN: 1474-6670. DOI: https://doi.org/10.3182/20050703-6-CZ-1902.01893.

[99] U. Forssell and L. Ljung. *Closed-loop identification revisited*. In: *Automatica* 35.7 (1999), pp. 1215–1241. ISSN: 0005-1098. DOI: https://doi.org/10.1016/S0005-1098(99)00022-9.

[100] L. Ljung. *System Identification: Theory for the User, 2nd Edition*. Prentice Hall PTR, 1999. ISBN: 978-0136566953.

[101] T. Söderström. *Errors-in-variables methods in system identification*. In: *Automatica* 43.6 (2007), pp. 939–958. ISSN: 0005-1098. DOI: https://doi.org/10.1016/j.automatica.2006.11.025.

[102] J. Schoukens; R. Pintelon; G. Vandersteen and P. Guillaume. *Frequency-domain system identification using non-parametric noise models estimated from a small number of data sets*. In: *Automatica* 33.6 (1997), pp. 1073–1086. ISSN: 0005-1098. DOI: https://doi.org/10.1016/S0005-1098(97)00002-2.

[103] R. Pintelon; J. Schoukens; G. Vandersteen and K. Barbé. *Estimation of nonparametric noise and FRF models for multivariable systems—Part II: Extensions, applications*. In: *Mechanical Systems and Signal Processing* 24.3 (2010), pp. 596–616. ISSN: 0888-3270. DOI: https://doi.org/10.1016/j.ymssp.2009.08.010.

[104] R. Pintelon and J. Schoukens. *System Identification: A Frequency Domain Approach, 2nd Edition*. Wiley-IEEE Press, 2012. ISBN: 978-0470640371.

[105] R. Pintelon; K. Barbé; G. Vandersteen and J. Schoukens. *Improved (non-)parametric identification of dynamic systems excited by periodic signals*. In: *Mechanical Systems and Signal Processing* 25 (2011), pp. 2683–2704. DOI: 10.1016/j.ymssp.2011.03.003.

[106] R. Pintelon; J. Schoukens; G. Vandersteen and K. Barbé. *Estimation of non-parametric noise and FRF models for multivariable systems—Part I: Theory*. In: *Mechanical Systems and Signal Processing* 24.3 (2010), pp. 573–595. ISSN: 0888-3270. DOI: https://doi.org/10.1016/j.ymssp.2009.08.009.

[107] H. Akaike. *A new look at the statistical model identification*. In: *IEEE Transactions on Automatic Control* 19.6 (1974), pp. 716–723. ISSN: 0018-9286. DOI: 10.1109/TAC.1974.1100705.

[108] R. Isermann and M. Münchhof. *Identification of Dynamic Systems : An Introduction with Applications*. Springer, 2011. ISBN: 978-3540788782.

[109] J. Schoukens; R. Pintelon; G. Vandersteen and P. Guillaume. *Frequency-domain system identification using non-parametric noise models estimated from a small number of data sets*. In: *Automatica* 33.6 (1997), pp. 1073–1086. ISSN: 0005-1098. DOI: https://doi.org/10.1016/S0005-1098(97)00002-2.

[110] P. Van. Overschee and B. L. De Moor. *Subspace Identification for Linear Systems : Theory - Implementation - Applications*. Springer, 1996. ISBN: 978-1461380610.

[111] T. Katayama. *Subspace Methods for System Identification*. Springer, 2005. ISBN: 978-1846281587.

[112] H. Kokal; E. Gruenbacher; L. del Re; M. Schmidt and M. Paulweber. *Bandwidth extension of dynamical test benches by modified mechanical design under adaptive feedforward disturbance rejection*. In: *Proceedings of the 2010 American Control Conference*. 2010, pp. 6151–6156. DOI: 10.1109/ACC.2010.5531597.

[113] R. Fletcher. *Practical Methods of Optimization, 2nd Edition*. Wiley, 2000. ISBN: 978-0471494638.

[114] L. Wu; X. Qiu and Y. Guo. *A simplified adaptive feedback active noise control system*. In: *Applied Acoustics* 81 (2014), pp. 40–46. ISSN: 0003-682X. DOI: https://doi.org/10.1016/j.apacoust.2014.02.006.

[115] B. Widrow. *Adaptive Inverse Control*. In: *IFAC Proceedings Volumes* 20.2 (1987). 2nd IFAC Workshop on Adaptive Systems in Control and Signal Processing 1986, Lund, Sweden, 30 June-2 July 1986, pp. 1–5. ISSN: 1474-6670. DOI: https://doi.org/10.1016/S1474-6670(17)55929-7.

[116] J. C. Burgess. *Active adaptive sound control in a duct - A computer simulation*. In: *Acoustical Society of America Journal* 70 (1981), pp. 715–726. DOI: 10.1121/1.386908.

[117] S. J. Elliott and P. Nelson. *The application of adaptive filtering to the active control of sound and vibration*. In: *NASA STI/Recon Technical Report N*. Vol. 86. 1985.

[118] B. Widrow and S. D. Stearns. *Adaptive Signal Processing*. Prentice Hall, 1985. ISBN: 978-0130040299.

[119] P. S. R. Diniz. *Adaptive Filtering: Algorithms and Practical Implementation, 4th Edition*. Springer, 2013. ISBN: 978-1461441052.

[120] G. Strang. *Linear Algebra and Its Applications, 4th Edition*. Thomson, Brooks/Cole, 2006. ISBN: 978-0030105678.

[121] C. Kelley. *Iterative Methods for Linear and Nonlinear Equations*. Society for Industrial and Applied Mathematics, 1995. DOI: 10.1137/1.9781611970944.

[122] J. R. Shewchuk. *An Introduction tothe Conjugate Gradient MethodWithout the Agonizing Pain*. In: *Carnegie Mellon University* (1994).

[123] G. K. Boray and M. D. Srinath. *Conjugate gradient techniques for adaptive filtering*. In: *IEEE Transactions on Circuits and Systems I: Fundamental Theory and Applications* 39.1 (1992), pp. 1–10. ISSN: 1057-7122. DOI: 10.1109/81.109237.

[124] D. J. Ewins. *Modal Testing: Theory, Practice and Application, 2nd Edition*. Wiley, 2009. ISBN: 978-0863802188.

[125] T. McKelvey. *Frequency Domain Identification Subspace methods and Periodic Excitation*. In: *2nd Russian Swedish Control Conference* (1995).

[126] Volkswagen. *MQB – der neue Modulare Querbaukasten, TDI und TSI – neue Motoren im MQB*. In: *Internationaler Presseworkshop, Wolfsburg* (2012).

[127] G. C. Calafiore and M. C. Campi. *The scenario approach to robust control design*. In: *IEEE Transactions on Automatic Control* 51.5 (2006), pp. 742–753. ISSN: 0018-9286. DOI: 10.1109/TAC.2006.875041.

[128] S. Skogestad and I. Postlethwaite. *Multivariable Feedback Control: Analysis and Design*. USA: John Wiley & Sons, 2005. ISBN: 0470011688.

[129] R. D. Braatz; P. M. Young; J. C. Doyle and M. Morari. *Computational complexity of $\mu$ calculation*. In: *1993 American Control Conference*. 1993, pp. 1682–1683. DOI: 10.23919/ACC.1993.4793162.

[130] I. R. Petersen; V.A. Ugrinovskii and A. Savkin. *Robust Control Design Using $H\infty$ Methods*. 2000.

[131] A. Packard and J. Doyle. *The complex structured singular value*. In: *Automatica* 29.1 (1993), pp. 71–109. ISSN: 0005-1098. DOI: https://doi.org/10.1016/0005-1098(93)90175-S.

[132] H. Werner. *Advanced Topics in Control*. In: *Technische Universität Hamburg (TUHH), Lecture Notes*. 2018.

[133] K. Zhou; J.C. Doyle and K. Glover. *Robust and Optimal Control*. Upper Saddle River, NJ, USA: Prentice-Hall, Inc., 1996. ISBN: 0-13-456567-3.

[134] J. Lunze. *Regelungstechnik 1: Systemtheoretische Grundlagen, Analyse und Entwurf einschleifiger Regelungen*. 7., neu bearb. Aufl. Springer, Berlin, 2008. ISBN: 3540689079.

[135] G. Zames. *Feedback and optimal sensitivity: Model reference transformations, multiplicative seminorms, and approximate inverses*. In: *IEEE Transactions on Automatic Control* 26.2 (1981), pp. 301–320. ISSN: 0018-9286. DOI: 10.1109/TAC.1981.1102603.

[136] J. C. Doyle; K. Glover; P. P. Khargonekar and B. A. Francis. *State-space solutions to standard H2 and H∞ control problems*. In: *IEEE Transactions on Automatic Control* 34.8 (1989), pp. 831–847. ISSN: 0018-9286. DOI: 10.1109/9.29425.

[137] C. Scherer. *H∞-Optimization without Assumptions on Finite or Infinite Zeros*. In: *SIAM Journal on Control and Optimization* 30.1 (1992), pp. 143–166. DOI: 10.1137/0330010.

[138] M. Sampei; T. Mita and M. Nakamichi. *An algebraic approach to H ∞ output feedback control problems*. In: *Systems and Control Letters* 14 (1990), pp. 13–24.

[139] P. Gahinet and P. Apkarian. *A Linear Matrix Inequality Approach to H ∞ Control*. In: *INTERNATIONAL JOURNAL OF ROBUST AND NONLINEAR CONTROL* 4 (1994), pp. 421–448.

[140] C. Scherer; P. Gahinet and M. Chilali. *Multiobjective output-feedback control via LMI optimization*. In: *IEEE Transactions on Automatic Control* 42.7 (1997), pp. 896–911. ISSN: 0018-9286. DOI: 10.1109/9.599969.

[141] P. P. Khargonekar and M. A. Rotea. *Mixed H2 H∞ control: a convex optimization approach*. In: *IEEE Transactions on Automatic Control* 36.7 (1991), pp. 824–837. ISSN: 0018-9286. DOI: 10.1109/9.85062.

[142] G. E. Dullerud and F. Paganini. *A Course in Robust Control Theory - A Convex Approach*. Springer, 2000. ISBN: 978-0387989457. DOI: 10.1007/978-1-4757-3290-0.

[143] J. Ackermann; A. Bartlett; D. Kaesbauer; W. Sienel and R. Steinhauser. *Robust Control: Systems with Uncertain Physical Parameters*. 1993. ISBN: 0387198431.

[144] M. Chilali and P. Gahinet. *H∞ design with pole placement constraints: an LMI approach*. In: *IEEE Transactions on Automatic Control* 41.3 (1996), pp. 358–367. ISSN: 0018-9286. DOI: 10.1109/9.486637.

[145] J. C. Doyle. *Synthesis of robust controllers and filters*. In: *The 22nd IEEE Conference on Decision and Control*. 1983, pp. 109–114. DOI: 10.1109/CDC.1983.269806.

[146] B. Wie and D. S. Bernstein. *A benchmark problem for robust control design*. In: *1990 American Control Conference*. 1990, pp. 961–962. DOI: 10.23919/ACC.1990.4790876.

[147] R. S. Vadamalu and C. Beidl. *Adaptive Filtering Methods for Active Torsional Vibration Reduction without Reference Sensing, under review*. 2018.

[148] A. Saberi; P. Sannuti and A. Stoorvogel. *Control of Linear Systems with Regulation and Input Constraints*. 1st. Springer-Verlag, 2000. ISBN: 1852331534.

[149] A. Pavlov; N. van de Wouw and H. Nijmeijer. *Uniform Output Regulation of Nonlinear Systems*. Birkhäuser Boston, 2006. ISBN: 978-0-8176-4465-9. DOI: https://doi.org/10.1007/0-8176-4465-2.

[150] C. I. Byrnes and A. Isidori. *Output regulation for nonlinear systems: an overview*. In: *International Journal of Robust and Nonlinear Control* 10.5 (1998), pp. 323–337. DOI: 10.1002/(SICI)1099-1239(20000430)10:5<323::AID-RNC483>3.0.CO;2-G.

[151] R. Marino and P. Tomei. *Output regulation for linear systems via adaptive internal model*. In: *IEEE Transactions on Automatic Control* 48.12 (2003), pp. 2199–2202. ISSN: 0018-9286. DOI: 10.1109/TAC.2003.820143.

[152] W. E. Larimore. *Canonical variate analysis in identification, filtering, and adaptive control*. In: *29th IEEE Conference on Decision and Control*. Vol. 2. 1990, pp. 596–604. DOI: 10.1109/CDC.1990.203665.

[153] M. Jansson. *Subspace Identification and ARX Modeling*. In: *IFAC Proceedings Volumes* 36.16 (2003). 13th IFAC Symposium on System Identification (SYSID 2003), Rotterdam, The Netherlands, 27-29 August, 2003, pp. 1585–1590. ISSN: 1474-6670. DOI: https://doi.org/10.1016/S1474-6670(17)34986-8.

[154] W. Michiels and S. Niculescu. *Stability, Control, and Computation for Time-Delay Systems*. Philadelphia, PA: Society for Industrial and Applied Mathematics, 2014. DOI: 10.1137/1.9781611973631.

[155] J. K. Hale and S. M. Verduyn Lunel. *Introduction to Functional Differential Equations*. Applied Mathematical Sciences, Springer-Verlag, 1993. ISBN: 978-0387940762.

[156] Z. Wu and W. Michiels. *Reliably computing all characteristic roots of delay differential equations in a given right half plane using a spectral method*. In: *Journal of Computational and Applied Mathematics* 236.9 (2012), pp. 2499–2514. ISSN: 0377-0427. DOI: https://doi.org/10.1016/j.cam.2011.12.009.